REPORT DOCUMENTATION PAGE

Form Approved
OMB No. 0704-0188

1. AGENCY USE ONLY (Leave blank)	2. REPORT DATE	3. REPORT TYPE AND DATES COVERED
	May 30, 1997	Final: 9/1/1992-11/30/1995

4. TITLE AND SUBTITLE
Brittle to Ductile Transitions in Cleavage Fracture: Experiments and Simulations

5. FUNDING NUMBERS
C-N00014-92-J-4022

6. AUTHOR(S)
A.S. Argon
Quentin Berg Professor of Mechanical Engineering

7. PERFORMING ORGANIZATION NAME(S) AND ADDRESS(ES)
Massachusetts Institute of Technology
Room 1-306
Cambridge, MA 02139

8. PERFORMING ORGANIZATION REPORT NUMBER

9. SPONSORING/MONITORING AGENCY NAME(S) AND ADDRESS(ES)
ONR Solid Mechanics Program
Attention of Dr. Roshdy Barsoum
ONR Code 1132
800 N. Quincy St. Balston Tower 1
Arlington, VA 22217-5000

10. SPONSORING/MONITORING AGENCY REPORT NUMBER

11. SUPPLEMENTARY NOTES
Final Report Text and Appendix containing publications.

12a. DISTRIBUTION/AVAILABILITY STATEMENT
Unlimited

12b. DISTRIBUTION CODE

13. ABSTRACT (Maximum 200 words)

Final report summarizing the experimental studies of crack arrest in Si single crystals and associated computer simulations of key crack tip processes controlling the brittle to ductile transition from cleavage to tough behavior.

14. SUBJECT TERMS
Experimental study of fracture transitions in brittle crystalline solids and associated simulations

15. NUMBER OF PAGES

16. PRICE CODE

17. SECURITY CLASSIFICATION OF REPORT	18. SECURITY CLASSIFICATION OF THIS PAGE	19. SECURITY CLASSIFICATION OF ABSTRACT	20. LIMITATION OF ABSTRACT
Unclassified	Unclassified	Unclassified	None

Massachusetts Institute of Technology
Department of Mechanical Engineering
Cambridge, MA 02139

BRITTLE-TO-DUCTILE TRANSITION IN CLEAVAGE FRACTURE: EXPERIMENTS AND SIMULATIONS

Final Report on ONR Contract
C-N00014-92-J-4022(*)
for the period of 9/1/1992 - 11/30/1995

Principal Investigator: A. S. Argon
Quentin Berg Professor of
Mechanical Engineering

Tel: (617) 253-2217
Fax: (617) 258-8742

ONR Program Director: Dr. R. Barsoum
Solid Mechanics Program
ONR Code 1132
800 N. Quincy Street - Balston Tower 1
Arlington, VA 22217-5000

(*) with support from DURIP Program through ARO under Contract DAAH04-93-G-0278 for purchase of computer workstations.

PROJECT SUMMARY

The brittle to ductile transitions of cleavage fracture in technologically important solids such as steel remains inadequately understood. The majority of previous studies of the phenomenon in all but Si have remained of an empirical nature directed toward finding rationale and processing procedures to decrease the brittle to ductile transition temperature to levels lower than what would be encountered during service. While this has been of unquestionable operational value it has resulted in little fundamental understanding of the basic phenomenon on which new developments in processing can be based.

The combination of experimental research carried out in the late 80s in the U.S., in Europe, USSR, and Japan on silicon and the associated mechanistic modeling at the atomic and microstructural levels has led to a new fundamental perspective on fracture transitions. The present ONR program has provided the major momentum for new breakthroughs.

In the following text we summarize the major achievements of this program both at the experimental and the modeling levels.

I. INTRODUCTION

The abrupt fracture transitions in cleavable solids from ductile to brittle (D–B) or from brittle to ductile (B–D) remain of prime technological importance. In engineering practice where reliable service performance in structures (particularly those constructed of steel) requires a certain level of fracture toughness under any adverse condition any abrupt excursion into brittle behavior is unacceptable. Over many decades certain empirical design strategies have evolved based on relatively simple tests of the fracture transition in quasi–static and impact experiments that prescribe safe ranges of service variables such as temperature, loading rate and of microstructure etc. In addition a large number of experimental alloy development studies have explored processing conditions that result in lowering the D–B transition temperature. While these studies and processing developments have been of unquestionable utility, they have shed little light on the fundamental mechanisms or processes that govern the transition, necessary for definitive control of the phenomenon.

From the few comprehensive investigations such as that of Hahn et al (1959) on "E" steel and the several searching experimental studies of Knott and co–workers (see Lin et al, 1987 for example) it has become clear that the D–B transition involves a successful "injection" of a supercritical cleavage microcrack into a receptive environment in which it can continue to propagate by cleavage without becoming re–arrested in a B–D transition (Argon 1987, Jokl et al, 1989). In polycrystalline material the arrest usually occurs at a grain boundary where the mismatch of the cleavage planes between adjacent grains produces the required hesitation to initiate plastic crack tip shielding processes. Continued propagation of the crack in a brittle cleavage–mode requires re–initiating a new microcrack in the next grain or achieve a crack break–through into the next grain onto a cleavage plane. In a single crystal the arrest involves a sequence of crack tip initiated inelastic shielding process. While this scenario has been well recognized, definitive analyses of it are few (see Lin et al, 1987). From these more comprehensive investigations it has become clear that in addition to the basic requirement of cleavability of a material the fundamental ingredient of the fracture transition phenomenon is the B–D transition involving the arrest of a propagating brittle cleavage crack. At a given temperature for a given microstructure, and rate of loading where any and all injected cleavage microcracks can be arrested the material has effectively undergone a transition to ductile behavior.

For this reason, in recent years, fundamental experimental studies have concentrated on processes that govern the B–D transition in either a static stress relaxation mode (George and Michot, 1993) a dynamic mode (Brede and Haasen, 1988, Samuels and Roberts, 1989, Hirsch et al, 1989) or a crack arrest mode (Brede et al, 1991, Hsia and Argon, 1994). These experimental studies have been paralleled by a host of searching theoretical modeling studies of the phenomenon. Below we take account of the most important key developments that has emerged from the research program.

II. REVIEW OF THE BRITTLE TO DUCTILE TRANSITION

A. General Phenomenology

Modern fundamental research on this subject has received its initial stimulus from an important theoretical study of Rice and Thomson (1974) who introduced a fundamental criterion that successfully classified materials as "cleavable" and thus, potentially prone to a fracture transition and "non cleavable" and, therefore, free of this phenomenon. In the former class of materials there exists an energy barrier to dislocation nucleation from the crack tip that is on the verge of propagation, whereas no such barrier exists for the non–cleavable solids, which as a result are intrinsically ductile. The cleavable solids with the energy barriers to nucleation of dislocations can, in principle, also behave in a ductile manner above a so–called brittle to ductile transition temperature T_{BD}, for a given rate of loading, when the thermal energy is sufficient to furnish the required activation to overcome the energy barrier, within the allotted time.

Experimental evidence suggests that in a certain class of cleavable solids the rate controlling process of the B–D transition is indeed simply the nucleation of an embryonic dislocation from the crack tip into a dislocation–free crack tip environment. This class of materials includes the body centered cubic transition metals Fe, Cr, Mo, W, (but not Ta, Nb, and perhaps V), the soft ionic compounds of the NaCl structure, hexagonal close packed metals Zn, Cd, and possibly, in principle all other crystalline solids in which dislocation velocities are strongly stress dependent. Other evidence suggests that in semi–conducting solids such as Si and Ge, with the diamond cubic structure, in most other semi–conducting solids such as GaAs, GaP, GaAsP, etc., in water ice, in most oxides, carbides, all covalent compounds, and perhaps most inter–metallic compounds in which dislocation velocity is very weakly stress dependent, the rate controlling process of the B–D transition should be the rate of motion of the emitted dislocations away from the crack tip. This behavior has been very well established in Si by a series of definitive experiments (St John, 1975, Brede and Haasen 1988, Hirsch et al 1989, George and Michot 1993). The principal differentiating feature of the cleavable solids is a substantial lattice resistance to dislocation motion at low temperatures.

Much evidence points in the direction that those solids in which the rate controlling process of the fracture transitions is the nucleation of an embryonic dislocation from the crack tip, possess ridge–like lattice potentials governing dislocation motion, where a thermally assisted double kink nucleation is the key process and the kink motion along the dislocation line is unhindered. In contrast, the materials in which the rate controlling process of the fracture transition is the rate of motion of dislocations away from the crack tip, are those in which overcoming the lattice potential to dislocation motion requires not only the nucleation of a double kink but also the repeated overcoming of substantial energy barriers to kink motion along the dislocation line.

While the above two alternatives of crack–tip initiated processes are considered fundamental in governing the brittle to ductile transition temperature, T_{BD}, in the test scenario of a dislocation free (or deficient) material, stress induced dislocation rearrangements in the background can provide significant modulations of behavior and can shift the T_{BD} downward as well as softening the transition. This possibility which is not considered intrinsic, since it is subject to elimination by aging effects, has received a large amount of attention ranging from qualitative treatments (Ashby and Embury, 1985, Hirsch et al, 1989) to more quantitative treatments (Suo et al, 1993, Nitzsche and Hsia, 1994) for the quasi–static monotonic loading case, to dynamic studies of shielding of a propagating cleavage crack (Freund and Hutchinson, 1985). This background inelastic polarization effect has not been considered to be of principal concern since it can be rendered ineffective by aging treatments.

B. Models and Simulations

The more recent ground–breaking theoretical developments were initiated by a comprehensive examination of the experimental facts of the B–D transition by Argon (1987) who concluded that the activation configuration governing the transition must be a dislocation of fractional strength, and pointed out that determination of such configurations requires accurate information on the ideal interplanar shear resistance profiles and how such profiles are affected by tension. Since that time Rice (1992) and Rice and co–workers (1992) have demonstrated in 2–D analyses, based on the well known Peierls approach for considering interplanar shear interactions through an elegant conservative tension - shear potential, that for cracks under a mixed mode of loading, the instability in the athermal emission of a line dislocation is reached when the crack front undergoes an inelastic Burgers displacement that forms only half a core of a dislocation. At this stage the energy release rate, G, from the crack tip field reaches a critical value $G_c=\gamma_{us}$, the unstable stacking energy associated with rigidly translating two halves of a crystal, across the slip plane, by half an atomic spacing. While this new insight has produced considerable activity in the determination of this new material parameter by a variety of fundamental methods such as the embedded atom method (Sun et al, 1993), or first principles calculations (Kaxiras and Duesbery, 1993) the required analysis of 3–D activation configurations lagged behind. An interesting but quite approximate analysis of Schöck & Püschl (1991) for saddle–point configurations of emitted dislocations at crack tips under Mode II loading lacked precision for the determination of the T_{BD}. On the other hand a more elegant perturbation analysis of Rice and Beltz (1994), developed around the last stable 2–D equilibrium state of $G\leq\gamma_{us}$, was precise, but gave unsatisfactory results at lower levels of G/γ_{us}, of interest to assess the conditions that govern the T_{BD}. It is important to note that the solution of saddle point configuration problems requires the development of special methodology since they constitute unstable equilibrium states in multi–parameter potential energy spaces. Apart from the quite approximate approach of Schöck and Püschl (1991), referred to above, such methodology in general had not been developed for such problems. Moreover, all the elegant developments of Rice and co–workers remained on slip planes passing through the crack front, while nearly all experimentally observed emission configurations are found to be on oblique slip planes, making an angle with both the plane of the crack and the crack front, as shown in Fig. 1. As pointed

out by Argon (1987) such planes should be preferred for reasons of high peak stress but require specialized considerations of crack tip inelastic response. Methodology to analyse such configurations by known dislocation field solutions near cracks was not available, until the present.

A new variational boundary integral (VBI) technique developed recently by Ortiz and coworkers (see Bower and Ortiz 1990, Xu and Ortiz 1993, Xu, Ortiz and Bower, 1994) for the solution of curved crack front configurations, involved in crack trapping by fibers and propagation of delamination fronts on fibers in composites (Xu, Bower and Ortiz, 1994), offered a new and general methodology for the solution of complex unstable crack front (or planar plastic zone front) problems. This numerical method uses continuous distributions of curved dislocations to represent both the real opening displacements of a crack and the inelastic displacements of planar plastic zones by one and the same continuous methodology. It requires only the statement of the specific combined shear and opening resistances of the crack faces and the planar inelastic zones attached to these cracks, through a tension-shear potential, for analysis of any arbitrary 3–D form. Moreover, the methodology can be applied, by a special procedure of constraints to both stable and unstable configurations permitting the accurate determination of saddle–point configurations and their energies. This VBI methodology was used by us in a definitive and comprehensive manner on most of the possible modes of dislocation nucleation from crack tips. The results are presented in Section III - B below.

Fundamental new developments on the subject of B–D transitions controlled by dislocation mobility away from the crack tip have been fewer than for the problem of crack tip dislocation nucleation discussed above. In Si, where the experiments on the B–D transitions have been most definitive as discussed in the introduction, and where many accurate measurements of the stress dependence of dislocation velocity are available (see Nadgornyi, 1988), there had been little work done on the atomic level mechanisms that govern the very unusual, nearly linear stress dependence of this velocity. In a detailed examination of the core re–arrangements on 30^{o} partial dislocations, involved in kink motion, Bulatov et al (1995) have now established the kinematics and energetics of several rate controlling processes of glide that are directly a consequence of the substantial difficulty of translating kinks along dislocations. These developments are not only important in furnishing a definitive model for dislocation motion in Si, but also for providing the required methodology for a fully atomistic simulation of the dislocation nucleation process from crack tips. Moreover, the methodology for analyzing saddle–point configurations for kink motion should also find direct applicability in the motion of screw dislocations in BCC metals and the details of the embryonic activation configurations of the rate controlling dislocation nucleation at crack tips. Such studies, however, have not been pursued further to maintain the focus on the key process of crack tip phenomena.

In neither the dislocation nucleation process nor the motion of dislocation groups away from the crack tips, has any serious consideration been given to the behavior of the oblique planes on which nearly all the dislocation activity has been observed. Moreover, apart from a relatively simple analysis of Zhou and Thomson (1991) there have been no serious simulations of heterogeneous nucleation of dislocations from crack tips. These have now largely been carried-out by us, and the findings are presented in Section III-B below.

III SIGNIFICANT RESEARCH RESULTS

A. Experimental Research Program

The experimental program has been designed to provide direct support for our theoretical modeling studies. As stated in Section II above, the present material of choice has been dislocation free Si single crystals in which the investigation is based primarily on arresting propagating cleavage cracks in a sample with a temperature gradient.

In the experimental program, large, double cantilever shaped Si single crystal platelets have been used to propagate cleavage cracks on the {110} type cleavage planes, up a temperature gradient, at different imposed velocities, until they became arrested at the appropriate brittle to ductile transition temperature, T_{BD}. In the chosen geometrical setting the crack is propagated in the <110> type direction which probes incipient dislocation activity on two complementary, symmetrically situated *oblique* {111} slip planes, making an angle of 35.4° with the cleavage crack plane and an angle of 54.6° with the crack front or alternatively on two complementary {111} planes normal to the cleavage plane and making an angle of 35.3° with the crack front.

In these experiments the nature of dislocation nucleation and motion that governs the brittle to ductile transitions have been studied in detail and are still being related to the simulations. Such dislocation activity has been monitored by etch pitting and by the Berg–Barrett x–ray topographic imaging technique (see Barrett, 1952). A specific aspect of the simulation is to determine the activation energy of the fundamental arrest process that governs the fracture transition temperature, T_{BD}, and how this relates to the velocity of the cleavage crack that is being arrested.

The preliminary results have been published (see 1-1 in the Appendix). A final manuscript describing the most recent experimental results on crack arrest modes in Si single crystals is in preparation.

B. Simulation of Activation Configurations of Dislocation Loops Emanating from Crack Tips

As discussed in Section II above two types of different crack tip response have been identified. In one class of materials of which Si is an example, the brittle to ductile transition is governed by the mobility of dislocations away from the crack tips. Here, nucleation and motion of kinks on partial dislocations are the rate controlling processes, and the energy barriers to kink motion become of major importance, but ultimately the transition is governed by the sluggish motion of crack tip shielding groups of dislocations. In most body centered cubic transition metals such as, e.g., Fe, Cr, Mo, and W, however, the present evidence indicates that kink mobility on dislocations is not subject to important energy barriers and that in these metals nucleation of a double–kink type embryonic dislocation configuration should be the fundamental process at the crack tip. These two processes are depicted in Figs 2a and 2b. It is assumed that these two variants of the activation process do not only govern the lattice

resistance to dislocation motion but also the resistance to the fundamental brittle to ductile transition in fracture at the tips of cleavage cracks. Accordingly, two separate simulations have been carried out. In the first simulation, discussed below, the actual activation barriers to dislocation nucleation have been investigated by the very versatile VBI method, pioneered by Xu and Ortiz, (1993), which makes use of the Peierls approach to dealing with non–linear dislocation core configuration problems. In this VBI method, continuously distributed packets of dislocations represent both the elastic crack face displacements and the combined inelastic shear and opening mode displacements on the potential slip planes contacting the crack front, subjected to mixed mode loading. A fundamental ingredient describing the inelastic response of the potential slip plane was a conservative tension – shear potential that represents the material response to combined large interplanar shear and opening displacements. Two important modifications were incorporated into the interplanar tension-shear potential consisting of a means of introducing a parameterized skew symmetry to better model differences between covalent solids and close packed metals and an all-important free surface ledge production resistance associated with the first few rows of atoms near a free surface.

With these modifications the VBI method was used to determine the saddle point configurations and their energetics for the three different modes depicted in Fig. 3. These included the modes of nucleation of dislocation embryos on a) inclined planes at arbitrary angles of inclination with the crack plane; b) on specific oblique planes representative of α-Fe; and finally c) on cleavage ledges on the crack front for the most likely geometries appropriate for α-Fe.

Figures 4a-4d show a specific set of activation configurations of dislocation embryos consisting of infinitesinal dislocaton packets nucleated in Mode II loading at systematically decreasing levels if driving force G/G_c where $G_c = \gamma_{us}$ (the unstable stacking energy) is the critical energy release rate for the last athermal configuration where the dislocation can be released from all points of the crack front simultaneously. In the figure the curved fronts represent the level contours of the total integrated elastic crack face displacements (for $x/b \leq 0$) and the inelastic Burgers shear displacements (for $x/b \geq 0$) that make up the extended embryo. Figure 4e gives the resulting dependence of the activation free energy of these embryo configurations on the normalized driving force G/G_c. These early results which do not consider the surface ledge production resistance translate into transition temperatures T_{BD} that are more than a factor 10 too high compared with expectations. When the surface production resistance was included, the energy barriers to embryo formation became unattainably high, leading to the conclusion that this mode, which had been considered by all investigators up to the present, can never be the preferred one.

Since slip activity associated with the fracture transition is very often found to be on oblique planes a proper analysis of dislocation embryo formation on the oblique plane (112) was investigated in α - Fe for a cleavage crack on the (001) plane with the crack front parallel to the [110] direction which is the preferred orientation of cleavage crack in this material. Figures 5a and 5b show respectively a saddle point configuration of a dislocation embryo on the (112)

plane at $G_I/G_c = 1.86$ and the dependence of the saddle point energies on the level of the normalized driving force G_I/G_{Ic}. Since the brittle crack can propagate at $G_I/G_c = 1.0$, it is clear from Figure 5b that the activation energy for this mode of nucleation is also extremely high, pushing the T_{BD} levels to values even higher than what it is for the inclined planes. This is inspite of the fact that the maximum stress at the crack tip is higher than what is encountered in the inclined planes.

Taking a cue from the many experimental observations of George and Michot (1993) that dislocation nucleation along the crack front occurs heterogeneously, at cleavage surface ledges, an analysis of this mode of nucleation was performed for the same (112) slip plane in the form of a cleavage surface ledge at the crack front as depicted in Fig. 3. This mode combines a number of advantages such as formation of a nearly pure screw type embryo, without any surface production along the ledge front and with a uniformly high area - averaged resolved shear stress. the result of the analysis is shown in Figs. 6a-6c, where Figs 6a and 6b show two saddle point configurations for G_{III}/G_{IIId} of 0.75 and 0.5 (with $G_{III} = K^2_{III}/2\mu = (0.35)^2 K_I^2/2\mu$), and Fig. 6c gives the dependence of the saddle point energies for embryo formation on the normalized level of G_{III}/G_{IIIcd} (where $G_{IIIcd} = \gamma_{us} = K^2_{IIIcd}/2\mu = K_{IIIcd} = 0.35K_{IC}$).

Finally, the energetics of the three different modes of nucleation: on the inclined planes; on the oblique planes; and on the cleavage surface ledges are compared in Fig. 7, where they are all referred to the normalized crack driving force of G_{ICd}/G_{IC}. Clearly, it is only the heterogeneous nucleation mode on the cleavage surface ledges that has the appropriate levels of saddle point energy that can be attained at reasonable temperatures. Indeed, an analysis for typical conditions for α-Fe indicates that in this mode of nucleation the brittle to ductile transition temperature should be around room temperature.

The results of these simulations have been published in various forms. (See 1-2, 1-3, and 1-5, 1-6, 1-7 in the Appendix)

C. Simulation of Kink Motions on Partial Dislocations in Silicon

Until the present time direct atomistic simulations of dislocation motion in Si were too difficult, and the computational costs involved were too high. Attempts utilizing molecular dynamics were found to be neither effective (energy barriers are too high) nor informative (difficult to capture saddle–point configurations among the partially directed random atomic motions). In the course of the present research we have developed new and very effective numerical methods that have made it feasible to study the relevant atomic level saddle–point mechanisms by static computations of the constrained unstable equilibrium configurations. In the present research a very large collection of

important component atomic mechanisms have been identified, involving not only kinks and their motion, but also their interaction with anti–phase defects, arising from dislocation core reconstruction phenomena, and other transitory atom complexes. An exciting aspect of these developments (Bulatov, et al, 1995) is that they can be verified or even tested, in principle, by pulsed internal friction experiments of the type that have been carried out by the Russian group of Nikitenko and Farber (1989), with whom some contact for a possible collaboration has been investigated but was found to be too cumbersome to pursue further.

These computations which presently utilize well chosen pair potentials of the Stillinger–Webber type, or hybrid potentials that have been development by Kaxiras, (1994) are quite computer intensive. For this reason we sought and have received support from the DURIP program through ARO to purchase computer hardware. This equipment in the form of two advanced work stations has been in place since Sept. 1994.

IV PUBLICATIONS

Copies of all publications that have resulted from this research program are attached in the Appendix.

References

Argon, A.S., (1987), Acta Metall., 35, 185.

Ashby, M.F., and Embury, (1985), Scripta Metall., 19, 557.

Barrett, C.S., (1952) "Structure of Metals", (Second edition), McGraw–Hill: New York

Bower, A.F., and Ortiz, M. (1990), J Mech. Phys. Solids, 38, 443.

Brede, M., and Haasen, P., (1988), Acta Metall., 36, 2003.

Brede, M., Hsia, K.J., and Argon, A.S., (1991), J. Appl. Phys., 70, 661.

Bulatov, V.V., Yip, S., and Argon, A.S., (1995), Phil. Mag., 72, 453.

Freund, L.B., and Hutchinson, J.W., (1985), J. Mech. Phys. Solids, 33, 169.

George, A., and Michot, G., (1993), Mater. Sci. Engng., A164, 118.

Hahn, G.T., Averbach, B.L., Owen, W.S., and Cohen, M., (1959) in "Fracture", edited by Averbach, B.L., Felbeck, D.K., Hahn, G.T., and Thomas, D.A., MIT Press: Cambridge, MA p.91.

Hirsch, P.B., Roberts, S.G., Samuels, J., and Warren, P.D., (1989), in "Advances in Fracture Research", edited by Salama, K., Ravi–Chandar, K., Taplin, D.M.R., and Rama Rao, P., Pengamon Press, Oxford Vol 1, p. 139.

Hsia, K.J., and Argon, A.S., (1994), Mater. Sci. Engng., A176, 111.

Jokl, M.L., Vitek, V., McMahon, C.J., and Burgers P., (1989), Acta Metall., 37, 87.

Kaxiras, E., (1994), private communication.

Kaxiras, E., and Duesbery M.S., (1993), Phys. Rev., Lett., 70, 3752.

Lin, T., Evans, A.G., and Ritchie, R.O., (1987), Met. Trans., 18A., 641.

Nadgornyi, E., (1988), "Progress in Materials Science" edited by Christian, J–W., Haasen, P., and Massalski, T.B., Pergamon: Oxford, vol. 31.

Nikitenko, V.I., and Farber, B. Ya, (1989) in "Structure and Properties of Dislocations in Semi–Conductors – 1989", edited by Roberts S.G., Holt, D.B., and Wilshaw, P.R., The Institute of Physics, Bristol, England (Series no 104), p. 257.

Nitzsche, V.R., and Hsia, K.J., (1994), Mater. Sci. Engng., A176, 155.

Rice, J.R., (1992), J. Mech. Phys. Solids., 40, 235.

Rice, J.R., and Thomson, R., (1994), Phil. Mag., 29, 73.

Rice, J.R., Beltz, G.E., and Sun. Y., (1992), in "Topics in Fracture and Fatigue", edited by Argon, A.S., Springer: New York, p. 1.

Rice, J.R., and Beltz, G.E., (1994), J. Mech. Phys. Solids., 42, 333.

Samuels, J., and Roberts, S.G., (1989), Proc. Roy. Soc., A421, 1.

Schöck, G., and Püschl, W., (1991), Phil. Mag., A64, 931.

Sun, Y., Beltz, G.E., and Rice, J.R., (1993), Mater. Sci. Engng., A170, 67

St John, C., (1975), Phil. Mag., 32, 1193.

Suo, Z., Shih, C.F., and Varias, A.G., (1993), Acta Metall. Mater., 41, 1551

Xu, G., and Ortiz, M., (1993), J. Num. Methods Engng., 36, 3675.

Xu, G., Argon, A.S., and Ortiz, M., (1995), Phil. Mag.,.72,415.

Xu, G., Argon, A.S., and Ortiz, M., (1996), Phil. Mag., submitted for publication.

Xu, G., Bower, A.F., and Ortiz, M, to be published.

Zhou, S.J., and Thomson, R., (1991), J. Mater. Res. 6, 639.

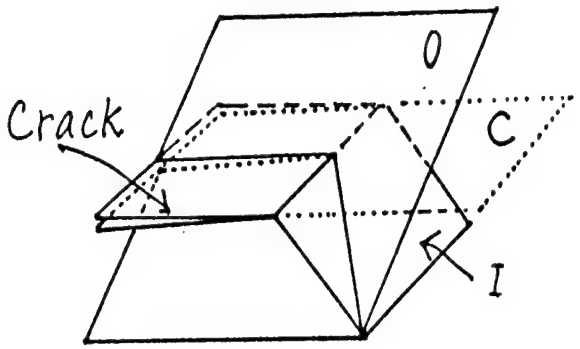

Figure 1 Cleavage crack;
inclined (I), oblique (o)
slip planes

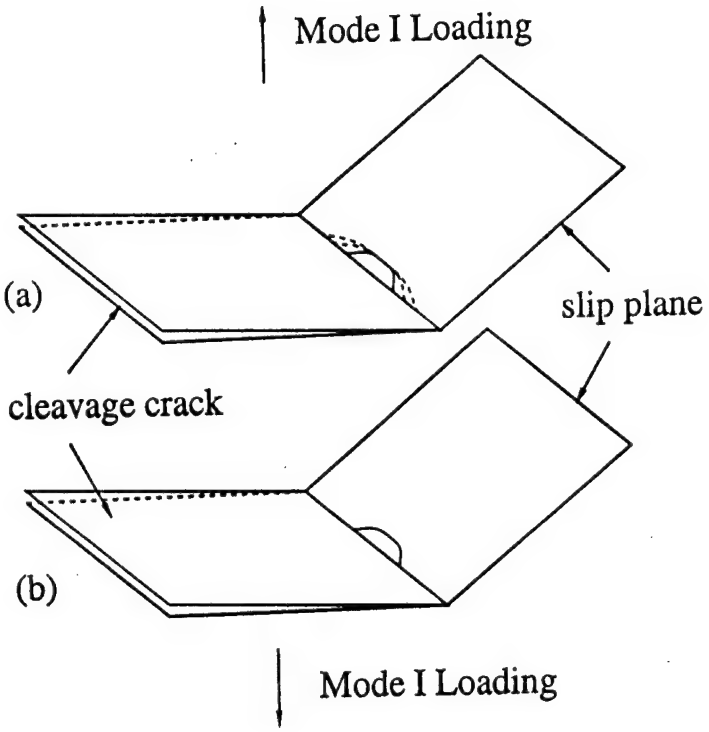

Figure 2

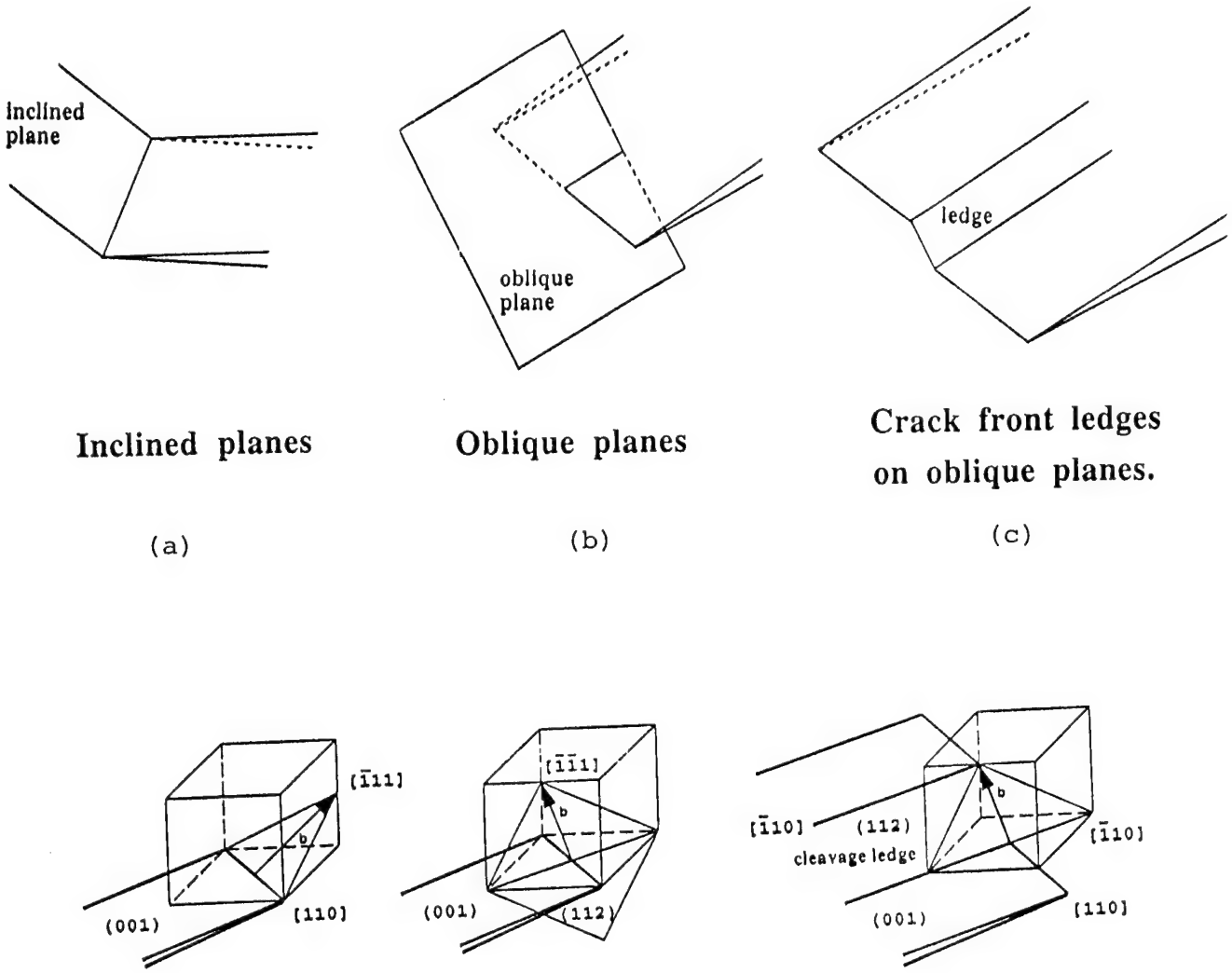

Fig. 3. Three different modes of dislocation nucleation from a crack tip considered in simulations: (a) on inclined planes; (b) on oblique planes; (c) on crack front cleavage ledges. Top figures are generic, bottom figures represent specific geometries applicable to alpha iron

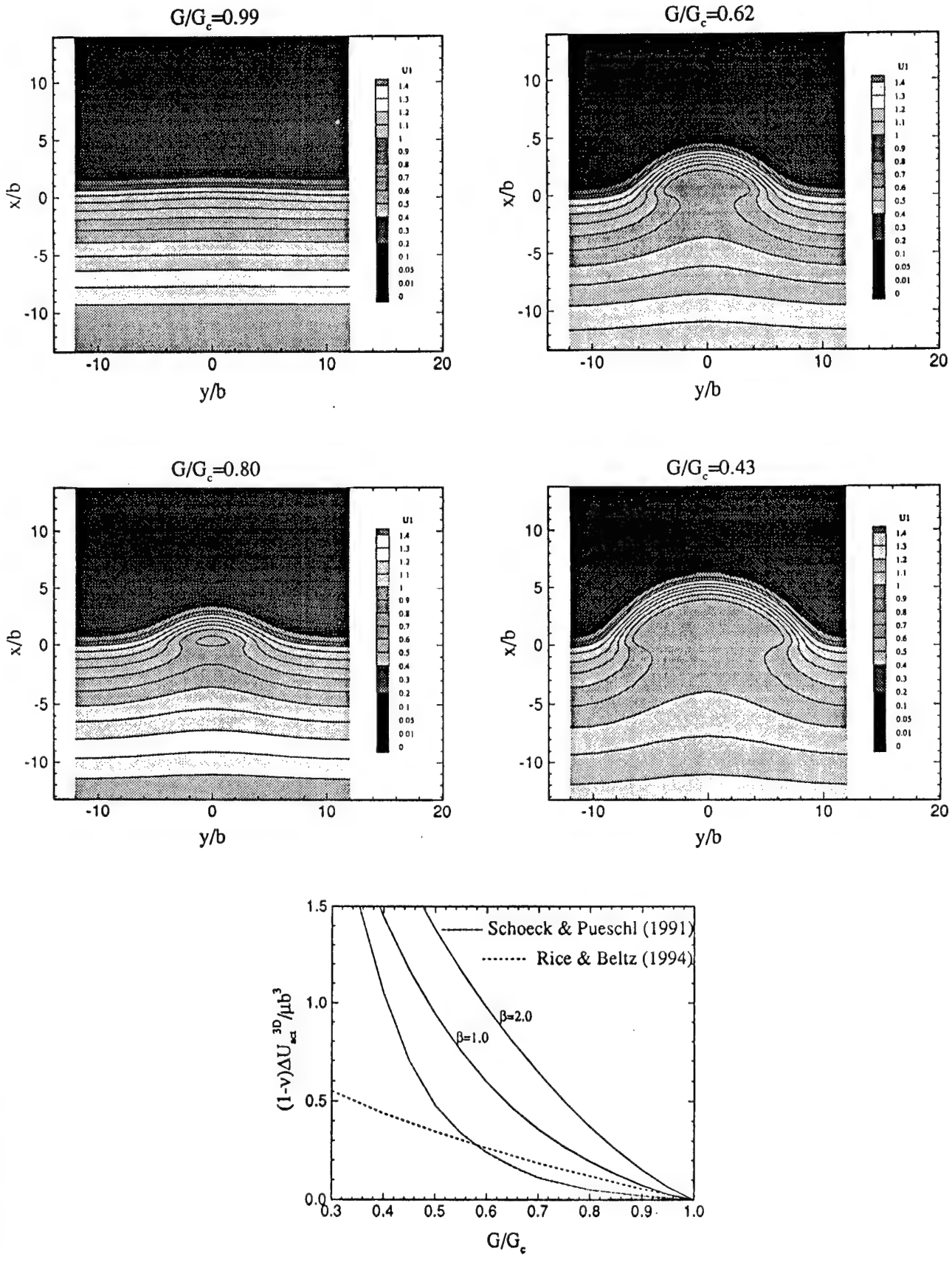

Fig. 4 Saddle point activation configurations of a dislocation embryo of continuously distributed infinitesimal dislocations at four levels of driving force under Mode II loading (a-d); resulting dependence of activation energies on normalized driving force.

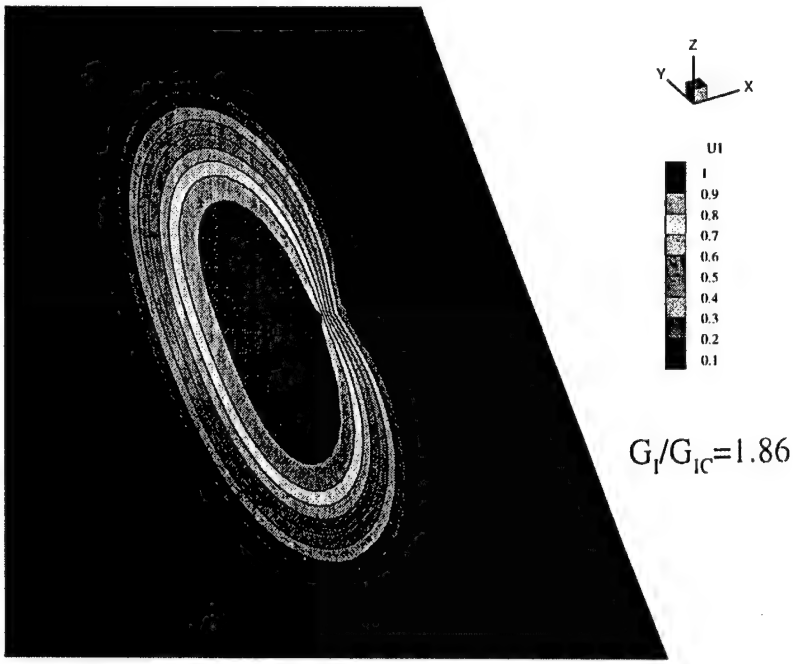

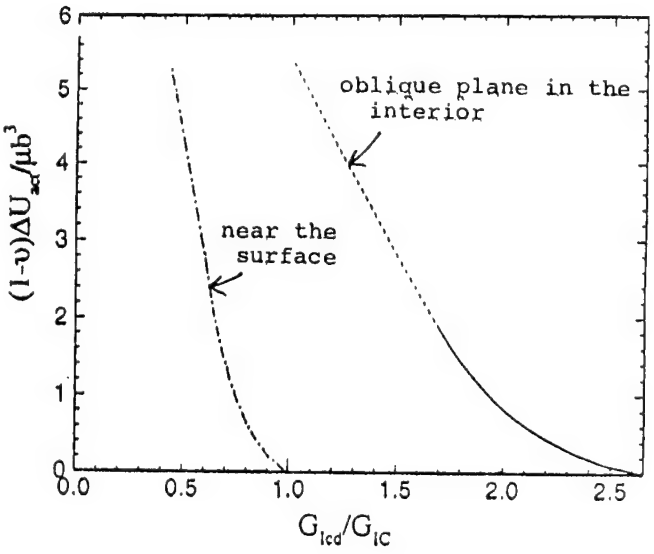

Fig. 5 Dislocation embryo formation on the oblique plane (112) in alpha iron for a cleavage crack on (001) with front parallel to the [110] direction: (a) typical saddle point configuration; (b) dependence of activation energy on normalized crack driving force.

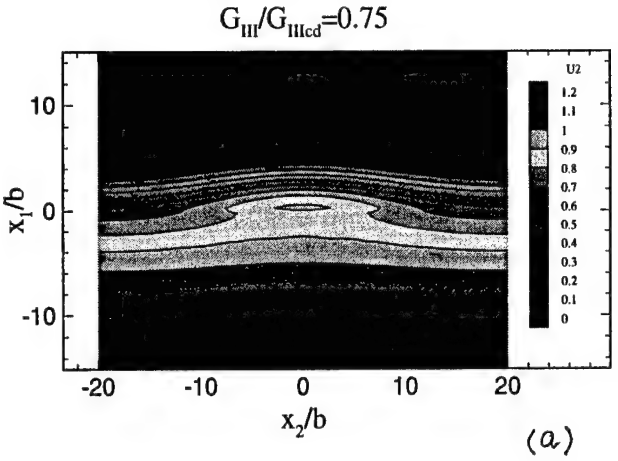

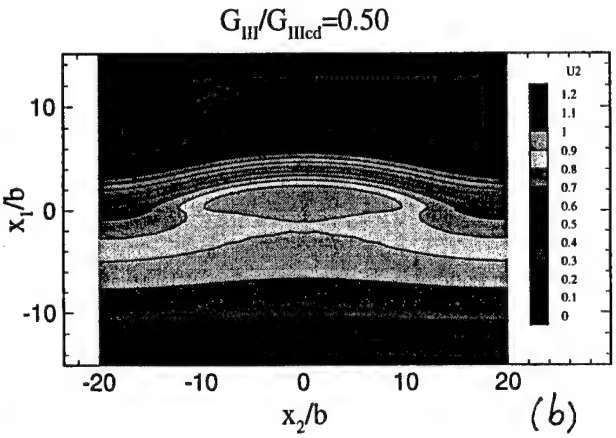

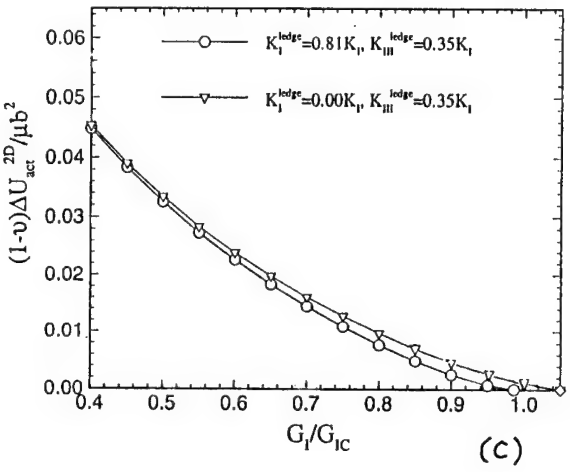

Fig. 6 Dislocation embryo formation on a crack front cleavage ledge containing an oblique (112) plane, under combined Mode III and Mode I: (a) embryo configuration under a normalized driving force 0.75; (b) under a lower driving force of 0.5.

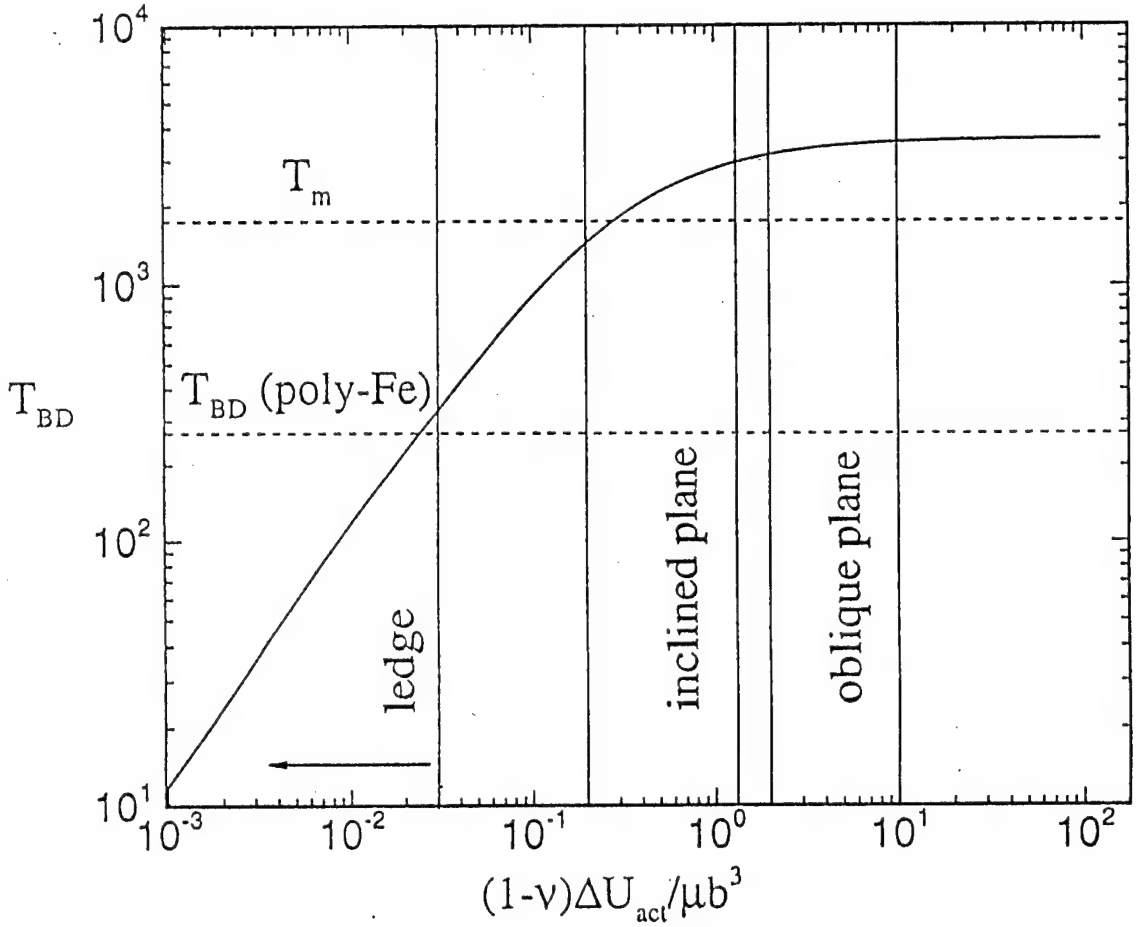

Fig. 7 Estimated B-D transition temperatures for α-iron based on a nucleation based crack arrest scenario involving the various modes of arrest considered in the simulations, compared with the experimental B-D transition temperature.

APPENDIX

Journal and Conference Papers Published
during the reported Research Period

REPORT DOCUMENTATION PAGE

Form Approved
OMB No. 0704-0188

1. AGENCY USE ONLY (Leave blank)	2. REPORT DATE	3. REPORT TYPE AND DATES COVERED
	May 22, 1997	Final: 9/1/1992-11/30/1995

4. TITLE AND SUBTITLE
Experimental Study of the Mechanics of Brittle-to-Ductile Transitions of Cleavage Fracture in Si Single Crystals

5. FUNDING NUMBERS
C-N00014-92-J-4022

6. AUTHOR(S)
K.J. Hsia and A.S. Argon

7. PERFORMING ORGANIZATION NAME(S) AND ADDRESS(ES)
Massachusetts Institute of Technology
Room 1-306
Cambridge, MA 02139
(A.S. Argon)

8. PERFORMING ORGANIZATION REPORT NUMBER
1-1

9. SPONSORING/MONITORING AGENCY NAME(S) AND ADDRESS(ES)
ONR Solid Mechanics Program (Attn: Dr. R. Barsoum)
ONR Code 1132
800 N. Quincy Street-Ballston Tower 1
Arlington, VA 22217-5000

10. SPONSORING/MONITORING AGENCY REPORT NUMBER

11. SUPPLEMENTARY NOTES
Paper published in "Materials Science and Engineering", A176, 111-119 (1994) (Reprints attached)

12a. DISTRIBUTION/AVAILABILITY STATEMENT
Unlimited

12b. DISTRIBUTION CODE

13. ABSTRACT *(Maximum 200 words)*

The micromechanisms of brittle-to-ductile transition (BDT) of cleavage fracture in Si single crystals have been investigated using a recently developed novel experimental technique. The crack arrest tests were performed by propagating a cleavage crack with a quasi-steady state velocity against a temperature gradient. Constant K specimens with cracks on {111} and {110} cleavage planes were used. A laser imaging technique was used to measure the crack velocity. The crack arrest temperature {BDT temperature} was determined as a function of crack velocity. An etch-pitting technique was used to study the dislocation structure at or near the crack arrest front. The results indicate that high dislocation mobility and a high dislocation density are needed to arrest a running cleavage crack. Preliminary evidence has confirmed that for Si crystals, the rate-limiting mechanisms for the BDT is dislocation motion rather than dislocation nucleation.

14. SUBJECT TERMS
Experimental study of fracture transitions brittle fracture; ductile behavior; Si single crystal

15. NUMBER OF PAGES
18

16. PRICE CODE

17. SECURITY CLASSIFICATION OF REPORT	18. SECURITY CLASSIFICATION OF THIS PAGE	19. SECURITY CLASSIFICATION OF ABSTRACT	20. LIMITATION OF ABSTRACT
Unclassified	Unclassified	Unclassified	None

Materials Science and Engineering, A176 (1994) 111–119

Experimental study of the mechanisms of brittle-to-ductile transition of cleavage fracture in Si single crystals

K. J. Hsia
University of Illinois at Urbana-Champaign, Urbana, IL 61801 (USA)
A. S. Argon
Massachusetts Institute of Technology, Cambridge, MA 02139 (USA)

Abstract

The micromechanisms of brittle-to-ductile transition (BDT) of cleavage fracture in Si single crystals have been investigated using a recently developed novel experimental technique. The crack arrest tests were performed by propagating a cleavage crack with a quasi-steady state velocity against a temperature gradient. Constant K specimens with cracks on {111} and {110} cleavage planes were used. A laser imaging technique was used to measure the crack velocity. The crack arrest temperature (BDT temperature) was determined as a function of crack velocity. An etch-pitting technique was used to study the dislocation structure at or near the crack arrest front. The results indicate that high dislocation mobility and a high dislocation density are needed to arrest a running cleavage crack. Preliminary evidence has confirmed that for Si crystals, the rate-limiting mechanism for the BDT is dislocation motion rather than dislocation nucleation.

1. Introduction

The phenomenon of brittle-to-ductile transition (BDT) in cleavage fracture has been studied by many researchers for decades, but the fundamental mechanisms during the BDT have been investigated only recently. Recent theoretical developments have indicated that the fundamental phenomenon of BDT is governed at the tips of propagating cleavage cracks by basic atomistic processes. Two distinct processes, brittle fracture by breaking bonds between atoms along cleavage planes and ductile behaviour by generating dislocations in slip planes, compete against each other at propagating crack tips. While the cleavage fracture process is fairly well understood by means of an energetic consideration, dislocation generation and its effects on a propagating cleavage crack are not yet fully understood mechanistically.

Dislocation generation at crack tips involves two successive stages: *dislocation nucleation* at or near the crack tip and *dislocation motion* away from the crack tip region. Two different groups of intrinsically brittle materials exist: the ones in which dislocation mobility is relatively high compared to the barrier to dislocation nucleation, and the ones in which dislocation nucleation is relatively easy but mobility is low. In the former group the rate-limiting phenomenon which determines the BDT is the competition between dislocation nucleation and cleavage crack propagation, whereas in the latter it is the competition between dislocation motion induced crack tip shielding or blunting and cleavage fracture. It is expected that the BDT behaviour of these two groups of materials have different characteristics.

In a pioneering attempt to model the competition between cleavage crack growth and dislocation emission from the crack tip, Rice and Thomson [1] performed an activation analysis in which the total energy change due to the formation of a dislocation half loop at the crack tip was calculated as a function of loop radius and dislocation core cut-off radius. In their analysis, a linear elastic crack tip stress field was used, and the materials were assumed to behave as a continuum up to the crack tip. Their model was very successful in distinguishing intrinsically brittle from intrinsically ductile materials, but the predicted critical activation energies for the intrinsically brittle materials to initiate plastic deformation were one or more orders of magnitude too high than that achievable by thermal activation. Argon [2] pointed out that the linear elastic solution was no longer applicable in the region very close to the crack tip where a dislocation loop was formed. A Peierls [3] type periodic resistance to the dislocation emission must then be used in a more accurate analysis. Cheung *et al.* [4] used a molecular dynamics approach to determine the non-linear crack tip field, and with this and several other stress field coupling effects, they reduced the critical activation energy for

0921-5093/94/$7.00
SSDI 0921-5093(93)02552-E

α-iron by a factor of 15. Since their analysis did not use a Peierls-type core description and because of the unrealistic orientation of their model, the predicted energy barrier for dislocation emission was still about one order of magnitude too high. The two biggest uncertainties in these models have been the dislocation core cut-off radius and the absence of stress relaxation accompanying dislocation emission. Recently, Rice [5] developed a model which took into account the non-linear interaction of atoms at the core based on the Peierls model. This model avoids the ambiguity of core cut-off radius, and identifies the saddle point instability configuration as a partially nucleated dislocation and calculates its energy barrier per unit length exactly. However, the model only considers the case where the crack front and slip plane are coincident. Later, the model was extended to consider the cases where the crack front is not coincident with slip plane but still passes through it, and the effect of tension across the slip plane [6].

The above models are applicable to the material systems in which dislocation nucleation is the rate-controlling mechanism for the BDT. Except for the earlier and more approximate model by Argon [2], none of these more recent models is capable of predicting the BDT temperature for different crack velocities or different strain rates.

The BDT due to dislocation motion induced crack tip shielding and blunting has also been studied by a number of researchers. Ashby and Embury [7] developed a model based on polarization of existing background dislocations adjacent to a crack tip, and discussed the effect of crack tip dislocation density on the BDT. Argon [2] considered a steady state propagating crack which drags a plume of dislocations with it. By taking into account the shielding effects, he obtained a relationship of the BDT temperature as a function of crack velocity. Hirsch *et al.* [8], on the other hand, pointed out the importance of the local inhomogeneity of both the shielding process and the brittle cleavage reinitiation process, and developed an approximate model based on shielding the critical portions of the crack front. For a stationary crack under different loading rates, their model was capable of predicting the BDT temperature in Si single crystals. Most recently, Brede [9] provided an elegant model for the BDT in which the crack tip shielding by dynamic reverse pile-ups along two specific slip planes in Si single crystals is considered. While still quite approximate, this model has captured most of the phenomena in the BDT in Si.

Many experimental observations strongly support the theory that competition between dislocation generation and cleavage fracture at or near the crack tip determines the BDT [10–17]. A large amount of experimental effort has been expended to study the BDT in Si single crystals because of the availability of well characterized dislocation-free Si crystals with known dopant levels, and the sharp transition temperature exhibited in this material. St John [10] first studied the crack tip dislocation activities by testing a tapered double cantilever beam specimen at different temperatures, and observed a rapid increase of dislocation activity near or at the transition temperature. Brede and Haasen [13] and Michot [12] conducted similar experiments on Si single crystals with different impurity (doping) concentration, and demonstrated the connection between the BDT temperature and dislocation mobility as a function of loading rate. Samuels and Roberts [14] used a four-point bending specimen and observed that dislocation activities occurred at only a few preferred sites along the crack. *In situ* TEM experiments of Chiao and Clarke [15] on Si and of Dewald *et al.* [16] on GaAs and MgO clearly showed dislocation emission and dislocation loop expansion processes from a sharp crack tip. These experiments have demonstrated that the dislocation emission process is favoured at only a few "catalytic" sites along the crack front where secondary perturbations exist.

The question still remains whether the BDT is controlled by dislocation nucleation or by dislocation motion for a specific material. The effects of crack velocity or strain rate on the BDT are not well understood either. To answer these questions, definitive experimental information is needed. In this paper, we shall first briefly describe an experimental technique developed by Brede *et al.* [17] and modified by us, and then present preliminary results of our experiments in Si single crystals.

2. Experimental procedure

Since the cleavage fracture process is nearly temperature-independent, whereas the dislocation generation from a crack tip is strongly temperature-dependent, a definitive way to study the mechanisms of the BDT is to maintain a strong temperature gradient on a sample of cleavable material, and to propagate a cleavage crack with steady state velocity from the low-temperature, brittle side towards the high-temperature, ductile side. The crack arrest temperature (the BDT temperature) can then be measured as a function of crack velocity. This experiment not only provides accurate information on the BDT temperature for different crack velocities, but also permits the determination of the rate-limiting mechanism through studying the dislocation structures on fracture surfaces.

For Si single crystals, some experimental evidence that the BDT is controlled by dislocation motion have been provided by Brede and Haasen [13] and by Samuels and Roberts [14]. They observed separately that near the BDT temperature, dislocations can nucleate from crack tips at a stress intensity substantially lower than the critical stress intensity for cleavage fracture. Yet cleavage fracture could occur when the applied loading rate is high. The deficiency of their experimental technique is the static nature of the test. Their samples are always loaded from a stationary position in a uniform temperature environment so that during loading, the crack tip experiences a full range of stress intensity from zero to the critical level. Because of this, at around the transition temperature, their crack tip may no longer be sharp or predictably shielded as the critical stress intensity is approached due to dislocation activities at lower stress intensity levels. Moreover, at different loading rate, the crack tip conditions near the BDT may not be the same, making it difficult to single out the most important mechanism which controls the BDT.

In the current experiments, tests are conducted with a cleavage crack propagating with a controlled steady state speed against a temperature gradient. The initiation of crack propagation from the low-temperature side guarantees the initial brittle mode of fracture and a sharp initial crack tip. The steady state growth of the crack ensures that the crack tip stress intensity is kept constant at the critical stress intensity, and the crack face profile remains unchanged (presumably the crack tip is still sharp) during the course of cleavage crack growth until the BDT occurs. This technique avoids many ambiguities concerning the conditions under which the BDT occurs, and concentrates on the most important mechanism for the BDT, *i.e.* the competition between cleavage fracture and dislocation activities at a sharp crack tip.

2.1. Experimental setup

The experimental technique, first developed by Brede *et al.* [17], was further modified by us. The basic setup is shown in Fig. 1. The fracture specimen is put in a vacuum chamber mounted on an Instron loading frame. The sample is heated from one side and cooled from the other to achieve the required temperature gradient. Thermocouples are attached on the sample surface to measure the temperature distribution. The sample is loaded with a constant displacement rate at the loading pins so that ideally a steady state and controlled crack velocity could be obtained in constant K samples. Different crack velocities can be achieved by applying different loading rates.

A laser imaging technique has been adopted to measure the crack velocity. The optical system used in

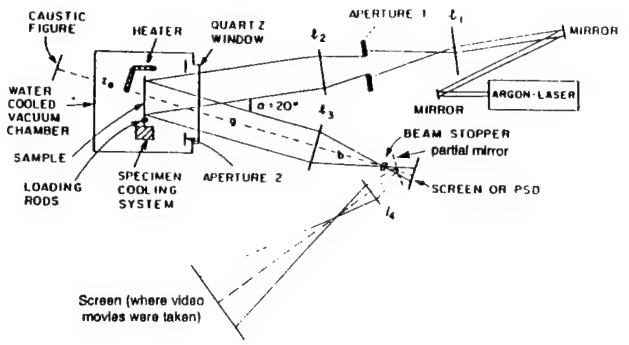

Fig. 1. Experimental setup of the loading system and crack velocity measuring system.

the tests is shown in Fig. 1. The laser beam from an argon ion laser is collimated by lenses l_1 and l_2, and reflected by the optically polished sample surface. A real image of the crack is formed on the screen behind the lens l_3 on the image plane of the sample surface. To obtain a dark field image (bright crack image on a dark background), a beam stopper is placed at the focal point of l_3 so that the reflected parallel light from the sample surface is completely blocked, and only the scattered light from the crack edges is allowed to pass the stopper and form a bright image. Typical images of the crack are shown in Figs. 2(a) and 2(b) which were taken by an EktaPro high-speed video camera with a speed of 1000 frames per second. The image of the sharp crack (nearly atomically sharp before the load is applied) is shown on the left of the picture as a short bright line. The somewhat bright region in the middle of the picture and the two parallel lines are the scattered light from the window edge, and thus irrelevant to the test results. Figure 2(b) shows the image of the same crack in Fig. 2(a) as it is propagating under the applied load. The current time is shown near the upper-left corner as 0.362 s after the test was started.

A position-sensitive detector (PSD), which converts the optical crack length information into voltage signals, was used to measure the crack length in real time. The data were then recorded by a storage oscilloscope and processed with a PC. The PSD was calibrated by the high-speed video camera. The calibration result is shown in Fig. 3 where the measurements of crack length as a function of time from the PSD and the high-speed video camera are presented. Although a low level of noise and some distortion of results from the measurements by the PSD were observed, the overall performance of the PSD was satisfactory. Therefore, the PSD was used throughout the rest of the experiments, particularly for monitoring the high-speed cracks.

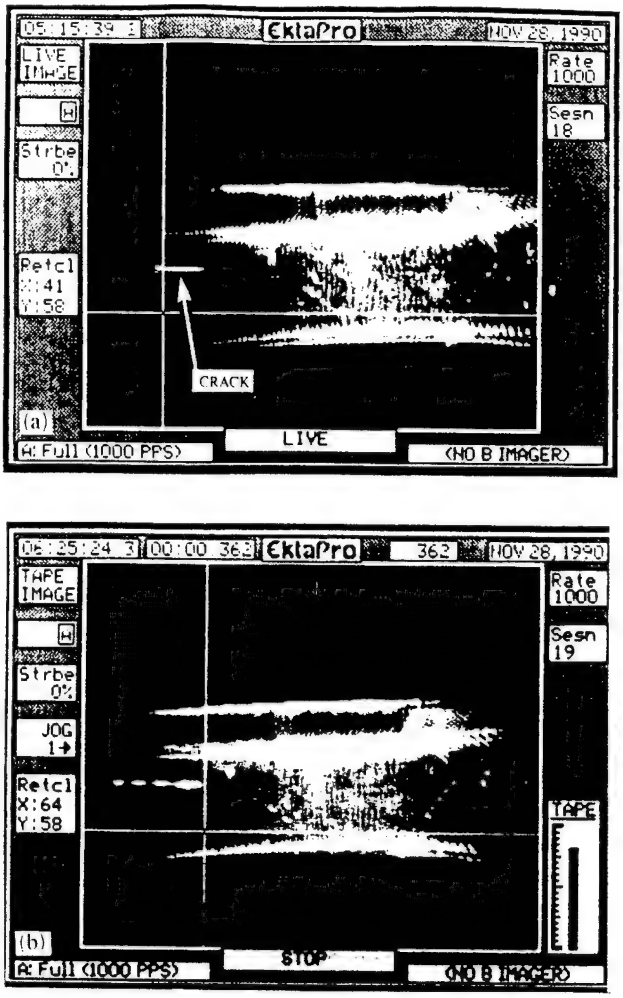

Fig. 2. High-speed video pictures of the dark field image of the sharp cracks: (a) before load is applied; (b) during loading, after a certain amount of crack propagation.

2.2. Material studied and sample preparation

The material used in this study was Si single crystals, although the technique could have been developed on other materials as well. Si was chosen to be studied first because it has been studied extensively in the past, and excellent information exists about its properties; moreover, it exhibits a very sharp BDT phenomenon. Most of the samples were cut from a heavily doped n-type crystal by electric discharge machining (EDM). A few samples were cut from a heavily doped p-type crystal. Heavily doped crystals were used because of the conductivity requirement for EDM machining. Two different sample orientations were tested: one with {111} crack plane and ⟨110⟩ crack growth direction, and the other with {110} crack plane and ⟨110⟩ crack growth direction. It is known that {111} planes in Si are primary cleavage planes whereas {110} planes are secondary cleavage planes. But low-temperature fracture tests revealed that the fracture surfaces of {110} oriented samples are much smoother than those of {111} orientation. Thus, the experimentally measured values of fracture toughness for these two orientations are very close, with the {110} orientation having even a somewhat lower toughness [12].

To achieve well controlled cleavage crack growth, constant stress intensity samples shown in Fig. 4 were used [18]. An atomically sharp pre-crack was generated in each specimen by pushing a tungsten-carbide wedge very slowly into the slot to open up the crack. Strengtheners (strips of Si) were glued on both sides of the specimen to prevent the crack from running all the way through the specimen, and to control the pre-crack length. Examination of the fracture surfaces after the tests revealed that very consistent pre-cracks are produced by this crack initiation technique.

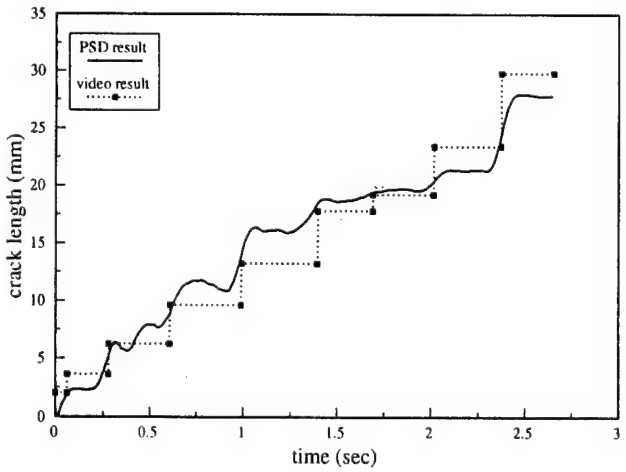

Fig. 3. Crack propagation result obtained with both the PSD and high-speed video for an uncoated specimen at room temperature.

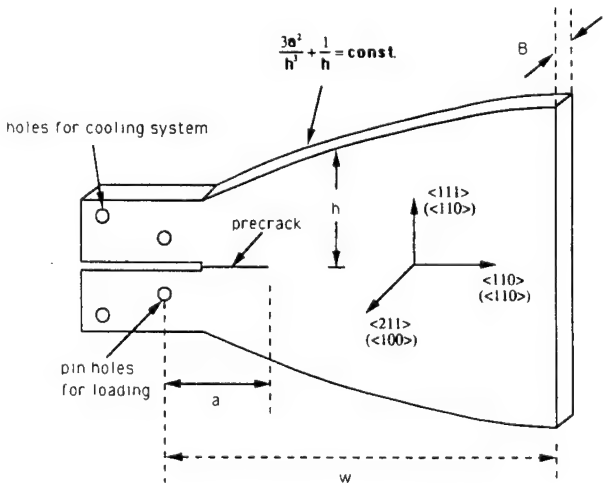

Fig. 4. Geometry of constant K specimens.

A serious problem encountered in experiments was that the cleavage cracks would not grow with a steady state velocity, but in a jerky manner (*i.e.* alternative jumps and stops). Figure 3 shows a typical room temperature test result in which repeated crack jumps are observed until the final unstable crack growth breaks the specimen apart. This behaviour is believed to be associated with the slight excess of the crack initiation fracture toughness over the crack growth fracture toughness. It will be shown later that the crack velocity is far below the elastic wave velocity in the material, and thus no dynamic effect should be present. This jerky behaviour could not be overcome by changing loading conditions or specimen geometry, and required the introduction of a parallel means of damping the oscillations.

To eliminate the crack jumps, such damping was introduced by coating a thin film of ductile metal on the sample surface. On both sides of the specimen, an Si_3N_4 film of 100 nm thickness was first coated to serve as a diffusion barrier between the Si and the metal thin film (otherwise the interdiffusion at elevated temperatures would change the microstructure of the metal thin film and adversely affect the reflectivity of the surface [19]). A 15 nm layer of Ti and a 1 μm thickness of Pt were then subsequently coated to provide the required damping. This technique has proven to be very effective in stabilizing the crack velocity. Figure 5 shows the crack propagation result, obtained by two independent data acquisition systems—the PSD and video camera, of a coated specimen loaded at room temperature. Compared with the behaviour of the uncoated specimen in Fig. 3, the crack propagation velocity in a coated specimen is substantially stabilized, although slight fluctuations are still present. The crack velocity as a function of time, shown in Fig. 6, was obtained by differentiation of Fig. 5. It is clear that a relatively steady state crack propagation can be achieved.

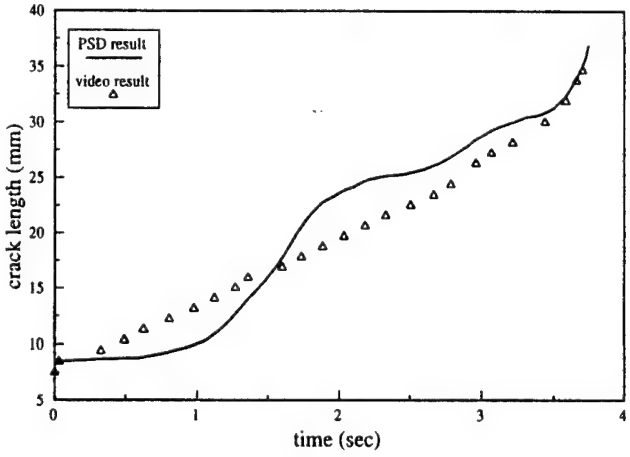

Fig. 5. Crack propagation result at room temperature for a coated specimen.

3. Experimental results

The experimental result of a typical crack arrest test at elevated temperatures with a temperature gradient is shown in Fig. 7. In processing the data acquired by the PSD, a proper smoothing algorithm was employed to filter out undesirable noise. Figure 7 shows the crack length as a function of time. Initially, the crack was stationary. Upon loading with a constant displacement rate at the loading pins, the crack started to propagate in the low-temperature region, until the crack tip reached the critical temperature and was arrested. In this specific test, the loading was continued after the crack was arrested, but the crack stayed at the arrest

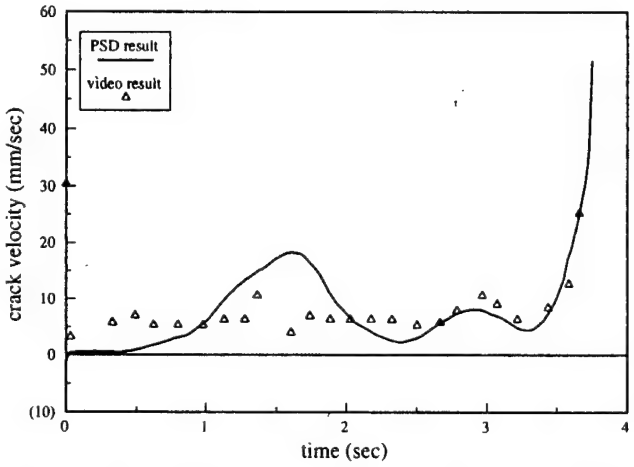

Fig. 6. Crack velocity as a function of time for a coated specimen.

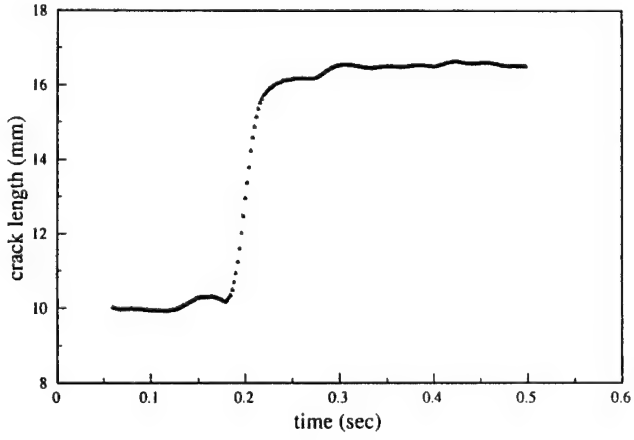

Fig. 7. Crack arrest test result at elevated temperature.

location for a while and underwent blunting. Eventually, upon continued loading, crack propagation re-initiated, and an unstable cleavage fracture occurred which broke the sample. The data for the final fast fracture is not shown on the plot. It can be seen that although the loading continued, the crack stayed at the arrest location for a substantially long time resulting in a significant elevation of K_{IC} for a re-start. The whole process can in fact be viewed as first a transition from the brittle, cleavage fracture mode to the ductile mode, and then a change of fracture mode from ductile blunting to re-initiation of an unstable cleavage fracture. The main interest of the present work is the first transition. The implications of these two changes of mode will be discussed later.

By differentiation, the crack velocity can be obtained as a function of time or crack length. Since there is a one-to-one correspondence between temperature and the crack tip location, a relation between crack velocity and temperature can be obtained. The result is plotted in Fig. 8, which shows that the cleavage crack first accelerated at a temperature level below the BDT, and then decelerated until the crack tip reached the temperature of 900 K, where it completely stalled (zero velocity). This temperature was thus taken to be the BDT temperature for this specific crack velocity. It is noted that if the crack arrest were caused purely by plastic flow induced crack tip shielding, the velocity drop should have been more steep. Therefore, the deceleration of the crack could be due partly to the decrease of crack tip driving force caused by crack acceleration, and partly to the nucleation of a few sluggish dislocations for which some experimental evidence will be shown shortly. Nevertheless, the final arrest of the crack must be caused by generation of extensive plastic flow. It should also be noted that the peak crack velocity is less than 0.25 m s^{-1}. The Rayleigh wave velocity in Si is 5.84 km s^{-1}. Thus, this crack velocity is far below the range where dynamic effects could be important.

To visualize the dislocation activities at the crack tip around the crack arrest location, the fracture surface was etched with Sirtl etchant and examined by means of light optical microscopy and scanning electron microscopy (SEM).

Figure 9(a) shows an SEM picture of an etched {110} fracture surface around the crack arrest location. This picture corresponds to the test results shown in Figs. 7 and 8. The diamond-shaped dislocation etch pits on the {110} cleavage plane are clearly seen. The loading was continued after the crack was arrested until a final unstable fracture occurred. A distinct crack arrest front is clearly shown. On one side of the front is

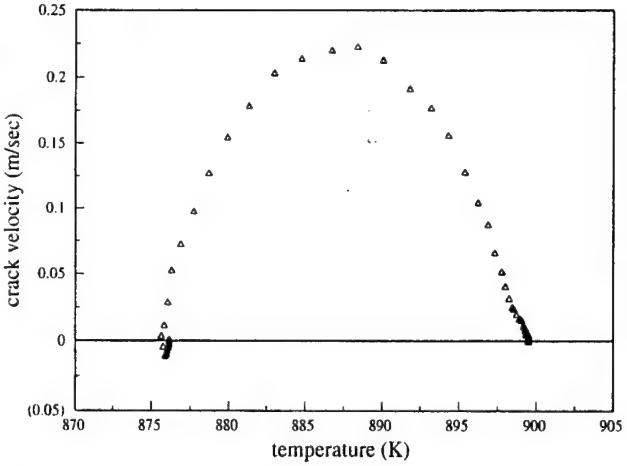

Fig. 8. Crack velocity as a function of temperature for the crack arrest test in Fig. 7.

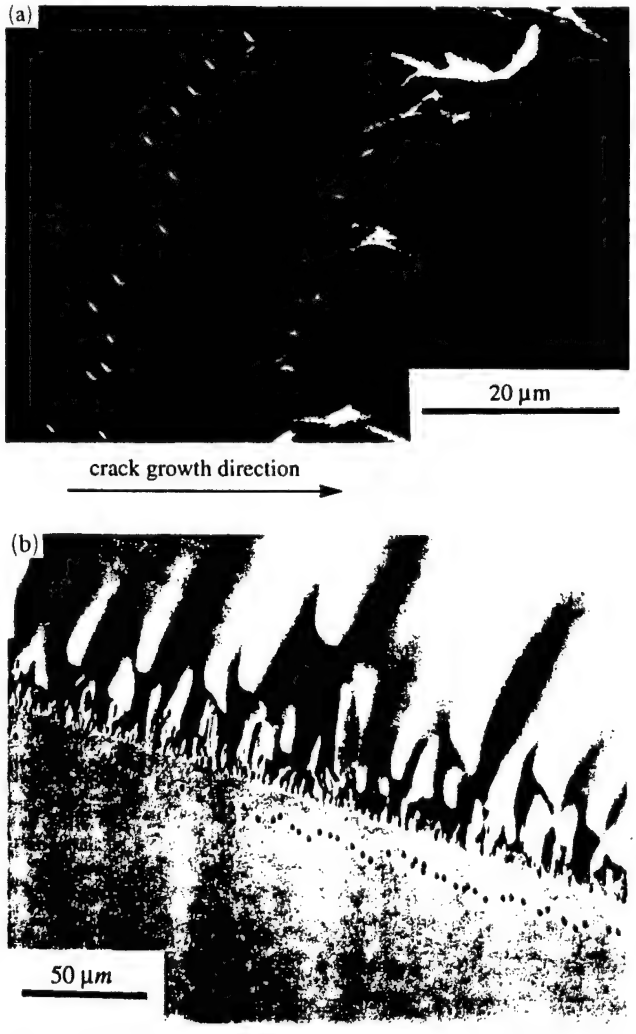

Fig. 9. Etched {110} fracture surface around the crack arrest front: (a) SEM picture with a high magnification; (b) optical micrograph with a low magnification.

the cleavage fracture surface which is smooth and featureless. On the other side is the roughened, wavy surface representing a substantial amount of dislocation activity. In fact, most of the dislocation induced plastic flow occurred right on the arrest front where, although the individual dislocation etch pits cannot be identified, some dimples are seen which are indications of clusters of dislocations upon etching. The dislocation density at the arrest location is too high for resolving individual etch pits. So it is most likely that before the final unstable fast fracture occurred, the crack experienced considerable ductile blunting. Furthermore, because of inhomogeneous nucleation of dislocations at the crack tip, the crack front is no longer sharp and straight after the blunting. Beyond the crack arrest location, a tortuous cleavage fracture surface following the no-longer straight crack front is observed. But the crack surface gradually smoothened itself out to return to the original cleavage plane.

It is interesting to note the presence of a line of dislocations formed before the crack reached the final arrest front. This can be seen more clearly in Fig. 9(b), taken with Nomarski contrast microscopy. It shows the same fracture surface shown in Fig. 9(a), but with a lower magnification. It should be mentioned that this phenomenon is not always repeatable. A more typical fracture surface would have the distinct crack arrest front with few individual dislocation etch-pits around it. This line of dislocations was most likely generated due to a hesitation of the running crack during which the dislocations had just enough time to move out of the fracture surface. Nevertheless, this line of dislocations demonstrated that even though dislocation nucleation conditions can be met at a propagating crack tip or that the crack can move with some dislocations attached to it as considered by Argon [2], this may not result in a BDT unless a critical grouping of crack tip dislocations having the appropriate mobility is established. Therefore, from the limited information, we can nevertheless conclude that in Si single crystals, dislocation mobility is likely to be the rate-limiting mechanism which controls the BDT, in agreement with the conclusions reached by other investigators (Brede and Haasen [13] and Hirsch *et al.* [8]) based on somewhat different experimental evidence.

A more typical fracture surface around the crack arrest front is shown in Figs. 10(a) and 10(b). These are from the two opposing pieces of the same specimen. Only one side was etched to study the dislocation structure and compare the etched and unetched surfaces. Although the crack arrest front is still clearly seen, few (if any) individual dislocation etch pits are visible. Nevertheless, the extensive dislocation activities near the crack arrest front did change the crack front morphology substantially, so that when the crack

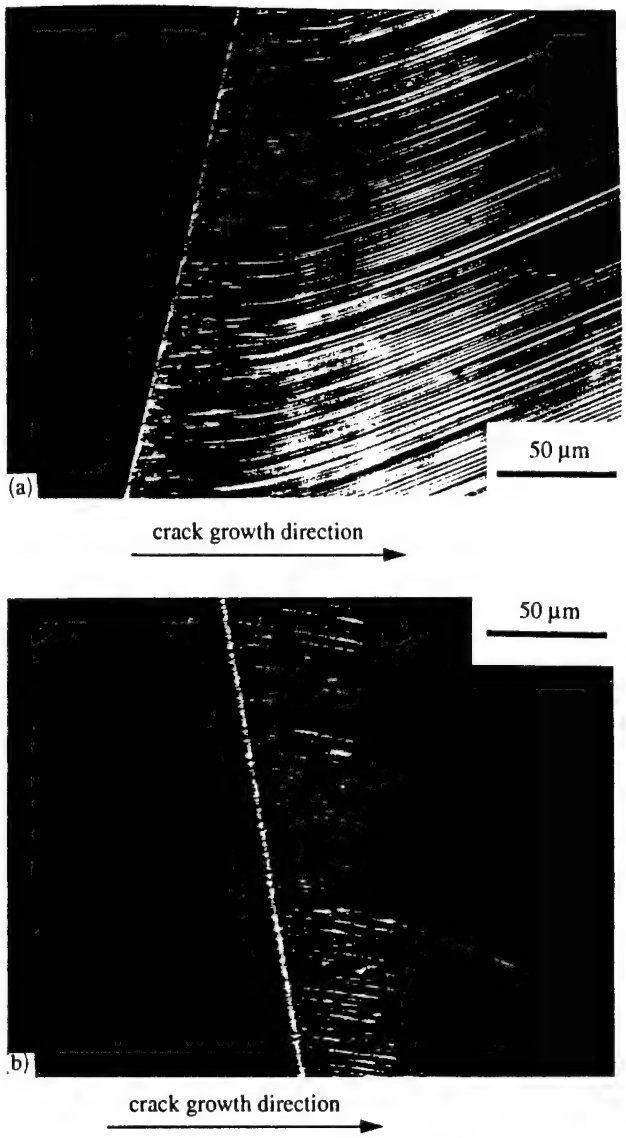

Fig. 10. {110} fracture surface of a typical crack arrest front; (a) before etching; (b) after etching.

started to grow again under continued loading, the fracture surface was no longer the smooth, cleavage surface, but a wavy one. Another evidence of dislocation activity near the crack arrest comes from the comparison of the etched and unetched surfaces. Before etching, the fracture surfaces of the two pieces were identical, except that they were mirror images of each other. However, it was observed that, after etching, the band on the crack arrest front widened up dramatically. This can only be explained by the existence of dislocation loops within the crack arrest front which, upon etching, formed dimples on the fracture surface. The formation of a wavy crack front upon generation of dislocations is an indication that, as argued by Hirsch and

Roberts [20], dislocation nucleation is not homogeneous, but from a limited number of sources along the crack front. The nucleation of dislocations from the primary sources may in fact suppress the nucleation in their neighbourhood. The continued nucleation of dislocations from these primary sources would then change the straight cleavage crack front into a wavy one. If this is true, the wave length of the waviness could be well correlated to the characteristic spacing of primary dislocation nucleation sources along the crack front.

Some additional evidence to support the conclusion that dislocation mobility controls the BDT in Si crystals comes from the portion of the fracture surface where fast cleavage fracture occurred at a temperature well above the BDT temperature (the final unstable crack growth region). There, scattered dislocation clusters such as the one shown in Fig. 11 were consistently observed. The mechanism to trigger the generation of these dislocations is still unclear, but the shielding effect due to their generation was apparently inadequate to slow down or arrest the fast propagating cleavage crack, although the dislocations could nucleate and their mobility was high enough to form complete loops which extended deep into the material.

4. Discussion and conclusions

The novel experimental technique developed by Brede *et al.* [17] and modified by us has proven to be an effective way to study the micromechanisms of the BDT in cleavable material systems. This technique provides the means to measure accurately the BDT temperature for a propagating cleavage crack without explicitly differentiating the controlling crack tip mechanism of the phenomenon. The measured BDT temperature by this technique could also be called the crack arrest temperature, which could be somewhat different from the BDT temperature measured by the static tests, though they relate fundamentally to the same phenomena.

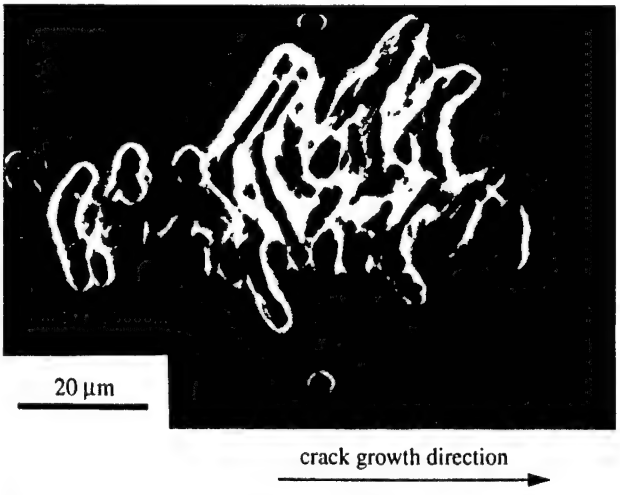

Fig. 11. Traces of dislocations during fast fracture at a temperature higher than the BDT temperature.

The preliminary experimental results on Si single crystals reported here have demonstrated that although dislocations can be emitted from the crack tip, they do not always provide enough blunting or shielding to result in the BDT. Therefore, it is concluded that in this material, dislocation mobility, rather than dislocation nucleation, is the rate-limiting mechanism for the BDT. Similar behaviour has been observed by Dewald *et al.* [16] in other material systems such as GaAs and MgO. They observed, using an *in situ* TEM technique, that although dislocations could be generated at or around a cleavage crack tip, this did not prevent the crack from propagating in a cleavage manner. Such observations of cleavage cracks carrying with them expanding plumes of dislocations had, of course, been made in studies on LiF by Burns and Webb [21].

Based on the preliminary experimental results, it is conceived that for a propagating cleavage crack in Si single crystals, dislocations can be continuously nucleated from the crack tip within a temperature range slightly below the crack arrest temperature. However, they cannot move deep into the specimen to result in effective shielding because of low mobility. As the crack passed by, it was likely that these dislocations were drawn out of the fracture surface by the image forces since the specimen was still in the high-temperature environment. But this dislocation activity is still expected to contribute to the fracture energy for propagating cracks. The energy release rate of fracture in this case will be slightly higher than at ambient temperature. It could also slow down the running crack slightly, as observed in Fig. 8.

The current experimental results also clearly demonstrated that in this material, reaching the crack arrest temperature does not always bring about general yielding of the specimen. If loading is continued, a change of fracture mode from crack blunting to re-initiation of cleavage (ductile to brittle transition) could still happen. This is in fact consistent with the mobility limiting mechanism of the BDT. After the crack was arrested, upon continued loading the fracture mode is determined essentially by the competition between the loading rate and the expansion rate of the crack tip plastic zone. This is the situation similar to those encountered in the static experiments [10, 12–14]. When dislocations are sluggish, the expansion rate of the plastic zone may not be able to keep up with the applied loading rate, and thus a re-initiation of

cleavage fracture such as the unstable crack growth observed in our experiments could result. On the other hand, for materials in which dislocation mobility is high, such as in some b.c.c. transition metals and perhaps some intermetallic compounds, once dislocations are nucleated, they are driven away by the crack tip stress field with a very high velocity, setting up little back stress at the crack tip. Because of this, the dislocation activity near the crack tip could continue unabated to result in even increasing blunting and ductile tearing. In these materials, a ductile to brittle transition could only happen under high strain rates by initiating a new microcrack in the blunted zone as is expected to happen in the usual DBT transition [22].

Clearly, the results we have reported here must be considered only preliminary, establishing the validity and utility of our experimental technique. Some further investigations of both theoretical and experimental nature are presently in progress and will be reported elsewhere.

Acknowledgments

This research was supported by the Department of Energy through Grant DE-FG02-87ER45294-A003. KJH is also partly supported by the National Science Foundation through Grant No. MSS 92-09309. Helpful discussions with Dr. Markus Brede are acknowledged. Help from Mr. T. Mower at MIT Lincoln Lab with the coating of specimens is appreciated.

References

1 J. R. Rice and R. Thomson, *Phil. Mag., 29* (1974) 73.
2 A. S. Argon, *Acta Metall., 35* (1987) 185.
3 R. E. Peierls, *Proc. Phys. Soc., 52* (1940) 23.
4 K. S. Cheung, A. S. Argon and S. Yip, *J. Appl. Phys., 69* (1991) 2088.
5 J. R. Rice, *J. Mech. Phys. Solids, 40* (1992) 239.
6 J. R. Rice, G. E. Beltz and Y. Sun, in A. S. Argon (ed.), *Topics in Fracture and Fatigue*, Springer, New York, 1992, p. 1.
7 M. F. Ashby and J. D. Embury, *Scripta Metall., 19* (1985) 557.
8 P. B. Hirsch, S. G. Roberts and J. Samuels, *Proc. R. Soc. London, A421* (1989) 25.
9 M. Brede, *Acta Metall. Mater., 41* (1993) 211.
10 C. St John, *Phil. Mag., 32* (1975) 1193.
11 J. J. Gilman, C. Knudsen and W. P. Walsh, *J. Appl. Phys., 29* (1958) 600.
12 G. Michot, *Crystal Properties and Preparation, 17/18* (1988) 55.
13 M. Brede and P. Haasen, *Acta Metall., 36* (1988) 2003.
14 J. Samuels and S. G. Roberts, *Proc. R. Soc. London, A421* (1989) 1.
15 Y.-H. Chiao and D. R. Clarke, *Acta Metall., 37* (1987) 203.
16 D. K. Dewald, T. C. Lee, I. M. Robertson and H. K. Birnbaum, *Scripta Metall., 23* (1989) 1307.
17 M. Brede, K. J. Hsia and A. S. Argon, *J. Appl. Phys., 70* (1991) 758.
18 S. Mostovoy, P. B. Crosley and E. J. Ripling, *J. Materials, 2* (1967) 661.
19 K. J. Hsia and A. S. Argon, unpublished research (1991).
20 P. B. Hirsch and S. G. Roberts, *Phil. Mag., A64* (1991) 55.
21 S. J. Burns and W. W. Webb, *J. Appl. Phys., 41* (1970) 2086.
22 L. B. Freund and J. W. Hutchinson, *J. Mech. Phys. Solids, 33* (1985) 169.

REPORT DOCUMENTATION PAGE

Form Approved
OMB No. 0704-0188

1. AGENCY USE ONLY (Leave blank)	2. REPORT DATE	3. REPORT TYPE AND DATES COVERED
	May 22, 1997	Final: 9/1/1992-11/30/1995

4. TITLE AND SUBTITLE
Nucleation of Dislocations from Crack Tips under mixed modes of loading: Implications for Brittle against Ductile Behavior of Crystals

5. FUNDING NUMBERS
C-N00014-92-J-4022

6. AUTHOR(S)
G. Xu, A.S. Argon and M. Ortiz

7. PERFORMING ORGANIZATION NAME(S) AND ADDRESS(ES)
Massachusetts Institute of Technology
Room 1-306
Cambridge, MA 02139
(A.S. Argon)

8. PERFORMING ORGANIZATION REPORT NUMBER
1-2

9. SPONSORING/MONITORING AGENCY NAME(S) AND ADDRESS(ES)
ONR Solid Mechanics Program (Attn: Dr. R. Barsoum)
ONR Code 1132
800 N. Quincy Street-Ballston Tower 1
Arlington, VA 22217-5000

10. SPONSORING/MONITORING AGENCY REPORT NUMBER

11. SUPPLEMENTARY NOTES
Paper published in "Philosophical Magazine", 72, 415-451 (1995)
(Reprints attached)

12a. DISTRIBUTION/AVAILABILITY STATEMENT
Unlimited

12b. DISTRIBUTION CODE

13. ABSTRACT *(Maximum 200 words)*

The variational boundary integral method of Xu and Ortiz is taken as a basis for studying dislocation nucleation from atomically sharp cracks under combined mode I - mode II loading. The tension-shear potential of Rice et al. is extended to allow for skewness in the shear resistance curve and to account for the surface production resistance which accompanies ledge formation. The calculated unstable equilibrium configurations of the incipient dislocations and the dependence of the associated activation energies on crack tip energy release rate are found to differ from the Rice-Beltz perturbation solution and the Schöck-Püschl more approximate solution. Simulations of dislocation nucleation on inclined slip planes reveal that, while tension softening facilitates nucleation, surface production resistance impedes it. The extent to which these two effects influence critical conditions for dislocation nucleation is quantified. The calculations suggest that homogeneous dislocation nucleation on inclined planes is not favored for materials with all but the lowest of unstable stacking-energy-to-surface-energy ratios. This emphasizes the importance of heterogeneous dislocation nucleation and nucleation on oblique slip planes on which free surface production should play a much weaker role. The implications of these findings on the nucleation-controlled brittle-ductile transition in cleavage fracture are discussed.

14. SUBJECT TERMS
Initiation of ductile behaviior from crack tips.
Dislocation emission simulation.

15. NUMBER OF PAGES
36

16. PRICE CODE

17. SECURITY CLASSIFICATION OF REPORT	18. SECURITY CLASSIFICATION OF THIS PAGE	19. SECURITY CLASSIFICATION OF ABSTRACT	20. LIMITATION OF ABSTRACT
Unclassified	Unclassified	Unclassified	None

PHILOSOPHICAL MAGAZINE A, 1995, VOL. 72, NO. 2, 415–451

Nucleation of dislocations from crack tips under mixed modes of loading: implications for brittle against ductile behaviour of crystals

By G. XU, A. S. ARGON†

Department of Mechanical Engineering, Massachusetts Institute of Technology, Cambridge, Massachusetts 02139, USA

and M. ORTIZ

Division of Engineering, Brown University, Providence, Rhode Island 02912, USA

[*Received 7 October 1994 and accepted 21 January 1995*]

ABSTRACT

The variational boundary integral method of Xu and Ortiz is taken as a basis for studying dislocation nucleation from atomically sharp cracks under combined mode I–mode II loading. The tension–shear potential of Rice *et al.* is extended to allow for skewness in the shear resistance curve and to account for the surface production resistance which accompanies ledge formation. The calculated unstable equilibrium configurations of the incipient dislocations and the dependence of the associated activation energies on crack tip energy release rate are found to differ from the Rice–Beltz perturbation solution and the Schöck–Püschl more approximate solution. Simulations of dislocation nucleation on inclined slip planes reveal that, while tension softening facilitates nucleation, surface production resistance impedes it. The extent to which these two effects influence critical conditions for dislocation nucleation is quantified. The calculations suggest that homogeneous dislocation nucleation on inclined planes is not favoured for materials with all but the lowest of unstable stacking-energy-to-surface-energy ratios. This emphasizes the importance of heterogeneous dislocation nucleation and nucleation on oblique slip planes on which free surface production should play a much weaker role. The implications of these findings on the nucleation-controlled brittle–ductile transition in cleavage fracture are discussed.

NOMENCLATURE

- b magnitude of Burgers vector
- c uniaxial strain elastic modulus
- G_{cd} critical driving force to nucleate a dislocation
- G_I crack driving force under mode I loading
- G_{II} crack driving force under mode II loading
- G_{Ic} critical cleavage crack driving force under mode I loading
- h interatomic layer spacing
- K_{IId} critical stress intensity factor K_{II} to nucleate a dislocation
- T_{BD} brittle-to-ductile transition temperature
- ΔU_{act}^{2D} activation energy per unit length for nucleating a straight dislocation in two dimensions

† Author for correspondence.

$\Delta U_{\mathrm{act}}^{\mathrm{3D}}$ activation energy for nucleating a dislocation loop in three dimensions
β skewness parameter for the shear resistance
γ_{s} surface energy
$\gamma_{\mathrm{us}}^{(\mathrm{u})}$ unrelaxed unstable stacking energy
$\gamma_{\mathrm{us}}^{(\mathrm{r})}$ relaxed unstable stacking energy
δ_r inelastic shear displacement between adjacent atomic layers
δ_{tip} interlayer inelastic displacement at the crack tip
δ_0 inelastic opening displacement between adjacent atomic layers
Δ_r shear displacement between adjacent atomic layers
Δ_0 opening displacement between adjacent atomic layers
θ angle of inclination between slip plane and the crack surface
λ decay parameter for the shear resistance to surface production
μ shear modulus
ν Poisson's ratio
σ tensile stress between adjacent atomic layers
τ shear stress between adjacent atomic layers
τ_r periodic shear resistance between adjacent atomic layers
τ_{s} shear resistance to surface production
ϕ oblique angle between the Burgers vector and the crack front
Φ inelastic potential between adjacent atomic layers
Ψ potential between adjacent atomic layers

§ 1. Introduction

The transition in the behaviour of materials from brittle to ductile continues to be of major scientific and technological interest. It was recognized early that cleavable materials are distinguished by having substantial energy barriers to dislocation nucleation from atomically sharp cracks on the verge of propagation (Armstrong 1966, Kelly, Tyson and Cottrell 1967, Rice and Thompson 1974). Moreover, pioneering experiments carried out on initially dislocation-free Si (St John 1975, Brede and Haasen 1988, Hirsch, Samuels and Roberts 1989) have demonstrated that, at least in this material, the brittle-to-ductile transition is not controlled solely by dislocation nucleation but also by the mobility of trains of dislocations nucleation from crack tips (Chiao and Clarke 1989, Samuels and Roberts 1989, George and Michot 1993) have established that dislocation nucleation is heterogeneous, singling out geometrical crack-tip imperfections.

Evidently, a full understanding of these processes necessitates some degree of atomistic modelling (for example Bulatov, Yip and Argon 1995). Despite being deficient in this respect, continuum approaches of the Peierls type have revealed useful insights (Rice 1992, Rice Beltz and Sun 1992, Sun Beltz and Rice 1993, Schöck 1991). For instance, continuum theories have in their own way confirmed that the saddle-point configuration of a nucleating dislocation consists entirely of dislocation core material, and that the accurate modelling of the atomic-level decohesion and shear response is of vital importance for the theory to be predictive. Within this framework, Rice and Beltz (1994) have computed saddle-point energies of three-dimensional dislocation nuclei by a first-order perturbation analysis. The activation energies obtained by this means differ somewhat from those determined by Schöck and Püschl (1991) by a different approach.

The analyses of Schöck and Püschl (1991) and Rice and Beltz (1994), while three dimensional, severely limit the range of possible geometries available to the incipient

dislocation loop: the former by prescribing its shape to be rectangular, and the latter by considering the dislocation to be nearly straight, in the spirit of perturbation theory. Here we present an analysis of dislocation nucleation from a crack tip which is free of *a priori* restrictions on the shape of the dislocation. Our calculations are based on a numerical method developed by Xu and Ortiz (1993) for the analysis of three-dimensional cracks in linear elastic solids. Because the method regards the crack as a continuous distribution of dislocation loops, it is readily extended to account for systems of interacting cracks and discrete dislocations such as envisaged here. This approach introduces no artificial discontinuity between elastic crack opening and inelastic interplanar separation. Additionally, we introduce a non-sinusoidal interplanar potential in the manner of Foreman, Jaswon and Wood (1951), as well as additional modifications to account for the resistance due to surface production. While the present analysis is restricted to isotropic elasticity in dealing with dislocation line properties, generalizations to anisotropic elasticity are straightforward but will not be pursued here. In this paper we further restrict our attention to geometries in which dislocation nucleation occurs on a slip plane containing the crack front.

Following a brief description of the numerical procedure in § 2, and a derivation of the modified interplanar potential in § 3, in § 4 we consider the problem of the nucleation of a straight dislocation within the plane of the crack under the action of pure mode II loading, with particular emphasis on the effect of departures from Frenkel's sinusoidal shear resistance relation. The analytical results of Rice and Beltz (1994) provide a direct test of the accuracy of the numerical procedure. In § 5 we broaden the scope of the analysis by allowing for arbitrary dislocation configurations, and the results are compared with the approximate analyses of Rice and Beltz (1994) and Schöck and Püschl (1991). In § 6 we turn to the tension-softening effect under mixed mode I–mode II loading. Our results reveal the dependence of the critical mode II stress intensity factor K_{IId} for dislocation emission on the applied mode I stress intensity factor K_{I}. We also compute the dependence of the critical energy release rate for dislocation emission on the phase angle of the applied loads, and compare the results with the analytical relation proposed by Sun *et al.* (1993). In § 7, we generalize the interplanar potential to account for the shear resistance due to surface production in cases where the slip plane intersects a free surface. The resulting interplanar potential is taken as a basis for the analysis of dislocation emission into inclined slip planes emanating from the crack front. The particular cases of α-Fe and Si are considered in some detail. Finally, in § 8 some general remarks are added, evaluating the present findings.

§ 2. Method of analysis

Our analysis builds on recent theoretical developments in the modelling of dislocation nucleation at a stressed crack tip (Beltz and Rice 1991, Rice 1992, Rice *et al.* 1992, Sun *et al.* 1993, Rice and Beltz 1994). In consonance with these developments, we consider a semi-infinite crack with a straight crack front lying on a slip plane in an elastically isotropic solid. We additionally assume that the crack surfaces do not interact and that, beyond the crack front, the shear separation resistance τ and tension separation resistance σ follow as functions of the inelastic displacements δ_r and δ_θ on the slip plane. A precise definition of δ_r and δ_θ has been given by Rice (1992) and Sun *et al.* (1993). As the crack is subjected to combined mode I–mode II loading, an incipient dislocation can form progressively and reach a nucleation configuration, where it is emitted into the slip plane as the load reaches a critical value. Consideration

Fig. 1

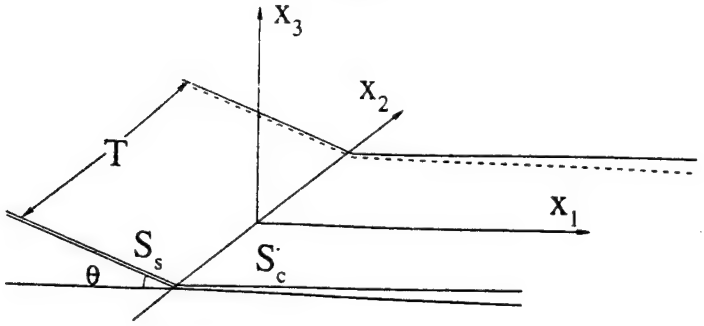

A semi-infinite crack with an inclined slip plane coincident with the crack front.

of a mode I loading component enables a systematic study of the tension-softening effect, as modelled by the modified interplanar potential to be introduced subsequently.

The geometry of the problem is illustrated in fig. 1. A semi-infinite atomically sharp crack and an inclined slip plane containing the crack front are subjected to a remote load, resulting in dislocation nucleation along the slip plane. The crystal is idealized as an isotropic linear elastic solid with shear modulus μ and Poisson's ratio ν. This description applies everywhere in the crystal except for the relative displacement of the atomic layers bounding the slip plane, which is governed by a Peierls interlayer potential. The remote loading, characterized by stress intensity factors K_{I}, K_{II} and K_{III}, induces a standard K field in the absence of a dislocation.

The profile of the nucleated dislocation and the crack opening displacement $\mathbf{u}$ follow by minimization of the potential energy

$$\Pi[\mathbf{u}] = W[\mathbf{u}] + V[\mathbf{u}] - P[\mathbf{u}], \tag{1}$$

where W is elastic strain energy, V the interlayer energy and P the potential energy of the applied forces. By representing the inelastic displacement along the slip plane and the opening displacement of the crack as a continuous distribution of dislocation loops, and using known expressions for the interaction energy between dislocation loops (Hirth and Lothe, 1982), Xu and Ortiz (1993) derived the general form of the strain energy

$$\begin{aligned} W[\mathbf{u}] = {} & \frac{\mu}{4\pi}\int_{S_c+S_s}\int_{S_c+S_s}\frac{[\mathbf{e}_i\cdot(\mathbf{n}\times\nabla u_j)_2][\mathbf{e}_j\cdot(\mathbf{n}\times\nabla u_i)_1]}{R}\,\mathrm{d}S_1\,\mathrm{d}S_2 \\ & -\frac{\mu}{8\pi}\int_{S_c+S_s}\int_{S_c+S_s}\frac{[\mathbf{e}_i\cdot(\mathbf{n}\times\nabla u_i)_1][\mathbf{e}_j\cdot(\mathbf{n}\times\nabla u_j)_2]}{R}\,\mathrm{d}S_1\,\mathrm{d}S_2 \\ & +\frac{\mu}{8\pi(1-\nu)}\int_{S_c+S_s}\int_{S_c+S_s}[\mathbf{e}_i\times(\mathbf{n}\times\nabla u_i)_1]\cdot\mathbf{T}\cdot[\mathbf{e}_j\times(\mathbf{n}\times\nabla u_j)_2]\,\mathrm{d}S_1\,\mathrm{d}S_2, \end{aligned} \tag{2}$$

where S_c and S_s represent the crack surface and the slip plane respectively, $(.)_1$ and $(.)_2$ denote two different points on the surfaces S_c and S_s, R is the distance between these two points, $\mathbf{e}_i$, $i = 1, 2, 3$, are Cartesian basis vectors, $\mathbf{n}$ is the normal vector to the crack surface or the slip plane, and $\mathbf{T}$ is a tensor with components

$$T_{ij} = \frac{\partial^2 R}{\partial x_i\,\partial x_j}. \tag{3}$$

The interlayer energy is expressible as

$$V[\mathbf{u}] = \int_{S_s} \Phi[\mathbf{u}]\, \mathrm{d}S, \tag{4}$$

where $\Phi[\mathbf{u}]$ is the interplanar potential defined per unit area of the slip plane. Suitable expressions for Φ are derived in § 3. Finally the potential energy of tractions $\mathbf{t}$ applied on the crack surfaces is

$$P[\mathbf{u}] = \int_{S_c} \mathbf{t}\cdot\mathbf{u}\, \mathrm{d}S. \tag{5}$$

In subsequent analyses, the crack surfaces are presumed to be free of applied tractions, and, consequently, $\mathbf{t} = \mathbf{0}$.

To solve for the displacements $\mathbf{u}$ numerically, the analysis has to be reduced to a bounded domain. Following the treatment of semi-infinite periodic cracks given by Xu and Ortiz (1993), this reduction can be achieved by writing

$$\mathbf{u} = \bar{\mathbf{u}} + \boldsymbol{\delta}, \tag{6}$$

where $\bar{\mathbf{u}}$ is the displacement of a standard K field for a reference semi-infinite crack. Choose Cartesian axes such that the crack occupies the domain $x_3 = 0$, $x_1 > 0$. Then, $\bar{\mathbf{u}} = \mathbf{0}$ for $x_1 < 0$ and

$$\bar{u}_1 = \frac{K_\mathrm{I}}{\mu}\frac{4(1-\nu)}{(2\pi)^{1/2}}\, x_1^{1/2}, \tag{7a}$$

$$\bar{u}_2 = \frac{K_\mathrm{II}}{\mu}\frac{4(1-\nu)}{(2\pi)^{1/2}}\, x_1^{1/2}, \tag{7b}$$

$$\bar{u}_3 = \frac{K_\mathrm{III}}{\mu}\frac{4}{(2\pi)^{1/2}}\, x_1^{1/2}, \tag{7c}$$

for $x_1 \geqslant 0$. The term $\bar{\mathbf{u}}$ matches the behaviour of the opening displacements for large x_1, that is far from the crack front. Consequently, the remaining term $\boldsymbol{\delta}$, which is the primary unknown in the calculations, may be expected to decay rapidly to zero with x_1. This situation is exploited by setting $\boldsymbol{\delta} = \mathbf{0}$ for $x_1 \geqslant x_1^c$, that is beyond some distance x_1^c from the crack front. Far from the crack front on the slip plane, $\boldsymbol{\delta}$ may also be expected to become negligibly small. In this manner, $\boldsymbol{\delta}$ can be restricted to a finite domain $\hat{S}_c \cup \hat{S}_s$, where $\hat{S}_c$ lies on the crack surface and $\hat{S}_s$ on the slip plane. Noting that $P[\bar{\mathbf{u}}] = 0$ on $\hat{S}_c$ and the interlayer potential only applies on the slip plane, the potential energy of the crack-slip plane system can then be written as

$$\Pi[\bar{\mathbf{u}} + \boldsymbol{\delta}] = W[\bar{\mathbf{u}} + \boldsymbol{\delta}] + V[\boldsymbol{\delta}] = W_1[\bar{\mathbf{u}}] + W_1[\boldsymbol{\delta}] + W_2[\bar{\mathbf{u}}, \boldsymbol{\delta}] + V[\boldsymbol{\delta}], \tag{8}$$

where we identify $W_1[\bar{\mathbf{u}}]$ as the self-energy of the system, free of inelastic modifications, $W_1[\boldsymbol{\delta}] + V[\boldsymbol{\delta}]$ as the self-energy of the system of inelastic modifications consisting of the distributed dislocations and the interplanar interaction energy on the slip plane, and where $W_2[\bar{\mathbf{u}}, \boldsymbol{\delta}]$ is the interaction energy of the initial unmodified system with the second system of modifications.

Then,

$$W_1[\delta] = \frac{\mu}{4\pi}\int_{\hat{S}_c+\hat{S}_s}\int_{\hat{S}_c+\hat{S}_s}\frac{[\mathbf{e}_i\cdot(\mathbf{n}\times\nabla\delta_j)_2][\mathbf{e}_j\cdot(\mathbf{n}\times\nabla\delta_i)_1]}{R}\,dS_1\,dS_2$$
$$-\frac{\mu}{8\pi}\int_{\hat{S}_c+\hat{S}_s}\int_{\hat{S}_c+\hat{S}_s}\frac{[\mathbf{e}_i\cdot(\mathbf{n}\times\nabla\delta_i)_1][\mathbf{e}_j\cdot(\mathbf{n}\times\nabla\delta_j)_2]}{R}\,dS_1\,dS_2$$
$$+\frac{\mu}{8\pi(1-\nu)}\int_{\hat{S}_c+\hat{S}_s}\int_{\hat{S}_c+\hat{S}_s}[\mathbf{e}_i\times(\mathbf{n}\times\nabla\delta_i)_1]\cdot\mathbf{T}\cdot[\mathbf{e}_j\times(\mathbf{n}\times\nabla\delta_j)_2]\,dS_1\,dS_2, \quad (9)$$

and

$$V[\delta] = \int_{\hat{S}_s}\Phi[\delta]\,dS. \quad (10)$$

Following the treatment of semi-infinite periodic cracks given by Xu and Ortiz (1993), the interaction energy W_2 of the displacement $\bar{\mathbf{u}}$ of the standard K field and the inelastic displacement correction $\boldsymbol{\delta}$ can be written as

$$W_2[\bar{\mathbf{u}},\boldsymbol{\delta}] = -K_I Q_I[\boldsymbol{\delta}] - K_{II}Q_{II}[\boldsymbol{\delta}] - K_{III}Q_{III}[\boldsymbol{\delta}], \quad (11)$$

where

$$Q_I[\boldsymbol{\delta}] = \int_{\hat{S}_c+\hat{S}_s}\mathbf{n}\cdot\boldsymbol{\sigma}_I\cdot\boldsymbol{\delta}\,dS, \quad (12a)$$

$$Q_{II}[\boldsymbol{\delta}] = \int_{\hat{S}_c+\hat{S}_s}\mathbf{n}\cdot\boldsymbol{\sigma}_{II}\cdot\boldsymbol{\delta}\,dS, \quad (12b)$$

$$Q_{III}[\boldsymbol{\delta}] = \int_{\hat{S}_c+\hat{S}_s}\mathbf{n}\cdot\boldsymbol{\sigma}_{III}\cdot\boldsymbol{\delta}\,dS, \quad (12c)$$

and $\boldsymbol{\sigma}_I$, $\boldsymbol{\sigma}_{II}$ and $\boldsymbol{\sigma}_{III}$ are stresses of K fields in modes I, II and III respectively for unit stress intensity factor. The integration is partly extended over the real crack surface since the crack front of the reference semi-infinite crack is actually located some distance from the physical crack front. This treatment allows us to use a non-singular Dugdale–Barenblatt crack as a reference crack, so that the quality of the solution can be improved (Xu and Ortiz 1993).

The unknown displacements $\boldsymbol{\delta}$ follow by rendering the potential energy $\Pi[\bar{\mathbf{u}}+\boldsymbol{\delta}]$ stationary. Noting that the first term on the right-hand side of eqn. (8) is independent of $\boldsymbol{\delta}$ and can therefore be disregarded, the variation leads to the Euler equation

$$\frac{\partial W_1[\boldsymbol{\delta}]}{\partial\boldsymbol{\delta}} + \frac{\partial V[\boldsymbol{\delta}]}{\partial\boldsymbol{\delta}} - K_I\frac{\partial Q_I[\boldsymbol{\delta}]}{\partial\boldsymbol{\delta}} - K_{II}\frac{\partial Q_{II}[\boldsymbol{\delta}]}{\partial\boldsymbol{\delta}} - K_{III}\frac{\partial Q_{III}[\boldsymbol{\delta}]}{\partial\boldsymbol{\delta}} = \mathbf{0}. \quad (13)$$

This equation is of integral type, by virtue of the first term, and nonlinear, by virtue of the second term. A finite-element method of spatial discretization of eqn. (13) has been given by Xu and Ortiz (1993) in the case $V=0$. The extension to the case $V\neq 0$ is straightforward and leads to a system of nonlinear equations which can be solved by a Newton–Raphson iteration.

A non-trivial complication arises in applying this program, owing to the loss of stability of the equations beyond the critical load. This difficulty may be circumvented by recourse to displacement control. For purposes of illustration, consider the pure mode II case corresponding to $K_I = K_{III} = 0$. Under these conditions, the finite-

Fig. 2

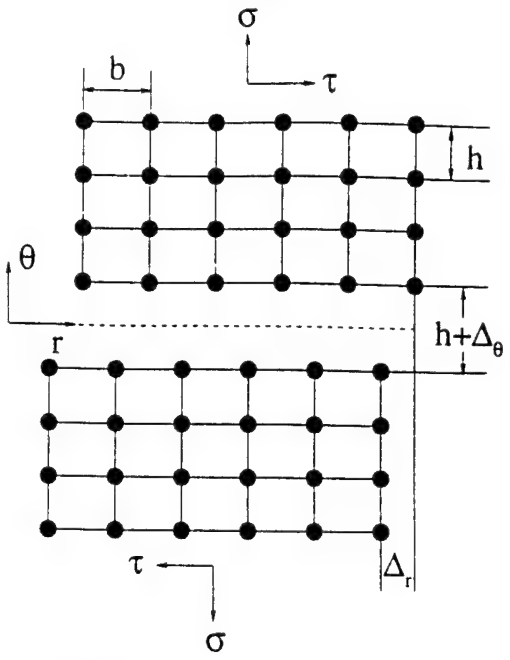

Block-like lattice sliding and opening displacement of atomic layers bounding a slip plane.

element discretization of the crack–slip plane system results in a system of equations of the form

$$\mathbf{F}(\boldsymbol{\delta}) = K_{\mathrm{II}}\mathbf{f}, \tag{14}$$

where $\boldsymbol{\delta}$ now denotes the array of nodal values of the field $\boldsymbol{\delta}(\mathbf{x})$, $\mathbf{F}$ is the internal force array, and $\mathbf{f}$ is the external force array normalized to $K_{\mathrm{II}} = 1$. Instead of enforcing the value of K_{II}, which is not possible beyond the critical point, we augment the system (14) by the addition of the kinematic constraint

$$\mathbf{f}\cdot\boldsymbol{\delta} - \bar{\delta} = 0. \tag{15}$$

Here, $\mathbf{f}\cdot\boldsymbol{\delta}$ is the displacement parameter conjugate to K_{II} and $\bar{\delta}$ its prescribed value. The unknowns of the combined system of eqns (14) and (15) are $\boldsymbol{\delta}$ and K_{II}. Thus K_{II} is not prescribed but computed as a function of the effective displacement $\bar{\delta}$, which can be increased monotonically from zero. Linearization of eqns (14) and (15) yields an incremental system of the form

$$\begin{bmatrix} \mathbf{K} & -\mathbf{f} \\ -\mathbf{f}^T & 0 \end{bmatrix}\begin{bmatrix} \Delta\boldsymbol{\delta} \\ \Delta K_{\mathrm{II}} \end{bmatrix} = \begin{pmatrix} 0 \\ -\Delta\bar{\delta} \end{pmatrix}, \tag{16}$$

where $\mathbf{K}$ is a symmetric tangent stiffness matrix. The form of eqn. (16) is indeed characteristic of a system with equality constraints enforced by Lagrange multipliers.

§ 3. An atomic level interlayer potential for tension–shear coupling

A coupled tension–shear interlayer potential which combines the Frenkel sinusoidal law and the Rose–Ferrante–Smith (1981) universal binding relation was derived by Beltz and Rice (1991). Following their development, we envisage two rigid half-crystals sliding uniformly across a slip plane of thickness h (fig. 2). Let Δ_r and Δ_θ

denote the shear and opening relative displacements respectively across the slip plane; τ and σ are the shear and normal resistances respectively acting between the blocks. The inelastic relative displacements δ_r and δ_θ are then defined as

$$\delta_r = \Delta_r - \frac{h\tau(\Delta_r, \Delta_\theta)}{\mu}, \tag{17a}$$

$$\delta_\theta = \Delta_\theta - \frac{h\sigma(\Delta_r, \Delta_\theta)}{c}, \tag{17b}$$

where $c = \lambda + 2\mu$ is the uniaxial strain elastic modulus.

The point of departure in the Beltz–Rice theory is an interplanar traction displacement relation of the general form

$$\tau(\Delta_r, \Delta_\theta) = A(\Delta_\theta) \sin\left(\frac{2\pi\Delta_r}{b}\right), \tag{18a}$$

$$\sigma(\Delta_r, \Delta_\theta) = \left(B(\Delta_r)\frac{\Delta_\theta}{L} - C(\Delta_r)\right)\exp\left(-\frac{\Delta_\theta}{L}\right), \tag{18b}$$

where $A(\Delta_\theta)$, $B(\Delta_r)$ and $C(\Delta_\theta)$ are functions to be determined. In eqns (18*a*) and (18*b*), b denotes the Burgers displacement and L the characteristic length of the decohesion process. This length is found to scale with the Thomas–Fermi screening distance in elemental metals (Rose *et al.* 1981). In simple tension, σ reaches its maximum level at $\Delta_\theta = L$.

Beltz and Rice (1991) determined the functions $A(\Delta_\theta)$, $B(\Delta_r)$ and $C(\Delta_\theta)$ by enforcing selected subsidiary constraints. Firstly, the traction–displacement relations are required to reduce to Frenkel's sinusoidal form and the Rose–Ferrante–Smith universal binding relation in simple shear and tension respectively. This gives

$$\tau(\Delta_r, 0) = \frac{\pi\gamma_{us}}{b}\sin\left(\frac{2\pi\Delta_r}{b}\right), \tag{19a}$$

$$\sigma(0, \Delta_\theta) = \frac{2\gamma_s}{L}\frac{\Delta_\theta}{L}\exp\left(-\frac{\Delta_\theta}{L}\right), \tag{19b}$$

where γ_s is the surface energy and $\gamma_{us}^{(u)}$ the unstable stacking energy parameter introduced by Rice (1992), defined as the (maximum) energy attained at the unstable equilibrium configuration in simple shear in the absence of opening displacement. If $\Delta_r = b^*$ in this configuration, then

$$\gamma_{us}^{(u)} = \int_0^{b^*} \tau(\Delta_r, 0)\,\mathrm{d}\Delta_r. \tag{20}$$

For slip along a translation vector of the lattice, such as attends a perfect dislocation, the symmetry of the lattice necesitates $b^* = b/2$. By contrast, the precise value of b^* for slip associated with a partial dislocation does not follow from symmetry considerations alone and requires an atomistic calculation for its determination.

Finally, the assumption of the existence of a joint potential $\Psi(\Delta_r, \Delta_\theta)$ for the traction displacement relations (18*a*) and (18*b*) requires that the Maxwell reciprocal relation

$$\frac{\partial\tau}{\partial\Delta_\theta} = \frac{\partial\sigma}{\partial\Delta_r} \tag{21}$$

be satisfied. In addition, the shear resistance must approach zero as the normal displacement increases to infinity, that is $\tau \to 0$, as $\Delta_\theta \to \infty$. The functions $A(\Delta_\theta)$, $B(\Delta_r)$ and $C(\Delta_r)$ which satisfy these constraints are

$$A(\Delta_\theta) = \frac{\pi\gamma_{us}}{b}\left(1 + \frac{1}{q}\frac{q-p}{1-p}\frac{\Delta_\theta}{L}\right)\exp\left(-\frac{\Delta_\theta}{L}\right), \tag{22a}$$

$$B(\Delta_r) = \frac{2\gamma_s}{L}\left[1 - \frac{q-p}{1-p}\sin^2\left(\frac{\pi\Delta_r}{b}\right)\right], \tag{22b}$$

$$C(\Delta_r) = \frac{2\gamma_s}{L}\frac{p(1-q)}{1-p}\sin^2\left(\frac{\pi\Delta_r}{b}\right), \tag{22c}$$

with

$$q = \frac{\gamma_{us}^{(u)}}{2\gamma_s}, \tag{23a}$$

$$p = \frac{\Delta_\theta^*}{L}. \tag{23b}$$

In these relations, Δ_θ^* is the relaxed opening displacement corresponding to a vanishing normal traction, $\sigma = 0$, at the unstable equilibrium configuration in shear. The parameter p is sometimes referred to as the dilation parameter. The parameters p and q jointly characterize the tension–shear coupling in the traction–displacement relations. The associated tension–shear potential is

$$\Psi(\Delta_r, \Delta_\theta) = 2\gamma_s\left[1 - \left(1 + \frac{\Delta_\theta}{L}\right)\exp\left(-\frac{\Delta_\theta}{L}\right) + \sin^2\left(\frac{\pi\Delta_r}{b}\right)\left(q + \frac{q-p}{1-p}\frac{\Delta_\theta}{L}\right)\exp\left(-\frac{\Delta_\theta}{L}\right)\right]. \tag{24}$$

A similar potential in which $p = q$ was earlier introduced by Needleman (1990) in the context of interfacial debonding. The relaxed unstable stacking energy $\gamma_{us}^{(r)}$ is defined as the energy in the relaxed unstable equilibrium configuration in shear, and it follows from the relation

$$\frac{\gamma_{us}^{(r)} - \gamma_{us}^{(u)}}{\gamma_{us}^{(u)}} = \frac{1-q}{q}\left(1 - \frac{1}{1-p}\exp(-p)\right). \tag{25}$$

In Frenkel's sinusoidal model, the unrelaxed unstable stacking energy $\gamma_{us}^{(u)}$ is given by

$$\gamma_{us}^{(u)} = \frac{\mu b^2}{2\pi^2 h}. \tag{26}$$

However, atomistic calculations using the embedded-atom method (Sun *et al.* 1993) and the density functional theory (Kaxiras and Duesbery 1993) show that eqn. (26) often overestimates $\gamma_{us}^{(u)}$. The values of the unstable stacking energy for Si, Ni_3Al, Fe, Ni and Al calculated from eqn. (26) are given in the table, where the elastic constants at different temperatures are also collected (Simmons and Wang 1971, Curnich 1972). The corresponding values of the unrelaxed unstable stacking energy $\gamma_{us}^{(u)}$ and relaxed unstable stacking energy $\gamma_{us}^{(r)}$ as calculated by Sun *et al.* (1993) and by Kaxiras and Duesbery (1993) are also displayed in the table for comparison. The discrepancies

Material properties.

Material and slip system	T (K)	c_{11} (10^5 MN m^{-2})	c_{12} (10^5 MN m^{-2})	c_{44} (10^5 MN m^{-2})	μ (10^5 MN m^{-2})	c' (10^5 MN m^{-2})	a_0 (Å)	γ_{us}^{sin} (J m^{-2})	$\gamma_{us}^{(r)}$ (J m^{-2})	$\gamma_{us}^{(u)}$ (J m^{-2})	$2\gamma_s$ (J m^{-2})	β	p	q	L/b
Si($\frac{1}{6}$)[$\bar{2}$11](111) (m1)	77·2	1·677	0·650	0·804	0·610	2·064	5·41	1·932	1·91	2·02	3·12	0·96	0·376	0·647	0·156
Si($\frac{1}{2}$)[0$\bar{1}$1](111) (m2)	77·2	1·677	0·650	0·804	0·610	2·064	5·41	1·932	1·67	1·81	2·68	1·07	0·452	0·675	0·144
Ni_3Al($\frac{1}{6}$)[$\bar{2}$11](111) (m3)	—	2·160	1·390	1·240	0·670	3·300	3·57	0·350	0·316	0·348	3·30	1·01	0·140	0·105	0·312
Fe($\frac{1}{2}$)[111](1$\bar{1}$0) (m4)	4·2	2·431	1·381	1·219	0·756	3·125	2·87	1·166	0·438	0·517	3·33	2·25	0·217	0·155	0·187
Fe($\frac{1}{2}$)[$\bar{1}\bar{1}$1](112) (m5)	4·2	2·431	1·381	1·219	0·756	3·125	2·87	1·010	0·497	0·581	3·80	1·74	0·210	0·153	0·215
Ni($\frac{1}{6}$)[$\bar{2}$11](111) (m6)	0	2·612	1·508	1·317	0·807	3·632	3·51	0·414	0·226	0·260	2·87	1·59	0·152	0·091	0·279
Ni($\frac{1}{2}$)[0$\bar{1}$1](111) (m7)	0	2·612	1·508	1·317	0·807	3·632	3·51	1·243	—	1·176	2·87	1·06	0·323	0·410	0·161
Al($\frac{1}{6}$)[$\bar{2}$11](111) (m8)	0	1·143	0·619	0·316	0·280	1·215	4·05	0·166	0·080	0·092	1·13	1·80	0·147	0·081	0·282
Al($\frac{1}{2}$)[0$\bar{1}$1](111) (m9)	0	1·143	0·619	0·316	0·280	1·215	4·05	0·498	—	0·418	1·13	1·19	0·301	0·370	0·163

Fig. 3

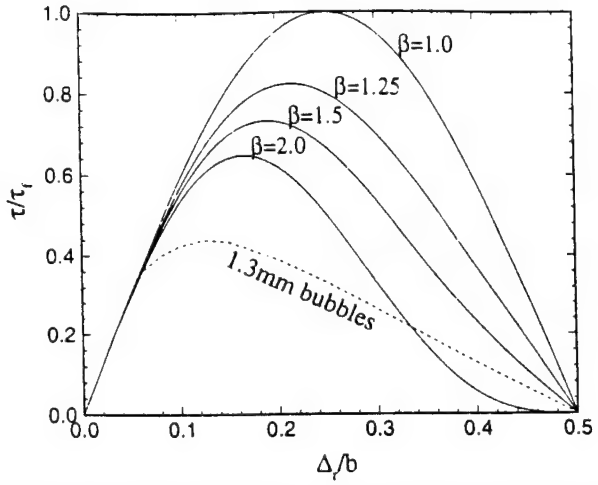

Shear stress τ against shear displacement Δ_r as a function of β.

between eqn. (26) and the atomistic calculations suggest that Frenkel's sinusoidal relation does not model the interlayer shear resistance accurately.

This was recognized by Foreman *et al.* (1951), who noted that the stress required to move a dislocation is usually far less than that which is predicted by the model of Peierls (1940) and Nabarro (1947), which is based on Frenkel's relation. Foreman *et al.* (1951) demonstrated that, when skewed shear resistance profiles are used in the Peierls–Nabarro model, wider dislocation cores are obtained which move at substantially reduced levels of stress. In the present context, modifications of the interlayer potential such as suggested by Foreman *et al.* (1951) will also be found to have a strong effect on activation energies for dislocation emission. We note, parenthetically, that in the well known bubble model of Bragg and Lomer (1949), which has provided a useful analogue for exploring crystal defects and structure in amorphous materials, the interbubble potential is very markedly skewed (Lomer 1949, Shi and Argon 1982).

In order to reflect more realistically the shear resistance properties of materials in the spirit of Foreman *et al.* (1951), and to decouple the unstable stacking energy from the shear modulus, we represent the shear resistance relation by the general Fourier expansion

$$\tau(\Delta_r) = \sum_{n=1}^{\infty} \lambda_n \sin\left(\frac{2n\pi\Delta_r}{b}\right). \tag{27}$$

Evidently, Frenkel's relation (19 *a*) is recovered by retaining only the first component in the expansion. The identification of the Fourier coefficients λ_n of all orders would require a wealth of experimental data or a full atomistic calculation. In all subsequent developments, we shall truncate eqn. (27) beyond the second term, that is we shall presume that $\lambda_n \approx 0$ for $n > 2$. The second term in the expansion furnishes the lowest order correction to the sinusoidal relation and this provides a basis for a systematic investigation of the effect of deviations from Frenkel's model.

The parameters λ_1 and λ_2 in eqn. (27) are readily determined by requiring that the

initial slope match the shear modulus, that is

$$h \left. \frac{\mathrm{d}\tau}{\mathrm{d}\Delta_r} \right|_{\Delta_r = 0} = \mu, \tag{28}$$

and that the unstable stacking energy (20) take a prescribed value. These requirements yield

$$\lambda_1 = \frac{\pi \gamma_{us}^{(u)}}{b}, \tag{29a}$$

$$\lambda_2 = \frac{\pi \gamma_{us}^{(u)}}{b} \frac{1}{2} (\beta - 1). \tag{29b}$$

The new parameter

$$\beta = \frac{\gamma_{us}^{(sin)}}{\gamma_{us}^{(u)}} = \frac{\mu b^2}{2\pi^2 h \gamma_{us}^{(u)}}, \quad 1 \leqslant \beta \leqslant 2, \tag{30}$$

measures the skewness of the function $\tau(\Delta_r)$ and effectively decouples the shear modulus from the unstable stacking energy. Using eqns (29*a*) and (29*b*), eqns (17*a*) and (27) become

$$\tau = \frac{\pi \gamma_{us}^{(u)}}{b} \left[\sin\left(\frac{2\pi\Delta_r}{b}\right) + \frac{\beta - 1}{2} \sin\left(\frac{4\pi\Delta_r}{b}\right) \right], \tag{31a}$$

$$\delta_r = \Delta_r - \frac{b}{2\pi} \frac{1}{\beta} \left[\sin\left(\frac{2\pi\Delta_r}{b}\right) + \frac{\beta - 1}{2} \sin\left(\frac{4\pi\Delta_r}{b}\right) \right]. \tag{31b}$$

Evidently, Frenkel's model is recovered upon setting $\beta = 1$.

Complete traction–displacement relations can be derived following the Beltz–Rice approach as outlined above. The result is

$$\tau(\Delta_r, \Delta_\theta) = A(\Delta_\theta) \left[\sin\left(\frac{2\pi\Delta_r}{b}\right) + \frac{\beta - 1}{2} \sin\left(\frac{4\pi\Delta_r}{b}\right) \right], \tag{32a}$$

$$\sigma(\Delta_r, \Delta_\theta) = \left(B(\Delta_r) \frac{\Delta_\theta}{L} - C(\Delta_r) \right) \exp\left(-\frac{\Delta_\theta}{L} \right), \tag{32b}$$

with

$$A(\Delta_\theta) = \frac{\pi \gamma_{us}}{b} \left(1 + \frac{1}{q} \frac{q - p}{1 - p} \frac{\Delta_\theta}{L} \right) \exp\left(-\frac{\Delta_\theta}{L} \right), \tag{33a}$$

$$B(\Delta_r) = \frac{2\gamma_s}{L} \left\{ 1 - \frac{q - p}{1 - p} \left[\sin^2\left(\frac{\pi\Delta_r}{b}\right) + \frac{\beta - 1}{4} \sin^2\left(\frac{2\pi\Delta_r}{b}\right) \right] \right\}, \tag{33b}$$

$$C(\Delta_r) = \frac{2\gamma_s}{L} \frac{p(1 - q)}{1 - p} \left[\sin^2\left(\frac{\pi\Delta_r}{b}\right) + \frac{\beta - 1}{4} \sin^2\left(\frac{2\pi\Delta_r}{b}\right) \right]. \tag{33c}$$

The corresponding potentials are then

$$\Psi(\Delta_r, \Delta_\theta) = 2\gamma_s \left\{ 1 - \left(1 + \frac{\Delta_\theta}{L} \right) \exp\left(-\frac{\Delta_\theta}{L} \right) + \left[\sin^2\left(\frac{\pi\Delta_r}{b}\right) + \frac{\beta - 1}{4} \sin^2\left(\frac{2\pi\Delta_r}{b}\right) \right] \left(q + \frac{q - p}{1 - p} \frac{\Delta_\theta}{L} \right) \exp\left(-\frac{\Delta_\theta}{L} \right) \right\} \tag{34}$$

and

$$\Phi(\delta_r, \delta_\theta) = \Psi(\Delta_r, \Delta_\theta) - \frac{h}{2\mu}\tau^2(\Delta_r, \Delta_\theta) - \frac{h}{2c}\sigma^2(\Delta_r, \Delta_\theta). \tag{35}$$

The relation between $\gamma_{us}^{(r)}$ and $\gamma_{us}^{(u)}$ is given by eqn. (25) independently of β. The values of p in the table are determined from eqn. (25). For Ni$(\frac{1}{2})[0\bar{1}1](111)$ and Al$(\frac{1}{2})[0\bar{1}1](111)$, the value of $\gamma_{us}^{(r)}$ is not available and p is determined by taking $\gamma_{us}^{(r)}/\gamma_{us}^{(u)} = 0{\cdot}9$, which is roughly in keeping with ratios computed for other materials (Sun *et al.* 1993). For Fe$(\frac{1}{2})[111](1\bar{1}0)$ we obtain the limiting value $\beta = 2$, which signals the largest possible departure from Frenkel's relation. By contrast, we obtain $\beta = 1$ for Si in the glide system $(\frac{1}{6})[\bar{2}11](111)$, in accordance with Frenkel's model. To complete the table, L is determined by matching the uniaxial strain modulus c, which yields the relation

$$L = \left(\frac{2\gamma_s h}{c}\right)^{1/2}. \tag{36}$$

Figures 4 and 5 show the dependence of τ on Δ_r for the materials in the table and the cases $\Delta_\theta = 0$ and $\Delta_\theta = L$ respectively. The tension-softening effect is clearly apparent in fig. 5. It is readily verified that the tension-softening effect is inversely proportional to the value of q, the ratio of the unstable stacking energy to the surface energy. Similarly, figs 6 and 7 show the dependence of σ on Δ_θ for the cases $\Delta_r = 0$ and $\Delta_r = b/2$ respectively. Interestingly, the cohesive strength is also reduced by a shear displacement Δ_r. However, this effect is less pronounced than the reduction of τ by Δ_θ. The strong reciprocal softening effects between shear and tension can ultimately be traced to the existence of an interatomic potential. While the softening of the shear resistance in tension is consistent with intuition, the converse softening of the tensile resistance in shear is less intuitive. Nevertheless, we shall accept the consequences of an interplanar potential and shall not pursue other possible coupling relations.

In closing this section we remark that Rice and Beltz (1994) suggested taking the interplanar spacing h in eqn. (26) as an adjustable parameter in order to relax the relation between the unstable stacking energy and the shear modulus. J. R. Rice (1994 private communication) has devised a two-parameter tension–shear interlayer potential which serves purposes similar to our present modelling.

§ 4. Two-dimensional dislocation nucleation under mode II loading

We begin by considering the simple case of a slip plane which lies in the extension of the plane of the crack. The crack is subjected to pure mode II loading resulting in a stress intensity factor K_{II}. The periodic shear resistance relation (31 *a*) and (31 *b*) is assumed to hold on the slip plane, with λ_1 and λ_2 given by eqns (29 *a*) and (29 *b*) and $\lambda_n = 0$ for $n > 2$. This problem has been investigated by Rice (1992) and Rice and Beltz (1994) for $\beta = 1$. They derived a relation between the inelastic shear displacement at the crack tip, $\delta_{tip} = \delta(0)$, and the applied energy release rate of the form

$$G_{II} = \frac{1-\nu}{2\mu}K_{II}^2 = \Phi(\delta_{tip}) = \int_0^{\delta_{tip}} \tau \, d\delta_r. \tag{37}$$

As G_{II} increases from zero to its maximum value G_{cd}, a stable cluster of distributed edge dislocations form on the slip plane and penetrate into the region ahead of the crack tip. The parameter δ_{tip} then measures the total Burgers vector of the dislocations. Because of the periodicity of the interplanar shear potential, an instability occurs at the critical point $G_{II} = G_{cd} = \gamma_{us}^{(u)}$, $\delta_{tip} = b^*$, beyond which a fully formed straight dislocation is

Fig. 4

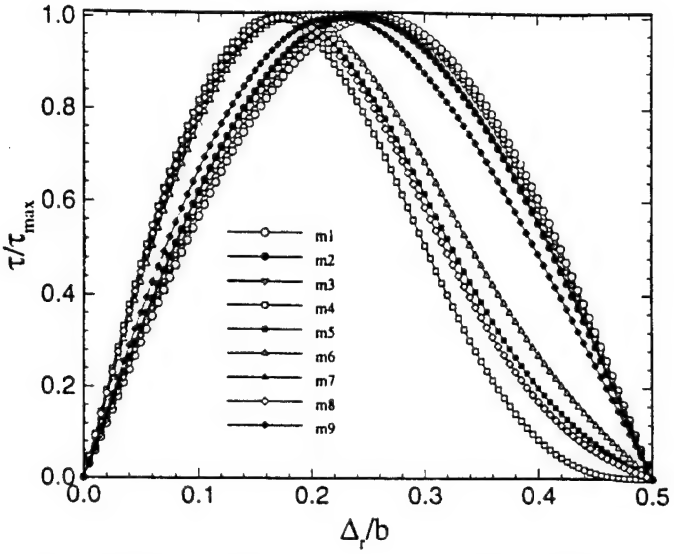

Shear resistance τ against displacement Δ_r for tensile opening displacement $\Delta_\theta = 0$. The nomenclature refers to the table.

Fig. 5

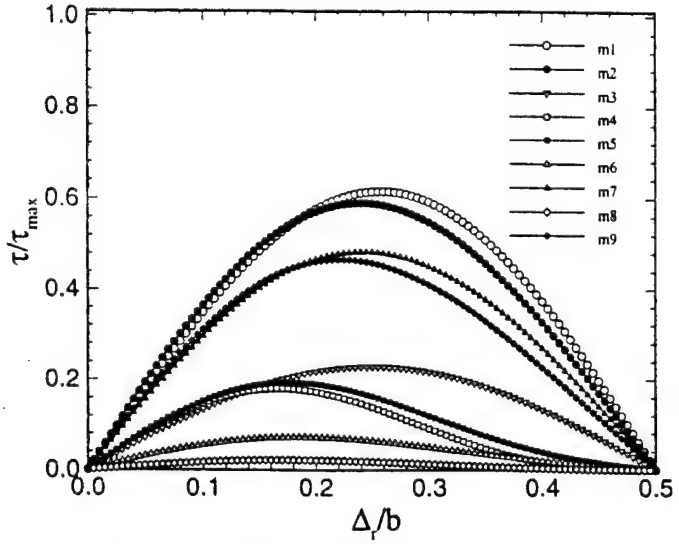

Shear resistance τ against displacement Δ_r for tensile opening displacement $\Delta_\theta = L$. The nomenclature refers to the table.

Fig. 6

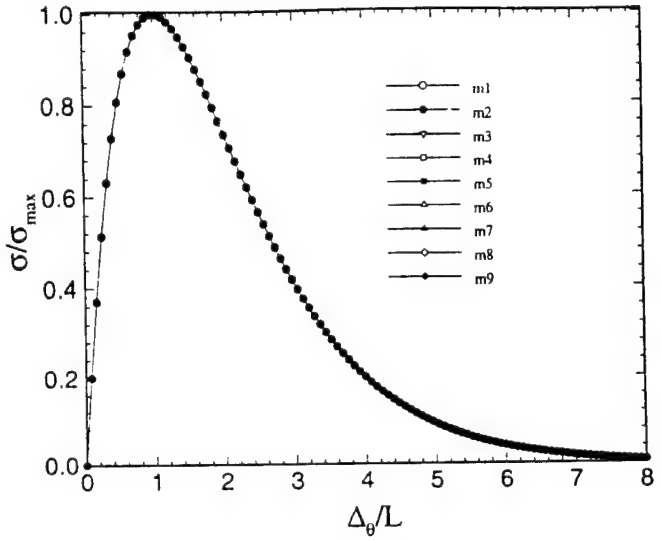

Tensile separation resistance σ against tensile displacement Δ_θ for a shear displacement $\Delta_r = 0$. The nomenclature refers to the table.

Fig. 7

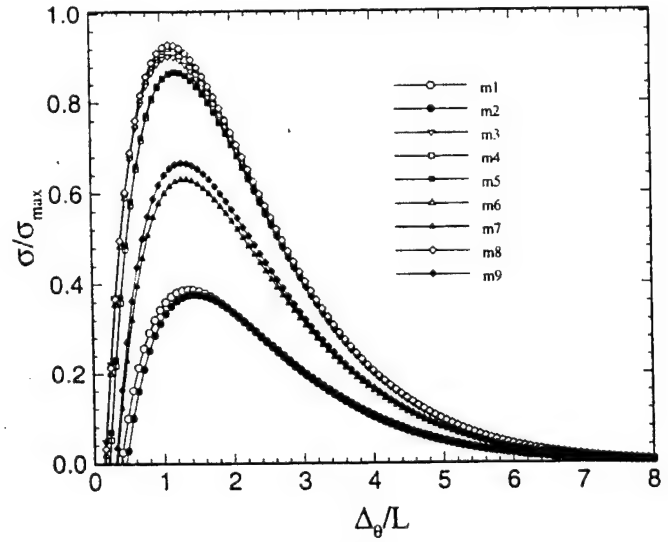

Tensile separation resistance σ against tensile displacement Δ_θ for a shear displacement $\Delta_r = b/2$. The nomenclature refers to the table.

Fig. 8

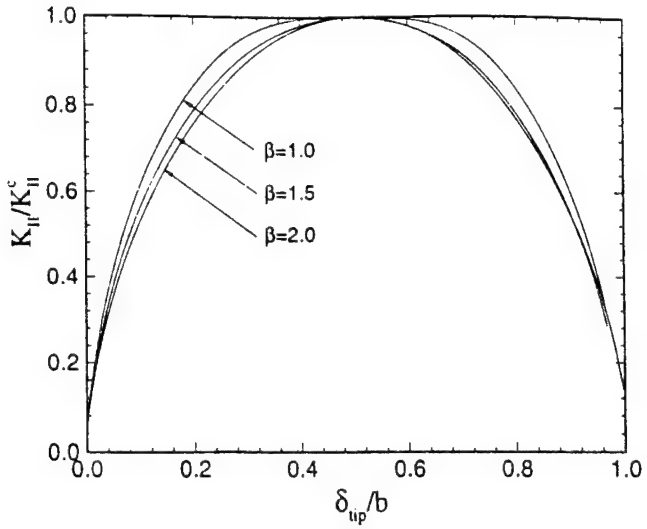

The variation in the inelastic shear displacement δ_{tip} at the crack tip with the applied stress intensity factor K_{II}.

Fig. 9

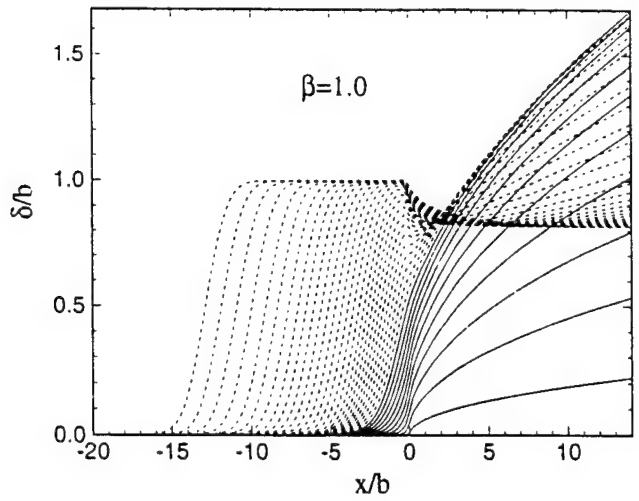

Successive profiles of the emitted dislocation in pure mode II, $\beta = 1{\cdot}0$.

emitted under decreasing G_{II}. It therefore follows that, for any $G_{II} < G_{cd}$, stable and unstable solutions exist corresponding to $\delta_{tip} < b^*$ and $\delta_{tip} > b^*$ respectively. These solutions are separated by an energy barrier

$$\Delta U_{act} = \Pi[\delta_{sad}(\mathbf{x})] - \Pi[\delta_{sta}(\mathbf{x})], \tag{38}$$

where $\Pi[\delta_{sad}(\mathbf{x})]$ and $\Pi[\delta_{sta}(\mathbf{x})]$ are the potential energies at the saddle point and stable equilibrium configurations respectively. ΔU_{act} may also be regarded as the activation energy required for bridging both configurations. In two dimensions, ΔU_{act} is defined necessarily as an energy per unit length.

In our calculations, the Burgers vector b is taken as the normalizing length parameter and Poisson's ratio ν is set to 0·3. Figure 8 shows the variation on δ_{tip} with the applied stress intensity factor K_{II}. The corresponding profile of the dislocation being emitted

Fig. 10

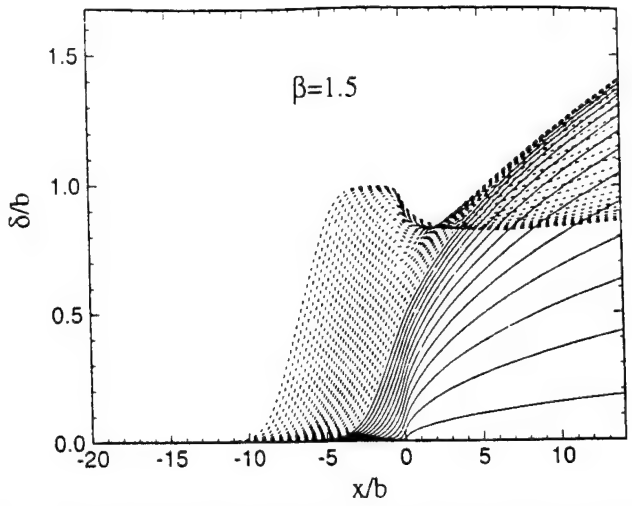

Successive profiles of the emitted dislocation in pure mode II, $\beta = 1{\cdot}5$.

Fig. 11

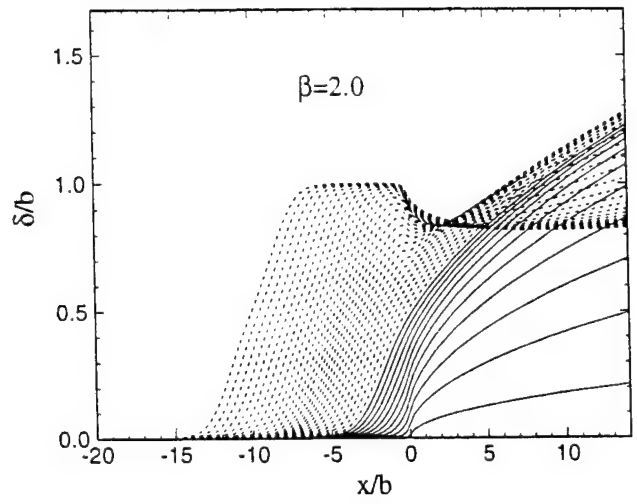

Successive profiles of the emitted dislocation in pure mode II, $\beta = 2$.

is shown in fig. 9 for $\beta = 1$, in fig. 10 for $\beta = 1{\cdot}5$ and in fig. 11 for $\beta = 2$. The solid curves in these figures represent the displacement profiles in the stable equilibrium configurations as G_{II} is increased from zero to G_{cd}. The broken curves correspond to the displacement profiles in the unstable configurations as G_{II} decreases from G_{cd}. The various levels of the opening front can be identified with reference to fig. 8. The unstable stacking energy $\gamma_{us}^{(u)}$ is kept constant in all three cases, which requires μ to be adjusted according to eqn. (30). Interestingly, the core width of the emitted dislocation depends sensitively on β. For large β the displacement distribution at the centre of the dislocation is flatter, in agreement with the results of Foreman *et al.* (1951).

The dependence of the two-dimensional activation energy Δu_{act}^{2D} per unit length on G_{II}/G_{cd} is shown in figs 12 and 13. It is seen from fig 12 that, for the same unstable stacking energy $\gamma_{us}^{(u)}$, the activation energy for dislocation emission increases with increasing β. This implies that the activation energy for dislocation emission does not

Fig. 12

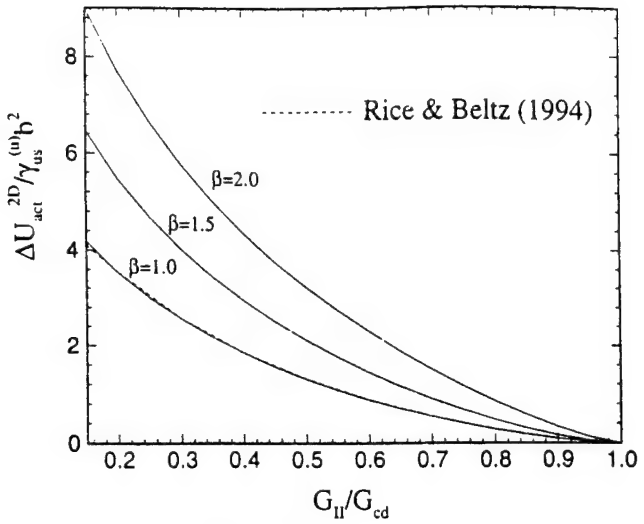

The activation energy per unit length for two-dimensional dislocation emission in pure mode II scaled by unstable stacking energy.

Fig. 13

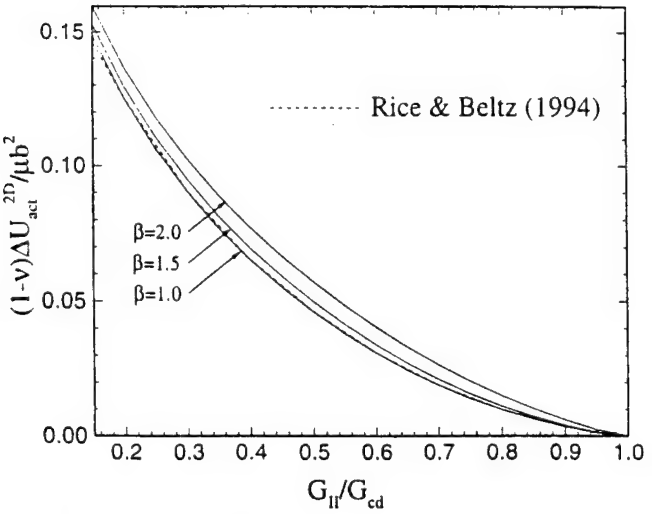

The activation energy per unit length for two-dimensional dislocation emission in pure mode II scaled by line tension.

strictly scale with $\gamma_{us}^{(u)}$ but also depends on the skewness of the shear resistance curve. By contrast, when scaled with the line energy, the activation energy depends less strongly on β as shown in fig. 13. In comparison, the figures also display the analytical results of Rice (1992). The close agreement with our calculations attests to the accuracy of the numerical procedure.

§ 5. Three-dimensional dislocation configurations and activation energies

The preceding two-dimensional analysis artificially restricts the emitted dislocation to be straight. The three-dimensional problem has been investigated by Schöck and Püschl (1991) and Rice and Beltz (1994). However, these analyses also restrict the

geometry of the emitted dislocation, by prescribing its shape to be rectangular (Schöck and Püschl 1991), or by assuming small deviations from the straight configuration (Rice and Beltz 1994). In this section, we present a three-dimensional analysis which allows for arbitrary dislocation shapes. The analysis is based on the numerical procedure outlined in § 2. In order to have a finite domain of analysis, we consider dislocation configurations which are periodic in the direction of the crack front. In this context, the activation energy is understood to be the activation energy per period. While the assumption of periodicity is in itself a geometrical restriction, its influence can be minimized by adopting a period T much larger than the lateral dimension of the protruding dislocation loops, since the interaction energy between the loops dies off quadratically with their separation.

We begin by considering the pure mode II case. Figure 14 shows the mesh used in the three-dimensional analysis. The period of the mesh in the x_2 direction is $T = 24b$. In order to trigger non-straight unstable solutions, a small perturbation of the form

$$\Delta\delta(x_1, x_2) = \varepsilon \cos\left(\frac{2\pi x_2}{T}\right) \exp\left(-\frac{x_1^2}{b^2}\right) \tag{39}$$

is introduced, with $\varepsilon = 0{\cdot}005b$, as the loading parameter G_{II} begins to decrease from the critical value G_{cd}. This type of approach is commonly adopted in post-buckling or post-bifurcation analyses and has been developed by a number of investigators (Koiter 1945, Hutchinson and Koiter 1970, Budiansky 1974). In this context, the most effective imperfection is found to coincide with the most critical buckling mode. In a similar vein, the x_2 dependence of $\Delta\delta$ adopted here is suggested by the analysis of Bower and Ortiz (1990) of unstable crack growth into a region of diminishing toughness, which shows that the long-wavelength distortions of the crack front are the most critical, and by the first-order perturbation analysis of Rice and Beltz (1994), which reveals similar trends. The longest wavelength which is allowed by the present model coincides with the period T of the mesh, which accounts for the term $\cos(2\pi x_2/T)$ in eqn. (39). A more systematic method for determinining the dominant unstable modes is provided by Vineyard's (1957) theory of rate processes. However, Vineyard's theory requires the solution of a full eigenvalue problem obtained by linearization at the critical point, which may be computationally costly, even if a subspace iteration procedure is considered in the manner of Clough and Pluzilu (1975). The simple approach adopted here appears effective, and therefore more rigorous alternatives will not be pursued.

The unstable (saddle-point) equilibrium configurations of the emitted dislocations are depicted in figs 15–18 for decreasing values of G_{II}/G_{cd}. The skewness parameter β is set to unity, which is representative of Si. Figs 19–22 concern the case $\beta = 2$, which is representative of Fe. The curves represent level contours of the ineleastic shear displacement δ_r in the x_1 direction. Remarkably, dislocation emission is seen to take place by the bulging out of a dislocation packet in the form of a 'double kink', which subsequently spreads out along the crack front at decreasing driving force G_{II}/G_{cd}. The kinks spread out more rapidly with increasing β. This effect may be attributable to the larger shear resistance in the direction of emission relative to the case of $\beta = 1$, where the drop of resistance is steeper in the forward direction.

The dependence of the activation energy on G_{II}/G_{cd} is shown in figs 23 and 24. The Rice–Beltz (1994) solution is tangential to the curve $\beta = 1$ at $G_{II}/G_{cd} = 1$ but diverges from it away from the critical point, as expected from the perturbative character of their analysis. By contrast, the Schöck–Püschl (1991) solution is less accurate in the vicinity of the athermal critical point but closer to the curve $\beta = 1$ elsewhere.

Fig. 14

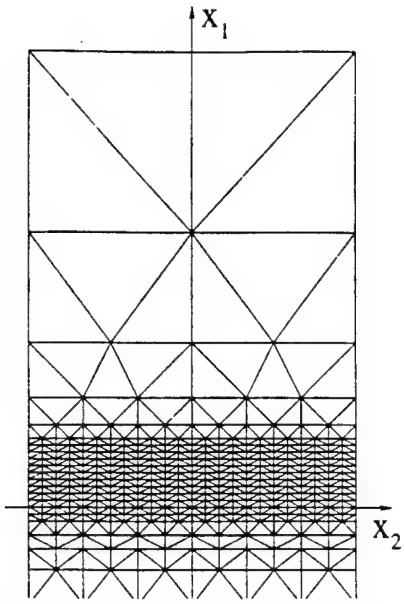

Mesh used in the analysis of three-dimensional dislocation nucleation. The period of the domain is $24b$.

Fig. 15

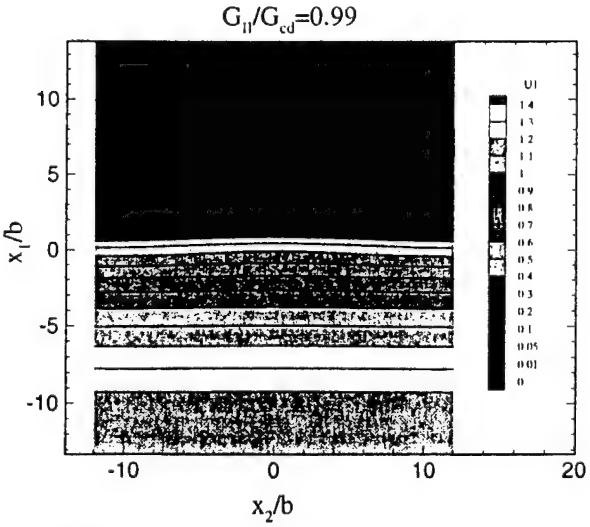

The saddle-point configuration at $G_{II}/G_{cd} = 0{\cdot}99$ in pure mode II loading, $\beta = 1$.

Fig. 16

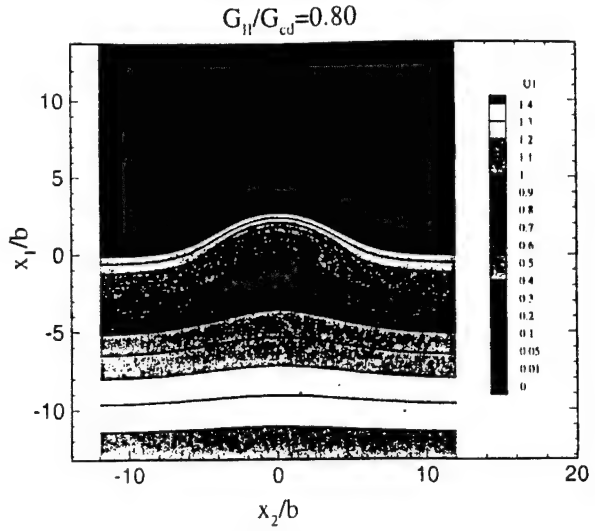

The saddle-point configuration at $G_{II}/G_{cd} = 0{\cdot}80$ in pure mode II loading, $\beta = 1$.

Fig. 17

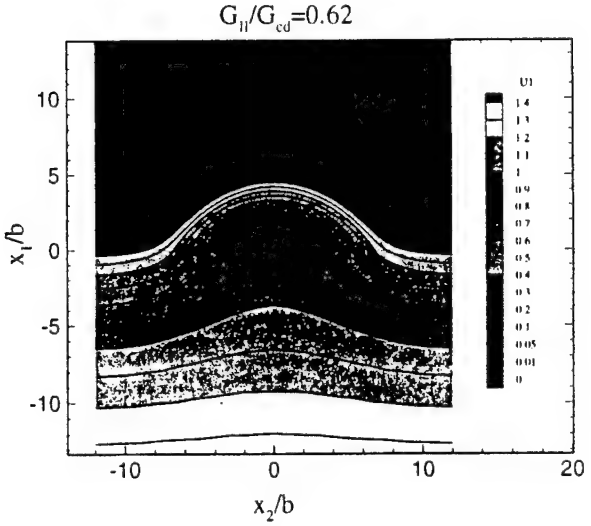

The saddle-point configuration at $G_{II}/G_{cd} = 0{\cdot}62$ in pure mode II loading, $\beta = 1$.

It should be carefully noted that the numerical solution underestimates the activation energy owing to the periodicity of the model and the resulting attraction between neighbouring kinks. This effect can be minimized by increasing the period T. The results are insensitive to T for $G_{II}/G_{cd} > 0{\cdot}5$. The activation energy for nucleating an isolated dislocation loop can be estimated by extrapolating the results from several periods to the limit $T \to \infty$. The result of this extrapolation is shown as the broken curve in fig. 25. From this estimate it may be concluded that a period of $T = 32b$ suffices to approximate closely the activation energy of an isolated dislocation loop over a broad range of G_{II}/ G_{cd}.

Fig. 18

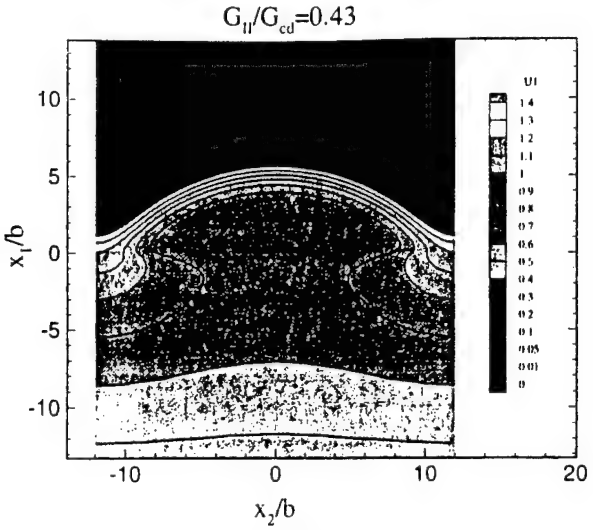

The saddle-point configuration at $G_{II}/G_{cd} = 0{\cdot}43$ in pure mode II loading, $\beta = 1$.

Fig. 19

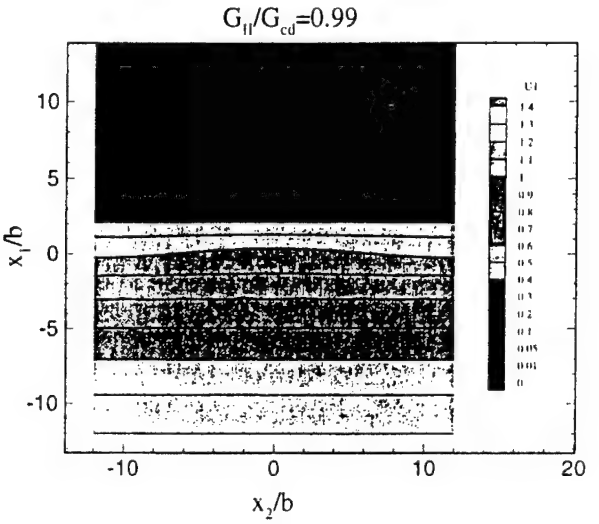

The saddle-point configuration at $G_{II}/G_{cd} = 0{\cdot}99$ in pure mode II loading, $\beta = 2$.

§ 6. Two-dimensional dislocation nucleation under mixed-mode loading

In this section we investigate a case which illustrates the tension-softening effect on dislocation emission. We envision a semi-infinite crack probing on the (112) slip plane of a b.c.c. crystal as shown in fig. 26. The crack front is parallel to the $[1\bar{1}0]$ direction and the Burgers vector is $\frac{1}{2}[\bar{1}\bar{1}1]$, that is perpendicular to the crack front. The crack is subjected to a combination of mode II and mode I loading. The tension–shear coupling constitutive relations (32 *a*), (32 *b*), (33 *a*), (33 *b*) and (33 *c*) are assumed to apply on the slip plane. We set $\beta = 1{\cdot}74$, which is representative of the system $(\frac{1}{2})[\bar{1}\bar{1}1](112)$ of α-Fe, and the remaining parameters are taken from the table.

Figure 27 shows the result of two-dimensional calculations giving the dependence of the critical mode II stress intensity factor K_{IId} for dislocation nucleation on the applied

Fig. 20

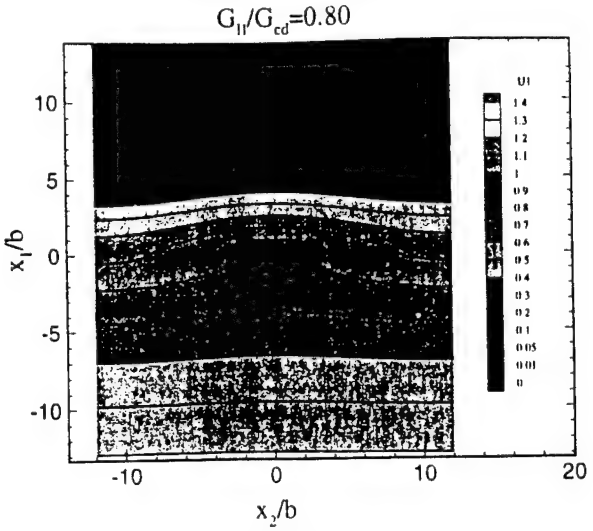

The saddle-point configuration at $G_{II}/G_{cd} = 0{\cdot}80$ in pure mode II loading, $\beta = 2$.

Fig. 21

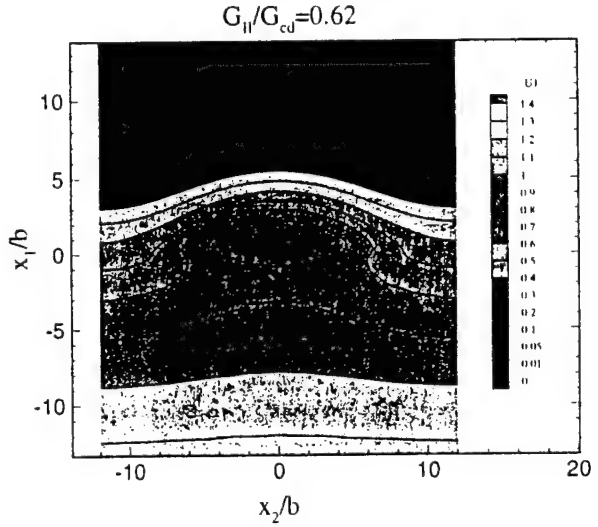

The saddle-point configuration at $G_{II}/G_{cd} = 0{\cdot}62$ in pure mode II loading, $\beta = 2$.

mode I stress intensity factor K_I. The method of analysis is as in § 4. Evidently, the application of mode I loading facilitates dislocation nucleation. However, the effect is small up to values of K_I of the order of 95% of the Griffith cleavage toughness K_{Ic}. The underlying reason for the weak mode I–mode II coupling is apparent in fig. 28, which depicts the sequence of opening and shear displacements for a loading program consisting of an initial increase of K_I from 0 to $0{\cdot}9K_{Ic}$ followed by displacement control in mode II at constant K_I. It is observed in this figure that the opening displacement δ_0 decays rapidly away from the crack front and does not significantly overlap with the dislocation core. This effectively precludes a strong tension–shear coupling except for values of K_I close to K_{Ic}. The broken curves in fig. 28 represent the two-dimensional unstable equilibrium configurations. The inset gives the variation in K_{II} with the crack

Fig. 22

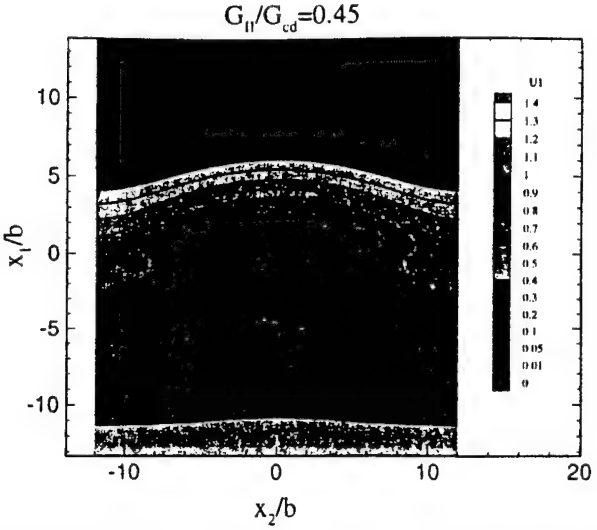

The saddle-point configuration at $G_{II}/G_{cd} = 0{\cdot}45$ in pure mode II loading, $\beta = 2$.

tip inelastic shear displacement at $K_I = 0{\cdot}9K_{Ic}$. The shear instability occurs at the peak of the curve, which determines the critical value K_{IId}. It is interesting to note that K_{IId} exhibits a sharp downturn as K_I approaches K_{Ic}. Our numerical simulations show that, at about $K_I \approx 0{\cdot}95K_{Ic}$, cleavage and dislocation nucleation occur simultaneously and the crack extends in a steady state.

The dependence of the critical energy release rate

$$G_{cd} = \frac{1-\nu}{2\mu}\,[K_I^2 + K_{IId}^2(K_I)] \tag{40}$$

for dislocation emission on the phase angle

$$\psi = \tan^{-1}\left(\frac{K_{IId}(K_I)}{K_I}\right) \tag{41}$$

is shown as the solid curve in fig. 29. For pure mode II loading ($\psi = 90°$), it follows that $G_{cd} = \gamma_{us}^{(r)}$ while, for pure mode I loading ($\psi = 0°$), one has $G_{cd} = 2\gamma_s$. On the basis of a shear-only model, Sun *et al.* (1993) obtained the elegant analytical relation

$$G_{cd} = \frac{\gamma_{us}}{\sin^2\psi} = \frac{1}{\sin^2\psi}\left[\gamma_{us}^{(r)} - \alpha(\gamma_{us}^{(u)} - \gamma_{us}^{(r)})\left(\frac{\pi}{2} - \psi\right)\right], \tag{42}$$

where γ_{us} is an effective unstable stacking energy for mixed-mode loading and α is a reduction coefficient which is determined by fitting the coupled shear-tension results. Equation (42) with $\alpha = 0{\cdot}856$ is plotted as the broken curve in fig. 29. The agreement with the numerical results is remarkably good in the range $\psi \geqslant 20°$.

§ 7. Dislocation nucleation on inclined slip planes

As a cleavage crack is subjected to a mode I loading, a dislocation may nucleate on a slip plane which is inclined to the plane of the crack. Furthermore, the Burgers vector of the dislocation in general will not be perpendicular to the crack front. A case in point concerns a crack lying in the cleavage plane (001) of an α-Fe crystal, its front in the [010] direction, emitting a dislocation of Burgers vector in the $[\bar{1}11]$ direction

Fig. 23

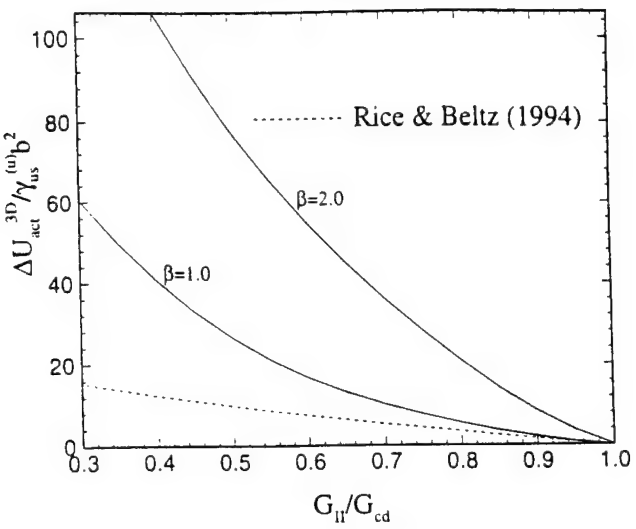

The activation energy for three-dimensional dislocation emission in pure mode II loading scaled by the unstable stacking energy $\gamma_{us}^{(u)}$.

Fig. 24

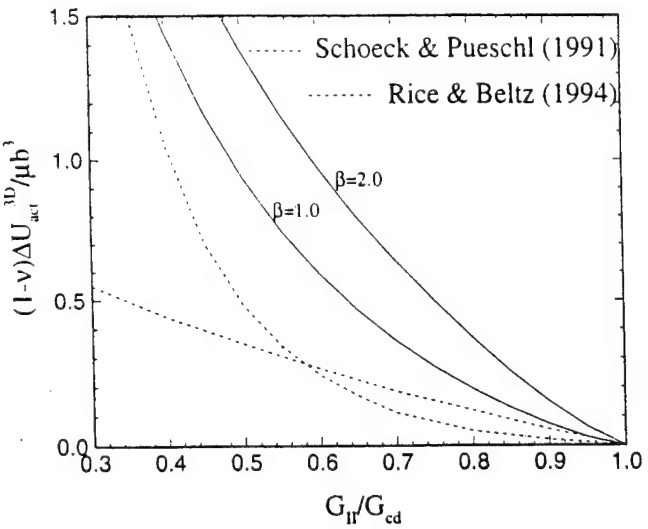

The activation energy for three-dimensional dislocation emission in pure mode II loading scaled by the line tension.

Fig. 25

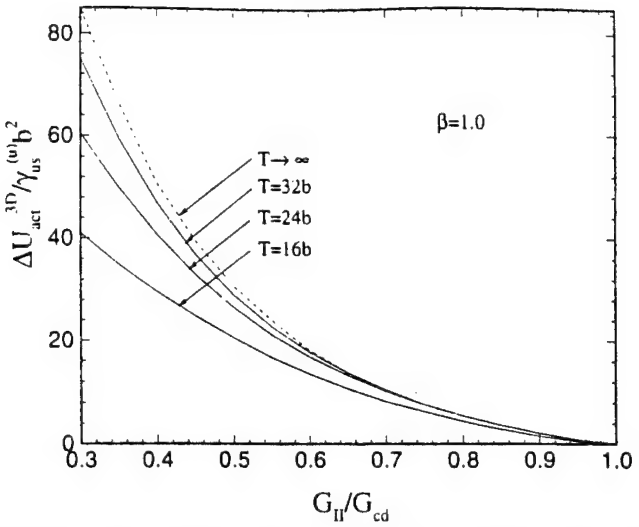

The effect of the size of the periodic cell on the activation energy for three-dimensional dislocation emission in pure mode II loading. The curve for a cell of infinite dimensions is obtained by extrapolation.

on the (101) plane as shown in fig. 30. In general, we shall let θ denote the angle between the slip plane and the crack surface, and ϕ the angle between the Burgers vector and a line perpendicular to the crack front in the slip plane. Using the effective stress intensity factor concept, Rice (1992) estimated the critical energy release rate for dislocation nucleation in two dimensions in an isotropic solid to be

$$G_{cd} = 8\,\frac{1 + (1-\nu)\tan^2\phi}{(1+\cos\theta)\sin^2\theta}\,\gamma_{us}. \tag{43}$$

The condition for the propagation of a cleavage crack is, on the other hand,

$$G_{Ic} = 2\gamma_s. \tag{44}$$

According to these criteria, crack tip blunting by dislocation emission precedes cleavage if $G_{cd} < G_{Ic}$, which requires

$$\frac{\gamma_s}{\gamma_{us}} > 4\,\frac{1 + (1-\nu)\tan^2\phi}{(1+\cos\theta)\sin^2\theta}. \tag{45}$$

Since γ_{us}, which is a measure of interplanar shear resistance, decreases with increasing temperature more rapidly than γ_s does, a condition such as eqn. (45) has the potential for explaining the brittle to ductile transition in intrinsically brittle materials. While the simple criterion (45) may help to explain the observed trends, quantitatively accurate predictions require careful consideration of such effects as tension softening (Sun *et al.* 1993) and the additional resistance due to surface production at the ledge formed when a dislocation is emitted on an inclined slip plane (see the papers by Zhou, Carlsson and Thomson (1994) based on a lattice Green function method, and by Kaxiras and Juan (1994) based on a first-principles approach).

The tension-softening effect can effectively be accounted for through a coupled tension–shear constitutive relation such as that considered in § 3. In order to account for the surface production resistance, we resort to the simple model sketched in fig. 31. Consider a quarter-space block sliding rigidly over a half-plane. Initially, the blocks are

Fig. 26

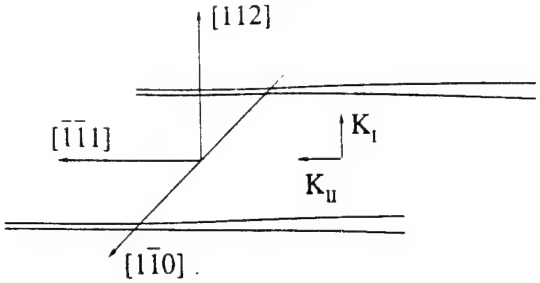

The geometry of a crack under mixed-mode loading.

Fig. 27

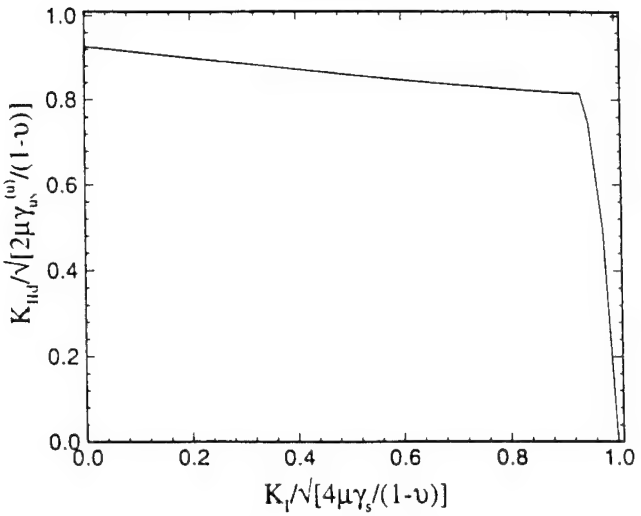

The dependence of the critical K_{II} on K_I for the nucleation of a dislocation in the $\frac{1}{2}[\bar{1}\bar{1}1](112)$ system of α-Fe.

Fig. 28

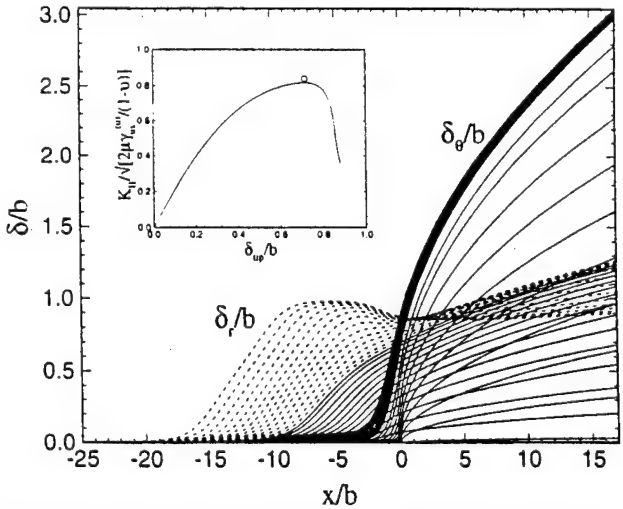

The sequence of shear and opening displacements in mixed-mode loading. K_I is increased from 0 to $0{\cdot}9K_{Ic}$ followed by displacement control in shear. The inset gives the variation in K_{II} with the crack tip inelastic shear displacement at $K_I = 0{\cdot}9K_{Ic}$.

Fig. 29

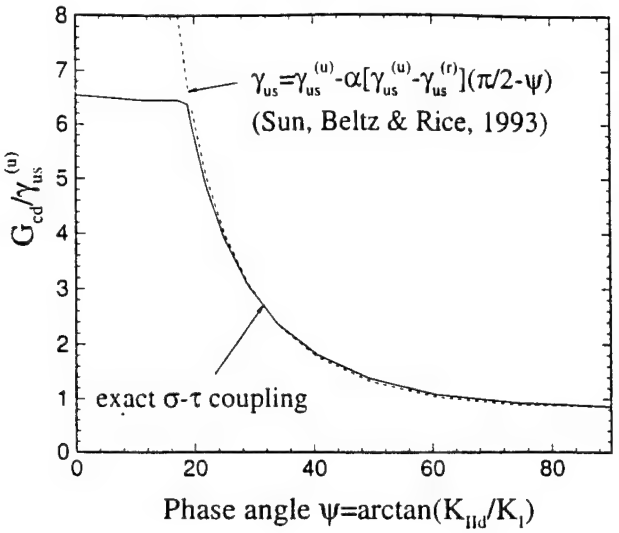

The dependence of the critical energy release rate G_{cd} on the phase angle ψ for dislocation nucleation in the $\frac{1}{2}[\bar{1}\bar{1}1](112)$ system of α-Fe.

Fig. 30

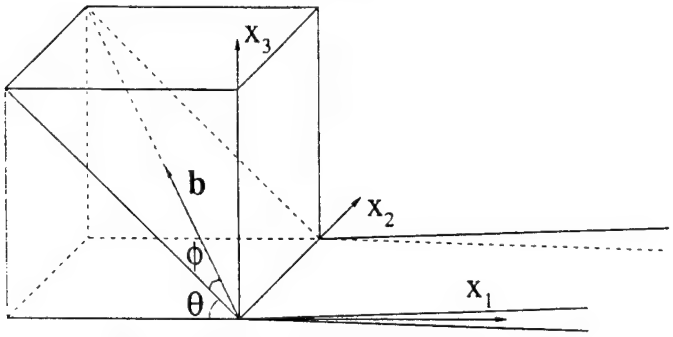

The geometry of a cleavage crack in α-Fe.

Fig. 31

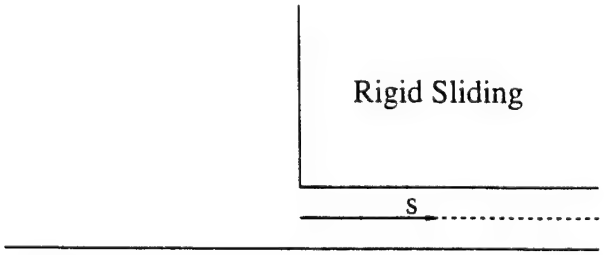

Model of surface production at a corner.

configured so that the free boundary is smooth. As the blocks slide, bonds are severed at the intersection between the slip plane and the free boundary at some expense in energy. We define the surface production resistance τ_s, as the shear resistance in excess of the shear resistance τ_r against slip alone in an infinite crystal. Intuitively, the surface production resistance should decrease rapidly from the corner and become vanishingly small several atomic spacings away from the corner. The work done against this resistance as the two blocks slide by one Burgers vector must equal to $\gamma_s b$, as required by energy conservation, which gives the condition

$$\int_0^\infty \int_0^b \tau_s \, \mathrm{d}\Delta_r \, \mathrm{d}s = \gamma_s b, \tag{46}$$

where s is the distance to the corner. Because of the periodicity of the lattice, τ_s may reasonably be expected to be itself periodic in Δ_r for fixed s. In addition, surface fields are often found to decay exponentially with depth (for example Midlin (1965)). Here again, the precise characterization of τ_s requires atomistic modelling. In lieu of this type of information, we postulate the following form:

$$\tau_s = \frac{\lambda \gamma_s}{b} \exp\left(-\frac{\lambda s}{b}\right)\left[1 - \cos\left(\frac{2\pi\Delta_r}{b}\right)\right], \tag{47}$$

which satisfies all the aforementioned constraints. In eqn. (47), the parameter λ represents the depth of decay of τ_s. In the limit of $\lambda \to \infty$, eqn. (47) reduces to two concentrated loads at $s = 0$, in accordance with the conventional description of surface tension. In the opposite limit of $\lambda \to 0$, the surface production resistance reduces to zero uniformly. The value of λ is expected to be in the range 1–2, and to be larger for covalent materials than for metallic materials. In addition, λ is an as yet unknown function of the inclination ϕ of the slip plane. In view of these uncertainties, we shall treat λ as a parameter and investigate its effect by varying it within its expected range.

We proceed to incorporate the surface shear resistance into a conservative interlayer potential. By definition of τ_s, the total shear resistance τ near the surface is

$$\tau = \tau_r + \tau_s, \tag{48}$$

where τ_r is the shear resistance against slip in an infinite crystal, which we take to be of the form (31 *a*) and τ_s is the excess shear resistance near the free surface, which we take to be of the form (47). Proceeding as in the treatment of the tension–shear coupling given in § 3, we find that

$$\tau(\Delta_r, \Delta_0; s) = A'(\Delta_0; s)\left[\sin\left(\frac{2\pi\Delta_r}{b}\right) + \frac{\beta - 1}{2}\sin\left(\frac{4\pi\Delta_r}{b}\right) + \frac{\rho(s)}{2\pi q} - \frac{\rho(s)}{2\pi q}\cos\left(\frac{2\pi\Delta_r}{b}\right)\right], \tag{49 a}$$

$$\sigma(\Delta_r, \Delta_0; s) = \left[B'(\Delta_r; s)\frac{\Delta_0}{L} - C'(\Delta_r; s)\right]\exp\left(-\frac{\Delta_0}{L}\right) \tag{49 b}$$

and

$$A'(\Delta_0; s) = \frac{\pi\gamma_{us}}{b}\left(1 + \frac{1}{q}\frac{q - p(s)\alpha(s)}{1 - p(s)}\frac{\Delta_0}{L}\right)\exp\left(-\frac{\Delta_0}{L}\right), \tag{50 a}$$

$$B'(\Delta_r; s) = \frac{2\gamma_s}{L}\left\{1 - \frac{q - p(s)\alpha(s)}{1 - p(s)}\left[\sin^2\left(\frac{\pi\Delta_r}{b}\right) + \frac{\beta - 1}{4}\sin^2\left(\frac{2\pi\Delta_r}{b}\right)\right.\right.$$

$$+\frac{\rho(s)}{2q}\frac{\Delta_r}{b}-\frac{\rho(s)}{4\pi q}\sin\left(\frac{2\pi\Delta_r}{b}\right)\Bigg], \tag{50b}$$

$$C'(\Delta_r;s)=\frac{2\gamma_s}{L}\frac{p(s)[\alpha(s)-q]}{1-p(s)}\left[\sin^2\left(\frac{\pi\Delta_r}{b}\right)+\frac{\beta-1}{4}\sin^2\left(\frac{2\pi\Delta_r}{b}\right)\right.$$

$$\left.+\frac{\rho(s)}{2q}\frac{\Delta_r}{b}-\frac{\rho(s)}{4\pi q}\sin\left(\frac{2\pi\Delta_r}{b}\right)\right], \tag{50c}$$

with

$$q=\frac{\gamma_{us}^{(u)}}{2\gamma_s}, \tag{51a}$$

$$\rho(s)=\lambda\exp\left(-\frac{\lambda s}{b}\right), \tag{51b}$$

$$p(s)=\frac{\Delta_\theta^*(s)}{L}, \tag{51c}$$

$$\alpha(s)=\frac{4q}{4q+\rho(s)}. \tag{51d}$$

The corresponding tension–shear potential now becomes

$$\Psi(\Delta_r,\Delta_\theta;s)=2\gamma_s\left\{1-\left(1+\frac{\Delta_\theta}{L}\right)\exp\left(-\frac{\Delta_\theta}{L}\right)\right.$$

$$+\left[\sin^2\left(\frac{\pi\Delta_r}{b}\right)+\frac{\beta-1}{4}\sin^2\left(\frac{2\pi\Delta_r}{b}\right)+\frac{\rho(s)}{2q}\left(\frac{\Delta_r}{b}\right)-\frac{\rho(s)}{4\pi q}\sin\left(\frac{2\pi\Delta_r}{b}\right)\right]$$

$$\left.\times\left(q+\frac{q-p\alpha(s)}{1-p}\frac{\Delta_\theta}{L}\right)\exp\left(-\frac{\Delta_\theta}{L}\right)\right\}. \tag{52}$$

Some limitations of the above model should be carefully noted. For instance, our approach does not explicitly account for the effects of local stress concentrations and reconstruction on the interlayer potential. It might also be more appropriate to replace Δ_r in eqn. (47) by the inelastic displacement δ_r. This, however, complicates the model by, for instance, rendering p coordinate dependent. Since p measures the relaxation of shear resistance as atoms move relative to each other, its effect on dislocation nucleation should decrease as the tensile stress increases. In the simple shear case, the critical energy release rate for dislocation nucleation is lowered by about 10% if relaxation is allowed for (Sun *et al.* 1993). However, this effect may be expected to be lessened in the presence of substantial tension softening, which is always present in situations where dislocation nucleation and cleavage fracture are in competition. For simplicitly, in calculations we have set $p=0$, corresponding to no relaxation.

We begin by considering an idealized configuration in which the Burgers vector is perpendicular to the crack front, that is $\phi=0°$. We set the ratio of Burgers vector to interplanar spacing $b/h=1$, Poisson's ratio $\nu=0{\cdot}3$ and skewness parameter $\beta=1$. Two slip planes at $\theta=45°$ and $\theta=90°$ are considered. The crack is subjected to pure mode I loading resulting in a stress intensity factor K_I. The possible energy release rate from the crack field given by

$$G_I=\frac{1-\nu}{2\mu}K_I^2 \tag{53}$$

Fig. 32

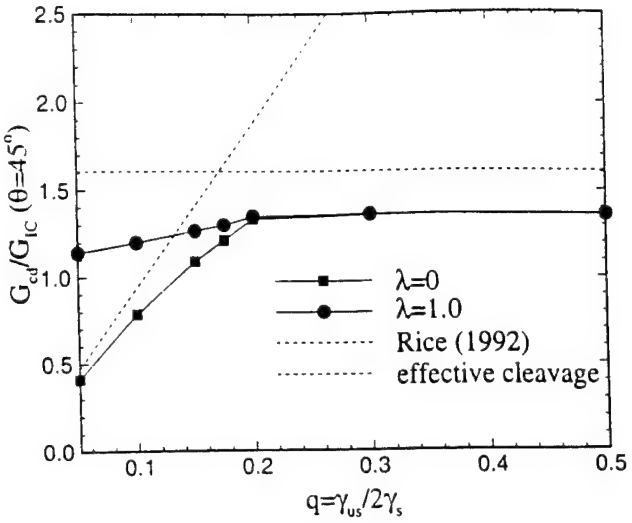

Dependence of the critical energy release rate G_{cd}/G_{Ic} on q for dislocation nucleation at 45°.

furnishes an alternative and more meaningful loading parameter. We note for later reference that the effective stress intensity factors acting on the slip plane are

$$K_{I}^{eff} = K_{I}\cos^{3}\left(\frac{\theta}{2}\right), \tag{54 a}$$

$$K_{II}^{eff} = K_{I}\cos^{2}\left(\frac{\theta}{2}\right)\sin\theta. \tag{54 b}$$

More precisely, K_{I}^{eff} and K_{II}^{eff} are the intensity factors at the tip of a small crack emanating from the crack tip in the direction of the slip plane (Cotterell and Rice 1980).

Figure 32 shows the dependence of the critical energy release rate G_{cd}/G_{Ic} for nucleation at 45° on the parameter $q = \gamma_{us}/2\gamma_s$. We recall that a high ratio G_{cd}/G_{Ic} is indicative of a tendency towards brittle behaviour, while a low value of G_{cd}/G_{Ic} denotes a propensity for ductile behaviour. In addition, a small value of q is expected to favour ductile behaviour, while a large value of q should promote brittle behaviour. These are, indeed, the trends revealed by eqn. (43) (Rice 1992). The expectation is therefore that G_{cd}/G_{Ic} be an increasing function of q. Our results do indeed exhibit this trend as shown in fig. 32. We note, however, that the dependence of G_{cd}/G_{Ic} on q is not linear, as predicted by Rice's approximate relation (43), as a consequence of the tension-softening effect. The departure from proportionality is more severe for large q, where G_{cd}/G_{Ic} reaches asymptotically a constant value. This constant is of the order of the energy release rate G_I/G_{Ic} required to cleave the slip plane, shown in fig. 32 as a broken line. Rice's relation closely matches the computed behaviour for $\lambda = 0$ in the range $q < 0{\cdot}15$. In all cases, however, Rice's relation overestimates G_{cd}/G_{Ic} relative to the computed values.

The effect of the shear resistance to surface production is accounted for in the calculations for $\lambda = 1$ and is neglected in the results for $\lambda = 0$. Interestingly, the surface production shear resistance results in significantly higher values of G_{cd}/G_{Ic} for $q < 0{\cdot}2$ and therefore causes a substantial embrittlement of the material. This result suggests that, even in nominally ductile materials, that is materials with small q, dislocation nucleation on inclined slip planes may not be energetically favoured at low

Fig. 33

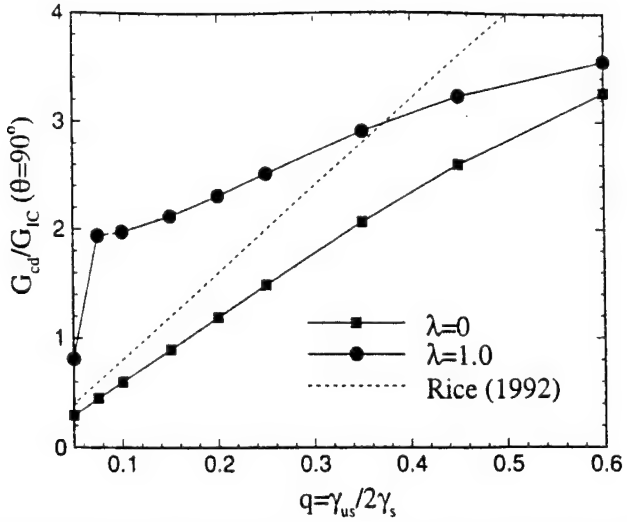

Dependence of the critical energy release rate G_{cd}/G_{Ic} on q for dislocation nucleation at 90°.

Fig. 34

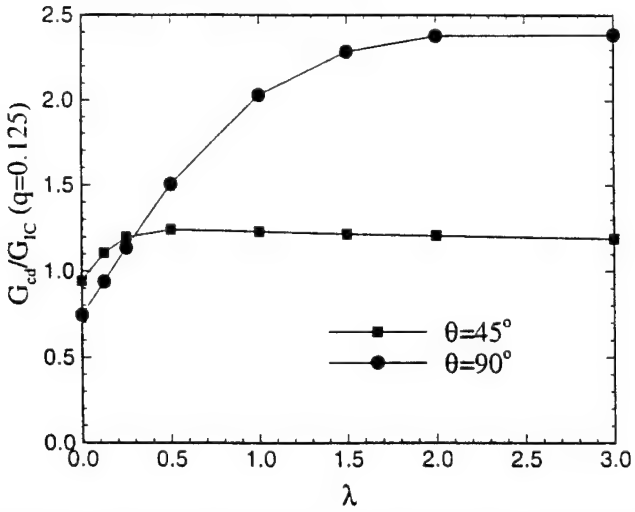

Dependence of the critical energy release rate G_{cd}/G_{Ic} on λ for dislocation nucleation at 45° and 90°.

temperatures. This, in turn, highlights the importance of other dislocation nucleation modes such as nucleation on oblique slip planes and/or inhomogeneous nucleation at the crack front, which have been amply observed experimentally (Chiao and Clarke 1989, Hirsch and Roberts 1991, George and Michot 1993).

Figure 33 shows G_{cd}/G_{Ic} for nucleation on slip planes at 90° as a function of q. While trends similar to the 45° case are evident from the figure, the rate at which the horizontal asymptote is approached is much slower in the 90° case. The result attest to the considerable difficulty in nucleating a dislocation loop at 90° against the surface production resistance.

The effect of the parameter λ on G_{cd}/G_{Ic} is shown in fig. 34 for a typical case of $q = 0{\cdot}125$. As pointed out earlier, the limit of $\lambda \to \infty$ corresponds to a conventional

treatment of surface production through surface tension. This limiting behaviour is ostensibly attained for $\lambda > 0{\cdot}5$ in the case of 45°, and for $\lambda > 2$ in the case 90°. Beyond these values, G_{cd}/G_{1c} is essentially independent of λ.

We conclude this section with a somewhat idealized study of dislocation nucleation in two representative materials, namely α-Fe and Si. For Fe, we consider as before the case of a crack lying in the (001) plane with its front in the [010] direction, emitting a dislocation of Burgers vector $\frac{1}{2}[\bar{1}11]$ on the (101) plane under the action of mode I loading. For Si, we consider the case of a crack lying in the $(\bar{1}10)$ plane with its front in the [110] direction, emitting a dislocation of Burgers vector $\frac{1}{2}[101]$ on the $(\bar{1}11)$ plane also under the action of mode I loading.

In both cases, there are four crystallographically equivalent slip systems converging on the crack tip. We note, however, that simultaneous emission on all four systems is unlikely owing to symmetry-breaking thermal fluctuations and heterogeneities along the crack front. Once a dislocation is nucleated in one system, the attendant stress relaxation makes it more difficult for the remaining dislocations to be emitted, at least while the dominant dislocation remains near the crack front. This scenario is borne out by observation (Chiao and Clarke 1989). We shall therefore adopt the constrained displacement hypothesis of Rice (1992) and Sun *et al.* (1993) according to which displacements, and the attendant shear resistance, take place predominantly in the direction of the dominant Burgers vector. This conjecture finds support in atomistic calculations (Yamaguchi, Vitek and Pope 1981, Sun *et al.* 1991, Kaxiras and Juan 1994).

When slip takes place at an angle $\phi \neq 0°$, corresponding to a Burgers vector which is not normal to the crack front, then condition (46) needs to be replaced by

$$\int_0^\infty \int_0^b \tau_s \, \mathrm{d}\Delta_r \, \mathrm{d}s = \gamma_s b \cos\phi, \tag{55}$$

and accordingly the surface production resistance relation (47) becomes

$$\tau_s = \frac{\lambda\gamma_s}{b} \exp\left(-\frac{\lambda s}{b}\right) \cos\phi \left[1 - \cos\left(\frac{2\pi\Delta_r}{b}\right)\right]. \tag{56}$$

As required, $\tau_s = 0$ when $\phi = 90°$. This corresponds to slip parallel to the crack front, which entails no surface production.

The material constants necessary to evaluate these two cases are taken from the table, except that p is set to 0. The calculated dislocation nucleation conditions for α-Fe and Si are $G_{cd}/G_{1c} = 1{\cdot}42$ and $G_{cd}/G_{1c} = 1{\cdot}23$ respectively. These are in good agreement with the results of the simulations of Sun *et al.* (1993). The calculations should be relatively insensitive to the choice of λ in view of the high tensile stresses and relatively large $\gamma_{us}/2\gamma_s$ ratios which are involved in both cases. Our results suggest that α-Fe and Si would be intrinsically brittle if dislocation nucleation were possible only on the inclined slip systems considered in the analysis. Further consideration of dislocation nucleation on oblique slip planes is required in order to strengthen these conclusions. It seems appropriate to emphasize at this point that, even if a material is not intrinsically brittle as regards the competition between dislocation emission and cleavage, other rate-limiting effects such as inadequate dislocation mobility away from the crack tip may cause the material to behave in a brittle manner. These effects are observed to play a particularly significant role in intermetallic compounds and semiconductor materials in which dislocation mobility is sluggish. Further large-scale

atomistic simulations and discriminating experimental studies are needed for developing a satisfactory understanding of these processes.

§ 8. Discussion

In the present paper we have employed the variational boundary integral method of Xu and Ortiz (1993) to study dislocation nucleation from atomically sharp cracks under combined mode I–mode II loading. In addition, we have extended the tension–shear potential of Rice *et al.* (1992) so as to allow for skewness of the shear resistance curve and to incorporate a surface production resistance which accompanies ledge formation. As a consequence of the skewness effect, our potential decouples the unstable stacking energy from the shear modulus.

Our simulations of dislocation nucleation in two dimensions using a sinusoidal shear resistance are in full agreement with the analytical results of Rice and Beltz (1994), which attests to the accuracy of the numerical procedure. With a shear resistance curve appropriately skewed so as to represent Fe, we find significant departures from the results based on Frenkel's sinusoidal relation, particularly as regards activation energies normalized by the unstable stacking energy. However, a considerable convergence of results is obtained where activation energies are normalized by line tension.

Our three-dimensional simulations of dislocation nucleation under pure mode II loading yield dislocation configurations which closely match the first-order perturbation results of Rice and Beltz (1994) near the critical point $G_{II} = G_{cd}$, that is in the range of validity of the perturbation analysis. However, the computed dislocation configurations depart sharply from the Rice–Beltz solution elsewhere. We find that the Schöck–Püschl (1991) unrelaxed approximate solution qualitatively captures the overall trends revealed by our analysis. When a mode I component is added to the loading, we find that tension softening facilitates dislocation nucleation, although significantly so only when K_I exceeds $0{\cdot}95K_{Ic}$.

Our simulations show that dislocation nucleation on inclined slip planes under mode I loading is impeded by surface production resistance, especially for low unstable stacking-energy–surface-energy ratios. For large ratios, tension softening is the dominant effect. Calculations tailored to α-Fe and Si suggest that dislocation emission on inclined slip planes is not operative at low temperatures.

The recent developments initiated by Rice and Beltz and by Schöck and Püschl have established that the activation configuration of a dislocation nucleating from the tip of a cleavage crack is made up of a fractional dislocation core, and that as a result the large discrepancy that existed in the energy predictions of the original Rice–Thompson (1974) model has been radically reduced. While the results of the present analysis, still based on continuum line notions of dislocations given in fig. 23 and fig. 24 are somewhat less favourable than those of either the Rice–Beltz (1994) or the Schöck–Püschl (1991) models, none of these has yet been able to close the gap.

To demonstrate the magnitude of the remaining gap, we consider the brittle-to-ductile transition as a thermally activated dislocation nucleation event, for which the event probability should scale with a given ratio of $\Delta U_{act}/kT$ as follows:

$$\frac{\Delta U_{act}}{kT} = \frac{\alpha\mu b^3}{(1-\nu)kT} = C, \tag{57}$$

where C depends on the particular scenario of the brittle to ductile transition event and is typically of the order of 10 as we show for a specific case in the Appendix, and where

α will depend on G_{II}/G_{cd} as given in fig. 24. We note that for a material such as α-Fe, where nucleation of a dislocation loop at the crack tip may indeed be the key event,

$$\frac{\mu b^3}{(1-\nu)k} \approx \frac{\mu_0 b^3}{(1-\nu)k}\left(1-\eta\frac{T}{T_m}\right). \tag{58}$$

In eqn. (58) we have taken note of the temperature dependence of the shear modulus in a first-order sense with η, typically being 0·5, where T_m is the melting point. For α-Fe, $\mu_0 b^3/(1-\upsilon)k \equiv T_0 = 1{\cdot}2 \times 10^5$ K, and $T_m = 1809$ K. Then the expected brittle-to-ductile transition temperature T_{BD} is related to $\alpha(G_{II}/G_{cd})$ by

$$\frac{T_{BD}}{T_0} = \left(\frac{C}{\alpha} + \eta\frac{T_0}{T_m}\right)^{-1}. \tag{59}$$

The results in fig. 24 do not consider the effect of tension–shear coupling nor the surface production resistance for nucleation on inclined slip planes. Not withstanding these reservations, it is interesting to estimate the T_{BD} for the arrest of a propagating cleavage crack. As we demonstrate in the Appendix for a realistic case of nucleation of a loop on a {112} plane where $G_{II}/G_{cd} = 0{\cdot}593$, the T_{BD} necessary to arrest a cleavage crack propagating with a velocity of, say, 1 cm s^{-1} on a (100) cleave should be 2630 K, or roughly a factor of ten above experimental expectations of -10°C.

While the present form of continuum analysis using the Peierls approach on the inclined planes could incorporate additional refinements such as anisotropy of the crystal and the actual geometry of the active Burgers vector in the slip plane, these are unlikely to be decisive. The present results have already demonstrated that the actual governing conditions must apply on the oblique slip planes where the surface production plays a smaller role and are most probably influenced by local heterogeneities as most of the experimental observations have indicated. Such analyses are now in progress. It is clear, however, that the final gap can only be closed by resorting to fully atomistic approaches for which the present method of analysis can furnish initial coordinates for the atoms making up the saddle-point configuration. Nevertheless, it is clear that a certain phase of the brittle to ductile transition in cleavage fracture which is controlled by dislocation nucleation as should be the case in b.c.c. metals (where the lattice resistance is governed by double kink nucleation and not by kink mobility) is now quite well understood, at least, semiquantitatively.

Acknowledgments

This research was supported by the Office of Naval Research (ONR) under Contract No. N00014-92-J-4022. M.O. gratefully acknowledges support from the ONR under Contract No. N00014-90-J-1758. We acknowledge a number of fruitful discussions with Professor J. R. Rice and Professor E. Kaxiras of Harvard University and Dr R. Thomson of the National Institute of Standards and Technology. The computations were carried out with the facilities of the Mechanics of Materials group at the Massuchusetts Institute of Technology and those of the Solid Mechanics group at Brown University. Moreover, G.X. gratefully acknowledges also the earlier guidance of Professor R. J. Clifton of Brown University on fracture on the atomic scale.

APPENDIX

Estimate of the brittle-to-ductile transition temperature

It is of interest to evaluate the present findings in terms of their predictive capability for the estimation of the brittle-to-ductile transition temperature, for example in α-Fe.

A number of different scenarios can be constructed to describe a brittle-to-ductile transition. We consider here a relatively precise process described by Argon (1987) in which a brittle cleavage crack in α-Fe propagates up a temperature gradient with a given constant velocity v until at a certain temperature T_{BD} it is arrested by a cascade of ductile processes initiated by the critical event of nucleation of a dislocation loop (or segment) from the crack tip. In this scenario the probability of activation of a transition event must be equal to the Mach number $m = v/c$ (c is the velocity of a sound wave) of a propagating crack, that is

$$\exp\left(-\frac{\Delta U_{act}}{kT_{BD}}\right) = m = \frac{v}{c}. \tag{A 1}$$

Thus

$$\frac{\Delta U_{act}}{kT_{BD}} = \frac{\alpha\mu b^3}{(1-\nu)kT_{BD}} = C = \ln\left(\frac{1}{m}\right), \tag{A 2}$$

where $\alpha = \alpha(G_{II}/G_{cd})$ is given in fig. 24 for $\beta = 2{\cdot}0$ (appropriate for α-Fe).

If account is also taken of the temperature dependence of the shear modulus of iron to first order effects through

$$\mu = \mu_0\left(1 - \eta\frac{T}{T_m}\right), \tag{A 3}$$

where μ_0 is the shear modulus at 0 K and η is typically of the order 0·5 for most metals, we find that

$$T_{BD} = T_0\left(\frac{\ln(1/m)}{\alpha} + \eta\frac{T_0}{T_m}\right)^{-1}, \tag{A 4}$$

where $T_0 \equiv \mu b^3/(1-\upsilon) = 1{\cdot}2 \times 10^5$ K and $T_m = 1809$ K for α-Fe.

We consider now the critical loop nucleation event to occur on the {112} plane for a (001) cleavage crack propagating in a ⟨001⟩ direction under a crack driving force $G_I = G_{Ic} = 2\gamma_s$. For such a crack the momentary driving force $G_{II}(\theta)$ probing the {112} slip plane should be given by

$$\frac{G_{II}(\theta)}{G_{Ic}} = \frac{K_{II}^2(\theta)}{K_{Ic}^2} = (\tilde{\sigma}^{I}_{r\theta}(\theta))^2 \tag{A 5}$$

where $\tilde{\sigma}^{I}_{r\theta}(\theta)$ is the angular factor for a mode I crack, and $\theta = 35{\cdot}2°$ for the {112} plane under consideration, for which $\tilde{\sigma}^{I}_{r\theta}(\theta) = 0{\cdot}275$. Taking $G_{cd} = \gamma_{us}^{(r)} = 0{\cdot}497\ \mathrm{J\,m^{-2}}$ (table) and $\gamma_s = 1{\cdot}95\ \mathrm{J\,m^{-2}}$ (Hirth and Lothe 1982), we estimate the driving force ratio G_{II}/G_{cd} for nucleation of a critical configuration on the inclined (112) plane to be

$$\frac{G_{II}}{G_{cd}} = \frac{G_{II}}{G_{Ic}}\frac{G_{Ic}}{G_{cd}} = (\tilde{\sigma}^{I}_{r\theta}(\theta))^2\frac{2\gamma_s}{\gamma_{us}^{(r)}} = 0{\cdot}593. \tag{A 6}$$

From fig. 24 for $\beta = 2{\cdot}0$ we determine that $\alpha = \Delta U_{act}(1-\upsilon)/\mu b^3 = 1{\cdot}0$ for the above estimate of the driving force ratio. Taking $m = 4 \times 10^{-6}$, that is $v = 1\ \mathrm{cm\,s^{-1}}$ we

calculated for $T_{BD} = 2630$ K from eqn. (A 4). This is roughly a factor of ten too high in relation to an experimental temperature that should be around -10°C.

References

ARGON, A. S., 1987, *Acta metall.*, **35,** 185.

ARMSTRONG, R. W., 1966, *Mater. Sci. Engng*, **1,** 251.

BELTZ, G. E., and RICE, J. R., 1991, *Modeling the Deformation of Crystalline Solids: Physical Theory, Application and Experimental Comparisons*, edited by T. C. Lowe, A. D. Rollett, P. S. Follansbee and G. S. Daehn (Warrendale, Pennsylvania: Metallurgical Society of AIME), p. 457.

BOWER, A. F., and ORTIZ, M., 1990, *J. Mech. Phys. Solids*, **38,** 443.

BRAGG, W. L., and LOMER, W. M., 1949, *Proc. R. Soc.* A, **196,** 171.

BREDE, M., and HAASEN, P., 1988, *Acta metall.*, **36,** 2003.

BUDIANSKY, B., 1974, *Advances in Applied Mechanics*, Vol. 14, edited by C.-S. Yih (New York: Academic Press), pp. 1–144.

BULATOV, V. V., YIP, S., and ARGON, A. S., 1995, *Phil. Mag.*, A, **72,** 453.

CHIAO, Y.-H., and CLARKE, D. R., 1989, *Acta Metall.*, **47,** 203.

CLOUGH, R. W., and PLUZILU, J., 1975, *Dynamics of Structures* (New York: McGraw-Hill).

COTTERELL, B., and RICE, J. R., 1980, *Int. J. Fract.*, **16,** 155.

CURNICH, L. R., 1972, Ph.D. Thesis, University of Minnesota.

FOREMAN, A. J., JASWON, M. A., and WOOD, J. K., 1951, *Proc. phys. Soc.* A, **64,** 156.

GEORGE, A., and MICHOT, G., 1993, *Mater. Sci. Engng*, A, **164,** 118.

HUTCHINSON, J. W., and KOITER, W. T., 1970, *Appl. Mech. Rev.*, **23,** 1353.

HIRSCH, P. B., and ROBERTS, S. G., 1991, *Phil. Mag.* A, **64,** 1353.

HIRSCH, P. B., SAMUELS, J., and ROBERTS, S. G., 1989, *Proc. R. Soc.* A, **421,** 25.

HIRTH, J. P., and LOTHE, J., 1982, *Theory of Dislocations* (New York: McGraw-Hill).

KAXIRAS, E., and DUESBERY, M. S., 1993, *Phys. Rev. Lett.*, **70,** 3752.

KAXIRAS, E., and JUAN, Y., 1994, (to be published).

KELLY, A., TYSON, W. R., and COTTRELL, A. H., 1967, *Phil. Mag.*, **15,** 567.

KOITER, W. T., 1945, Ph.D. Thesis, University of Delft.

LOMER, W. M., 1949, *Proc. R. Soc.* A, **196,** 182.

MIDLIN, R. D., 1965, *Int. J. Solids Struct.*, **1,** 417.

NABARRO, F. R. N., 1947, *Proc. phys. Soc.* A, **59,** 256.

NEEDLEMAN, A., 1990, *J. Mech. Phys. Solids*, **38,** 289.

PEIERLS, R. E., 1940, *Proc. phys. Soc.* A, **52,** 34.

RICE, J. R., 1992, *J. Mech. Phys. Solids.*, **40,** 235.

RICE, J. R., and BELTZ, G. E., 1994, *J. Mech. Phys. Solids*, **42,** 333.

RICE, J. R., BELTZ, G. E., and SUN, Y., 1992, *Topics in Fracture and Fatigue*, edited by A. S. Argon (Berlin: Springer), p. 1.

RICE, J. R., and THOMSON, R., 1974, *Phil. Mag.*, **29,** 73.

ROSE, J. H., FERRANTE, J., and SMITH, J. R., 1981, *Phys. Rev. Lett.*, **47,** 675.

SAMUELS, J., and ROBERTS, S. G., 1989, *Proc. R. Soc.* A, **421,** 1.

SCHÖCK, G., 1991, *Phil. Mag.* A, **63,** 111.

SCHÖCK, G., and PÜSCHL, W., 1991, *Phil. Mag.* A, **64,** 931.

SHI, L.-T., and ARGON, A. S., 1982, *Phil. Mag.* A, **46,** 255.

SIMMONS, G., and WANG, H., 1971, *Single Crystal Elastic Constants and Calculated Aggregate Peoperties* (Cambridge, Massachusetts; MIT Press).

SUN, Y., BELTZ, G. E., and RICE, J. R., 1993, *Mater. Sci. Engng.* A, **170,** 67.

SUN, Y., RICE, J. R., and TRUSKINOVSKY, L., 1991, *High-Temperature Ordered Intermetallic Alloys IV*, Materials Research Society Symposium Proceedings, Vol. 213, edited by L. A. Johnson, D. T. Pope and J. O. Stiegler (Pittsburgh, Pennsylvania: Materials Research Society), p. 243.

ST JOHN, C., 1975, *Phil. Mag.*, **32,** 1193.

VINEYARD, G. H., 1957, *Phys. Chem. Solids*, **3,** 121.

XU, G., and ORTIZ, M., 1993, *Int. J. numer. Methods in Engng*, **36,** 3675.

YAMAGUCHI, M., VITEK, V., and POPE, D., 1981, *Phil. Mag.* A, **43,** 1027.

ZHOU, S. J., CARLSSON, A. E., and THOMSON, R., 1994, *Phys. Rev. Lett.*, **72,** 852.

REPORT DOCUMENTATION PAGE

Form Approved
OMB No. 0704-0188

1. AGENCY USE ONLY (Leave blank)	2. REPORT DATE	3. REPORT TYPE AND DATES COVERED
	May 22, 1997	Final: 9/1/1992-11/30/1995

4. TITLE AND SUBTITLE
Development of a Variational Boundary Integral Method for the Analysis of Fully Three Dimensional Crack Advance Problems

5. FUNDING NUMBERS
C-N00014-92-J-4022

6. AUTHOR(S)
Guanshui Xu, Ali S. Argon, Michael Ortiz, and Allan Bower

7. PERFORMING ORGANIZATION NAME(S) AND ADDRESS(ES)
Massachusetts Institute of Technology
Room 1-306
Cambridge, MA 02139 (A.S. Argon)

8. PERFORMING ORGANIZATION REPORT NUMBER
1-3

9. SPONSORING/MONITORING AGENCY NAME(S) AND ADDRESS(ES)
ONR Solid Mechanics Program (Attn: Dr. R. Barsoum)
ONR Code 1132
800 N. Quincy Street - Ballston Tower 1
Arlington, VA 22217-5000

10. SPONSORING/MONITORING AGENCY REPORT NUMBER

11. SUPPLEMENTARY NOTES
Paper published in "Computational Mechanics '95", edited by S.N. Atluri G. Yagawa, and T.A. Cruze Springer: Berlin, vol. 2, pp 2874-2889 (1995)

12a. DISTRIBUTION/AVAILABILITY STATEMENT
Unlimited

12b. DISTRIBUTION CODE

13. ABSTRACT *(Maximum 200 words)*

A variational boundary integral method is developed for the analysis of three dimensional cracks of arbitrary geometry in both isotropic and anisotropic elastic solids. By representing the opening displacements of the crack as continuous distributions of infinitesimal dislocation loops and minimizing the corresponding potential energy of the solid, the kernels of the governing integral equations acquire milder singularities of type 1/R, and the resulting system of the equations is symmetric. The applicability of the method and the performance of the numerical scheme are demonstrated by a selection of examples. Based on the proposed integral equations, a first order perturbation method was developed for the analysis of instabilities of an initial planar semi-infinite crack growing subject to combined mode I and mode III loading. The full-field numerical simulations compare well with the predictions of the perturbation theory and with experimentally observed characteristic patterns of brittle fracture surface. The method has also been used to study the three dimensional aspects of toughening mechanisms including crack trapping, bridging and debonding in fiber reinforced brittle matrix composites. The extension of the method proves to be a very powerful and flexible tool in studies of nucleation of dislocations from crack tips on the atomic scale in fully three dimensional forms. These studies have provided straightforward solutions of several key problems such as determination of saddle point configurations of dislocation loops on both inclined and oblique slip planes for thermally assisted emission, and calculation of thermal activation energies for nucleation of embryonic dislocation loops as a function of crack front driving force.

14. SUBJECT TERMS
A comprehensive discussion of application areas of a variational boundary integral method of analysis

15. NUMBER OF PAGES
13

16. PRICE CODE

17. SECURITY CLASSIFICATION OF REPORT	18. SECURITY CLASSIFICATION OF THIS PAGE	19. SECURITY CLASSIFICATION OF ABSTRACT	20. LIMITATION OF ABSTRACT
Unclassified	Unclassified	Unclassified	None

in "Computational Mechanics '95", edited by S. N. Atluri, G. Yagawa and T. A. Cruse, (Springer: Berlin), vol 2, pp. 2874-2889 (1995).

Development of a Variational Boundary Integral Method for the Analysis of Fully Three Dimensional Crack Advance Problems

Guanshui Xu and Ali S. Argon

Department of Mechanical Engineering, M. I. T.
Cambridge, MA 02139

Michael Ortiz and Allan Bower

Division of Engineering, Brown University
Providence, RI 02912

Abstract

A variational boundary integral method is developed for the analysis of three dimensional cracks of arbitrary geometry in both isotropic and anisotropic elastic solids. By representing the opening displacements of the crack as continuous distributions of infinitesimal dislocation loops and minimizing the corresponding potential energy of the solid, the kernels of the governing integral equations acquire milder singularities of type $1/R$, and the resulting system of the equations is symmetric. The applicability of the method and the performance of the numerical scheme are demonstrated by a selection of examples. Based on the proposed integral equations, a first order perturbation method was developed for the analysis of instabilities of an initial planar semi-infinite crack growing subject to combined mode I and mode III loading. The full-field numerical simulations compare well with the predictions of the perturbation theory and with experimentally observed characteristic patterns of brittle fracture surface. The method has also been used to study the three dimensional aspects of toughening mechanisms including crack trapping, bridging and debonding in fiber reinforced brittle matrix composites. The extension of the method proves to be a very powerful and flexible tool in studies of nucleation of dislocations from crack tips on the atomic scale in fully three dimensional forms. These studies have provided straightforward solutions of several key problems such as determination of saddle point configurations of dislocation loops on both inclined and oblique slip planes for thermally assisted emission, and calculation of thermal activation energies for nucleation of embryonic dislocation loops as a function of crack front driving force. The findings of these studies have underscored the importance of quantum mechanics calculations for engineering applications and narrowed the gap for ultimately understanding the phenomena which govern brittle to ductile transitions in certain types of intrinsically brittle solids.

1. Introduction

This paper reports the recent development of a variational boundary integral method for the analysis of three dimensional cracks of arbitrary geometry in both isotropic and anisotropic linear elastic solids. A set of its applications to fully three dimensional crack growth in brittle materials and fiber reinforced composites, and dislocation nucleation from crack tips are also briefly demonstrated.

Numerous boundary integral methods which reduce the three dimensional crack problems to the solution of integral equations defined on the faces of the crack are presently in existence (Brebia, 1978, Banerjee and Butterfield, 1981, Atluri, 1986, Cruse, 1988, Aliabadi and Rooke, 1991). Most of these methods, however, make use of the Somigliana identity as a means of effecting the reduction to the boundary, which results in highly singular integral equations of difficult numerical treatment. Instead, here we propose to represent the opening displacements of the crack as continuous distributions of dislocation loops. The energy of the solid can then be computed from known expressions for the

interaction energy of a pair of dislocation loops (Hirth and Lothe, 1982, Lothe, 1982). The geometry of the loops and their Burgers vectors are readily related to the crack opening displacements, which are then determined by minimization of the total potential energy of the solid. Because the governing integral equations are derived from a variational principle, the systems of equations which result upon discretization of the crack are symmetric. The method shares this desirable property with the Galerkin boundary element formulation of Maier and Polizzotto (1987). The distributed dislocation loop representation gives rise to integral equations which are only mildly singular, which greatly facilitates their numerical treatment. The present work extends the formulation of Bui (1977), based on a double-layer potential, and the variational formulation of Clifton *et al.* (1981) based on the fundermental solution for a dislocation segment. Both of these formulations were restricted to planar cracks and mode I loading.

Crack growth is modeled by assigning a velocity to the crack front according to a pseudodynamic crack-tip equation of motion (Freund, 1990), and by enforcing a suitable kinking criterion such as the vanishing of the local mode II stress intensity factor (Cotterel and Rice, 1989). Other types of crack-tip equations of motion and kinking criteria, such as those adopted by Gao and Rice (1989), Fares (1989), Bower and Ortiz (1990,1991) and others, can be accommodated equally well. The analysis proceeds incrementally by a time-stepping procedure similar to that advocated by Fares (1989). The mesh is continuously adapted to the changing geometry of the crack.

Dislocation nucleation from crack tips is analyzed based on the Peierls concept, in which a tension-shear potential is assumed to hold along the favored slip plane emanating from a crack tip. The crack and the slip plane are viewed as a three dimensional crack system embedded in an elastic solid. The opening displacements of the crack and the interlayer displacements along the slip plane are solved uniformly by representing them as continuous distribution of infinitesimal dislocation loops. The saddle point configurations of the incipient dislocation and the dependence of the associated activation energies on crack tip energy release rate are also determined.

2. Boundary Integral Equation Formulation

Consider a three-dimensional crack of arbitrary geometry in an infinite elastic body subjected to general loading. Let the surface of the crack be S with contour $C = \partial S$, and let $\mathbf{u}(\mathbf{x})$, $\mathbf{x} \in S$, be the displacement jump across S, with components u_i relative to a Cartesian basis $\mathbf{e}_i$. Our first aim is to compute the strain energy of the cracked solid. This is accomplished by representing the opening displacements as a continuous distribution of dislocation loops, and subsequently using known expressions for dislocation loop energies.

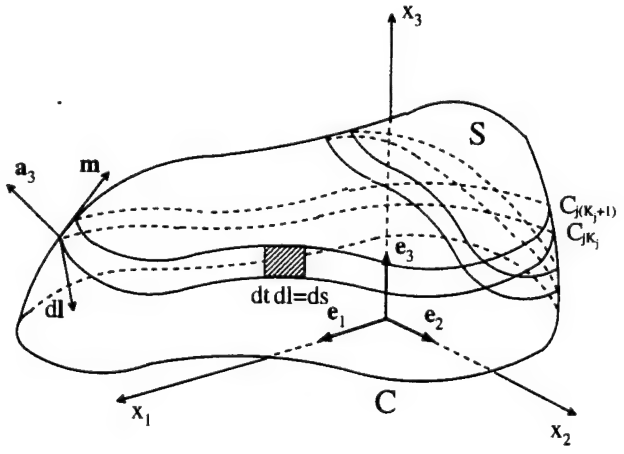

Fig. 1. Distributed dislocation loop representation of opening displacement field.

The dislocation distribution equivalent to $\mathbf{u}(\mathbf{x})$ is determined as follows. For $i = 1, 2, 3$, let C_{iK_i} be the level contours on S corresponding to values of $u_i = K_i \Delta u_i$ (no sum), $K_i = 0, 1, 2, \ldots N_i$. This defines three sets of level contours inscribed on the crack surface, Fig. 1. Since $u_i = 0$ at the crack front C, it follows that $C_{i0} = C$. We begin by replacing the original opening displacement field by

one consisting of discrete steps of magnitude Δu_i across the the level contours C_{iK_i}. Evidently, the stepwise opening displacement field so defined approaches $\mathbf{u}(\mathbf{x})$ as $\Delta u_i \to 0$. Each contour C_{iK_i} may be viewed as carrying a dislocation of Burgers vector

$$\mathbf{b}_i = \Delta u_i \mathbf{e}_i \qquad (no\ sum\ on\ i). \tag{1}$$

Note that, by definition, the Burgers vector for the loop C_{iK_i} points in the ith coordinate direction and has a constant magnitude equal to Δu_i. The elastic interaction energy between two dislocation loops C_1 and C_2 of Burgers vectors $\mathbf{b}_1$ and $\mathbf{b}_2$ in an infinite linear elastic solid is (Hirth and Lothe, 1982)

$$\begin{aligned} W_{12} =& \frac{\mu}{2\pi} \oint_{C_1} \oint_{C_2} \frac{(\mathbf{b}_1 \cdot d\mathbf{l}_2)(d\mathbf{b}_2 \cdot d\mathbf{l}_1)}{R} - \frac{\mu}{4\pi} \oint_{C_1} \oint_{C_2} \frac{(\mathbf{b}_1 \cdot d\mathbf{l}_1)(\mathbf{b}_2 \cdot d\mathbf{l}_2)}{R} \\ &+ \frac{\mu}{4\pi(1-\nu)} \oint_{C_1} \oint_{C_2} (\mathbf{b}_1 \times d\mathbf{l}_1) \cdot \mathbf{T} \cdot (\mathbf{b}_2 \times d\mathbf{l}_2), \end{aligned} \tag{2}$$

where $d\mathbf{l}_1$ and $d\mathbf{l}_2$ are vectors of infinitesimal length, tangent to C_1 and C_2, respectively, μ is the shear modulus, ν Poisson's ratio, R is the length of the relative position vector between C_1 and C_2, and

$$T_{ij} = \frac{\partial^2 R}{\partial x_i \partial x_j}. \tag{3}$$

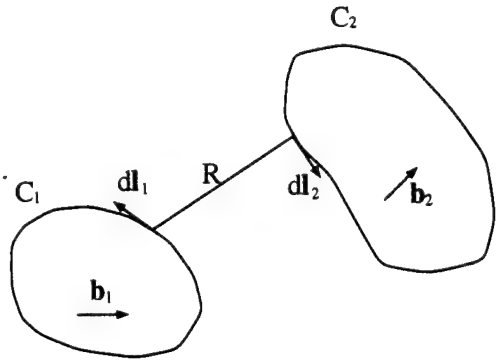

Fig. 2. Interacting dislocation loops.

Therefore, using the dislocation representation of the opening displacement and invoking the principle of superposition, the strain energy of the cracked solid follows as

$$\begin{aligned} W[\mathbf{u}] =& \frac{1}{2} \lim_{\Delta u_1, \Delta u_2, \Delta u_3 \to 0} \sum_{i=1}^{3} \sum_{j=1}^{3} \sum_{K_i=0}^{N_i} \sum_{K_j=0}^{N_j} \Big[\frac{\mu}{2\pi} \oint_{C_{iK_i}} \oint_{C_{jK_j}} \frac{(\mathbf{b}_i \cdot d\mathbf{l}_{jK_j})(d\mathbf{l}_{jK_j} \cdot d\mathbf{l}_{iK_i})}{R} \\ &- \frac{\mu}{4\pi} \oint_{C_{iK_i}} \oint_{C_{jK_j}} \frac{(\mathbf{b}_i \cdot d\mathbf{l}_{iK_i})(\mathbf{b}_j \cdot d\mathbf{l}_{jK_j})}{R} \\ &+ \frac{\mu}{4\pi(1-\nu)} \oint_{C_{iK_i}} \oint_{C_{jK_j}} (\mathbf{b}_i \times d\mathbf{l}_{iK_i}) \cdot \mathbf{T} \cdot (\mathbf{b}_j \times d\mathbf{l}_{jK_j}) \Big]. \end{aligned} \tag{4}$$

The factor $1/2$ in this expression compensates for the fact that the double sum accounts for the interaction energy between each pair of loops twice. The computation of the strain energy is completed by passing to the limit of $\Delta u_i \to 0$. To this end, let $\mathbf{m}$ be a unit surface vector (i. e., a unit vector tangent to S) normal to C_{iK_i}. Since C_{iK_i} is a level contour of u_i, it follows that

$$\mathbf{m} = \nabla u_i / \mid \nabla u_i \mid . \tag{5}$$

Let t measure the distance from the loop along $\mathbf{m}$, and let $\triangle t$ be the distance along $\mathbf{m}$ between the consecutive loops C_{iK_i} and $C_{i(K_i+1)}$, Fig. 1. The derivative of u_i with respect to t follows as

$$\frac{du_i}{dt} = \nabla u_i \cdot \mathbf{m} = \mid \nabla u_i \mid, \tag{6}$$

where use has been made of identity (5). Hence, for small $\triangle u_i$, one has

$$\triangle u_i \approx \mid \nabla u_i \mid \triangle t \tag{7}$$

and the Burgers vectors (1) become

$$\mathbf{b}_i \approx \mid \nabla u_i \mid \triangle t \mathbf{e}_i. \tag{8}$$

Furthermore, the line element along a contour may be expressed as

$$d\mathbf{l} = ds\mathbf{n} \times \mathbf{m} = ds\mathbf{n} \times \nabla u_i / \mid \nabla u_i \mid, \tag{9}$$

where ds is the element of arc length, and $\mathbf{n}$ is the unit normal vector to the surface. Substituting (8) and (9) into (5), and noting that in the limit of $\triangle u_i \to 0$, $\triangle t ds$ may be identified with the element of surface area dS, one finds,

$$\begin{aligned} W[\mathbf{u}] = & \frac{\mu}{4\pi} \int_S \int_S \frac{[\mathbf{e}_i \cdot (\mathbf{n} \times \nabla u_j)_2][\mathbf{e}_j \cdot (\mathbf{n} \times \nabla u_i)_1]}{R} dS_1 dS_2 \\ & - \frac{\mu}{8\pi} \int_S \int_S \frac{[\mathbf{e}_i \cdot (\mathbf{n} \times \nabla u_i)_1][\mathbf{e}_j \cdot (\mathbf{n} \times \nabla u_j)_2]}{R} dS_1 dS_2 \\ & + \frac{\mu}{8\pi(1-\nu)} \int_S \int_S [(\mathbf{e}_i \times (\mathbf{n} \times \nabla u_i)_1] \cdot \mathbf{T} \cdot [(\mathbf{e}_j \times (\mathbf{n} \times \nabla u_j)_2] dS_1 dS_2 \end{aligned} \tag{10}$$

where $(.)_1$ and $(.)_2$ denote two different points on S, and R is the distance between these two points. eq. (10) is the sought expression for the strain energy of the cracked solid. It takes the form of a double integral over the crack surface S. An advantage of the present formulation which is immediately apparent from (10) is that the kernels of all integrals have singularities of the type R^{-1}, i. e., are only mildly singular. This greatly facilitates their numerical treatment.

The above integral equation can be extented to anisotropic cases utilizing the interaction energy of two dislocation loops in anisotropic elastic solids (Lothe, 1982). The corresponding equations for eqns (2) and (10) are then,

$$\begin{aligned} W_{12} = \frac{1}{8\pi^2} \oint_{C_1} \cdot \oint_{C_2} \frac{1}{R} \int_0^{2\pi} & \mathbf{b}_1 \cdot [(d\mathbf{l}_1 \times \mathbf{z}, d\mathbf{l}_2 \times \mathbf{z}) \\ & - (d\mathbf{l}_1 \times \mathbf{z}, \mathbf{z}) \cdot (\mathbf{z}, \mathbf{z})^{-1} \cdot (d\mathbf{l}_2 \times \mathbf{z}, \mathbf{z})] \cdot \mathbf{b}_2 d\phi; \end{aligned} \tag{11}$$

$$\begin{aligned} W[\mathbf{u}] = & \frac{1}{16\pi^2} \int_S \int_S \frac{1}{R} \int_0^{2\pi} \mathbf{e}_i \cdot [(\mathbf{n} \times \nabla u_i)_1 \times \mathbf{z}, (\mathbf{n} \times \nabla u_j)_2 \times \mathbf{z}) \\ & - ((\mathbf{n} \times \nabla u_i)_1 \times \mathbf{z}, \mathbf{z}) \cdot (\mathbf{z}, \mathbf{z})^{-1} \cdot (\mathbf{z}, (\mathbf{n} \times \nabla u_j)_2 \times \mathbf{z})] \cdot \mathbf{e}_j d\phi dS_1 dS_2. \end{aligned} \tag{12}$$

where $\mathbf{z}$ is a unit vector perpendicular to $\mathbf{R}$, and ϕ is the angle between $\mathbf{z}$ and arbitrary chosen reference $\mathbf{z}_0$, perpendicular to $\mathbf{R}$. Let $\mathbf{a}$ and $\mathbf{b}$ be two vectors, $(\mathbf{a}, \mathbf{b})$ then denotes a matrix with elements

$$(\mathbf{a}, \mathbf{b})_{jk} = a_i c_{ijkl} b_l \tag{13}$$

where c_{ijkl} are the elastic coefficients.

The potential energy of the solid follows as the sum of the strain energy (10 or 12) and the potential energy of the applied loads. Without loss of generality, we shall confine our attention to the

case in which tractions T_i are applied directly to the faces of the crack. Then, the potential energy of the solid is

$$\Phi[\mathbf{u}] = W[\mathbf{u}] - \int_S \mathbf{T} \cdot \mathbf{u} dS. \tag{14}$$

For given tractions, the opening displacements of the crack may be obtained by minimizing the potential energy Φ. The distribution of stress intensity factors over the crack front C can then be extracted from the known opening displacements. As is evident from (14), Φ defines a positive definite quadratic form in $\mathbf{u}$. Consequently, Rayleigh-Ritz methods of approximation based on the constrained minimization of Φ over a finite dimensional interpolation space result in symmetric systems of equations. One such method based on a finite element discretization of the crack surface refers to our previous work (Xu and Ortiz, 1993), in which the treatment of singularity along the crack front, the singular integration, the calculation of stress intensity factors, and the treatment of the periodic semi-infinite cracks are addressed.

3. Non-planar Crack Growth under Mixed Mode Loding

Based on the proposed integral equations (14), a first order perturbation method is developed for calculating stress intensity factors at the tip of a slightly non-planar three–dimensional crack. The solution is used to analyze the instabilities of an initially planar semi–infinite crack subjected to combined mode I and mode III loading. It is shown that there is a critical ratio of mode III to mode I which causes the crack to deviate from its original plane, which is illustrated in Fig. 3 (Xu, *et al*, 1994a).

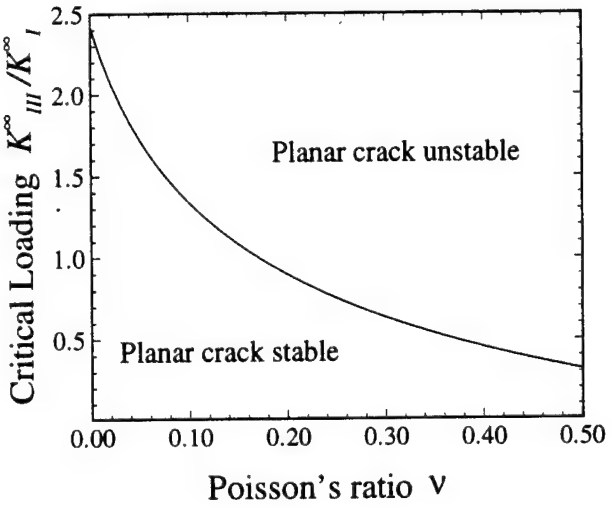

Fig. 3. Critical loading for a mode I–mode III crack to develop a wavy profile.

Our perturbation solution predicts the combination of remote loads which causes a planar semi–infinite crack to deviate from its initial plane. However, it gives little indication of the path followed by the crack during non–planar growth. We address this issue, using a full numerical analysis. Several authors have investigated the two–dimensional problem of a crack propagating under mixed mode I/mode II loading or under the T–stress component T_{22} (Cotterell and Rice, 1980). We therefore restrict our attention to cracks propagating under mixed mode I/mode III loads, or subjected to a remote T_{33} stress component.

The results of our simulations of crack growth are shown in Figs 4 and 5. An initial semi-infinite crack with the straight crack front is subjected to mixed mode I/mode III loads for two values of $K^{\infty}_{III}/K^{\infty}_{I}$. Fig. 4 is a three–dimensional view of the crack surface. To show the rate of growth of the amplitude of the waviness of the crack, a view of both cracks along the initial crack front is drawn in Fig. 5. In each figure, the out-of-plane displacement of the crack faces has been magnified 150 times, to show clearly the nature of the crack path. The amplitude of the waviness of the crack

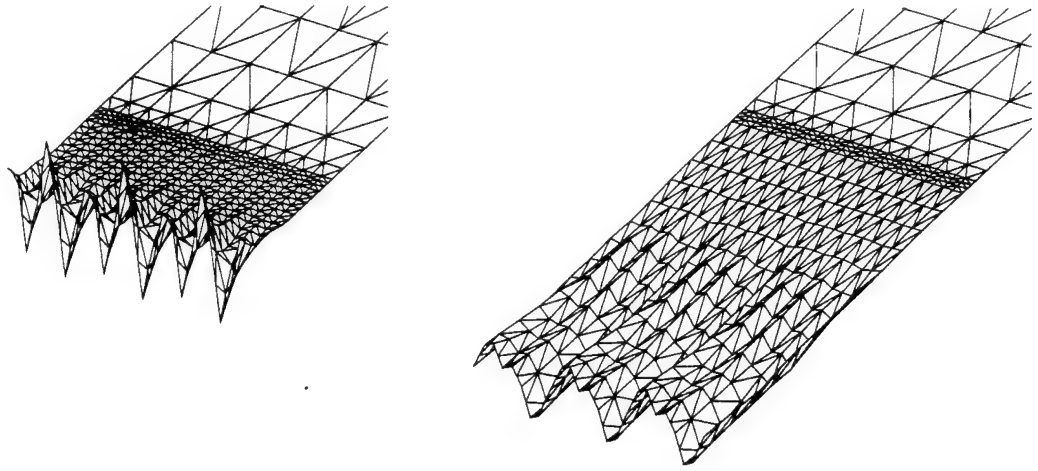

(a) (b)

Fig. 4. The path of an initially planar semi–infinite crack subjected to mixed mode I/mode III loading. Note that the out–of–plane displacement of the crack faces is magnified 150 ×. (a) $K^{\infty}_{III}/K^{\infty}_{I} = 2$; (b) $K^{\infty}_{III}/K^{\infty}_{I} = 0.2$.

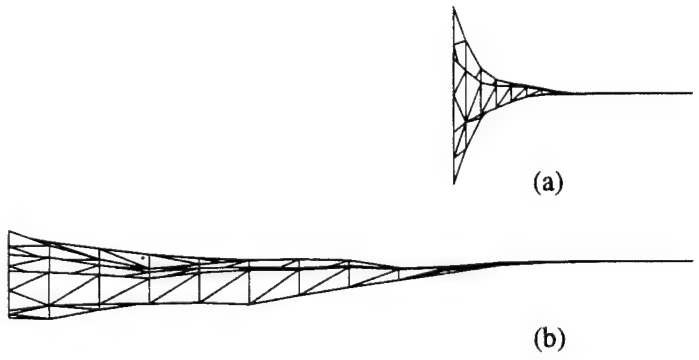

Fig. 5. A side view along the initial fronts of the cracks shown in Fig. 4.

faces is therefore greatly exaggerated. The loading applied to the crack shown in Fig. 4(a) is in the regime where unstable non–planar crack growth is predicted. As expected, the amplitude of the initial waviness of the crack grows exponentially as the crack propagates. The higher frequency components of the initial perturbation grow less rapidly than the low frequency ones, and the low frequency terms eventually dominate. The wavelength of the roughness of the crack faces therefore appears to increase as the crack grows. The pattern of fracture is remarkably close to the experimental observations reported by Sommer (1969). It should be noted that we have restricted our numerical analyses to conditions where the faces of the crack do not contact. In most practical situations, the crack propagates far enough to ensure that the roughness of the crack faces exceeds the crack opening displacements. The crack faces then touch, and the fracture process is considerably more complicated than the cases we consider here.

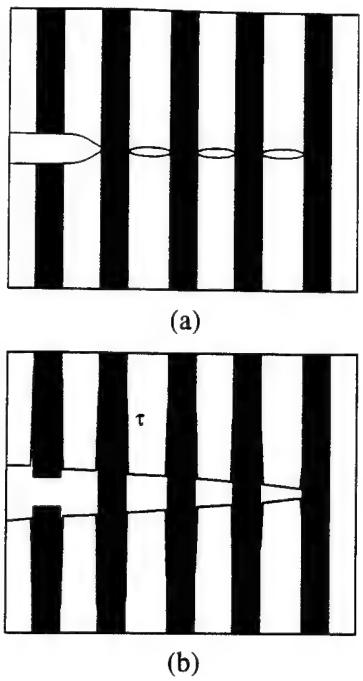

Fig. 6. Toughening mechanisms for a brittle matrix composite reinforced with: (a) perfectly bonded fibers; (b) weakly bonded fibers.

4. Three Dimensional Crack Growth in Fiber Reforced Composites

Fiber-reinforced composites have elicited considerable interest because of the potential for improving the toughness and strength of the composite in the fiber direction. We consider two main types of composites: those consisting of a brittle matrix reinforced with strongly-bonded ductile particles or fibers; and brittle-matrix composites reinforced with weakly-bonded brittle fibers. Brittle fibers have the appeal of enabling high-temperature performances that can not be attained with conventional metallic and organic fibers. Ductile fibers are normally strongly bonded to the matrix and are capable of undergoing large deformations in the wake of the crack, Fig. 6 (a). By contrast, the toughness of the brittle fibers is comparable to that of the matrix. Consequently, the matrix/fiber bond is commonly designed to be weak to avoid fiber fracture. This allows interfacial debonding and sliding, which in turn reduces the level of stress in the fibers and enables them to remain intact in the wake of the crack. The bridging fibers inhibit crack opening, providing an important source of toughness Fig. 6 (b) (Phillips, 1974; Marshall *et al.*, 1985). The success of this type of composite depends to a significant degree on the understanding and assessment of the relationship between the properties of the constituents – fiber, matrix and interface – and the overall mechanical performance of the composite.

We confine our attention to mode I matrix crack propagation normal to the fiber axis. The successive crack front profiles of a semi-infinite crack as it bypasses two successive rows of impenetrable fibers with unlimited bonding to the matrix are plotted in Fig. 7 together with the corresponding values of the applied stress intensity factors. The fibers are uniformly distributed with the ratio of the radius of the fiber to the distance between the fibers equal 0.25. As is evident from these figures, $K_{\rm I}^{\infty}$ must be steadily increased for the crack to bow through the first row of obstacles. At a critical configuration, however, the attraction between the two lobes of the crack approaching each other in the wake of the obstacles overcomes the fracture resistance of the matrix and the crack begins to grow unstably under decreasing applied load. The maximum value of $K_{\rm I}^{\infty}$ at the critical configuration is computed to be $2.36K_{\rm IC}^{\rm mat}$. The elevation in applied stress intensity factor over the toughness of the matrix required to bypass the first row of particles may be thought of as a measure of the toughening effect of the 'trapping' mechanism. Throughout the stable regime, the stress intensity factors $K_{\rm I}(s)$ remain close to $K_{\rm IC}^{\rm mat}$ at all points s of the front contained in the matrix. By contrast, the value of $K_{\rm I}(s)$ at points in contact with the particles rises sharply over $K_{\rm IC}^{\rm mat}$. $K_{\rm I}(s)$ attains its maximum at

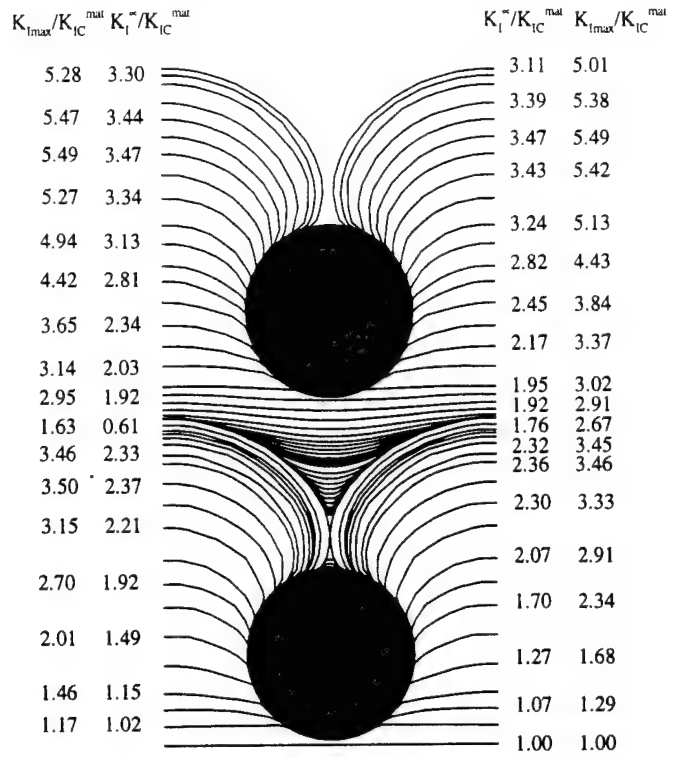

Fig. 7. The profile of a semi-infinite crack as it bypasses two successive rows of impenetrable particles. K_I^∞ is remote stress intensity, K_{IC}^{mat} is the toughness of the matrix. The fibers are uniformly distributed with the ratio of the radius of the fiber to the distance between the fibers equal 0.25.

the point s of first contact between the front and the particles, and rises to $K_{\mathbf{Imax}} = 3.46K_{\mathbf{IC}}^{\mathbf{mat}}$ at peak load.

A similar sequence of events takes place after the crack makes contact with the second array of obstacles. Initially, the crack grows stably under increasing load up to a maximum of $K_{\mathrm{I}}^{\infty} \approx 3.47K_{\mathrm{IC}}^{\mathbf{mat}}$. The difference between the two successive maxima of K_{I}^{∞} reflects the stabilizing effect of the first row of particles bypassed by the crack, and may be construed as a measure of the toughening effect of the 'bridging' mechanism. As before, the points of the front in contact with the second row of particles experience a sharp increase in the local value of the stress intensity factor, which attains a maximum of $5.49K_{\mathrm{IC}}^{\mathbf{mat}}$ at peak load.

The more detailed simulations of crack trapping (Xu and Ortiz, 1993; Xu, *et al.*; 1994b) also compare well with other simulations using different numerical schemes (Bower and Ortiz, 1990, 1991; Gao and Rice, 1989; Fares, 1989), and experimental studies of crack trapping in brittle heterogeneous solids (Mower and Argon, 1995).

The effect of debonding on crack trapping is determined by way of numerical simulation (Xu, *et al.*; 1994b). To simplify the calculations, for cracks which propagate along an interface we adopt a fracture criterion that requires the energy release rate along the propagation direction to be constant and equal to the interface fracture resistance. The influence of mode mixity on toughness is therefore neglected. Fig. 8 depicts the successive profiles adopted by the semi-infinite crack as it bypasses one of the uniformly distributed fibers with ratio $R/b = 0.25$ and $G_{int}/G_{mat} = 0.25$, where R is the radius of the fiber, b is the distance between two fibers, G_{int} and G_{mat} are fracture resistance of interface and matrix, respectively.

For design purposes, toughness increases by trapping have to be evaluated for different volume fractions of fibers as well as different interface fracture resistances. Fig. 9 shows the variation of the toughness increase due to crack trapping with interface toughness for various values of R/b. The toughness due to trapping increases with the interface fracture resistance. A larger areal concentration

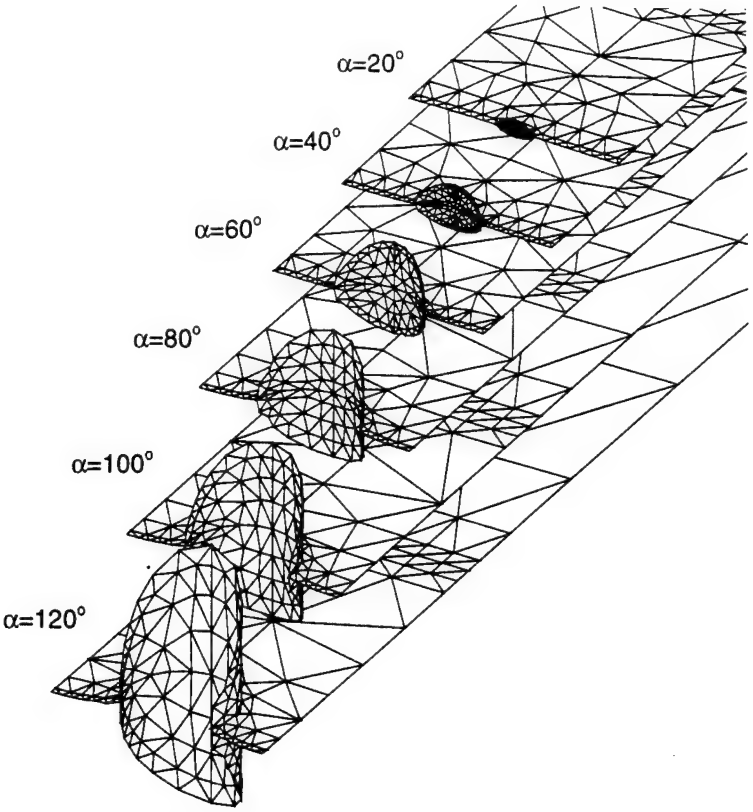

Fig. 8. Profiles of a semi-infinite crack as it bypasses weakly bonded fibers. α is a parameter describing the debonding along the fiber.

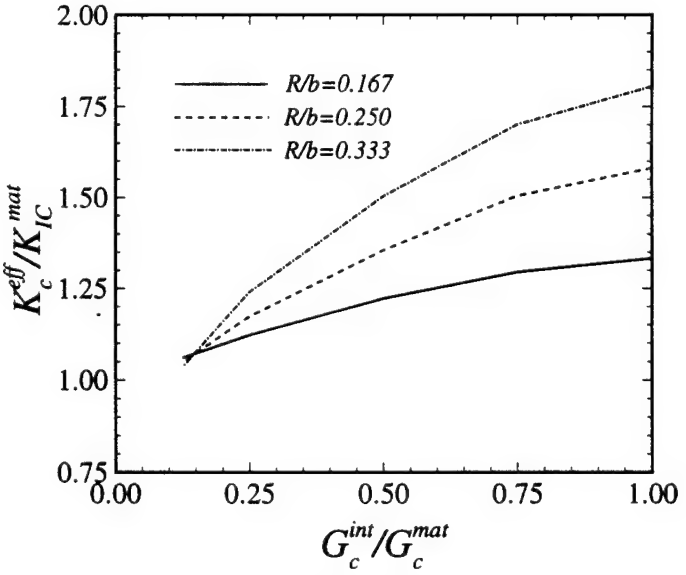

Fig. 9. Variation of effective trapping toughness with interface fracture resistance and fiber volume fraction.

of fibers on the crack front traps the crack more effectively than a lighter concentration. For all fiber volume fractions, it is possible for the effective toughness of the composite to be less than the matrix toughness if the interface fracture resistance is very small.

5. Dislocation Nucleation from a Crack Tip

The transition in the behavior of intrinsically brittle materials from brittle to ductile continues to be of major scientific and technological interest. It was recognized early on that cleavable materials are distinguished by having substantial energy barriers to dislocation nucleation from atomically sharp cracks on the verge of propagation (Armstrong, 1966; Kelly *et al.*, 1967; Rice and Thomson, 1974). Moreover, pioneering experiments carried out on initially dislocation-free Si (St John, 1975; Brede and Haasen, 1988; Hirsch *et al.*, 1989) have demonstrated that, at least in this material, the brittle to ductile transition (BDT) is not controlled solely by dislocation nucleation but also by the mobility of trains of dislocations emitted from the crack tip. Other experiments particularly designed to follow dislocation nucleation from crack tips (Chiao and Clarke, 1989; Samuels and Roberts, 1989; George and Michot, 1993), have established that dislocation nucleation is heterogeneous, singling out geometrical crack-tip imperfections.

Our analysis of this class of problems builds on recent theoretical developments in the modeling of dislocation nucleation at a stressed crack tip (Rice, 1992; Rice *et al.*, 1991; Rice and Beltz, 1994). In consonance with these developments, we consider a semi-infinite crack with a straight crack front embedded in an elastically isotropic solid. We additionally assume that the crack surfaces do not interact and that, beyond the crack front, the shear and tension separation resistances, τ and σ respectively, follow as functions of the inelastic displacements δ_r and δ_θ along the slip plane, in which dislocations may nucleate. The inelastic relative displacements δ_r and δ_θ are defined as

$$\delta_r = \Delta_r - h\tau(\Delta_r, \Delta_\theta)/\mu, \tag{15a}$$

$$\delta_\theta = \Delta_\theta - h\sigma(\Delta_r, \Delta_\theta)/c, \tag{15b}$$

where Δ_r and Δ_θ denote the shear and opening relative displacements between two interatomic layers, μ and c are the shear modulus and the uniaxial strain elastic modulus, respectively.

The profile of the nucleated dislocation and the crack opening displacement $\boldsymbol{\delta}$ follow by minimization of the potential energy

$$\Phi[\boldsymbol{\delta}] = W[\boldsymbol{\delta}] + V[\boldsymbol{\delta}] - P[\boldsymbol{\delta}]. \tag{16}$$

The interlayer energy $V[\boldsymbol{\delta}]$ is expressible as

$$V[\boldsymbol{\delta}] = \int_{S_,} \phi[\boldsymbol{\delta}] dS \tag{17}$$

where $\phi[\mathbf{u}]$ is the interplanar shear tension coupling potential defined per unit area of the slip plane. The associated traction-displacement relation may be modeled as

$$\tau(\Delta_r, \Delta_\theta) = A(\Delta_\theta)\Big[\sin\Big(\frac{2\pi\Delta_r}{b}\Big) + \frac{\beta-1}{2}\sin\Big(\frac{4\pi\Delta_r}{b}\Big)\Big], \tag{18a}$$

$$\sigma(\Delta_r, \Delta_\theta) = \Big[B(\Delta_r)\Big(\frac{\Delta_\theta}{L}\Big) - C(\Delta_r)\Big]\exp\Big(-\frac{\Delta_\theta}{L}\Big), \tag{18b}$$

where $A(\Delta_\theta)$, $B(\Delta_r)$ and $C(\Delta_r)$ can be determined by enforcing selected constrains (Rice *et al.*, 1991; Xu, *et al.*, 1995). β is a parameter that describes the skewness of the shear resistance profile (Xu, *et al.*, 1995) The resulting non-linear system can be solved by a Newton-Raphson iteration.

A non-trivial complication arises in applying this program, owing to the loss of stability of the equations beyond the critical load. This difficulty may be circumvented by recourse to displacement control. For purposes of illustration, consider the pure mode II case corresponding to $K_I = K_{III} = 0$. Under these conditions, the finite-element discretization of the crack/slip plane system results in a system of equations of the form

$$\mathbf{F}(\boldsymbol{\delta}) = K_{II}\mathbf{f}, \tag{19}$$

where $\boldsymbol{\delta}$ now denotes the array of nodal values of the field $\boldsymbol{\delta}(\mathbf{x})$, $\mathbf{F}$ is the internal force array, and $\mathbf{f}$ is the external force array normalized to $K_{II} = 1$. Instead of enforcing the value of K_{II}, which is not possible beyond the critical point, we augment the system (19) by the addition of the kinematic constraint

$$\mathbf{f}\cdot\boldsymbol{\delta} - \bar{\delta} = 0. \tag{20}$$

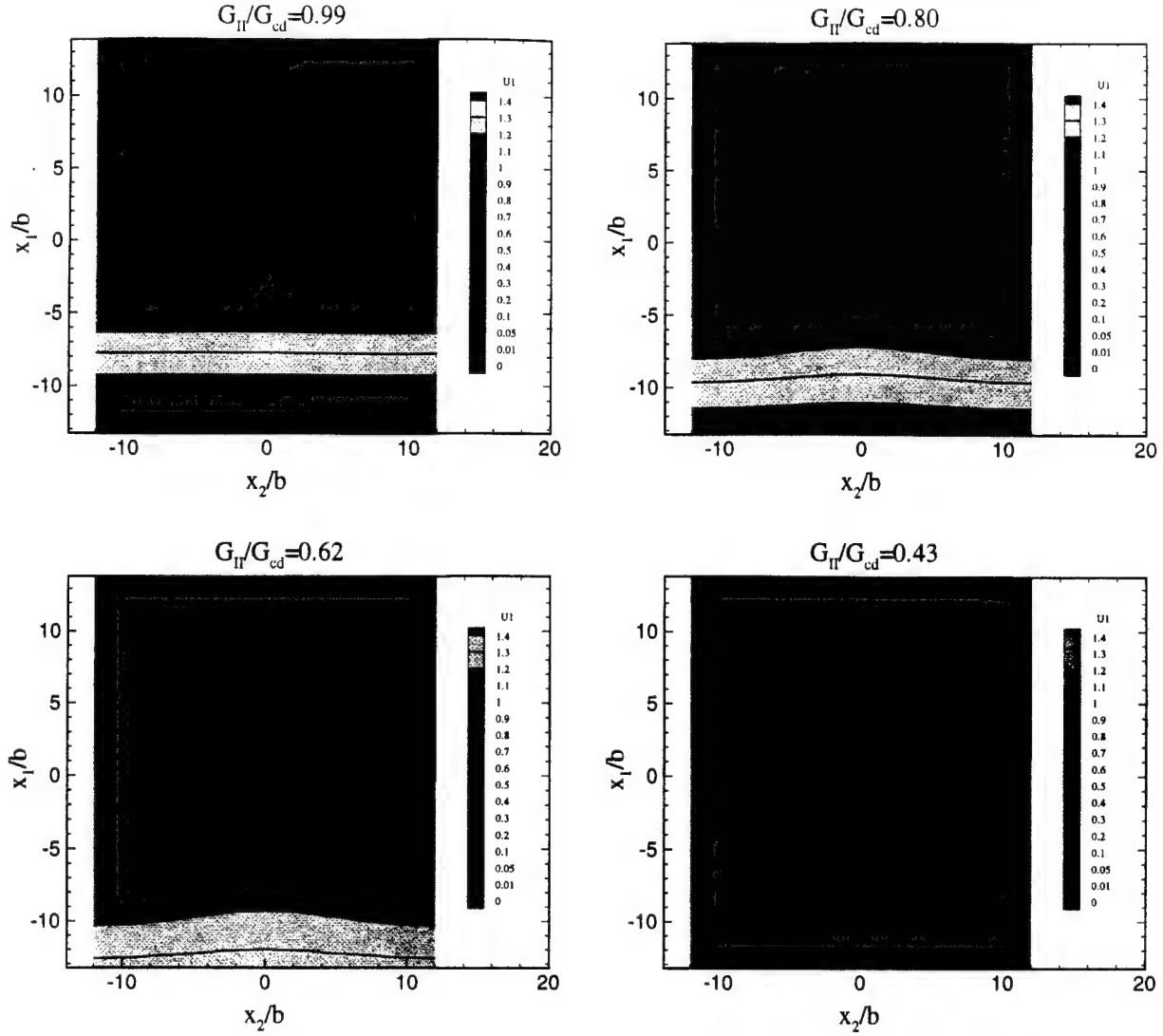

Fig. 10. Saddle point configurations of dislocation embryos at a crack tip for simple shear loading. The contour lines represent the shear displacement distributions of a dislocation emitting from the crack front at x=0. G_c is the critical loading for the nucleation of the dislocation. β=1.

Here, $\mathbf{f} \cdot \boldsymbol{\delta}$ is the displacement parameter conjugate to K_{II} and $\bar{\delta}$ its prescribed value. The unknowns of the combined system of equations (19) and (20) are $\boldsymbol{\delta}$ and K_{II}. Thus, K_{II} is not prescribed but computed as a function of the effective displacement $\bar{\delta}$, which can be increased monotonically from zero. Linearization of (19) and (20) yields an incremental system of the form

$$\begin{pmatrix} \mathbf{K} & -\mathbf{f} \\ -\mathbf{f}^T & 0 \end{pmatrix} \begin{pmatrix} \triangle\boldsymbol{\delta} \\ \triangle K_{II} \end{pmatrix} = \begin{pmatrix} 0 \\ -\triangle\bar{\delta} \end{pmatrix} \tag{21}$$

where $\mathbf{K}$ is a symmetric tangent stiffness matrix. The form of (21) is indeed characteristic of a system with equality constraints enforced by Lagrange multipliers.

As a demonstration, we consider the simple case of a slip plane which lies in the extension of the plane of the crack. The crack is subjected to pure mode II loading resulting in a stress intensity factor K_{II}. The unstable equilibrium (saddle point) configurations of the emitted dislocations are depicted in Fig. 10 for decreasing values of G_{II}/G_{cd}, where G_{cd} is the critical energy release rate for emitting an endless line of dislocation. The skewness parameter β is set to 1, which is representative of Si. The curves represent level contours of the inelastic shear displacement δ_r in the x_1-direction. Remarkably, dislocation emission is seen to take place by the bulging out of a dislocation packet consisting of a

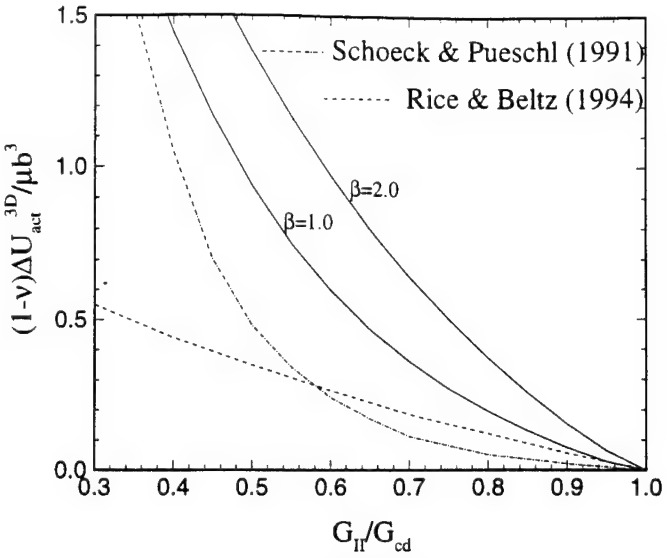

Fig. 11. The activation energy in pure Mode II loading, scaled with shear moduli μ for the dislocation emission in 3D

fractional dislocation in the form of a "double kink", which subsequently spreads out along the crack front at decreasing driving force G_{II}/G_{cd}.

The dependence of the activation energy on G_{II}/G_{cd} is shown in Fig. 11. Rice and Beltz's (1994) solution comes in tangent to the curve $\beta = 1$ at $G_{II}/G_{cd} = 1$ but diverges from it away from the critical point, as expected from the perturbative character of their analysis. By contrast, the Schöck and Püschl (1991) approximate solution is less accurate in the vicinity of the athermal critical point but closer to the curve $\beta = 1$ elsewhere.

6. Summary

We have summarized the recent development of a very flexiable variational boundary integral method for the analysis of the fully three dimensional crack advance problems. The applicability of the method and performance of the numerical scheme are demonstrated by the studies of the three dimensional dimensional crack growth in brittle materials and fiber reinforced composites, and dislocation nucleation from crack tips. The method also has important applications in fields such as surface crack propagation related failures in manufacturing industries, hydraulic fracturing in horizontal drilling techniques and the modeling of possible dynamic problems related to earthquakes. We are in the process of developing some of these applications.

Acknowledgement

This research was supported by the ONR under contract N00014-92-J-4022 at MIT, and also under the ONR contract N00014-90-J-1758 and the NSF grant DMR-9223683 at Brown University. Moreover, we are grateful for an ARO supplementary equipment grant P-33768-MA-RIP at MIT. We acknowledge a number of fruitful discussions with Profs. R. J. Clifton of Brown University, J. R. Rice and E. Kaxiras of Harvard University, and Dr. R. Thomson of NIST. The computations were carried out with the facilities of the Mechanics of Materials group at MIT. and those of the Solid Mechanics group at Brown University.

References

Aliabadi, M. H. and Rooke, D. P. (1991), *Numerical Fracture Mechanics*, Kluwer Academic Publishers.

Armstrong, R. W. (1966), *Mater. Sci. Eng.*, **1**, 251.

Atluri, S. N. (1986), *Computational Methods in the Mechanics of Fracture*, Elsevier Science Publishers B. V.

Brebbia, C. A. (1978) *The Boundary Element Method for Engineers*, Penteck Press, London.

Banerjee, P. K. and Butterfield, R. (1981), *Boundary Element Methods in Engineering Science*. McGrawHill.

Bower, A. F. and Ortiz, M. (1990), *J. Mech. Phys. Solids*, **38**(4), 443.

Bower, A. F. and Ortiz, M. (1991), *J. Mech. Phys. Solids*, **39**(6), 815.

Brede, M. and Haasen P. (1988), *Acta Metall.*, **36**, 2003.

Bui, H. D. (1977) , *J. Mech. Phys. Solids*, **25**, 29.

Chiao, Y.-H. and Clarke, D. R. (1989), *Acta Metall.*, **47**, 203.

Clifton, R. J. and Abou-Sayed, A. S. (1981), SPE/DOE Paper No. 9879, Low Permeability Symposium, Denver, Colorado.

Cotterell, B. and Rice, J. R. (1980), *Int. J. Fract.*, **16**(2), 155.

Cruse, T. A. (1988), *Boundary Element Analysis in Computational Fracture Mechanics*, Kluwer Academic Publishers.

Fares, N. (1989), *J. App. Mech.*, **56**, 837.

Freund, L. B. (1990), *Dynamic Fracture Mechanics*, Cambridge University Press.

Gao, H. and Rice, J. R. (1989), *J. App. Mech.*, **56**, 828.

George, A. and Michot, G. (1993), *Mater. Sci. Eng. A* **164**, 118.

Hirsch, P. B. and Roberts, S. G. (1991), *Phil. Mag. A*, **64**, 55.

Hirsch, P. B., Samuels, J. and Roberts, S. G. (1989), *Proc. Roy. Soc. A*, **421**, 25.

Hirth, J. P. and Lothe, J. (1982), *Theory of Dislocations*, 2nd ed., Wiley-Interscience, New York.

Kelly, A., Tyson, W. R. and Cottrell, A. H. (1967), *Phil. Mag.*, **15**, 567.

Lorth, J. (1982), *Phil. Mag. A*, **46**(1), 177.

Maier, G. and Polizzotto, C. (1987), *Comput. Methods App. Mech. Eng.*, **60**, 175.

Marshall, D. B., Cox, B. N. and Evans, A. G. (1985), *Acta Metall.*, **33**, 2013.

Mower, T. and Argon, A. S. (1995), to appear in *Mech. Mater.*

Peierls, R. E. (1940), *Proc. Phys. Soc. A*, **52**, 34.

Phillips, D. C. (1974), *J. Mater. Sci.*, **9**, 1847.

Rice, J. R. (1992), *J. Mech. Phys. Solids*, **40**, 235.

Rice, J. R. and Beltz, G. E. (1994), *J. Mech. Phys. Solids*, **42**, 333.

Rice, J. R. , Beltz, G. E. and Sun, Y. (1992), in *Topics in Fracture and Fatigue*, edited by Argon, A. S., Springer, Berlin.

Rice, J. R. and Thomson, R. (1974), *Phil. Mag.*, **29**, 73.

Samuels, J. and Roberts, S. G. (1989), *Proc. Roy. Soc. Lond. A*, **421**, 1.

Sommer, E. (1969), *Eng. Fract. Mech.*, **1**, 539–46.

Schöck, G. and Püschl, W. (1991), *Phil. Mag.*, **A64**, 931.

St John, C. (1975), *Phil. Mag.*, **32**, 1193.

Xu, G. and Ortiz, M. (1993), *Inter. J. Numer. Methods in Eng.*, **36**, 3675.

Xu, G., Argon, A. S. and Ortiz, M. (1995), *Phil. Mag. A*, in press.

Xu, G., Bower, A. F. and Ortiz, M. (1994a), *Int. J. Solids Structures*, **31**(16), 2167.

Xu, G., Bower, A. F. and Ortiz, M. (1994b), in *Fracture and Damage in Quasi-Brittle Structures*, edited by Z.P. Bazant, Z. Bittnar, M. Jirasek and J. Mazars, E & FN Spon, London, pp. 589-604.

REPORT DOCUMENTATION PAGE

Form Approved
OMB No. 0704-0188

1. AGENCY USE ONLY (Leave blank)	2. REPORT DATE	3. REPORT TYPE AND DATES COVERED
	May 22, 1997	Final: 9/1/1992-11/30/1995

4. TITLE AND SUBTITLE
Atomic Modes of Dislocation Mobility in Silicon

5. FUNDING NUMBERS
C-N00014-92-J-4022

6. AUTHOR(S)
V.V. Bulatov, S. Yip, and A.S. Argon

7. PERFORMING ORGANIZATION NAME(S) AND ADDRESS(ES)
Massachusetts Institute of Technology
Room 1-306
Cambridge, MA 02139 (A.S. Argon)

8. PERFORMING ORGANIZATION REPORT NUMBER
1-4

9. SPONSORING/MONITORING AGENCY NAME(S) AND ADDRESS(ES)
ONR Solid Mechanics Program (Attn: Dr. R. Barsoum)
ONR Code 1132
800 N. Quincy Street - Ballston Tower 1
Arlington, VA 22217-5000

10. SPONSORING/MONITORING AGENCY REPORT NUMBER

11. SUPPLEMENTARY NOTES
Paper published in"Philosophical Magazine" 72, 453-496 (1995)
(Reprint attached)

12a. DISTRIBUTION/AVAILABILITY STATEMENT
Unlimited

12b. DISTRIBUTION CODE

13. ABSTRACT *(Maximum 200 words)*

Mechanisms of partial dislocation mobility in the {111} glide system of silicon have been studied in full atomistic detail by applying novel effective relaxation and sampling algorithms in conjunction with the Stillinger-Weber empirical inter-atomic potential and simulation models of up to 90,000 atoms. Low-energy pathways are determined for the generation, annihilation and motion of in-core defects of the 30°-partial dislocation, specifically, the individual left and right components of a double-kink, an antiphase defect (APD), and various kink - APD complexes. It is shown that the underlying mechanisms in these defect reactions fall into three distinct categories, characterized by the processes of bond-breaking, bond switching, and bond exchange, respectively. The quantitative results reveal a strong left-right asymmetry in the kinetics of kink propagation and a strong APD-kink binding; these have not been recognized previously and therefore hold implications for further experiments. The present work also demonstrates the feasibility of the atomistic approach to modeling the kinetic processes underlying dislocation mobility in crystals with high Peierls barriers.

14. SUBJECT TERMS
A comprehensive modelling study of the atomic level process involved in the motion of particle dislocations in Si

15. NUMBER OF PAGES
43

16. PRICE CODE

17. SECURITY CLASSIFICATION OF REPORT	18. SECURITY CLASSIFICATION OF THIS PAGE	19. SECURITY CLASSIFICATION OF ABSTRACT	20. LIMITATION OF ABSTRACT
Unclassified	Unclassified	Unclassified	None

PHILOSOPHICAL MAGAZINE A, 1995, VOL. 72, NO. 2, 453–496

Atomic modes of dislocation mobility in silicon

By V. V. BULATOV, S. YIP and A. S. ARGON

Massachusetts Institute of Technology, Cambridge, MA 02139, USA

[*Received 4 January 1995 and accepted 28 January 1995*]

ABSTRACT

Mechanisms of partial dislocation mobility in the {111} glide system of silicon have been studied in full atomistic detail by applying novel effective relaxation and sampling algorithms in conjunction with the Stillinger–Weber empirical interatomic potential and simulation models of up to 90 000 atoms. Low-energy pathways are determined for the generation, annihilation and motion of in-core defects of the 30°-partial dislocation, specifically, the individual left and right components of a double-kink, an antiphase defect (APD), and various kink–APD complexes. It is shown that the underlying mechanisms in these defect reactions fall into three distinct categories, characterized by the processes of bond-breaking, bond switching, and bond exchange, respectively. The quantitative results reveal a strong left–right asymmetry in the kinetics of kink propagation and a strong APD–kink binding; these have not been recognized previously and therefore hold implications for further experiments. The present work also demonstrates the feasibility of the atomistic approach to modelling the kinetic processes underlying dislocation mobility in crystals with high Peierls barriers.

§ 1. INTRODUCTION

Among the many problems in deformation and fracture of crystalline solids where dislocation processes are the primary concern, the brittle-to-ductile transition (BDT) in cleavage fracture stands out as a particularly important phenomenon. In crystalline silicon, a material with characteristically high lattice resistance to dislocation motion (Peierls barrier), the transition is signalled by a sharp increase in the fracture energy, by five- to ten-fold, over a narrow temperature range of 3–4 K (St John 1975, Brede and Haasen 1988, Hirsch, Samuels and Roberts 1989, George and Michot 1993). In contrast to cleavable metals where BDT is governed by dislocation nucleation, the controlling mechanism in crystals with strong directional bonding, of which Si is prototypical, lies in the mobility of the dislocations. Additionally, the problem of dislocation mobility in Si holds interest from the standpoint of understanding electro-mechanical coupling effects in semiconductors, such as the reduction in activation barriers to dislocation kink motion through doping (George and Champier 1979) and the ability of dislocations to provide undesirable conduction paths or otherwise substantially affect the electronic properties of semiconductors.

Experimental and theoretical studies of dislocation mobility in Si have focused on the formation and propagation of dislocation double kinks (Hirsch, Ourmazd and Pirouz 1981, Hirth and Lothe 1982, Farber, Iunin and Nikitenko 1986). From measurements which give estimates of 0·6 and 1·6 eV, respectively, for the energy barriers to kink formation and kink motion (Farber *et al.* 1986), it is possible to infer that the potential energy contour for kink mobility must have deep reliefs, characterized by a significant *secondary* Peierls barrier. To elucidate the electronic effects on dislocation mobility, early calculations have dealt with atomic mechanisms deduced

primarily from ball-and-spoke models (Hirsch 1979, Jones 1980, Heggie and Jones 1983a, b), while later studies were concerned with calculating the structure and energetics of dislocation cores using empirical interatomic interaction models. Direct atomistic simulation of dislocation motion using interatomic potential functions also have been reported (Heggie and Jones 1987, Duesbery, Michel and Joos 1990, Duesbery, Joos and Michel 1991): however, such attempts have met with considerable difficulties.

Besides the problem of a high Peierls barrier, the simulation of dislocation mobility in Si entails other challenges. Because of the long-range elastic fields associated with dislocations and to a lesser extent with kinks, it is necessary to study fully three-dimensional (3D) simulation cells, with as many as 10^4 or even 10^5 atoms. When this is combined with the fundamental requirement common to all atomistic simulations, namely, the availability of reliable interatomic potentials, it becomes necessary to compromise between theoretical (physical) rigour and computational tractability. To ensure an adequate treatment of the configurational degrees of freedom involved in dislocation motion, the relative simplicity of empirical potential functions becomes an important advantage. On the other hand, because such descriptions have only limited transferability, it is also essential to apply first-principles methods (Bigger *et al.* 1992, Payne, Teter, Allan, Arias and Joannopoulos 1992) to further scrutinize the results obtained using empirical potentials wherever this is realistically possible. In essence this is the two-step approach which exploits the complementarity of both methods (Duesbery and Richardson 1991).

In the present paper we present a comprehensive study of the energetics involved in the mobility of the 30°-partial dislocation on the {111} glide plane in Si. Using an approach based on the Stillinger–Weber interatomic potential (Stillinger and Weber 1985), a set of newly developed methods for energy minimization and configuration sampling, and a periodic simulation cell with variable shape and volume to minimize the net internal stress, we have determinated the activation energies for formation and migration of in-core defects and their detailed atomic configurations, which arise in propagating the 30°-partial dislocation via the kink mechanism. The set of defects investigated consists of the isolated reconstructed partial dislocation, the antiphase defect (APD) which results from the reconstruction, and the two components (left and right) of a double kink, as well as complexes formed by the association of an APD with either the left or the right kink. From these results a picture has emerged of the complexity and richness of the structural and kinetic aspects of core-defect reactions underlying dislocation mobility. Specifically, the results suggest classifying each displacement event as involving bond breaking, bond switching, or bond exchange. The interpretation not only brings out a significant property of the Si lattice, but also points to a framework for investigating mobility of defect structures in general.

We begin in § 2 with a description of the simulation model of Si, the methodology of setting up the simulation cell, and the energy minimization and configuration sampling methods developed in this study. The Stillinger–Weber potential model is chosen for our work for its overall robustness in a large variety of applications, even though this potential is known to fail to give the correct reconstruction of the 90°-partial dislocation (Duesbery *et al.* 1991, Bigger *et al.* 1992). All the simulations, pertaining to both mobility and nucleation of the APD and kink defects, are presented in § 3 which begins with an overview of all the results prior to delving into their analyses in detail in the following subsections. This overview should provide sufficient insight into the complex processes investigated. Following the overview we discuss in detail first the

energetics and atomic configurations associated with the displacement of isolated APD, and right and left kinks, then the same analysis is carried out for the kink–APD complexes. For the nucleation study, results are given separately for the homogeneous processes of creating two APDs or a double kink in the dislocation core, and the heterogeneous reactions wherein a defect is already present. In § 4 we consider the general implications of the detailed mobility mechanisms presented in § 3 and arrive at their classification based on bond rearrangements. In the final section we conclude with a summary of the present results along with an outlook for future developments.

§ 2. Simulation details

2.1. *General considerations*

In this section we consider some of the relevant techniques of the simulations. A more detailed discussion will be given elsewhere.

The first step in the simulation was the choice of the Stillinger–Weber potential as a satisfactory empirical interatomic potential function for simulating the dislocation motion in Si (§ 2.2). In § 2.3 details of the simulation geometry and boundary conditions are presented. The core simulation methods developed specifically for studying the dislocation mobility in Si are discussed in § 2.4, 2.5 and 2.6. Nevertheless, before considering the simulation techniques in detail a few preliminary remarks are appropriate.

From the recent simulations (Duesbery *et al.* 1990, 1991) it has become clear that conventional molecular dynamics (MD) methods are unsuitable for simulating dislocation motion in Si even at high temperatures. This is because in Si and other similar materials with high Peierls barriers dislocation mobility is low, making atomic-scale events resulting in dislocation or kink motion as rare events. In MD, however, for much of the simulation time atoms sample various inconsequential configurations in stable equilibrium before any significant event actually occurs. Thus, MD is ineffective in sampling atomic processes commonly described as rare events (Carter, Ciccotti, Hynes and Kapral 1989).

In view of this difficulty with MD, it became necessary to develop efficient numerical methods for studying specific atomic mechanisms of dislocation motion such as those in Si. The methodology adopted consisted of static energy minimizations to study the topography of the many-body energy surfaces involved in the description of saddle-point configurations associated with dislocation motion.

For finding low-energy defect states relevant to dislocation motion we have adopted a modified simulated annealing technique introduced by Kirkpatrick (1984), which is presented in §2.4. Then, to find low-energy pathways connecting mechanically stable defect configurations, a new technique of gradual ascent was developed. In this technique sampling of the various pathways is accomplished by applying a local perturbation potential carefully chosen to avoid driving the system over excessively high barriers, as discussed in § 2.5. Lastly, in §2.6 a modification of the conjugate gradient relaxation method is presented that searches efficiently for saddle points of the N-body energy surface even when N is as large as 10^5.

By combining the methods introduced in the following subsections it was possible to identify important atomic mechanisms of dislocation motion in Si.

2.2. *Interatomic potential model of Si*

A conclusion that can be reached through examination of previous work is that none of the currently used empirical potentials developed for Si are particularly well suited to describing the highly distorted atomic environments characteristic of dislocation cores in this material (Duesbery *et al.* 1991). This is because the strength and character of covalent bonding in semiconductors are very sensitive to the details of local atomic geometry.

Typically, an empirical potential is constructed based on an *ad-hoc* choice of functional form containing a few (usually about 10) numerical parameters. The parameters are then fitted to a few judiciously selected material properties and, possibly, to some results of *ab-initio* quantum mechanical calculations (Stillinger and Weber 1985, Tersoff 1986). The function so established is then expected to provide a reasonable description of other properties as well, i.e. it is to be *transferable.*

Although, the above approach was successful in describing some properties of close-packed metals, a generally satisfactory empirical model of Si is yet to be found. While dozens of empirical potentials have been developed for Si, all suffer from lack of transferability. Nevertheless, the quest for appropriate empirical models continues, in spite of reservations about the applicability of simple empirical descriptions to such strongly bonded materials as silicon.

Although lack of transferability is a serious drawback, the empirical potentials can still be useful as interpolation or extrapolation functions. Thus, in a rather limited sense, an empirical description can still be of value in simulating systems with large numbers of atoms. However, as with any interpolation scheme, an empirical model works best for atomic configurations close to the states where exact solutions are known. Accordingly, we shall use our empirical models for simulations only where atomic environments are close to those where the model was shown to be applicable.

Of the available empirical potentials for Si that of Stillinger and Weber (SW) (1985) performed well specifically in describing the structure and energetics of 30°-partial dislocations in the {111} glide system (Duesbery *et al.* 1991). Since the mechanisms of motion of this particular partial dislocation were of interest, the SW empirical model was chosen for our simulations.

The SW function for Si has the following form;

$$\dot{U} = \sum f_2(r_{ij}) + \sum f_3(r_{ij}, r_{ik}, \theta_{jik}), \tag{1}$$

where f_2 is the two-body, and f_3 is the three-body energy contribution to the energy, r_{ij} is the distance between atoms i and j, θ_{jik} is the angle between two vectors connecting atom i to atoms j and k, respectively, and the sums run over all enclosed indices. The two-body energy term f_2 is of the Lennard–Jones type, while the three-body term f_3 is a product of radial distance and angle-dependent terms. Important for the subsequent discussion is the angle-dependent term in the three-body energy which is of the following form:

$$f_3 \sim (\cos \theta_{jik} + 1/3)^2. \tag{2}$$

This particular form was chosen to stabilize the open diamond cubic structure of Si by countering deviations of the cosine of the bonding angle from the tetrahedral value of $-1/3$.

2.3. *Geometry of simulation cell and boundary conditions*

Correct choice for boundary conditions (BC) is important for obtaining physically acceptable simulation results. First, BC should be flexible enough to permit atomic motions of interest to take place. On the other hand, BC must not introduce spurious effects. In the present study BC were chosen to reach a balance between flexibility and simplicitly, without compromising accuracy.

Specifically, periodic BC were chosen where bulk material is simulated by closing boundaries of the simulation volume on themselves in a three-dimensional torus. For additional flexibility, the Parrinello–Rahman constant-stress method was used that allows the periodic box to change its shape (Parrinello and Rahman 1982) in response to any imbalance between the desired and the actual stress in the simulation volume.

Other types of BC have also been suggested and were applied by others, including various modifications of the so-called 'flexible' BC, where the simulation volume was divided into two parts: the explicit atomic core (1), and the surrounding elastic continuum (2) (Hoagland, Hirth and Gehlen 1976). Then, by linking the two regions together 'smoothly' it becomes possible to obtain relaxed atomic structures of dislocations and cracks. Possibly the most satisfactory BC of this type were developed by Sinclair (1975).

More recently, the same basic idea was employed in more sophisticated ways through the use of the lattice Green's function method (Thomson, Zhou, Carlsson and Tewary 1992) and finite element methods based on non-local elasticity (Kohlhoff, Grumbsch and Fischmeister 1991). Also, free-surface BC were used in various modifications. Of those, the best results were obtained with surface tractions adjusted according to appropriate solutions of linear elasticity theory applicable to the outer medium (deCelis, Argon and Yip 1983, Cheung and Yip 1990).

The current status of development of BC for studying atomic mechanisms of fracture and plasticity in solids is such that none of the BC is ideal for all applications, and the correct choice depends on the objectives of a particular study. The specific periodic BC chosen by us proved to be reasonable, as was confirmed by the results presented in § 3.

Simulations of dislocations in the periodic BC present unique problems: because it is impossible to have only one dislocation in the simulation volume, one has to introduce a dislocation dipole in the periodic box even if only the properties of a single dislocation are of interest. The two dislocations then interact with each other and with all periodic images of themselves. If dimensions of simulation cells are small, the effective density of dislocations is high, which results in a substantial level of spurious stress in the simulation volume. Such undesirable effects, however, can be minimized by a proper choice of the size of the periodic box.

In some studies (Bigger *et al.* 1992) such distortion stress was substantially reduced by using a *quadrupole* dislocation arrangement in periodic BC. In the present simulations the choice has been made for a dipole in a relatively large box resulting in a relatively small distortion stress. Moreover, by allowing the box shape to change, the net stress in the simulation volume can be maintained at any desired level, including zero.

The X, Y and Z axes of the simulation cell were chosen parallel to the $[11\bar{2}]$, $[111]$ and $[\bar{1}10]$ directions respectively of the diamond cubic lattice of the Si single crystal. For the perfect arrangement of atoms a rectangular box was chosen with 30 atomic planes in the X and Y directions and 25 planes in the Z direction, containing on the whole 22 500 atoms. The general geometry of the periodic box is shown in fig. 1, along with

Fig. 1

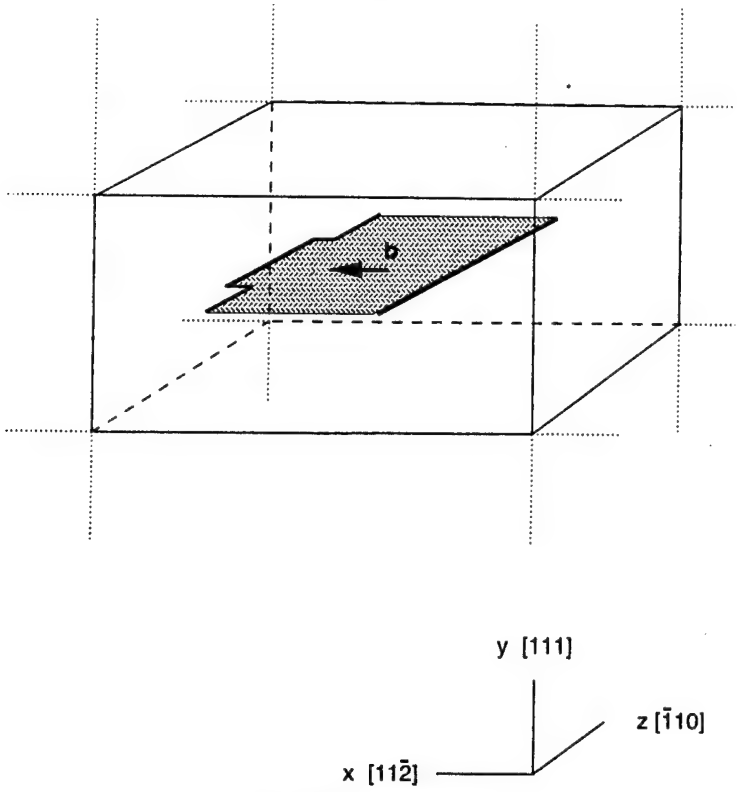

Simulation geometry.

a pair of dislocations lying in a (111), (XY), plane: one straight and the other kinked, and arranged parallel to the [$\bar{1}$10] (Z) direction.

In order to test the sensitivity of results to the size of the simulation cell, a few calculations were performed using a simulation volume four times the normal size, i.e. containing 90 000 atoms. For the case of two straight dislocations in a (111) glide plane, the excess energies per unit length of dislocation, computed for 22 500 and 90 000 atoms, agreed within 0·4%. Compared to the quality of the empirical potential model chosen for silicon, such accuracy is more than adequate. Nevertheless, a relatively large simulation volume is required to accommodate dislocations and kinks without any core overlap. Most of the simulations discussed below were performed using a simulation cell of the geometry described above with 22 500 atoms.

2.4. *Constrained simulated annealing technique*

It is known that the motion of kinks and other core defects controls the dislocation mobility in Si (Hirth and Lothe 1982). As stated above, the approach taken here is to study dislocation mobility indirectly by applying static minimization methods to obtain low-energy defect states and connecting them by low-energy pathways relevant to dislocation and kink motion. Here we introduce a numerical technique for finding the lowest energy minima on the N-body energy surface.

Although in some cases one may guess the relevant defect states by observing the symmetry of the crystalline lattice, it is desirable to avoid such guesswork and to follow more systematic ways of finding the lowest energy minima on the energy surface. For this purpose it is natural to adopt the simulated annealing (SA) approach, which has

been shown to provide a basis for very effective computational algorithms of *global optimization* (Otten and van Ginneken 1989, Press, Teukolsky, Vetterling and Flannery 1992). The advantage of the SA method, in contrast to the more conventional algorithms of local optimization such as steepest descent or conjugate gradients, lies in its ability to find the absolute (global) minimum of an object-function. The method is applicable to various complex problems, as was reviewed by Otten and van Ginneken (1989).

Consider the potential energy of an N-body system which can be viewed as a hyper-surface defined in the $3N$-dimensional space of atomic coordinates. Such an *energy surface* may have a very complex structure with topographical details of various scales and character. The idea of the SA method is to let the N-body system explore all these scales in succession, from the largest to the smallest, so that eventually it finds the lowest depth of its potential energy. This is done using Monte Carlo or MD sampling techniques applied first at a high temperature T. If the system is given enough time to wander at this initial temperature, it will sample all accessible regions of the $3N$-dimensional configurational space and reach (partial) *thermal equilibrium*. At this stage the system escapes freely from local minima of depth less than or of the order of kT, but other, higher barriers keep it confined generally within a low energy region.

Subsequently, temperature is decreased gradually according to a specified *annealing schedule*, and the system begins to feel smaller details of the energy landscape so that the location of the low-energy region is further refined. Although such a procedure of gradual refinement does not guarantee that the global (absolutely lowest) minimum will be eventually found, it can lead to energy minima acceptable in a practical sense. The key to success is in the appropriate choice of the annealing schedule (Otten and van Ginneken 1989, Press *et al.* 1992).

Although practical recipes have been suggested (Press *et al.* 1992), choosing the annealing schedule is still an art. The problem is that one has to have some initial information about the topography of the energy function in order to choose an optimal schedule. On the other hand, it is precisely the purpose of using the SA technique to explore this unknown topography. For that reason annealing schedules are usually chosen by trial and error. In spite of the above difficulty, SA is a very robust, although computationally demanding, numerical method for global optimization. With appropriate modifications, as discussed below, we have used it successfully to find the low-energy defect states in the dislocation cores relevant to dislocation mobility in Si.

By experimenting with annealing schedules we have found that for the specific purpose of finding low-energy defects in dislocation cores, the SA method should be modified to prevent *over-annealing*. Suppose one wishes to find the lowest energy kink states in the dislocation core (for more details see § 3.4). A possible geometry for such a simulation is given in fig. 1, where one of the two dislocations contains a double kink. Now, if the usual SA procedure were applied to this structural state, then during the initial stages of high-temperature annealing the system would evolve gradually so that the kinks would anneal out first, followed by the dislocations themselves. In the end, a perfect diamond cubic (DC) structure would result with no kinks, dislocations or any other defects present.

Clearly, the above result is due to the fact that the defect-free DC structure is by far the lowest energy state of the atomic model of Si. On the other hand, in order to use the SA method for finding metastable low-energy defect states it is necessary to find alternative ways of employing the method. Depending on the annealing schedule, some structural states with defects can be obtained by the usual SA algorithm. However, such cases of accidental success do not establish a systematic search procedure.

Fig. 2

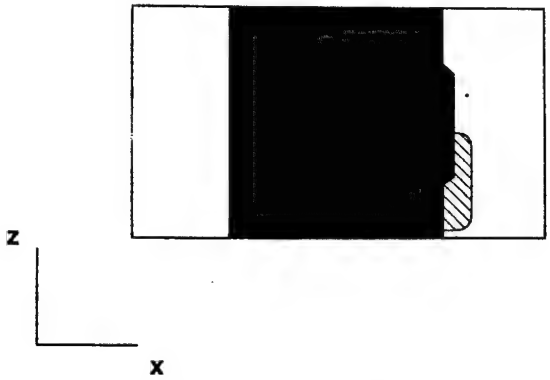

Simulated annealing constrained to a small region surrounding kink.

The search for low-energy defect states can be carried out more effectively if the system is prevented from visiting the many corners in the $3N$-dimensional space of atomic coordinates that are far removed from the relevant configurations of dislocation kinks. Practically, this is implemented by performing the SA search in a reduced subspace of atomic coordinates confined to a volume around the kink (fig. 2). This volume must be large enough to include all atoms in the core of a single kink, but it must not include the second kink or the second dislocation to prevent their mutual annihilation. Fortunately, the atomic models employed here, containing from 22 500 to 90 000 atoms were large enough to satisfy the above requirement.

We have established that volumes comprised of one to two thousand atoms in and around the kink core were sufficient for finding lowest energy states of kinks and other more complex defects, which are discussed in detail in § 3. The benefits of using such a modified SA technique are twofold. First, the kink will not anneal out and low-energy forms of it, whatever they are, will be eventually found in a systematic way. Second, the dimensionality of the search is greatly reduced from 22 500 (or 90 000) to 1000 (or 2000). Hence, the search requires much less computational effort.

It may be argued that, since most of the atomic coordinates are kept frozen during the constrained SA search, the minimum located will only be approximate. While this is true in certain cases, the position of the minimum can be further refined, after the search is completed in a reduced subspace, by performing local unconstrained minimisation in the full configurational space of all $3N$ atomic coordinates. Such a refinement usually requires only moderate computational effort, since the preceding constrained SA search brings the system already very close to the true minimum. In practice, a sequential procedure, consisting of a constrained SA search and subsequent unconstrained refinement, was found to be reliable and robust. This method was used extensively to search for the low-energy defect states relevant for dislocation motion to be discussed in § 3.

2.5. *Sampling by gradual ascent*

It has been mentioned earlier that a straightforward MD approach was not successful in simulating dislocation motions in Si. In this section, we consider some of the difficulties involved and an alternative approach based on the notion that the many-body energy function itself contains, in principle, all the information about rate-dependent properties of the system. In the same way that the energy minima correspond to various

mechanically stable structural states, so the dynamic evolution of the system is characterized by the low-energy paths which connect these minima in the $3N$-space. Specifically, the saddle points on such paths determine the kinetics of the mobility.

In standard formalism of transition state theory (TST) (Halsey, White and Eyring 1945) any rate-dependent process is considered to be a net result of transitions (or jumps) from one energy basin to another. The dominant contributions to the kinetic rates then come from the states near the lowest saddle points on the energy surface. Although dynamic effects are ignored (Carter *et al.* 1989), the low-energy paths connecting the energy minima and the saddle points are sufficient to determine transition rates.

In Si the dislocation motions generally require the breaking of strong covalent bonds. Consequently, the barriers for such motions are relatively high, of the order of 1 eV. At temperatures below melting, only the paths going over the lowest saddles are expected to contribute appreciably to the overall dislocation mobility. An efficient numerical algorithm for finding such low-energy paths on the energy surface is therefore needed.

It is clear that the problem of finding the paths with the lowest saddle points is considerably more challenging than that of finding the lowest minima. This is because one is dealing not with a single state, but an entire connected sequence of structural states. The problem is so complex that a systematic, general approach has yet to be established (Czerminski and Elber 1990). Among the numerical methods that have been developed, including a so-called local propagation technique (Cerjan and Miller 1981), various modifications of the 'reaction coordinate' approach (Czerminski and Elber 1990) and others (Stillinger and Weber 1982), the only systematic method suggested so far for finding optimal paths on the $3N$-dimensional energy surface is that of Elber and Karplus (EK) (1987). In spite of the promise of this method, the computational cost involved in optimizing the paths is extremely large for systems containing many atoms.

We now introduce a less systematic approach which we will call gradual ascent (GA); it was found to be quite efficient in finding the low-energy paths connecting two energy minima. Consider two different mechanically stable structural states of the system corresponding to minima labelled 1 and 2 on the energy surface. Suppose we wish to displace the system from 1 to 2 statically, by applying a local perturbation field superimposed on the N-body potential energy such that the latter is gradually deformed to bring minimum 1 closer to the first dividing saddle point. In this process, some up-hill displacement is necessary on the way, however, it is also important to avoid climbing up against very steep walls of the potential energy.

In the present study the system is driven uphill by connecting its current position in the configurational space (initially at minimum 1) directly to the configuration at minimum 2 with a harmonic spring potential of variable stiffness. Starting at zero stiffness and initial state 1, the stiffness is raised in small increments, and at each step the atomic positions are allowed to respond to the applied perturbation by minimizing the total (interatomic plus spring) energy.

In the beginning of this process, both the spring and interatomic energies are found to increase steadily with increasing stiffness. However at some point the spring energy reaches a maximum and then begins to drop. Such behaviour signals that the system has just been driven over the ridge. If the springs are released soon after this is observed, and a simple steepest descent search is applied, the system may be found in state 2, or in an intermediate minimum, say state 3. In the latter case, if reaching state 2 is still of interest, the system should be driven from state 3 toward state 2, and so on.

Although the outlined procedure will necessarily yield a path connecting states 1 and 2, it tends to find only the rather direct paths, and in a few instances it has failed to find the lowest saddles lying farther away from the straight path. In order to devise a more flexible algorithm a modification was introduced as follows. It is not surprising that, when driving the system uphill, some of the atoms offer more resistance to the applied perturbation than others. This suggests that it may be more efficient in sampling the atomic displacements not to increment the stiffness uniformly throughout. Instead, by allowing the atomic springs to vary individually, a flexible and more natural sampling procedure is obtained where the more resistive atoms are not displaced uphill as much as the less resistive ones.

With the above modification the GA algorithm has been used to find several low-energy paths relevant to dislocation mobility. In contrast, a more rigid search, where the stiffness was incremented uniformly for all springs, often resulted in higher energy paths. The conclusion is that the flexible GA algorithm is superior to the rigid GA search. For this reason, the former has been used almost exclusively in the present study.

To further test the effectiveness of our method in finding the lowest paths, we performed direct path optimizations using the EK procedure for two important cases of motion of the kink complexes (details given in § 3.4), and compared the results with those obtained using the GA algorithm. In both cases the lowest saddles obtained were essentially the same.

While this comparison does not demonstrate the general validity of the GA technique, it does indicate that GA is capable of giving correct results for the low-energy paths. Moreover, in addition to its high computational efficacy, the method can be used even when the final destination (minimum 2) is not known in advance. In fact, it was found that in many cases a crude guess about the destination state was sufficient as long as the subsequent search was flexible enough. An example of this is given in § 3.5, where homogeneous nucleation of kinks is discussed. In that case, both the final fully relaxed structure of a narrow double kink and a low-energy path for its formation were obtained by displacing the system from the initial state (a straight dislocation) to the final state (a wide rectangular double kink) using the flexible GA algorithm.

In summary we emphasize that the GA algorithm does not guarantee finding the lowest possible activation paths. The technique is not based on mathematical theorems, but is a result of attempts to find a practical alternative to other, more systematic but also computationally very demanding, numerical methods. In § 3 we present a number of important atomic mechanisms governing dislocation mobility in Si that were obtained by the GA method.

2.6. *An algorithm for accurate location of saddles*

In the GA method we have discussed so far, although the system is driven over ridges on the energy surface, there is no assurance that the crossing occurs at the lowest energy point, i.e. a saddle. Additional effort is required to determine the position of a saddle point. Most of the available methods for locating saddles appear to be either not robust, or computationally too costly, or both (Cerjan and Miller 1981, Stillinger and Weber 1982). Sinclair and Fletcher (SF) (1974) have suggested a modified conjugate gradient procedure for local minima as well as for saddles, at about the same computational cost. However, at times the SF method fails to converge to, or even misses, the saddles altogether (Sinclair and Fletcher 1974, Bulatov and Argon 1992). We have found that by combining the SF algorithm with an eigenmode analysis

a more robust algorithm is obtained. In this study more than a hundred saddle points have been accurately located using the modified SF technique.

To summarize, in this section we have discussed numerical methods that were employed in the present study. The intention was not. to provide a systematic introduction to the simulation methods (these are described elsewhere), but rather to clarify the various difficulties encountered in simulating dislocation motion in Si and how these can be circumvented in practical ways. Although development of new techniques was not an initial priority, substantial effort was invested in analysing in a controlled way the atomic level processes that govern dislocation motion. For this the focus was on finding both accurate and practical alternatives to more elaborate and much more costly computational procedures currently used in atomistic simulations. The numerical methods discussed above were designed with this specific purpose in mind. The results reported below justify our choice of the static relaxation approach for studying the kinematics and energetics of elementary processes involved in the motion of partial dislocations in Si.

§ 3. Simulation results

3.1. *An overview*

In our approach to identifying important mechanisms of dislocation motion in Si, we shall draw substantially on previous studies on this subject.

Silicon has a diamond cubic structure consisting of two interpenetrating fcc lattices displaced relatively to each other by one-quarter of the long diagonal of the cubic unit cell. Accordingly, as in the parent fcc lattice, {111} planes are the principle slip planes. Because of the non-primitive structure of the diamond cubic lattice, there are two distinct subsets of 111 slip systems, the shuffle and the glide sets (Hirth and Lothe 1982).

In principle, full dislocations of the shuffle subset should be more mobile than their glide counterparts (Duesbery and Richardson 1991). However, results of electron microscopy (Ray and Cockayne 1971) have shown that both static and mobile dislocations on {111} planes are dissociated, thus indicating that the shuffle set dislocations do not play a major role in crystallographic slip in Si since dissociation on the shuffle subset is hardly possible. That plastic slip in Si occurs predominantly on the glide subset has been also confirmed by direct lattice imaging (Duesbery and Richardson 1991).

Our attention will be concentrated on the {111} glide subset dislocations, which dissociate into Shockley partials of two types: 90°-(edge) partial and 30°-(mixed) partial. There is a growing consensus in the literature that these two partial dislocations contribute most prominently to the plastic properties of crystalline Si. Of the two, the 90°-partial has received so far more attention from the theorists due to its simpler structure. On the other hand, the 30°-partial is no less important, since it is involved in the dissociation of both screw and 60°-full dislocations. In comparison, the 90°-partial is involved only in the dissociation of the 60°-full dislocation.

In the present communication, results are presented of simulations performed with the specific purpose of studying the atomic modes of mobility of 30°-partial dislocations of the {111} glide subset of Si based on the Stillinger–Weber empirical model. The intent is to use a systematic approach to obtain in the end a reasonably complete picture of the motion of 30°-partials.

In this section we discuss the essential set of findings related to the motion of the 30°-partial dislocation in intrinsic Si. The essential set comprises the structure, energetics, and atomic mechanisms of nucleation and motion of various core defects on the 30°-partial dislocations in Si and a few associated configurations important for the mobility of this type of dislocation. For ready reference we give here a brief overview of the important results discussed in detail in the subsequent subsection.

First, a fully relaxed structure of the 30°-partial dislocation core is obtained and discussed. It is found, in agreement with the earlier studies, that this partial dislocation reconstructs by pairing up dangling bonds of the core atoms and forming bonded dimers in the core. This (2×1) reconstruction is strong, resulting in the formation of reconstruction, or so-called *antiphase defects* (APDs). Structure and energies of APDs and dislocation *kinks* are examined; it is established that the individual left and right components of a *double-kink* have vastly different structures, pointing to an intrinsic left–right asymmetry of the 30°-partial. These two kink forms are termed conventionally *left kink* (*LK*) and *right kink* (*RK*) (§ 3.2).

Second, low-energy paths for the displacement of LKs, RKs and APDs along the dislocation core are found and the corresponding energy barriers are calculated. The energy barrier to APD motion is very low (0·17 eV), compared to the motion barriers for both kinks, 0·74 for the RK and 0·82 for the LK. This difference in the motion barriers is related to the *lubricating* effect of a dangling bond involved in the motion of the APDs. Motion of both kinks is found to involve intermediate metastable configurations, identified as *alternative* forms of the kinks, *LK'* and *RK'*. The origin of these alternative structures is traced to the period doubling due to the (2×1) reconstruction (§ 3.3).

Third, interactions of the kinks with the APD are examined. Contrary to the earlier suggested picture of weak binding, the kinks and the APDs are found to bind strongly and form stable kink–APD complexes: the left kink-APD complex (LC) with binding energy of 0·51 eV and the right kink–APD complex (RC) with a binding energy of 0·84 eV. Structures of the complexes are such that the parent defects can no longer be recognized: the LC contains an atom with a dangling bond in its centre, while the RC is centred around a fivefold coordinated atom instead. Accordingly, motion barriers for the complexes differ by a factor of 5, with the LC motion barrier at 0·22 eV and the RC motion barrier at 1·04 eV. These findings point again to the observed lubricating effect of the dangling bonds and the left–right asymmetry in the core of the 30°-partial dislocation (§ 3.4).

Fourth, various atomic mechanisms for the nucleation of kinks and reconstruction defects are discussed in the last two subsections in the context of *defect multiplication reactions*. In order to choose between multiple possibilities, selection rules based on kink- and APD-numbers are introduced. Final selection of the candidates is made by inspection of the energy balance between reactants and products. It is found that the nucleation of kinks and APDs requires rather substantial energy when it occurs homogeneously, i.e. in the core of a perfectly reconstructed (defect-free) 30°-partial (§ 3.5). At the same time, the nucleations occur preferentially in the presence of in-core defects: double kinks are formed in the presence of an APD, while APD pairs are formed in the presence of a kink. These effects are generally attributed to the influence of the kink–APD binding which, if present during the nucleation event, reduces the nucleation barrier substantially (§ 3.6).

Fig. 3

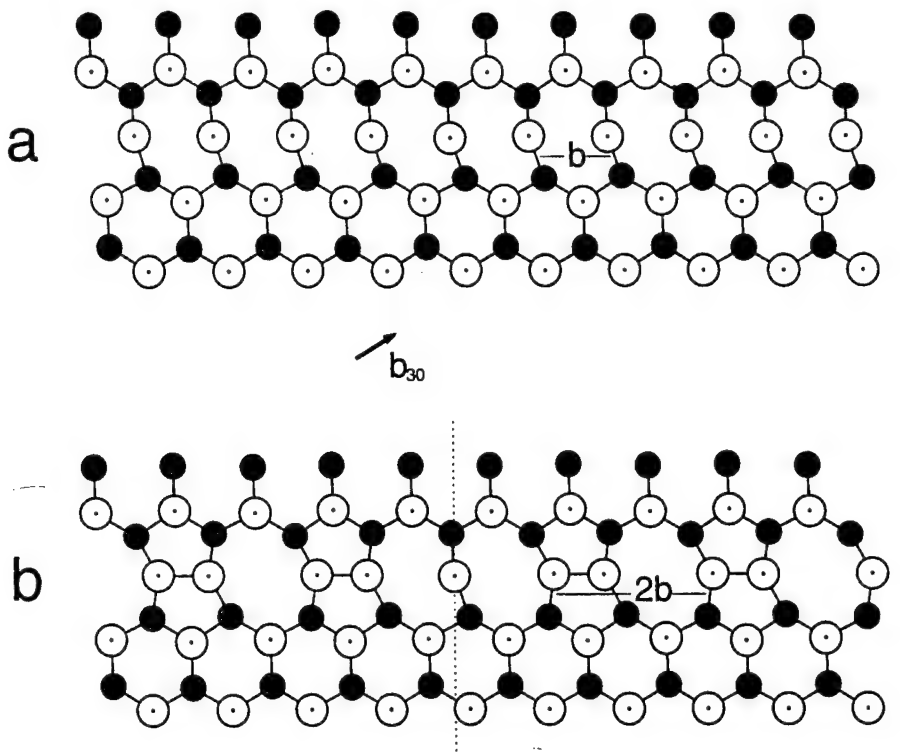

Core structure of 30°-partial dislocation : (*a*) unreconstructed and (*b*) reconstructed.

3.2. *Core structure and in-core defects of a 30°-partial dislocation*

3.2.1. *Core reconstruction and reconstruction defects*

The structure of an (unreconstructed) 30°-partial dislocation core on a {111} glide plane is given in fig. 3 (*a*), where a small cluster of atoms (80 out of 22 500) immediately above (open circles) and below (shaded circles) the glide plane is shown. Regular atoms in the diamond cubic structure have fourfold coordination: three bonds are shown as straight segments nearly parallel to the glide plane, while the fourth bond points up for the atoms above the glide plane (shown as dots in the centres of the open circles) and down for the atoms below (not shown).

Unlike regular atoms, atoms in the core have only three bonded neighbours,† each with one dangling bond. The fully relaxed core structure shown in fig. 3 (*a*), has an excess energy of 2·72 eV per repeat distance *b* along the dislocation line (*b* is also the Burgers vector length for the full screw and 60° dislocations).

Clearly, this excess energy is rather high and includes both the (elastic) energy due to distortions of the bond lengths and angles and the energies of dangling bonds on the atoms in the core. On the other hand, it was suggested earlier that partial dislocations in Si experience reconstruction where atoms in the core move closer to each other so that the unpaired electrons can form bonding orbitals (Alexander and Tiechler 1991).

For the 30°-partial dislocation, such reconstruction occurs via a particularly

† There are no explicit bonding terms in the SW potential function, so bonds are shown conventionally for each pair of atoms that are within a certain distance from each other which is chosen as 1·20 of the equilibrium bond length in the perfect diamond cubic lattice of Si.

symmetry-breaking atomic rearrangement shown in fig. 3 (*b*), where the repeat distance along the dislocation line doubles to become 2*b*. Although the reconstruction introduces additional distortions of the bond lengths and angles, such effect are clearly offset by a reduction in energy due to pairing up of the dangling bonds. As a result, the excess energy is significantly reduced to become 1·91 eV/*b*, indicating that the core of the 30°-partial dislocation must be strongly reconstructed.

Parenthetically, there is little use for a so-called *core energy* in atomistic simulations of dislocations. In fact, this parameter was initially introduced to eliminate the apparent divergence of the energy of a single dislocation treated as a line singularity in the continuous linear elastic field (Hirth and Lothe 1982). Clearly, in a discrete atomistic model such a problem never arises, since the nonlinear interactions are all appropriately accounted for. Therefore, no attempt has been made here to estimate the core energy which would have required a rather artificial separation of linear from nonlinear interactions. Instead, excess energy per unit length of the dislocations was used for comparison. Since the nonlinear interactions only gradually fade away, this also underscores the need for a rather more substantial environment in the dislocation model.

The excess energy of the dislocation, computed in the present simulation geometry, contains at least three distinct terms: excess energy of the isolated dislocation, energy of the long-range elastic interactions between dislocations in the dislocation dipole and their periodic images, and the stacking fault energy. The last term is zero for the SW potential since the cutoff range of the potential function is not long enough to include third-nearest neighbours for a given atom. Moreover, because the size and geometry of the simulation cell are such that dislocations and their images are always separated by distances not less than 13*b*, the interaction terms are also relatively small, as was already mentioned in § 2.

The symmetry-breaking reconstruction changes periodicity along the dislocation core, which may have profound effects on the electronic properties of Si with dislocations. One clear consequence of the reconstruction is that the size of the Brillouin zone in the direction along the dislocation core shortens by half. Various effects of the reconstruction on the electronic properties of Si are discussed by Alexander and Tiechler (1991).

Important for the present discussion is the fact that reconstruction of the 30°-partial is a very robust effect which has been reproduced in simulations based on various empirical interatomic potentials (Duesbery *et al.* 1991) as well as in calculations based on a semi-empirical tight binding approximation. Experimentally observed levels of the spin-resonance signals are consistent with the reconstructed core structure, where not more than 5% of in-core atoms can be associated with paramagnetic centres (Alexander and Tiechler 1991). The remaining signal may be related to the presence in the dislocation core of reconstruction defects.

Hirsch introduced the so-called APD of the reconstruction; since the symmetry can be broken in two ways, there must be domains in the dislocation core reconstructed in the two opposite senses, i.e. out-of-phase with each other (Hirsch 1980). The boundary between the perfectly reconstructed domains is then an APD, or simply a core atom which has a dangling bond between the two phases of the reconstruction. Such a defect is shown in the centre of fig. 3 (*b*) for the 30°-partial dislocation. Its energy was found to be 0·81 eV.

For the sake of comparison, it is convenient to introduce at this point an energy scale parameter. A natural choice for the SW model of Si is the depth of its two-body energy

Fig. 4

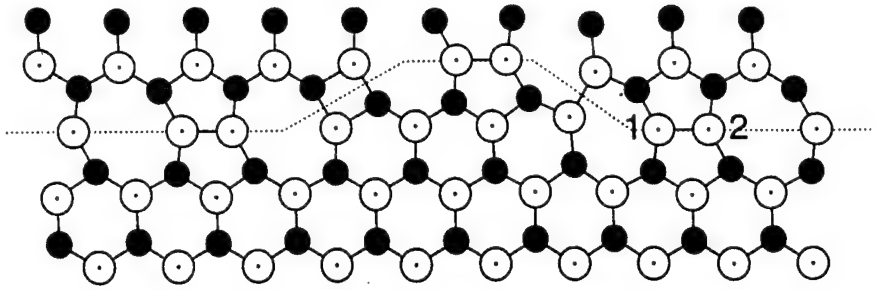

A narrow double kink in the reconstructed core of 30°-partial dislocation.

well, i.e. 2·17 eV. At the same time, this is also the cohesive energy per bond of diamond cubic Si, i.e. the energy to break a covalent bond.

Since breaking a reconstructed bond is required to produce two APDs, the APD energy should be close to 1·08 eV. Its actual value, 0·81 eV, is notably lower for several reasons. First, the reconstructed bond is 3% longer and, therefore, weaker than the regular bond. In addition, bond angles deviate from the ideal tetrahedral angle by up to 19° in the reconstructed configuration. Accordingly, when the reconstructed bond breaks, these and other distortions are relaxed, which accounts for the energy difference.

It is recognized that an APD is not a 'plasticity carrier' by itself, meaning that its motion does not produce any plastic strain. However, it is a natural and important by-product of reconstruction and should be anticipated to play a role in the nucleation and motion of dislocation kinks. Furthermore, Hirsch (1980) conjectured that APDs and kinks may bind weakly to each other forming kink–APD complexes. For these reasons, various aspects of APD–kink interactions will naturally appear in the following discussion.

3.2.2. *Structure and energy of kinks in the 30°-partial*

Dislocations move by nucleating and expanding double-kinks (Hirth and Lothe 1982). In bcc metals and some other materials with less directional bonding, the kinks can be wide, spreading over 10–20 repeat distances along the dislocation line. On the other hand, in Si and other materials with high Peierls barrier (or Peierls resistance) the kinks must be very narrow. In the Stillinger–Weber model discussed here, it is the directional nature of covalent bonding, modelled by the stiff angle-dependent part of the potential, that makes the kinks narrow. It is shown below that for the same reason dislocation kinks in Si have rather high energy too. This is consistent with the electron microscopy data showing that at moderate temperatures dislocations in Si are very straight and confined almost exclusively to lie along ⟨110⟩ directions (Duesbery and Richardson 1991).

Shown in fig. 4 is a small fragment of the 30°-partial dislocation core containing a closely spaced double-kink. The fully relaxed excess energy of this configuration is 1·51 eV, including the attractive kink–kink interaction for this spacing. At larger separations this energy reaches 1·60 eV and can be identified as the double-kink energy. In fact, in the linear elastic limit, kink–kink interaction energy is inversely proportional to the kink separation according to the following expression in isotropic elasticity (Hirth and Lothe 1982):

$$\Delta U_{\text{kink-kink}} = -\frac{\mu b^2 a^2}{8\pi x(1-\nu)}((1+\nu)\cos^2\alpha + (1-2\nu)\sin^2\alpha) = -\frac{A}{(x/b)}, \qquad (3)$$

where μ is the shear modulus, b is the dislocation Burgers vector, a is the kink height,

x is the distance between kinks, ν is Poisson's ratio and α is the angle between the Burgers vector b and the dislocation line. For the case of the 30°-partial and the SW interaction parameters, $A = 0{\cdot}277$ eV†.

Comparing eqn. (3) with a corresponding energy term computed directly from the atomistic model, we find, indeed, that at separations larger than 5–6b, kink–kink interaction is consistent with the linear elastic prediction. On the other hand, at smaller distances kink–kink interaction becomes strong and essentially non-linear, as discussed further in § 3.4. The above value of 1·60 eV for the double-kink energy is taken as the energy of the two kinks at a distance 6b from each other. Then, the remaining kink–kink interaction energy can be estimated from eqn. (3) as 0·046 eV. With this correction, the energy of two kinks an infinite distance apart from each other becomes 1·64 eV.

Although the formation of a double-kink requires the breaking of a reconstructed bond, the double-kink energy is lower than the ideal bond-breaking energy of 2·16 eV, apparently for the same reasons as previously discussed in the case of APD. Clearly, in the given geometry kinks appear only in pairs. It is then conventional to define a single-kink energy as one half of the double-kink energy, i.e. 0·82 eV. This value is almost identical with the APD energy of 0·81 eV, and agrees very well with previous calculations (Duesbery *et al.* 1991). The equal partitioning of the double-kink energy between the LK and the RK is still an issue which deserves some scrutiny, since structures of the two kinks are very different (fig. 4)‡. This is in contrast with the case of a double-kink in a 90°-partial (Heggie and Jones 1987), where both kinks have the same structure.

The origin of such asymmetry can be traced to the fact that whenever the Burgers vector has a non-zero screw component (i.e. no longer pure edge), it is possible to associate the sense of the dislocation to the direction of the screw component. Hence the asymmetry is not a result of our choice of the empirical force law, but is a consequence of the particular slip geometry of the 30°-partial in the diamond cubic lattice. It turns out that this asymmetry has important consequences and manifests itself profoundly in the ways that the 30°-partial dislocation moves, as we discuss in subsequent sections.

3.3. *Motion of isolated kinks and APDs*

3.3.1. *Overview*

Two defects can be considered isolated from each other if their interaction energy is negligible. In the model containing 22 500 atoms, the maximum defect separation is 12b, at which the kink–kink interaction energy is about 0·01 eV, two orders of magnitude smaller than the double-kink energy. All other interactions, such as kink–APD and APD–APD, are even weaker. Therefore, one may assume that the defects are well separated in that the presence of one defect does not affect the structural state of another at such distances. In other words, the defect cores do not overlap.

Kinks and APD are secondary defects in the core of the primary defect, the dislocation. Since a dislocation moves through the motion of kinks along it (Hirth and Lothe 1982), it is necessary to examine such motion. Although kink motion is

† Although diamond cubic Si is not isotropic, we have computed Voigt average values for μ and ν from the elastic constants c_{11}, c_{12} and c_{44} reported in Balamane, Halicioglu and Tiller (1992) for the SW empirical model.

‡ The energy of a single kink can be computed using a slightly different geometry of the periodic boundary conditions (Sinclair 1975). Results of such calculations will be reported elsewhere.

one-dimensional, there are many possible paths for the kink to move in the configurational space of participating atoms. Given that our goal is to find atomic mechanisms of the easiest motion, we will focus on those configurational paths associated with the lowest motion barriers.

Of the three relevant activation parameters, we will be concerned with only the activation energies in this communication. Results obtained for activation volumes will be reported elsewhere. In order to calculate the third activation parameter, activation entropy, a dynamic approach is required (Bennett 1975). This quantity will not be discussed here, since the substantial effort involved in dynamical simulations is not justified in view of the rather crude nature of the empirical force laws used to describe Si.

3.3.2. *Right kink motion*

Kink motion along the perfectly reconstructed dislocation core involves making and breaking of the reconstructed bonds (examine RK in fig. 4). One can imagine that a simple way for the RK to move is by breaking a reconstructed bond 1–2 on the right of the kink, and then forming another bond on the left as the RK moves to the right. Such a path indeed has been found using the GA sampling method. The path runs through a few intermediate minima, with the highest point on the path corresponding to an energy barrier of 1·87 eV. This is somewhat higher than the energy required to break a reconstructed bond (1·63 eV, almost exactly twice the APD energy). An additional 0·2 eV is required to move the kink after the reconstructed bond on the right is broken. This last stage of the motion is relatively easy, although the overall barrier is high due to the energy of bond breaking.

It is important to ascertain whether the above mechanism has the lowest possible energy barrier. It was found that a lower-energy motion mode does indeed exist that does not require the breaking of a bond completely, but involves a more coordinated atomic rearrangement where, at the same time as one bond is weakening, another one is forming (fig. 5). While the end result of such motion is the same, i.e. RK motion, kinematically it is a totally different mechanism. Because this path involves bond switching rather than bond breaking, the overall barrier is substantially lower than before, i.e., 0·74 eV compared to 1·87 eV. Shown in fig. 5 (*a*, *b*, *c*) are three sequential stages of RK motion that correspond to the first half of the kink translation to the right. The energies of the states *a*, *b* and *c* are marked by the corresponding letters on the energy *versus* motion coordinate† plot of fig. 5 (*d*). The initial configuration is an

† Notion of a motion coordinate is in some sense arbitrary. Indeed, as discussed by Bennett (1975) it is possible to use different combinations of the atomic coordinates to specify a motion (or reaction) coordinate. However, any physical quantity, e.g. activation energy or entropy, that is computed numerically will be independent of the particular choice of motion coordinate used for such a computation. For example, the mode of motion illustrated in fig. 5 can be equally well represented by the distance between atoms 1 and 2 and, alternatively, by an appropriate measure of local strain. Notice that both of the above measures change monotonically from the initial to the final state. In fact, for the sake of discussion we will often line up the stationary points on the energy plot with certain characteristic positions in the corresponding configurations. In particular, these points are chosen as the centres of symmetry for the configurations in fig. 5 (*a*), (*c*). Since the structure in fig. 5 (*b*) lacks symmetry, we choose the position of atom 4 as a geometrical centre, on the grounds that it experiences the largest displacement from its position in the initial structure to the final structure. In the following we will often omit discussions of the particular choices of reaction coordinates used to show the correspondence between structural states and energies.

Fig. 5

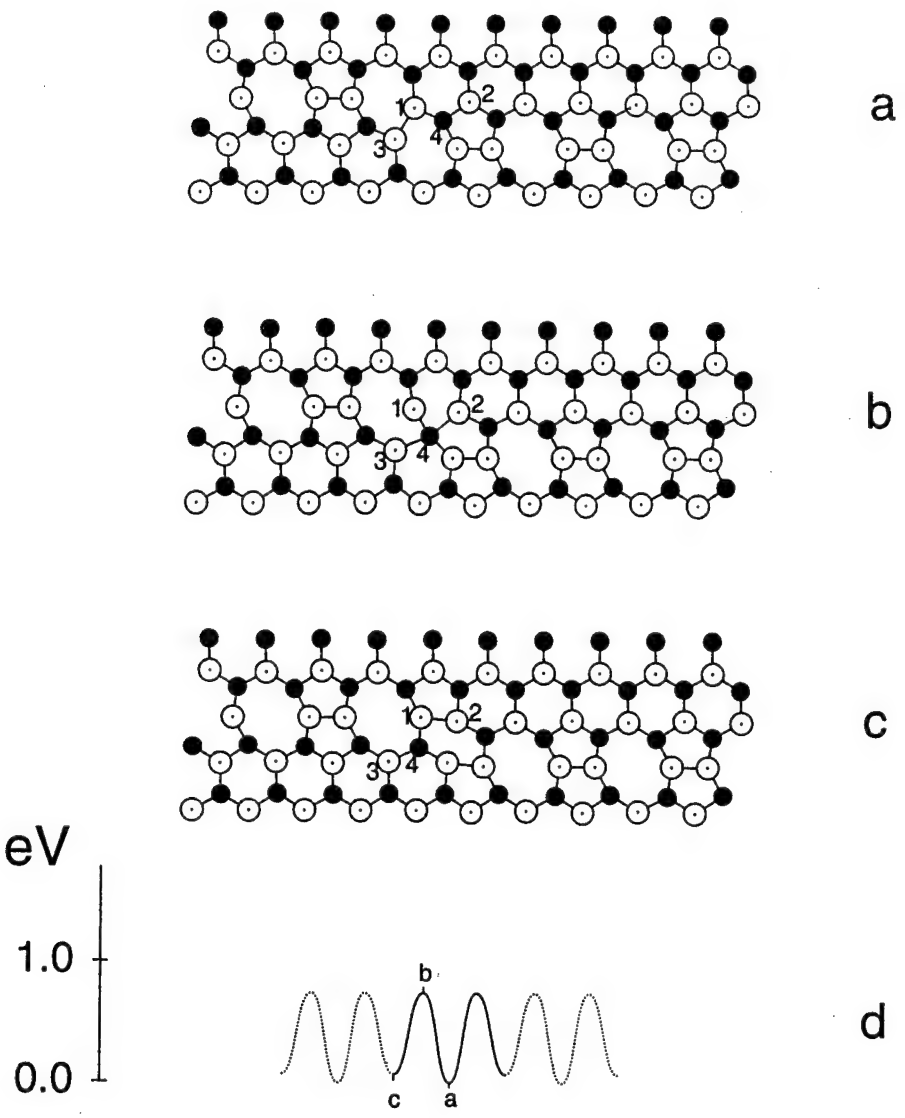

Lowest energy path found for motion of right kink.

isolated RK in the minimum configuration. Notice that in going from fig. 5 (*a*) to fig. 5 (*b*), bond 1–3 breaks while at the same time bond 3–4 is formed. Figure 5 (*b*) actually corresponds to a saddle point separating two adjacent minima. This barrier is 0·74 eV. Past the saddle, a new minimum is reached which is almost as deep as the initial state: its energy is only 0·07 eV higher. This last stage involves breaking bond 2–4 and simultaneously forming bond 1–2 (fig. 5 (*c*)).

This small difference in energies indicates that, at low temperatures when unknown entropy terms may be neglected, it is likely to find a RK in either of the two states shown in fig. 5 (*a*) and (*c*). To distinguish between these two forms of right kink, the abbreviation RK is reserved in the following only for the regular right kink shown in fig. 5 (*a*). At the same time, the abbreviation RK′ denotes the alternative structure shown in fig. 5 (*c*).

The right kink moves by $1b$ by transforming RK into RK′, or RK → RK′. Further motion to the right occurs over another barrier of the same height so that RK′ transforms back into the form RK, now having translated by a full period $2b$ to the right. The sequence of atomic motions in this second step is reverse to the one just discussed. Evidently, the existence of the alternative state RK′ for the right kink is related to the period doubling in the reconstructed core of the 30°-partial. The existence of an alternative stable kink structure has not been previously recognized, as the right kink has been identified as the structure shown in fig. 5 (*a*). In the present study the alternative structure RK′ occurs as an intermediate state of motion in the complete sequence of RK → RK′ → RK. Also we have found RK′ directly by random search using the constrained simulated annealing technique. In fact, the RK′ form appears clearly in the configuration reported in an earlier MD simulation using the same potential function (Duesbery *et al.* 1990). Although the authors concluded that no substantial motion was produced, the presence of RK′ indicates that some kink motion had apparently occurred in the simulation, but had not been noticed.

It is important to note that an attempt to move RK using the more straightforward ascent technique resulted in sampling the high-energy path involving bond breaking discussed earlier, in the sequence RK + bond → APD + RK + APD → bond + RK. On the other hand, the low-energy mechanism RK → RK′ → RK was found only using a modified GA sampling method, where the relative resistance of different atoms to moving up the potential energy surface was taken into account. The fact that no paths for RK motion of energies lower than 0·74 eV were found, indicates that the sequence RK → RK′ → RK is possibly the path of lowest energy available for right kink motion.

In the following, except for special circumstances, only the lowest paths are reported for various processes involving the core defects.

3.3.3. *Motion of left kink*

Motion of the left kink shown in fig. 6 is similar to the low-energy sequence for the right kink discussed above. Again, the lower-energy mechanism involves bond switching: the left kink LK (fig. 6 (*a*)) moves by transforming into an intermediate configuration LK′ (fig. 6 (*c*)) passing through the barrier state shown in fig. 6 (*b*). The barrier height is 0·82 eV, which is close to that of RK, at 0·74 eV. The left kink moves in the sequence LK → LK′ → LK, by which full translation over $2b$ is completed.

Despite the similarity, the two low-energy paths are quite different. The intermediate state LK′ has 0·42 eV higher energy than LK. Accordingly, such a state was not frequently found in the constrained simulated annealing search. Unlike RK′, this state should not be populated appreciably in equilibrium at moderate temperatures. Rather, its significance is in providing an intermediate *landing state* on the low-energy motion path. Here again, by comparing atomic mechanisms of motion of the two kinks, the asymmetry between left and right becomes apparent.

3.3.4 *APD motion*

Inspection of fig. 3 (*b*) shows that an APD can move if a reconstructed bond breaks, say immediately to the left of the APD. Afterwards the APD may bond to its immediate-neighbour atom, while the adjacent atom, leftmost of the three, is left with a dangling bond. Through this exchange the APD is translated by $2b$ to the left. Such a mechanism was found to have a rather high energy barrier of 1·65 eV.

Fig. 6

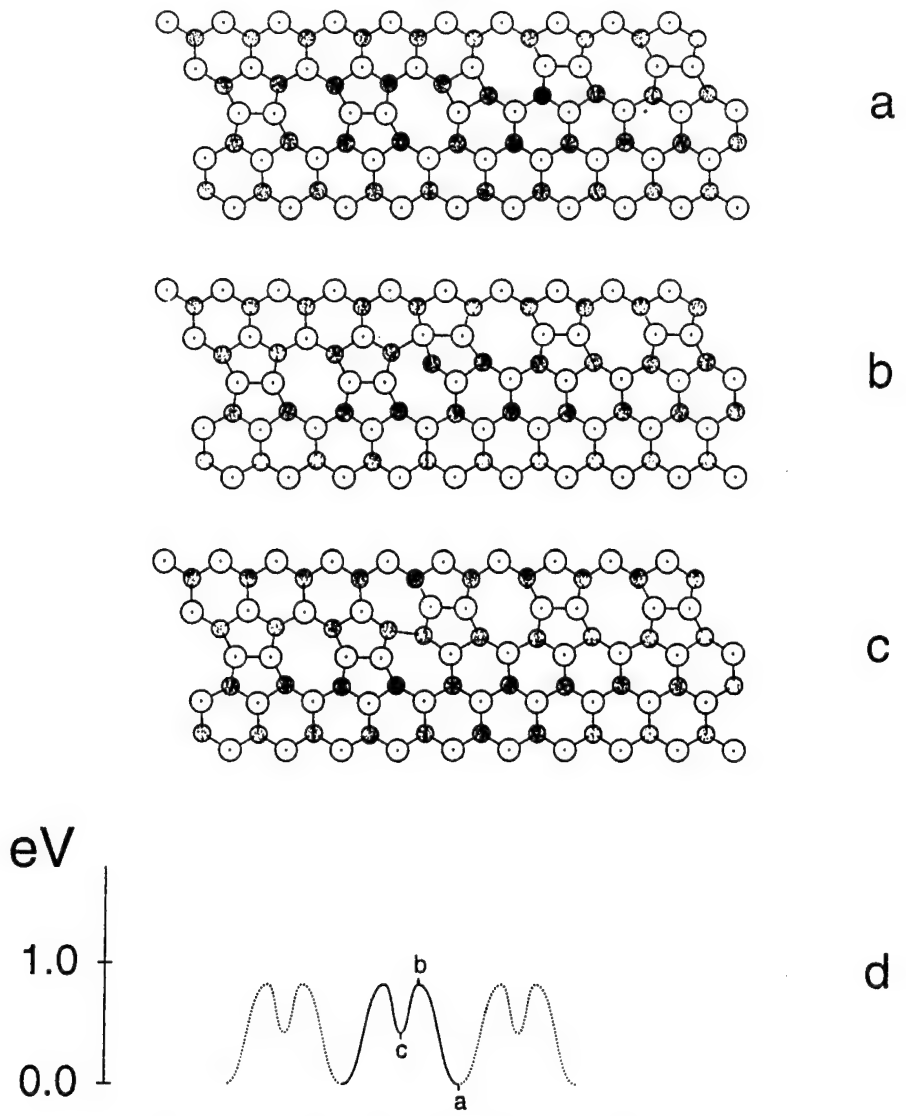

Lowest energy path found for motion of a left kink.

It was found, however, that an APD can break up the two atoms in the reconstructed pair more effectively by attacking the reconstructed bond, in the manner shown in fig. 7 (*a–d*). We note that this costs little energy, since, having one fewer bond than a regular atom, the APD can undergo relatively large in-plane displacements without perturbing its three bonds and their bond angles. In the ensuing barrier configuration of fig. 7 (*d*), the APD attaches itself to the reconstructed bond on the left. At the saddle point configuration, two bonds coexist, which results in a very low barrier, i.e. 0·17 eV. Completion of the full cycle of APD displacement occurs by the breaking of the co-existing bond on the left.

It may appear that some of the configurations shown in fig. 7 are quite similar to each other. Indeed, the similarity points to a typical feature of the energy profiles obtained for mechanisms involving an APD, namely the three very low barriers, each only about 0·01 eV high. Since these barriers are substantially lower than kT even at

Fig. 7

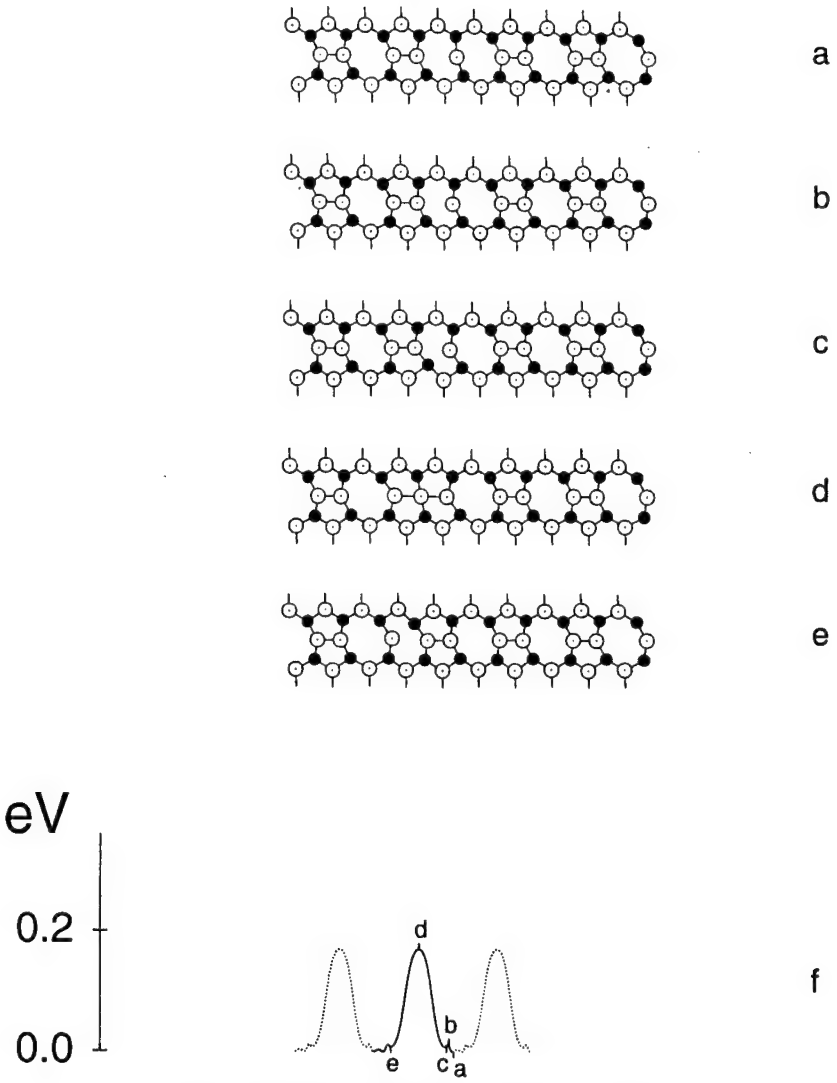

Lowest energy path found for motion of APD.

room temperature, they have little effect on the APD motion. Moreover, some of these details are likely to be spurious features of the SW potential. We believe that the small middle hump is a consequence of the angular part of the SW potential function which enforces tetrahedral bond arrangements. In addition to the minimum energy structure shown in fig. 7 (*a*), there exists an equivalent state where the APD bends to the right (not shown). The central hump appears because the bond angles are close to 120° in the neutral position, which is penalized in the SW model by some additional bond bending energy of the order of 0·01 eV for each 120° angle.

This discussion is provided to demonstrate our reasons for ignoring details of this nature in the results to follow. On the other hand, the point of real importance is that the overall barrier for APD motion is about one-fifth of the motion barriers for isolated LK and RK. This is due to the ease with which the APD makes itself available for bond switching, whereas no such flexibility is present in the motions of kinks. While such low barriers may, in part, be attributed to the SW potential, APD-assisted bond

switching, or bond exchange, is a possible kinematical mode for defect mobility. To explore this further we will in the next section examine the effects of kink–APD interactions on the mechanisms of kink motion.

3.4. *Kink–APD complexes and their motions*

3.4.1. *Overview*

Interaction of the secondary defects (kinks, APD, etc.) in the dislocation core at large separations is relatively weak. As was discussed earlier, such interaction is well described by appropriate relations of linear elasticity. It is important and possible to examine, within the present computational approach, the interaction of kinks and APDs in the nonlinear range, i.e. when the defect cores overlap. In this section we study short-range kink–APD interactions, leaving the nonlinear kink–kink interaction for the following section 3.5.

Because point defects are associated with distortions of atomic positions giving rise to an excess of energy, there is always a possibility that two (or more) defects can lower their energy by clustering together. When this is energetically beneficial, the defects are said to bind. Since the early work of Hirsch the general notion was that of weak binding where a kink and an APD are adjacent, as shown in Hirsch's fig. 5 (Hirsch 1980); the binding was thought to result from the mutual accommodation of the individual elastic distortions. As shown in the previous section, such interaction can produce only a relatively weak binding, of the order of kT (see also Heggie and Jones (1983a, b)). It will be seen in the following that such a picture of weak binding is incorrect. In fact, kink–APD binding is strong and results in the formation of new stable defects, or kink–APD complexes, where identities of the constituent species are drastically altered from their forms in isolation.

For a system with interacting defects the lowest energy bound states can be effectively found by applying the technique of the constrained SA method. As was emphasized earlier, a constraint is often required to make the system sample regions of the configurational space that are of primary interest and prevent it from over-annealing. Using such constraints, an extensive search was performed for configurations in which a kink and an APD are bound. A few such states were found for each kink–APD pair. It is significant that a single, lowest-energy state, discussed below, was repeatedly obtained for each kink, starting from different initial configurations.

3.4.2. *Left kink–APD complex*

The lowest energy configuration found for the left kink–APD pair is shown in fig. 8 (*d*). The binding energy of LK and APD in this state is 0·51 eV, which is rather large. Moreover, in the obtained structure of the complex the individual components, LK and APD, can no longer be recognized†. Indeed, a new configuration is obtained where an atom with a dangling bond sits right in the centre of the now unrecognizable left kink. This renders the earlier suggested picture of weak binding due to elastic

† To see this one has to compare structures of the APD shown in fig. 3 (*b*) and of the left kink shown in fig. 4 with the structure of their bound state of fig. 8 (*d*).

Fig. 8

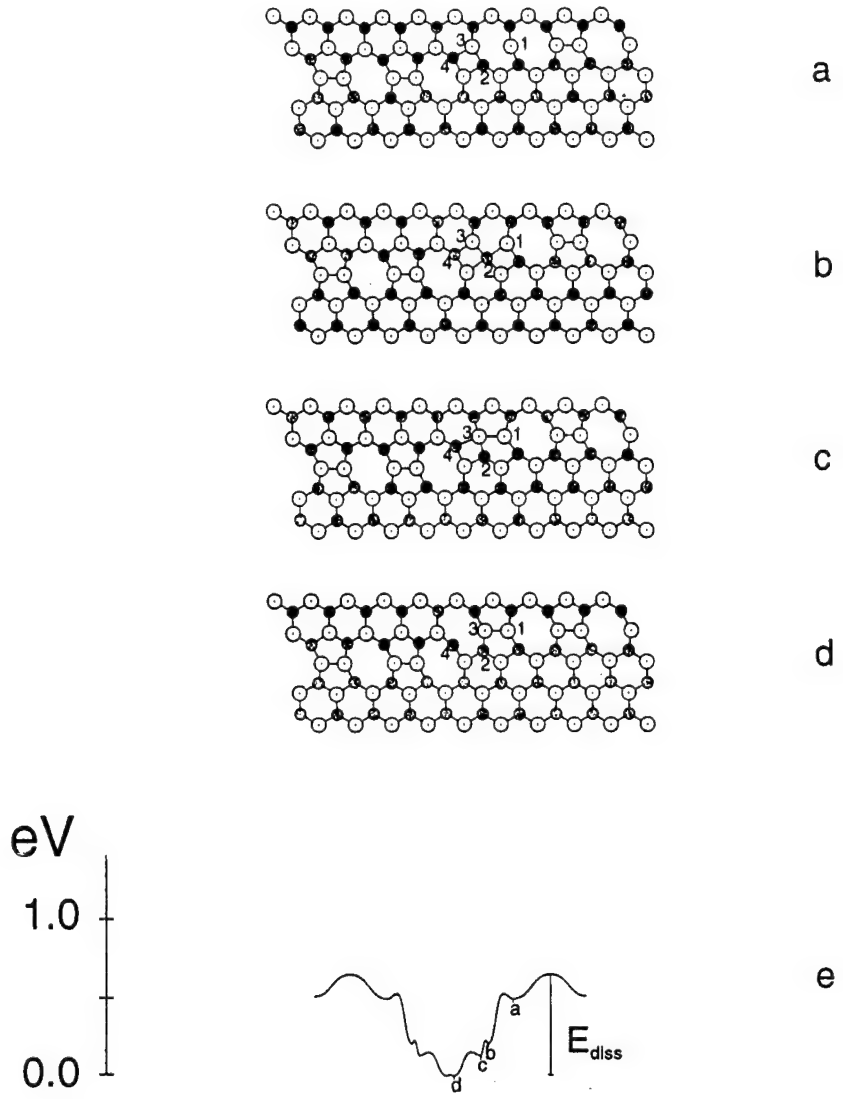

A low energy path for formation of a left kink–APD complex.

accommodation invalid. Quite the contrary, the binding observed here is strong both in terms of energetics and structure. Hence, it is appropriate to classify such a bound state as a new defect, the left kink–APD complex (LC), with its own characteristic energy and core structure.

In order to understand better the role that LC plays in dislocation motion, possible mechanisms for the formation and motion of this complex were examined. A possible mechanism for LC formation, identified using the GA sampling method, is shown in fig. 8. In the initial state (fig. 8 (*a*)), LK and APD are positioned next to each other, but are still resolvable. The transformation occurs when the APD (atom 1) attacks atom 2 (fig. 8 (*b*)), which results in the formation of an additional bond 1–2. Subsequently, bond 1–2 itself breaks to allow formation of a new reconstructed bond 1–3 (fig. 8 (*c*)). Bond 1–3 grows stronger at the expense of bond 3–4 which breaks to complete the LC

formation (fig. 8 (*d*)). Associated with this sequence, which can be written as LK + APD → LC, is the energy *versus* reaction coordinate plot shown in fig. 8 (*e*).

The same sequence of atomic rearrangements, in the reverse direction, describes the dissociation of LC into LK and APD, LC → LK + APD. It is worthwhile to note that the barriers separating state (*a*) from state (*b*) is too low to stabilize dissociation; this means that if dissociation proceeds only to the state (*a*), then the low-energy bound state will be restored immediately. However, the dissociated state has a better chance of surviving if the next barrier on the right from state (*a*) is swept over. This barrier corresponds to the motion of the APD component going to the right. If this barrier can be overcome (the appropriate configuration is not shown), the barrier to transform back into the bound state becomes comparable to the barrier for further separation of LK and APD.

It is helpful to distinguish precursor states, like state (*a*) in fig. 8, from fully developed states of the defect reactions. In the present case the full barrier E_{diss} for LC dissociation is 0·66 eV, which is notably higher than the pre-barrier 0·52 eV (between (*d*) and (*a*)).

In the bound state (fig. 8 (*d*)) the dangling bond, initially located on atom 1, moves on to atom 4 which belongs to a different atomic row (below the glide plane). Clearly, LC in this configuration is a kink and an APD at the same time. Indeed, it is a step in the dislocation line, just like a kink, but it is also an APD in the sense that it divides two perfectly reconstructed segments in the dislocation core. It is of interest to see whether a LC can move with the same ease as an APD.

The lowest-energy atomic mechanism found for LC motion is illustrated in fig. 9. The overall barrier for such motion is only 0·22 eV, which is roughly one-quarter of the barrier for isolated LK motion. Apparently, by binding to the left kink, the APD strongly affects the operating mechanism of motion of the resulting complex LC.

The atomic mechanism of the easy motion is shown in fig. 9 (*a–e*). Again, as was the case for APD motion, the atom with the dangling bond has substantial freedom to move in the direction along the core. Consequently, it takes little energy for the LC atom to attack the reconstructed bond on its left (fig. 9 (*a*, *b*)). This triggers subsequent bond switching, leading to the state shown in fig. 9 (*c*). In the geometric centre of this on-barrier configuration is an atom with five nearest neighbours.† From there, the full cycle of LC transport to the left is completed by a similar, but inverted sequence of atomic motions (fig. 9 (*d*, *e*)) .

For comparison, both energy profiles for LC motion (solid line) and for LC formation/dissociation (dotted line) are shown in fig. 9 (*f*) in the same coordinates. Clearly, the LC stays well below the dissociated state at all times during its motion. This means that the discussed low-energy mechanism does not require LC to separate into LK and APD even for a short time. Accordingly, the *lubricating* effect of the dangling bond is very substantial, reducing the overall barrier for the left kink motion from 0·82 eV to 0·22 eV.

3.4.3. *Right kink–APD complex*

Using the constrained SA method it was found that the right kink, RK, binds to an APD even stronger than the left kink does. The binding energy for a RK–APD pair was

† In state (*c*) of fig. 9 the central atom appears over-coordinated (five nearest neighbours). This is in contrast with APD and LC atoms that are under-coordinated. Such odd coordinations were often found whenever a dangling bond was involved in transformation or motion.

Fig. 9

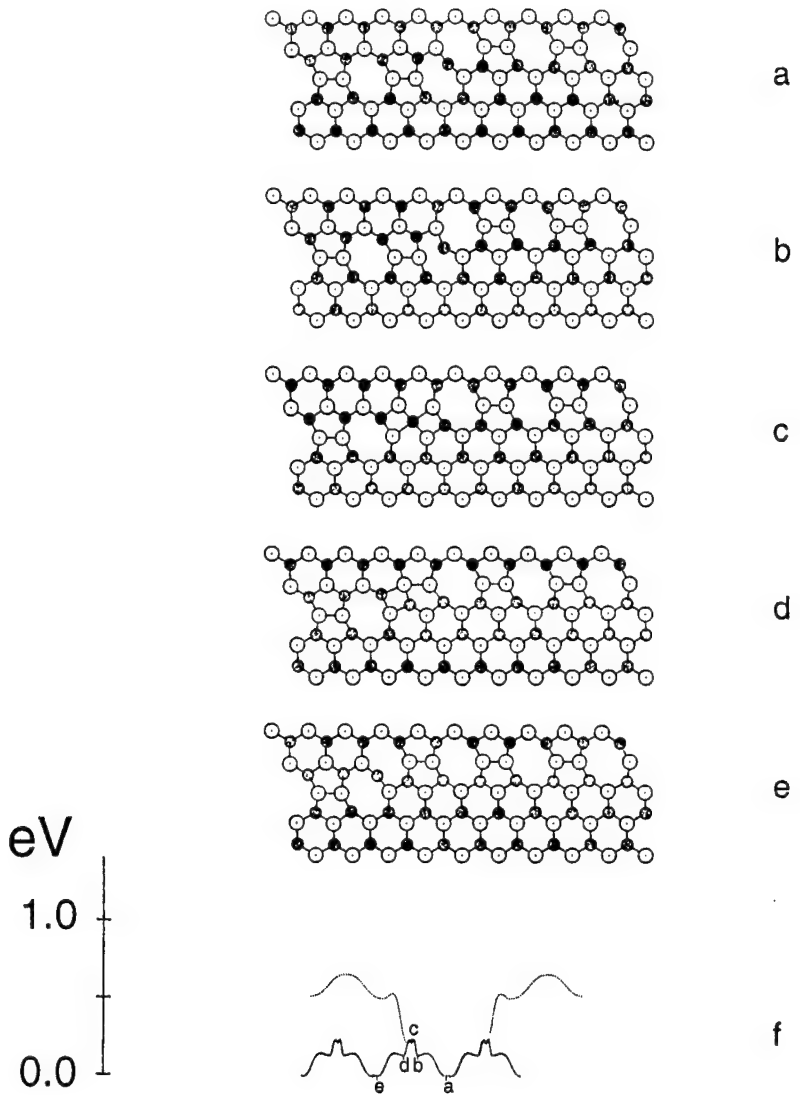

Lowest energy path for motion of left kink–APD complex.

found to be 0·84 eV, substantially larger than the 0·51 eV found for the LC. The resulting configuration of a strongly bound right kink–APD complex (RC) can be seen in fig. 10(*e*), where atom 3 in the geometric centre of RC has five nearest neighbours. In principle, such local atomic arrangement must have higher energy than the regular four-fold coordination. However, the formation of an extra reconstructed bond 1–2 seemingly makes up for the difference; the resulting binding is strong.

It is apparent, by comparing core structures and binding energies of the two complexes, LC and RC, that a left–right asymmetry inherent for the 30°-partial shows itself very clearly. It then follows that the mechanisms of formation and motion of these two core defects may well be different too. Thus we now consider the low-energy paths found for RC formation and motion and compare them with the results obtained for LC.

It is easiest to grasp the essentials of RC formation by comparing the two configurations show in fig. 10(*d*) and (*e*). The complex is formed by the APD

Fig. 10

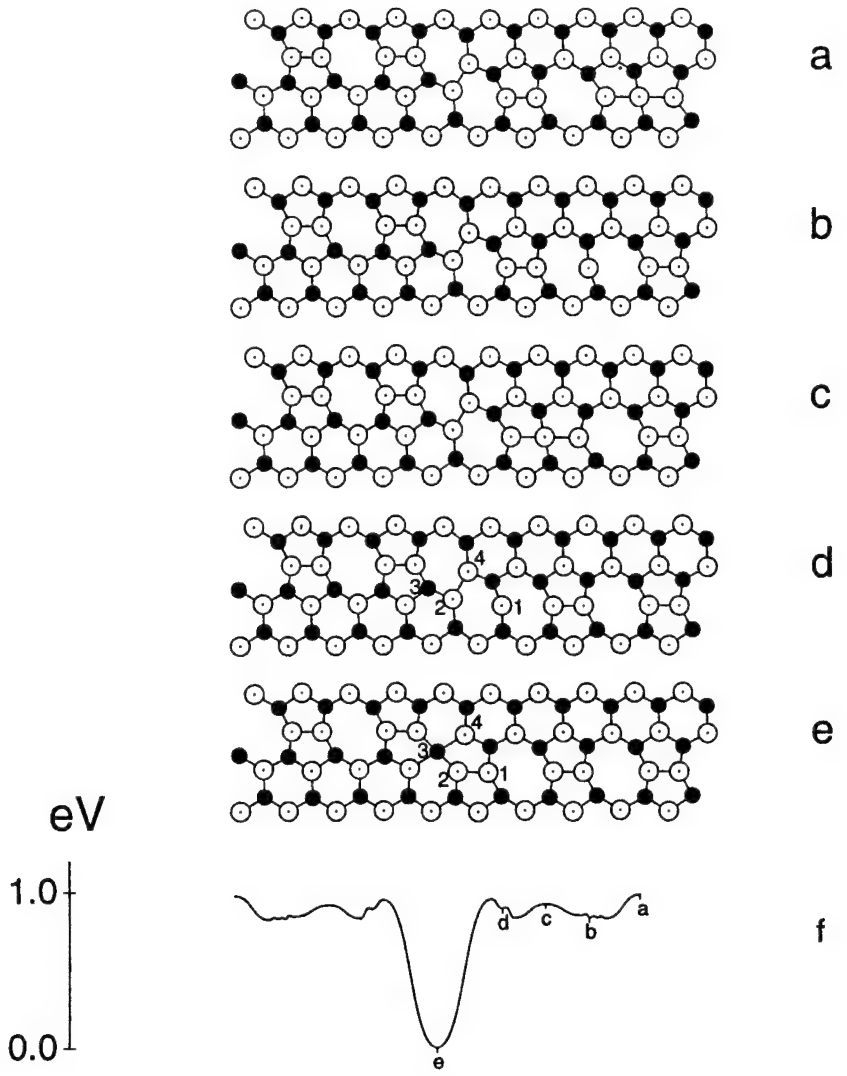

A low energy path for formation of a right kink–APD complex.

(atom 1) attacking its neighbour (atom 2). This triggers an atomic reconfiguration, the formation of reconstructed bond 1–2. At the same time atom 3 acquires an extra neighbour (atom 4). The final configuration (fig. 10(*e*)) is a RC, formed as a product of the defect association reaction RK + APD → RC.

Considering the reverse process of RC dissociation, RC → RK + APD, the first barrier (0·95 eV) is slightly higher than the second barrier (0·94 eV), as seen on the energy plot. This second barrier corresponds to a saddle configuration of the APD component moving away from the RK to the right. The third barrier is still somewhat higher (0·97 eV). However, all subsequent barriers for APD motion farther to the right are essentially of the same height. This indicates that at distances as small as 4*b*, kink–APD interaction can be neglected. Accordingly, 0·97 eV is taken to be the dissociation barrier, since no other path of lower energy was found.

Additional comparison was made between RC and LC in terms of their motion

Fig. 11

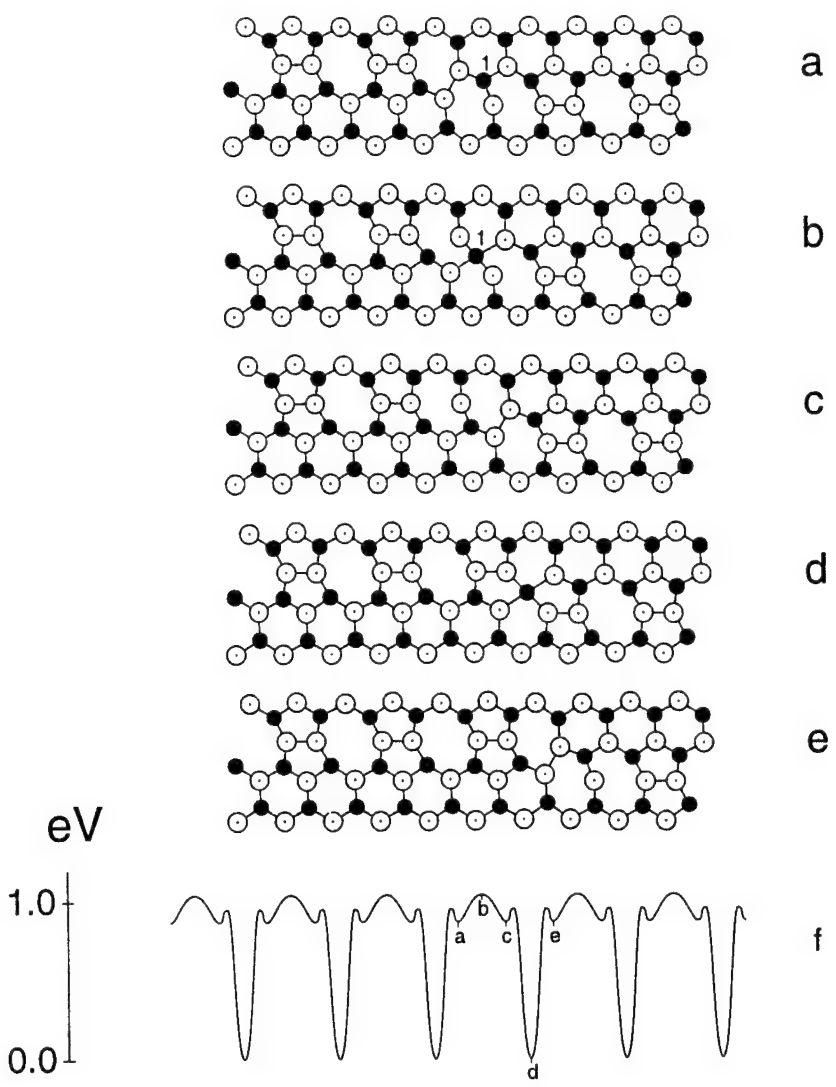

Lowest energy path for motion of a right kink–APD complex.

barriers. In this case, extensive search by GA sampling produced a relatively low-energy path associated with an unusual sequence of atomic motions.

A full period of RC motion is shown in fig. 11, where upon going from fig. 11 (*a*) to fig. 11 (*e*) the RC moves a distance 2*b* to the right. The sequence begins with the configuration where an APD is immediately on the right of RK (fig. 11 (*a*)). Then atom 1 makes a move resulting in the APD moving through the RK to the left, and, at the same time, RK moves a distance 1*b* to the right (fig. 11 (*c*)). On the way the barrier configuration (fig. 11 (*b*)) is passed where atom 1 has five bonded neighbours. The energy barrier for such atomic reconfiguration is relatively low (0·16 eV).

Further motion to the right occurs by absorbing the APD from behind and forming the RC, as shown in fig. 11 (*d*). By this the kink moves further to the right by *b*/2. Then the complex dissociates by emitting the APD to the right. At the same time, the kink centre moves to the right by another *b*/2, completing a full period of RC motion

(fig. 11 (*e*)). The latter configuration is equivalent to the initial one (fig. 11 (*a*)) except that the RC has moved 2*b* to the right.

In the above sequence, RK + APD → APD + RK → RC → RK + APD, the APD component is regenerated after being absorbed in the complex for one half of the motion cycle. Consequently, the other half is relatively easy due to the lubricating effect of the APD. Nevertheless, the motion barrier is high (1·04 eV), since dissociation of the strongly bound complex RC is involved.

As was shown in the previous section the right kink has two equally important forms, RK and RK′. However, our attempts at finding low-energy mechanisms for RC motion involving RK′ did not produce any results. The reasons for this appears to be a subtle kinematical distinction between these two forms of the right kink and their relation to the complex RC. In fact, the difference is seen clearly when the two reactions are compared: RK + APD ↔ RC and RK′ + APD ↔ RC.

When a RC dissociates into APD and RK, as shown in fig. 11 (*d*, *e*), both RK and APD appear on the right relative to the previous position of the complex RC. This way, the coordinated motion of *both defects* to the right is maintained. On the other hand, RC can also dissociate into APD and RK′, as illustrated in fig. 12. The barrier for such dissociation is practically the same as for the previously studied mechanism, i.e. 1·03 eV. However, this last dissociation is different in that APD and RK′ move in the opposite directions from the position of RC. Therefore, even if kink RK′ does appear on the right from RC, as in fig. 12 (*e*), the APD appears on the left instead. Accordingly, this second dissociation can contribute only to splitting of the two defects but not to their coordinated motion in the same direction.

It follows from the above discussion that the most probable way for the RC to move is by complex dissociation into RK and APD followed by APD-assisted bond switching. At the same time, the barrier of 1·04 eV obtained for such a mode is not only much higher than the barrier for LC motion (0·22 eV), but even higher than the motion barrier of an isolated kink RK (0·74 eV). Such difference in motion barriers for RC and LC is a strong manifestation of the left–right asymmetry, characteristic of the 30°-partial dislocation. The LC moves easily because a highly mobile three-fold coordinated atom with a dangling bond makes bond switching easy. On the other hand the 5-fold coordinated atom in the centre of RC is surrounded by its four in-plane bonded neighbours. There appears to be no other way to make such a defect move than by destroying it via dissociation.

To test the reliability of our method of gradual ascent we have carried out path optimisations using the method of Elber and Karplus (1987) for the two cases of complex motions discussed in this and the previous sections. Because of the very high computational cost of EK path optimizations, it was not practical to use the method to study all possible defect motions and reactions. We therefore chose the RC and LC motions for EK path optimizations since they involve greatly different barrier heights. The EK optimizations were performed using discretized paths represented by 50 straight segments connected in a chain. A Monte Carlo SA technique was used to search for the low-energy chain configurations. The results were in agreement with the numbers obtained earlier using the GA method: the highest point on the optimal path for LC motion was 0·22 eV above the minimum, and the barrier for RC motion was 1·04 eV.

If the SW empirical model of Si were completely accurate, then the conclusion to draw from these results would be that by binding to LK and to RK the APD affects the

Fig. 12

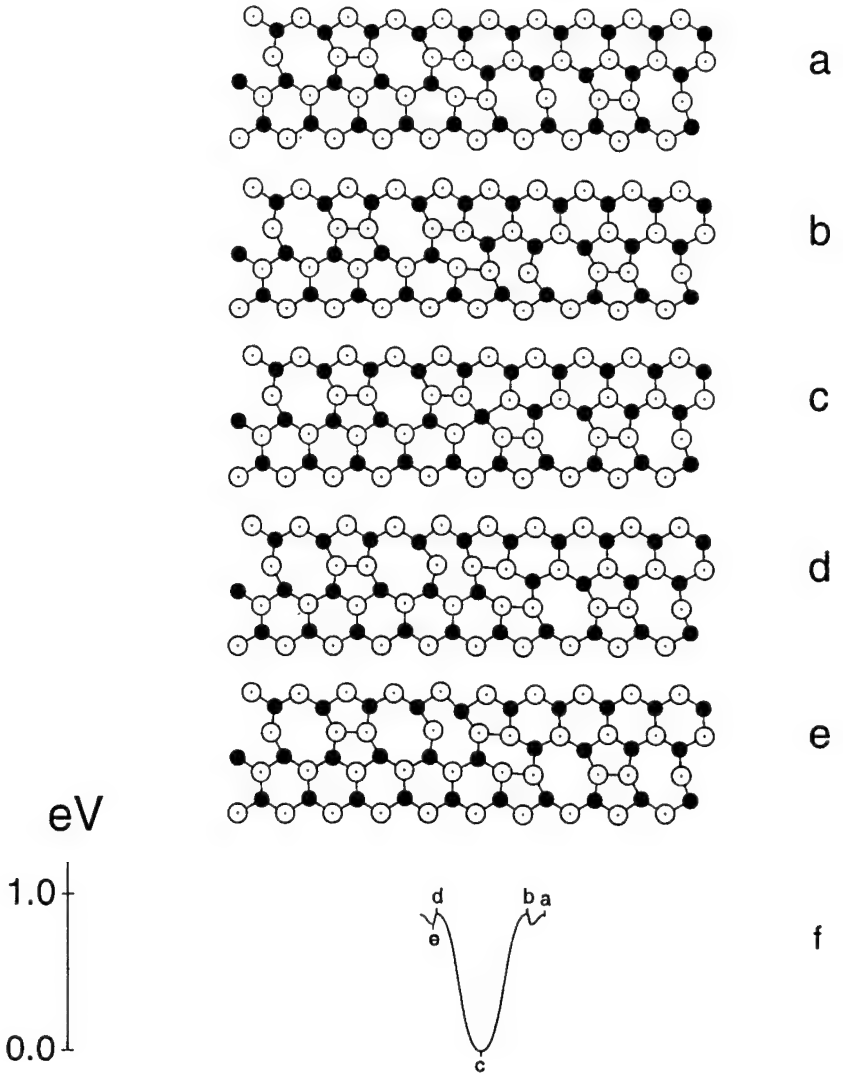

Another low energy path for formation of a right kink–APD complex.

motion of the resulting complexes differently. Indeed, the APD lubricates the motion of LC but immobilizes RC.

3.5. *Homogeneous nucleation of kinks and APDs*

In the previous sections, relevant motion mechanisms were identified for the five core defects: APD, LK, RK, LC and RC. In order to obtain a more complete picture of the processes involved in the motion of the 30°-partial, atomic mechanisms for nucleation of these defects must be considered. In this section, mechanisms for homogeneous nucleation of kinks and APDs are examined. These will be contrasted in the following sections with mechanisms of heterogeneous nucleation which involve pre-existing defects in the dislocation core.

As the first case of interest, fig. 13 shows a mechanism for double-kink nucleation, found using the gradual ascent method. The mechanism is homogeneous, in the sense

Fig. 13

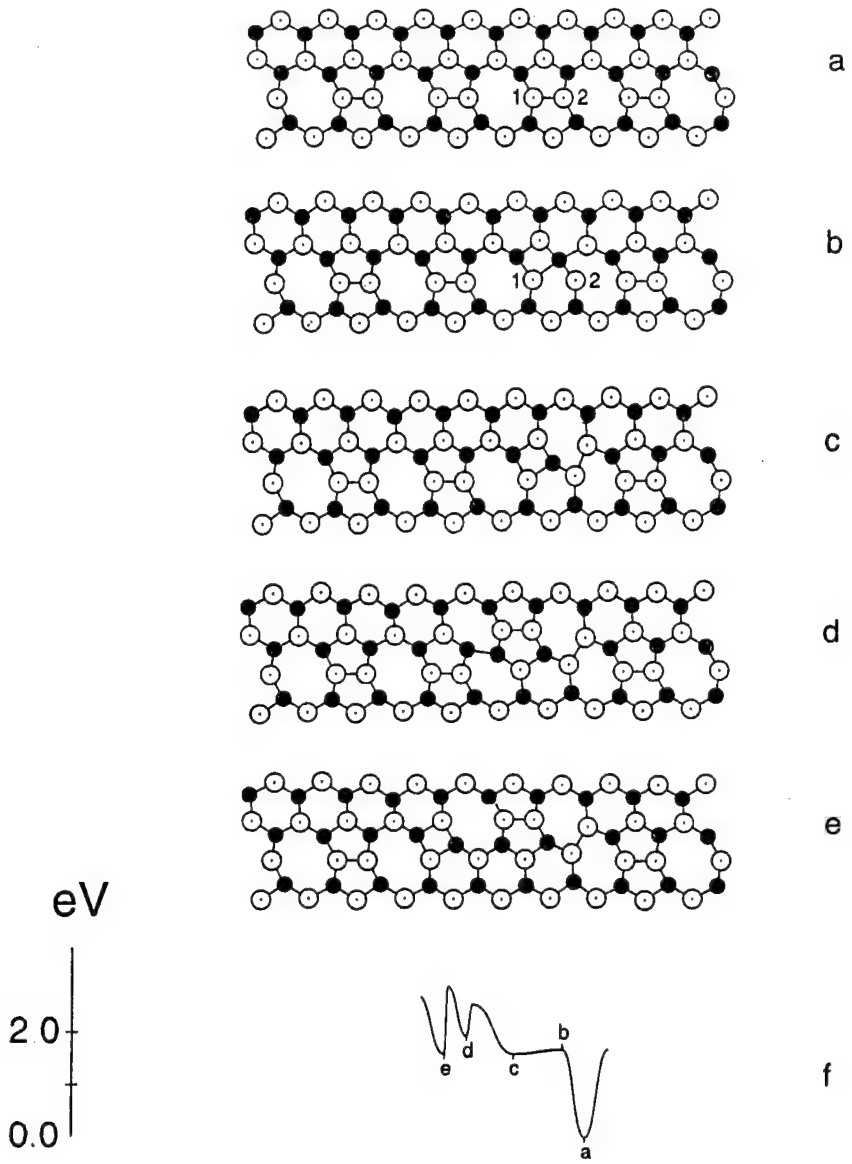

A low energy path for double-kink nucleation in a perfectly reconstructed core.

that initially there were no defects in the dislocation core. On going from fig. 13 (*a*) to fig. 13 (*c*) the reconstructed bond 1–2 breaks, which requires overcoming a barrier of 1·58 eV (fig. 13 (*b*)). The resulting structure shown in fig. 13 (*c*) contains two adjacent kinks, RK and LK. However, this embryonic state is not stable and may return back to the straight dislocation; the barrier for such a reverse process is only 0·07 eV.

To become more stable the double kink must expand. This can be accomplished in two ways, by moving RK to the right or by moving LK to the left. Actually, the barriers for these two paths are close, 2·51 eV for the expansion to the right and 2·54 eV for the expansion to the left. Of the two mechanisms, only the double-kink expansion to the left is shown in fig. 13. The LK moves to the left by transforming into the higher energy LK′ state (fig. 13 (*d*)). On further motion LK′ transforms back into LK, but is

now separated from RK by $3b$ (fig. 13 (*e*)). The total energy barrier, with respect to the initial state of the straight dislocations, is 2·88 eV†.

Further separation of the kinks involves essentially the same mechanisms, discussed earlier in the context of kink motions. The heights of subsequent barriers and minima on the energy profile change with kink separation, modulated by attractive kink–kink interaction. As mentioned before, such attractive interaction is well described by a linear elastic term (eqn. (1)) at kink–kink separations larger than $5 - 6b$. At shorter distances kink–kink interaction systematically deviates from the linear form of eqn. (3) and becomes strongly nonlinear when LK and RK are next to each other. In its extreme form, such nonlinearity is seen in fig. 13 (*b*), which shows atomic positions in the embryonic barrier configuration. In this case the core overlap of the kinks is such that individual kinks can not be recognized.

For our discussion it is important to note that the energy barrier for the above mechanism is rather high. On the other hand, the sequence shown in fig. 13, if read in the reverse direction, is a low energy path for the LK + RK recombination. Relative to the initial state of two kinks an infinite distance apart from each other, the recombination barrier is determined by the motion barriers of the kinks. The smallest of the two barriers gives an estimate of the recombination barrier as 0·74 eV.

In close analogy with the above mechanism for the double kink nucleation, nucleation of an APD pair on a fully reconstructed straight dislocation requires breaking a reconstructed bond and moving one APD away by $2b$. The corresponding sequence and the energy plot are not shown, since these are rather trivial. The pre-barrier for such a process is 1·63 eV. The full barrier is 1·79 eV. Further search revealed that there are other mechanisms for APD generation, which have lower energy barriers. Such (heterogeneous) mechanisms will be discussed in the next section.

The homogeneous mechanism discussed here is important for APD + APD recombination. Clearly, the barrier for APD recombination is equal to the APD motion barrier (0·17 eV).

To summarize the discussion given in this section, we state that energy barriers for homogeneous nucleation of double kinks and APDs are high. In order to find other, easier ways to generate kinks and APDs we have examined various paths originated at the pre-existing defects in the dislocation core, such as APDs, kinks and their complexes.

3.6. *Heterogeneous mechanisms for nucleation of kinks and APDs*

3.6.1. *Overview*

We now focus on kink and APD generation mechanisms mediated by the presence of another defect in the core. A general scheme for the defect reactions in question is $A \rightarrow B + C \ldots$. Here, A is a defect in the dislocation core which serves as nucleation site for two or more defects, B, C, etc. In the case of the 30°-partial, where at least five defect

† To plot the energy for the path under discussion an appropriate measure of local strain was used as the reaction coordinate (fig. 13 (*f*)). In the discussed case this was a convenient choice, since the strain changes monotonically on going from fig. 13 (*a*) to fig. 13 (*e*). With such a choice, however, subsequent configurations and the corresponding points on the energy plot appear somewhat misaligned.

Table 1. Five major defects and their kink and APD numbers.

Defect	Kink number	APD number
APD (antiphase defect)	0	1
LK (left kink)	−1	0
RK (right kink)	+1	0
LC (left complex)	−1	1
RC (right complex)	+1	1

species can participate in various defect multiplication reactions, the number of possible combinations is large.†

Fortunately, it is possible to substantially reduce this number by cutting off in advance most of the combinations as either kinematically impossible or, otherwise, not important. For that, it is instructive to observe that kinks can only appear and disappear in pairs: one left kink and one right kink. The same is true about APDs, although in this case there is no difference between left and right APDs. Such observations can be reformulated in terms of appropriate selection rules.

It is convenient to assign certain characteristic numbers to each participating defect. These are listed in table 1. The APD bears one unit of apd-number, but has zero kink-number. On the other hand, the kinks bear no apd-number, but have non-zero kink-numbers, i.e. -1 for LK, $+1$ for RK. It then follows that the complexes have non-zero apd- and kink-numbers; LC has one unit of apd-number and its kink-number is -1, while RC has one unit of apd-number and kink-number of $+1$.

Based on the above classification, two simple selection rules are:

(1) Defect reactions changing total (algebraic) sum of the kink-numbers are kinematically impossible.
(2) Allowed defect reactions should either leave total apd-number unchanged or change it by two at a time.

Clearly, all four reactions examined earlier in the previous sections do not violate these rules:

(1) $0_{0,0} \leftrightarrow \mathrm{LK}_{-1,0} + \mathrm{RK}_{+1,0}$,
(2) $0_{0,0} \leftrightarrow \mathrm{APD}_{0,1} + \mathrm{APD}_{0,1}$,
(3) $\mathrm{LC}_{-1,1} \leftrightarrow \mathrm{LK}_{-1,0} + \mathrm{APD}_{0,1}$,
(4) $\mathrm{RC}_{+1,1} \leftrightarrow \mathrm{RK}_{+1,0} + \mathrm{APD}_{0,1}$,

where the first number in each pair of subscripts is a kink-number, and the second number is an apd-number of a given defect.

We have seen that the first two reactions of homogeneous nucleation have rather high barriers. In contrast, the last two reactions, if read from left to right, have reasonably low barriers and can be considered as alternative mechanisms for defect multiplication. In fact, energy considerations provide one more guiding principle by which the number of relevant mechanisms which deserve closer examination can be further reduced.

For every reaction involving core defects, it is a simple matter to obtain a lower-bound estimate for the total energy barrier. As an example, consider the following

† To keep our discussion focused we do not consider the alternative kink states LK′ and RK′ as separate entities.

reaction of (homogeneous) nucleation: $0 \rightarrow LC + RC$. Apparently, a total barrier for such a reaction can not be lower than its total energetic effect, i.e. the energy of reaction products minus the energy of the initial state. In the present case the energetic effect is equal to the sum of energies of the two isolated complexes, LC and RC. The LC energy is computed as the sum of energies of LK and APD, minus their binding energy in the complex, i.e. $0{\cdot}82 + 0{\cdot}81 - 0{\cdot}51 = 1{\cdot}12$ eV. Likewise, RC energy is found to be 0·79 eV. Therefore, the total energy of formation of the pair is 1·91 eV. Since the overall barrier can only be higher, this reaction is not of considerable interest..

For the same reason, reactions of the types $A \rightarrow B + C + D$, $A \rightarrow B + C + D + E$, and the like, can be ignored due to their excessively high energies. There are only four allowed defect multiplication reactions with relatively low energetic effects that have not yet been discussed and therefore deserve attention:

(1) $APD \rightarrow LK + RC$ (energetic effect is 0·80 eV),
(2) $APD \rightarrow LC + RK$ (1·13 eV),
(3) $LK \rightarrow LC + RC$ (1·11 eV),
(4) $RK \rightarrow RC + APD$ (0·78 eV).

The first two reactions correspond to possible mechanisms for kink pair generation, mediated by the presence of an APD. The last two mechanisms may contribute substantially to APD production. All these possibilities are discussed below.

3.6.2. *APD-assisted nucleation of kinks*

It has been suggested previously that nucleation of double kinks occurs more frequently in the presence of APD (Heggie and Jones 1983a, b). Here we examine such APD-assisted mechanisms for kink nucleation. In the presence of an APD, one of the two kinks can be formed directly in a bound state, i.e. in a complex. In this case, the energetic effect of such a nucleation reaction is reduced by the amount of the binding energy. Furthermore, if such binding occurs in the course of nucleation, the overall nucleation barrier may be offset by the same amount too. To see if this is indeed the case, GA searches were performed for low-energy paths for the following multiplication reactions:

(1) $APD \rightarrow LK + RC$,
(2) $APD \rightarrow LC + RK$

The results are presented in figs. 14 and 15.

Both sequences develop from the same initial state of a single APD in an otherwise straight 30°-partial. However, the end results are different. The first sequence shown in fig. 14 produces two kinks, one left and one right. Of the two, the right kink appears directly in the form of a RC. In this sequence the APD (atom 1) attaches to atom 2 making it the centre of a forming RC complex. At the same time, bond 4–5 breaks and atoms 3 and 4 move closer to each other to form a reconstructed bond. In the configuration shown in fig. 14 (*b*) the system appears at the top of an energy barrier of 1·25 eV. From here the energy decreases by a bond-switching mechanism in which bond 6–3 breaks but bond 5–6 forms. The resulting state consist of a right complex RC and an LK.

Characteristically, the left kink appears in the high-energy LK′ configuration (fig. 14 (*c*)). This embryonic state must develop further by moving one of its kinks away from the other. Clearly, since the barrier for RC motion is high (> 1 eV), it must be the motion of LK′ to the left that completes the nucleation sequence, as shown in

Fig. 14

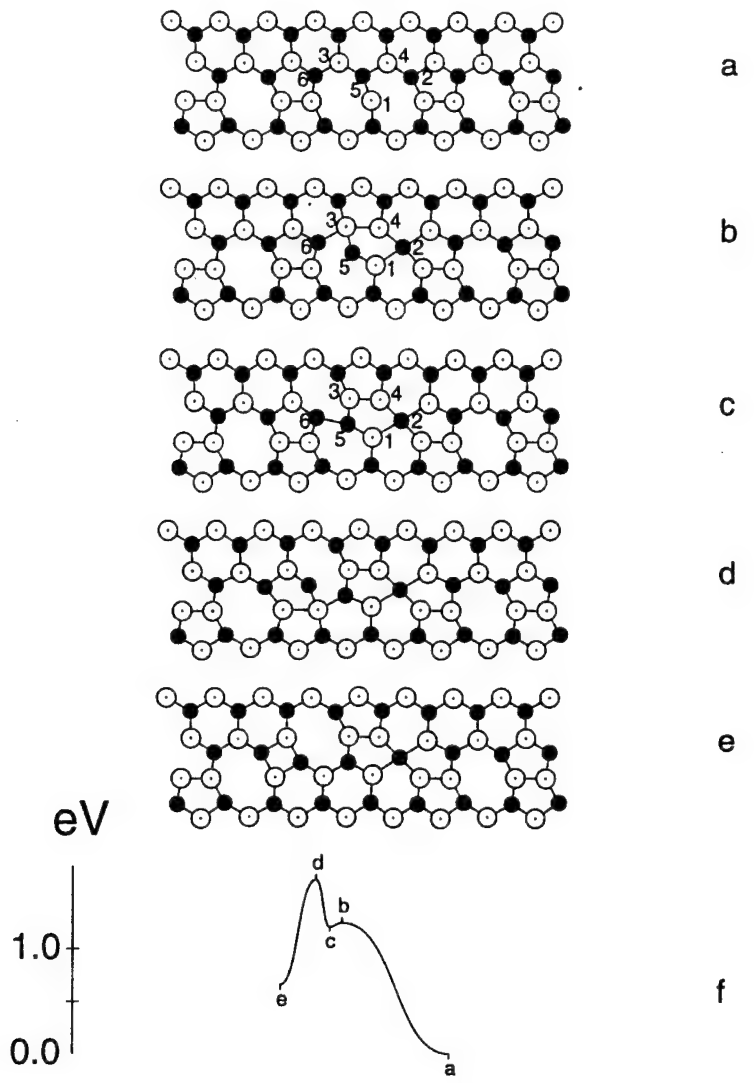

A low energy path for APD-assisted double-kink nucleation by the APD → LK + RC reaction.

fig. 14 (*d*, *e*). The barrier to such motion is 1·65 eV (relative to the initial state), and the energy of the final state shown in fig. 14 (*e*)) is 0·66 eV.

Unexpectedly, the total barrier to double-kink nucleation by the above mechanism is relatively high, at 1·65 eV. This is because RC formation in this case is kinematically coupled with the formation of LK′, the higher-energy state of the left kink. Indeed, the energy reduction due to binding is nearly matched by the excess energy of the LK′ kink. It is only in the final state (LK + RC) shown in fig. 14 (*e*) that the energy benefit of binding clearly appears.†

The second path for double-kink nucleation on an APD is shown in fig. 15, resulting in the formation of a LC–RK pair. The mechanism involves switching two pairs of bonds simultaneously, which is triggered by an APD-attack on bond 2–3. As a result,

† All further attempts to find a lower energy path leading eventually to LK + RC failed, so that the barrier remained at 1·65 eV.

Fig. 15

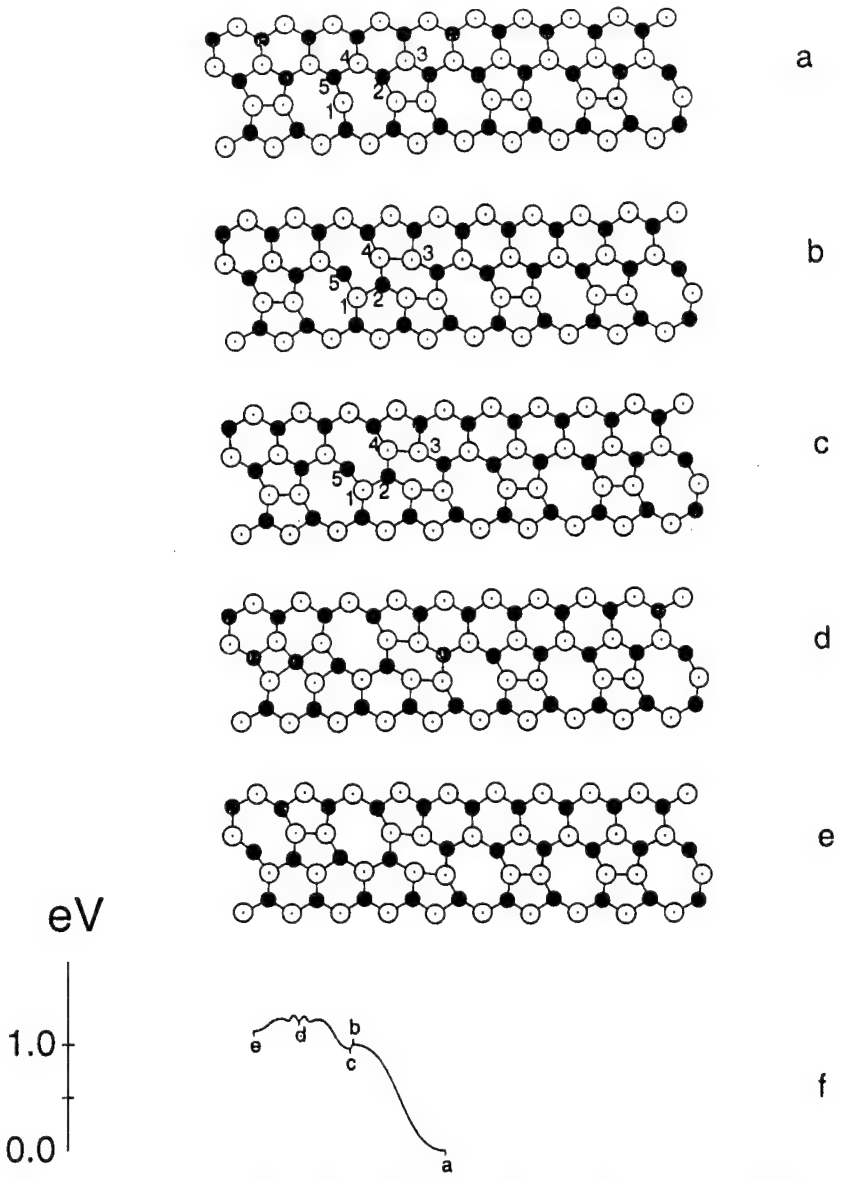

Another low energy path for APD-assisted double-kink nucleation by the APD → LC + RK reaction.

bond 2–3 breaks, making it possible for atoms 1 and 2 to bond instead. Simultaneously, bond 4–5 breaks, giving way to formation of the reconstructed bond 3–4. The right kink is formed in its RK′ state (fig. 15 (*c*)), whereas the left kink appears in the bound state LC. Two configurations, the barrier state (fig. 15 (*b*)) and the embryo (fig. 15 (*c*)) are almost indistinguishable. Accordingly, the barrier for the reverse transformation, from (*c*) back to (*a*), is very low (0·04 eV).

The nucleation is completed by LC moving away from RK to the left (fig. 15 (*c–e*)), which is a motion requiring very low energy. The resulting barrier for this mechanism is 1·28 eV, which is markedly lower than the 1·65 eV for the mode discussed above involving the RC. Clearly, only in the second sequence of APD → LC + RK is the nucleation barrier reduced substantially by the intervening binding. In contrast to that, the energy for the APD → LK′ + RC reaction remains high.

The above disparity is mostly due to the following two factors. The first is that the left kink appears, in the APD → LK′ + RC reaction, in the LK′ form, which has 0·40 eV excess energy compared to the LK form. This partly negates the barrier reduction due to binding. On the other hand, in the other reaction of APD → LC + RK′ the right kink appears in the RK′ form, which has almost the same energy as the RK form. Another distinction between the two multiplication reactions is in the different ways the two double kinks expand from the embryonic states. The first double kink LK′ + RC expands by moving its LK′ component, while the second double kink LC + RC′ does it by moving the LC. Because LC motion is easier, the total energy barrier for the second nucleation is lower.

The above comparison shows that, although lower bounds for the energy barriers of various defect reactions can be given based on the energies of the involved species, the only way to actually find these barriers is by making the defects move in some ways. In fact, simple energy balance considerations predict that the second mechanism (APD → LC + RK) may have a higher energy barrier, contrary to what was found. This underscores the importance of explicit sampling of various atomic modes involved in dislocation motion. The GA sampling used in the present work provides full details of defect motions and reactions, including very strong nonlinear interactions of the defects.

3.6.3. *Heterogeneous nucleation of APDs on kinks*

The core reconstruction and the resulting APDs in the core are responsible for the observed complex mechanisms of motion of the 30°-partial dislocation. Consequently, the net kinetics of dislocation motion must be dependent on the concentration of APDs; the mechanisms of formation of these are discussed below.

The direct bond-breaking mode resulting in the formation of two APDs is one possible mechanism, which has a high barrier (1·79 eV). Among the other atomic mechanisms discussed so far, two modes of complex dissociation result in APD production: the sequence RC → APD + RK has a barrier of 0·97 eV, and the sequence LC → APD + LK has a barrier of 0·66 eV. The second of the two barriers is lower due to the weaker binding of APD to the left complex.

Two additional low-energy mechanisms of APD generation, i.e. heterogeneous nucleation of APDs on kinks, should be noted. Specifically, the following two reactions are considered: LK → LC + APD (1) and RK → RC + APD (2). There is some analogy with the heterogeneous double-kink generation discussed in the preceding section, but now one of two nucleated APDs is free, while the other is formed directly bound to the kink. The barriers for such reactions are expected to be low because the bond-breaking energy can be partly offset by the binding energy in a forming complex.

Shown in fig. 16 is a particularly simple path for APD nucleation on an LK. Kinematically, an APD and an LC are formed by breaking bond 1–2 in the LK core (fig. 16 (*a–c*)). The corresponding pre-barrier is 1·17 eV, lower than the energy required to break a reconstructed bond in the core (1·64 eV). The difference is apparently due to the fact that bond 1–2 is initially weaker than an ordinary reconstructed bond. Hence, it takes less energy to break bond 1–2. Equivalently, it is the LC binding energy (0·51 eV) that makes up the difference (1·64 − 0·51 = 1·13 eV).

The lowest energy path to separate the nucleated pair is to move the APD to the left away from the LC (fig. 16 (*d–e*)). The total energy barrier is relatively low (1·30 eV), indicating that this mechanism provides an effective path for APD generation.

Another possible mechanism of APD nucleation involves the alternative state of the

Fig. 16

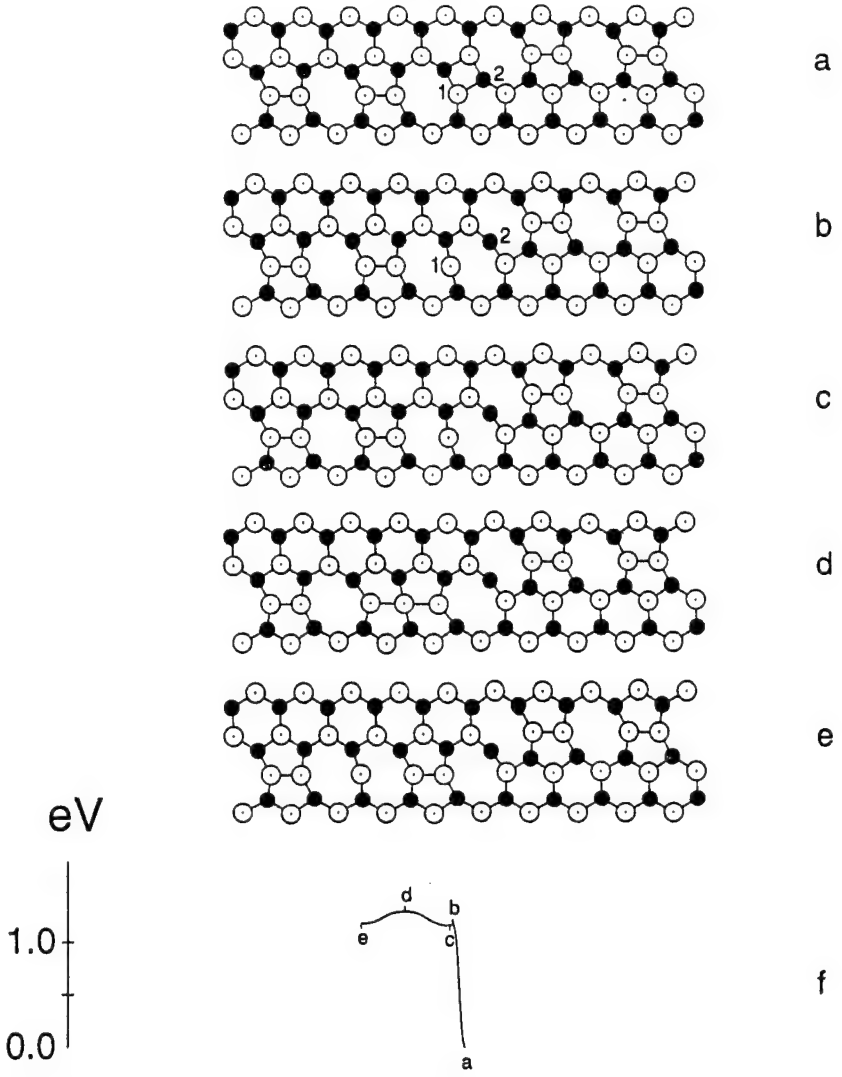

A low energy path for APD generation by the LK → LC + APD reaction.

left kink LK′. However, the sequence LK′ → LC + APD was found to have a higher barrier. Taking into account that the LK′ state is already 0·4 eV higher in energy than LK, this mechanism should not contribute substantially to APD production.

Yet another atomic mechanism for APD nucleation, this time on the right kink, is illustrated in fig. 17. It involves breaking the reconstructed bond 1–2 accompanied by formation of another reconstructed bond, 2–3 (fig. 17 (*a*, *b*)). Subsequent atomic reconfiguration results in the formation of an RC with atom 4 in the centre (fig. 17 (*c*)). To complete the reaction the APD moves away to the right, separating itself further from the RC (fig. 17 (*d*, *e*)). The pre-barrier for this nucleation reaction is 0·91 eV, and the full barrier is 1·02 eV.

A similar atomic mode was identified for the sequence involving the alternative state of the right kink: RK′ → RC + APD. Although the details are different here, the total energy barrier is roughly the same (1·01 eV). This value is notably lower than those of the total energy barriers for the other modes of APD production, with the exception

Fig. 17

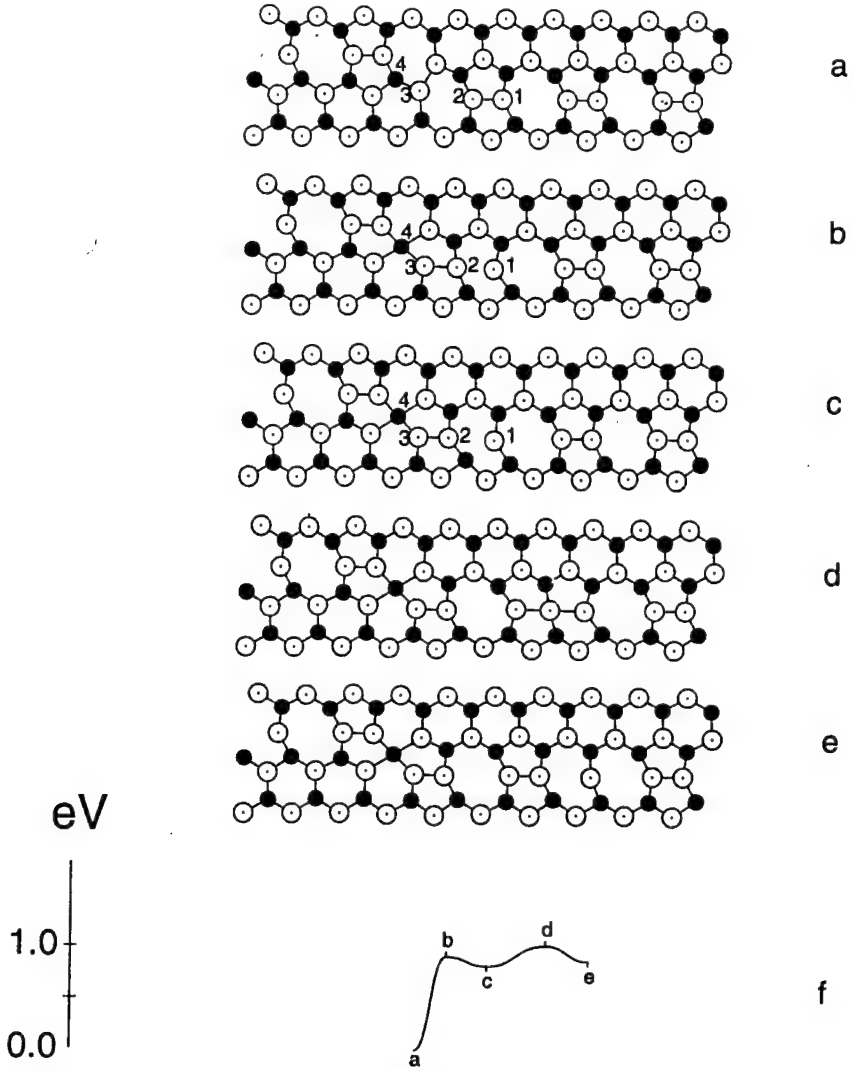

A low energy path for APD generation by the RK → RC + APD reaction.

of the LC dissociation reaction. Therefore, both of the sequences, RK → RC + APD and RK′ → RC + APD are important for APD generation.

That a RK (in both forms) is a more preferred site for APD nucleation than a LK is a consequence of the higher binding energy of the right complex. This points again to the left–right asymmetry characteristic of the 30°-partial, discussed in some detail earlier above.

§ 4. Implications for the kinetics of dislocation motion

The mechanisms discussed above do not exhaust all possible atomic modes that can contribute to dislocation mobility since there can be a much larger number of modes that can make dislocations move. However, the guiding principles chosen to navigate in this sea of atomic mechanisms were the following:

(1) From the rich spectrum of possible atomic mechanisms only those in the lower ranges of energy barriers are examined.

(2) Moving from the low-energy side of the spectrum to the higher, a minimally sufficient set of mechanisms must be identified that would provide the means for production and motion of the relevant defect species.

On the operational side, the present approach combines three different numerical methods:

(1) A constrained variant of the SA technique is used to isolate low-energy defect states in the dislocation core. At this stage the major defect species are identified as APD, LK, LK′, LC, RK, RK′ and RC.
(2) The GA technique is employed to search for low-energy paths associated with nucleation and motion of the defects. The candidates are chosen by inspection of the possibilities based on selection rules for the defect reactions.
(3) Stationary points (minima and saddles) are found lying on the low-energy paths. These are used to compute activation energies and to examine the kinematics of various atomic mechanisms of dislocation motion.

Obviously, the overall picture of the motion of the 30°-partial dislocation presented here is incomplete; we have not considered such important intrinsic defects as vacancies and interstitials and their interaction with dislocations and kinks, nor the effects of doping on the atomic interactions. These issues remain for later studies. However, the present work is a rather comprehensive study of the defect reactions involving only the kinks and the APDs. Indeed, mechanisms other than those discussed above have energies too high to deserve careful examination. An example of a high-energy barrier mechanism is the homogeneous nucleation of a pair of left and right complexes, $0 \rightarrow LC + RC$. While kinematically possible, such a mechanism must have an energy barrier not lower than the energetic effect of 1·91 eV of the corresponding multiplication reaction. On the other hand, some of the defect recombination reactions are not discussed above because their energy barriers and kinematics are very simple. A good example is the reverse reaction of recombination, of $LC + RC \rightarrow 0$. The barrier for the reaction is equal to the motion barrier of the LC defect, i.e. 0·22 eV. Hence, this mechanism is important for defect recombination. Likewise, every multiplication mechanism discussed in the previous sections has a reverse sequence. For most of such (associative) reactions, the full barriers are identified as the minimum of the motion barriers for participating defects.

For ready reference, the important energy parameters for the atomic mechanisms that have been studied are listed in table 2 (for the defect motions) and table 3 (for the defect reactions). The second and third columns of table 3 are for the energies of the embryonic pre-nucleus states (second column), and for the energies of fully separated defects (third column). For the reactions where both energies are close, only one number is given in the table. Likewise, both pre-barriers and full barriers (for complete separation) are given in the fourth and fifth columns, respectively.

A clearer picture of energy barriers involved in dislocation motion is given in fig. 18, where the barriers are grouped into three categories of mechanism: (1) very fast, (2) slower but important, and (3) too slow—inoperative. The rationale behind this division is that there are clear gaps in the spectrum of activation barriers separating the three groups of mechanisms. Mechanisms in the first group are termed fast due to their very low energy barriers. Mechanisms in the middle group must be slower. At the same time, this group includes the lower-energy modes for the production of all major defects and their motions and is, therefore, important. Mechanisms in the upper group are called

Table 2. Defect energies and motion barriers.

Defect	Energy (eV)	Motion barrier (eV)
APD	0·81	0·17
LC	1·12 $U_{lk} + U_{apd} - U_{bind}$	0·22
RK → RK′ → RK	0·82/0·89† 0·5 (U_{rk+lk})	0·74
LK → LK′ → LK	0·82/1·22† 0·5 (U_{rk+lk})	0·82
RC	0·79 $U_{rk} + U_{apd} - U_{bind}$	1·04

† Energies separated by / are for the normal and alternative forms of kinks.

Table 3. Energies and energy barriers for defect reactions.

	Energy of the products (eV)		Reaction barrier (eV)	
Reaction	Embryo	Separated	Pre-barrier	Full barrier
0 → apd + apd	1·62		1·63	1·79
0 → LK + RK	1·51	1·60	1·58	2·88
apd → LK′ + RC → LK + RC	1·21	0·66	1·25	1·65
apd → LC + RK′ → LC + RK	0·96	1·13	1·00	1·28
RK → RC + apd	0·82	0·87	0·91	1·02
LK → LC + apd	1·16	1·18	1·17	1·30
RC → RK + apd	0·88	0·84	0·95	0·97
LC → LK + apd	0·49	0·51	0·52	0·66

inoperative because, although they include some defect production or motion mechanisms, there are already lower-energy mechanisms for the same purpose in the two lower groups, which should be naturally selected.

Another principle behind the above classification is the kinematical characteristics common to the motions from each of the three groups. Indeed, all mechanisms from the high-energy group involve, in one way or another, breaking a full-strength reconstructed bond, as was discussed for the case of the homogeneous kink and APD nucleations. Accordingly, the corresponding energy barriers are above 1·6 eV. Mechanisms in the middle group also involve bond breaking, but are always accompanied by simultaneous formation of another bond. Such bond-switching mechanisms have lower energies centred approximately around 0·8–1·0 eV, which is close to one-half of the energy required to break a reconstructed bond. Both of the APD nucleation reactions on kinks are in this category. Lastly, all the low-energy mechanisms involve bond exchange between two atoms, one with a broken (dangling) bond and another a normally bonded atom. The atom with a broken bond restores normal four-fold bonding at the expense of another atom left with a dangling bond instead. In such a case, it is the participation of a dangling bond which makes the energy barrier relatively low, such as the barriers for APD and LC motions at about 0·2 eV.

The above classification gives a way to assess the results obtained in this study,

Fig. 18

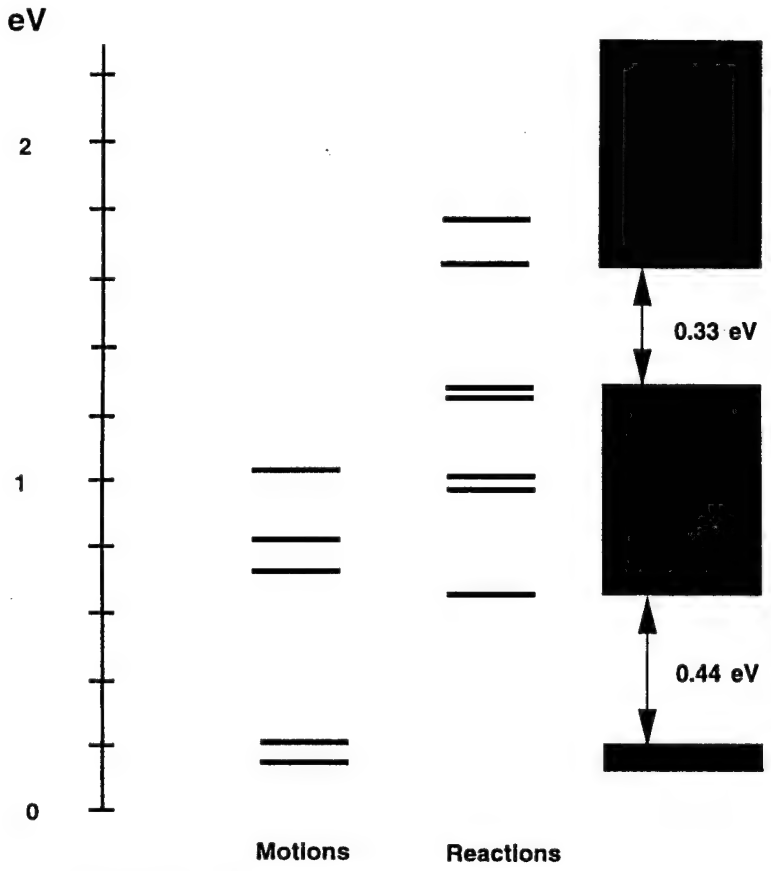

Atomic mechanisms grouped by their energy barriers.

making the overall picture much clearer. Clearly, the energy barriers are closely related to the kinematics of underlying atomic mechanisms. On the other hand, there are only three kinematical forms identified above as: bond breaking, bond switching, and bond exchange. Consequently, it is the energies associated with these kinematical elements that largely determine the barriers to various atomic motions. Given the approximate nature of the SW model of Si used in this study, it is of primary importance to obtain more reliable values for the energies of the three major kinematical types. Such more precise calculations can be performed based on the density functional theory (DFT) in the local density approximation (LDA) (Payne *et al.* 1992). One result of the present study is that targets for such calculations are now better defined.

In fact, this work provides a very important input for such first-principles calculations by isolating the atomic mechanisms that are worth looking at. On the other hand, first-principles results also can be used to develop a better empirical potential capable of reproducing the atomic mechanisms of dislocation motion more reliably. In such a way, the empirical and first-principles approaches can complement each other well in furnishing a more reliable quantitative description of dislocations in Si. The unique strength of each approach is exploited: large-scale empirical simulations

are best used to identify the most important elements of dislocation motion, while DFT/LDA calculations should then permit a more accurate description.

It remains to be determined how much of the picture that has been developed of the defect reactions and motions is indeed relevant for the overall dislocation mobility in Si. Ultimately, the DFT/LDA approach should be used to test the quality of the present results. Some calculations have already been carried out by us based on a semi-empirical tight binding potential that was shown to give a reasonable description of the dislocation reconstructions in Si (Bigger *et al.* 1992). Preliminary results of these calculations seem to support the present conclusions. This indicates that at least part of the picture discussed above may survive future scrutiny. It appears that the present results can be trusted to the extent that the employed empirical model is capable of describing specific slip geometry of the diamond cubic lattice of Si.

Another remaining challenge is to incorporate the detailed local kinematics and energetics of defects and their motions into an overall kinetic model for the motion of a whole dislocation that can then permit comparisons with experiments on dislocation mobility. Such models are presently being developed by us.

§ 5. Conclusions

We have presented an extensive study of the energetics and atomic configurations of the essential in-core defects that participate in the dislocation glide of the 30°-partial on the {111} slip plane of Si. Results were obtained on mobility and nucleation of these defects by using the Stillinger–Weber potential and a simulation methodology that overcomes some of the difficulties encountered previously. The latter consists of using a large and flexible simulation cell where possible artifacts due to periodic image forces are minimized, and a set of novel techniques for sampling and relaxation of statically displaced atomic configurations. Specifically, these techniques are a simulated annealing approach constrained to an appropriate volume surrounding the defect structure and a method, denoted as gradual ascent (GA), for generating a defect structure by imposing an external field of flexible atomic springs. By further combining GA with a conjugate gradient algorithm supplemented by eigenmode analysis, an effective procedure is thus obtained for the determination of atomic configurations and corresponding energies at saddle-point positions.

Several general implications have emerged from the considerable body of detailed results on atomic mechanisms discussed here, which lend insight to the understanding of dislocation mobility in crystalline solids with high Peierls barriers. First is the effect of reconstruction which is manifest in the central role of the APD and the kink–APD complexes. Without quantitative results on the formation and migration energies for the defects, accessible only through atomistic simulation, it was not possible previously to go beyond qualitative considerations and speculations. A second general feature discovered from our results is the left–right asymmetry in the mobility of the 30°-partial via the kink mechanism. This is an intrinsic property of the screw dislocation in the diamond cubic lattice; the effect is potentially experimentally detectable (Farber *et al.* 1986). Lastly, the natural grouping of mechanisms into bond breaking, bond switching and bond exchange means that the formidable complexity of defect reactions involved in kink mobility may be somewhat reduced by ignoring most of the bond-breaking processes as being energetically unfavourable.

We are quite mindful that all the results presented are obtained using the Stillinger–Weber potential. While we have made certain allowances for the empirical nature of this model in interpreting the various findings, we also recognize the need to

reanalyse the key results from the present work using more rigorous methods. This is a logical next step for future work. Besides the first-principles methods based on the density functional theory within the local density approximation (Payne *et al.* 1992, Bigger *et al.* 1992), it would also be of interest to apply the computationally less demanding methods based on the tight binding semi-empirical approach (Bigger *et al.* 1992). For this purpose the present study provides an important input in the form of one-dimensional adiabatic paths on the energy surface corresponding to some of the most relevant atomic mechanisms of dislocation mobility.

Acknowledgment

This work has been supported by the Office of Naval Research, through grants N00014-92-J-1957 and N00014-92-J-4022, as part of the ONR Coordinated Program on Mechanics and Atomistics of Mechanical Behavior. Further salary support was derived from a post-doctoral fellowship from the Allied Signal Corporation for which we are grateful to Dr L. Davis. We acknowledge a number of useful discussions with M. Duesbery and E. Kaxiras on theoretical aspects and with B. Ya. Farber on experimentally verifiable implications.

References

Alexander, H., and Tiechler, H., 1991, *Materials Science and Technology*, Vol. 4, edited by W. Schroter (New York: VCH), Ch. 6.

Balamane, H., Halicioglu, T., and Tiller, W. A., 1992, *Phys. Rev.* B, **46,** 2250.

Bennett, C. H., 1975, *Exact Defect Calculations in Model Substances, in Diffusion in Solids*, edited by J. J. Barton and A. S. Norwich (New York: Academic Press), p. 73.

Bigger, J. R. K., McInnes, D. A., Sutton, A. P., Payne, M. C., Stich, I., King-Smith, R. D., Bird, D. M., and Clarke, L. J., 1992, *Phys. Rev. Lett.*, **69,** 2224.

Brede, M., 1993, *Acta metall. mater.*, **41,** 211.

Brede, M., and Haasen, P., 1988, *Acta metall.*, **36,** 2003.

Bulatov, V. V., and Argon, A. S., 1992, *Phys. Rev.* A, **46,** 5275.

Carter, E. A., Ciccotti, G., Hynes, J. T., and Kapral, R., 1989, *Chem. Phys. Lett.*, **156,** 472.

Cerjan, C. H., and Miller, W. H., 1981, *J. chem. Phys.*, **75,** 7800.

Cheung, K. S., and Yip, S., 1990, *Phys. Rev. Lett.*, **65,** 2804.

Czerminski, R., and Elber, R., 1990, *J. chem. Phys.*, **92,** 5580.

deCelis, B., Argon, A. S., and Yip, S., 1983, *J. appl. Phys.*, **54,** 4864.

Duesbery, M. S., Joos, B., and Michel, D. J., 1991, *Phys. Rev.* B, **43,** 5143.

Duesbery, M. S., Michel, D. J., and Joos, B., 1990, *Mater. res. Soc. Symp. Proc.*, **163,** 941.

Duesbery, M. S., and Richardson, G. Y., 1991, *CRC Crit. Rev. solid state mater. Sci.*, **17,** 1.

Elber, R., and Karplus, M., 1987, *Chem. Phys. Lett.*, **139,** 375.

Farber, B. Ya., Iunin, Yu. L., and Nikitenko, V. I., 1986, *Phys. stat. sol.* (a), **97,** 469.

George, A., and Champier, G., 1979, *Phys. stat. sol.* A, **53,** 529.

George, A., and Michot, G., 1993, *Mater. Sci. Engng.*, **A164,** 118.

Halsey, G., White, H. J., and Eyring, H., 1945, *Text res. J.*, **15,** 295.

Heggie, M., and Jones, R., 1983a, *Phil. Mag. B*, **48,** 365; 1983b, *Ibid.*, **48,** 379; 1987, *Inst. Phys. Conf. Ser.*, **87,** 367.

Hirsch, P. B., 1979, *J. Phys.*, **40,** C6-117; 1980, *J. Microsc.*, **118,** 3.

Hirsch, P. B., Ourmazd, A., and Pirouz, P., 1981, *Inst. Phys. Conf. Ser.*, **60,** 29.

Hirsch, P. B., Samuels, J., and Roberts, S. G., 1989, *Proc. roy. Soc. Lond.*, A, **421,** 25.

Hirth, J. P., and Lothe, J., 1982, *Theory of Dislocations* (New York: Wiley), Chap. 8.

Hoagland, R. G., Hirth, J. P., and Gehlen, P. C., 1976, *Phil. Mag.*, **34,** 413.

Jones, R., 1980, *Phil. Mag.* B, **42,** 213.

Kirkpatrick, S., 1984, *J. stat. Phys.*, **34,** 975.

Kohlhoff, S., Gumbsch, P., and Fischmeister, H. F., 1991, *Phil. Mag.* A, **64,** 851.

ONSAGER, L., and MACHLUP, S., 1953, *Phys. Rev.*, **91,** 1505.
OTTEN, R. H. J. M., and VAN GINNEKEN, L. P. P. P., 1989, *The Annealing Algorithm* (Boston: Kluwer).
PARRINELLO, M., and RAHMAN, A., 1982, *J. chem. Phys.*, **76,** 2662.
PAYNE, M. C., TETER, M. P., ALLAN, D. C., ARIAS, T. A., and JOANNOPOULOS, J. D., 1992, *Rev. mod. Phys.*, **64,** 1045.
PRESS, W. H., TEUKOLSKY, S. A., VETTERLING, W. T., and FLANNERY, B. P., 1992, *Numerical Recipes*, second edition (Cambridge: University Press), p. 436.
RAY, I. L. F., and COCKAYNE, D. J. H., 1971, *Proc. roy. Soc. Lond.* A, **325,** 543.
ST JOHN, C., 1975, *Phil. Mag.*, **32,** 1193.
SINCLAIR, J. E., 1975, *Phil. Mag.*, **31,** 647.
SINCLAIR, J. E., and FLETCHER, R., 1974, *J. Phys. C,* **7,** 864.
STILLINGER, F. H., and WEBER, T. A., 1982, *Phys. Rev.* A, **25,** 978; 1985, *Phys. Rev.* **B31,** 5262.
TERSOFF, J., 1986, *Phys. Rev. Lett.*, **56,** 632.
THOMSON, R., ZHOU, S. J., CARLSSON, A. E., and TEWARY, V. M., 1992, *Phys. Rev.* B, **46,** 10613.

REPORT DOCUMENTATION PAGE

Form Approved
OMB No. 0704-0188

1. AGENCY USE ONLY (Leave blank)	2. REPORT DATE	3. REPORT TYPE AND DATES COVERED
	May 22, 1997	Final: 9/1/1992-11/30/1995

4. TITLE AND SUBTITLE
Kinetics of Dislocation Emission from Crack Tips and the Brittle to Ductile Transition of Cleavage Fracture

5. FUNDING NUMBERS
C-N00014-92-J-4022

6. AUTHOR(S)
A.S. Argon, G. Xu and M. Ortiz

7. PERFORMING ORGANIZATION NAME(S) AND ADDRESS(ES)
Massachusetts Institute of Technology
Room 1-306
Cambridge, MA 02139 (A.S. Argon)

8. PERFORMING ORGANIZATION REPORT NUMBER
1-5

9. SPONSORING/MONITORING AGENCY NAME(S) AND ADDRESS(ES)
ONR Solid Mechanics Program (Attn: Dr. R. Barsoum)
ONR Code 1132
800 N. Quincy Street - Ballston Tower 1
Arlington, VA 22217-5000

10. SPONSORING/MONITORING AGENCY REPORT NUMBER

11. SUPPLEMENTARY NOTES
Paper published in "Materials Res. Soc. Proc.", vol. 409, 29-44 (1996)
(Reprint attached)

12a. DISTRIBUTION/AVAILABILITY STATEMENT
Unlimited

12b. DISTRIBUTION CODE

13. ABSTRACT *(Maximum 200 words)*

Several activation configurations of dislocation embryos emanating from cleavage crack tips at the verge of propagating have been analyzed in detail by the variational boundary integral method, as central elements of the rate controlling process of nucleation governed fracture transitions from brittle cleavage to tough forms, as in the case for BCC transition metals. The configurations include those on inclined planes, oblique planes and crack tip cleavage ledges. Surface ledge production resistance is found to have a very strong embrittling effect. Only nucleation on oblique planes near a free surface and at crack tip cleavage ledges are found to be energetically feasible to explain brittle-to-ductile transition temperatures in the experimentally observed ranges.

14. SUBJECT TERMS
A summary of previous computational simulations of the brittle ductile transitions in fracture.

15. NUMBER OF PAGES
15

16. PRICE CODE

17. SECURITY CLASSIFICATION OF REPORT	18. SECURITY CLASSIFICATION OF THIS PAGE	19. SECURITY CLASSIFICATION OF ABSTRACT	20. LIMITATION OF ABSTRACT
Unclassified	Unclassified	Unclassified	None

KINETICS OF DISLOCATION EMISSION FROM CRACK TIPS AND THE BRITTLE TO DUCTILE TRANSITION OF CLEAVAGE FRACTURE.

A.S. Argon *, G. Xu *†, M. Ortiz ‡
* Massachusetts Institute of Technology, Cambridge, MA 02139
† present address: Terra Tek, Inc, 420 Wakara Way, Salt Lake City, Utah 84108
‡ California Institute of Technology, Pasadena, CA 91125

ABSTRACT

Several activation configurations of dislocation embryos emanating from cleavage crack tips at the verge of propagating have been analyzed in detail by the variational boundary integral method, as central elements of the rate controlling process of nucleation governed fracture transitions from brittle cleavage to tough forms, as in the case for BCC transition metals. The configurations include those on inclined planes, oblique planes and crack tip cleavage ledges. Surface ledge production resistance is found to have a very strong embrittling effect. Only nucleation on oblique planes near a free surface and at crack tip cleavage ledges are found to be energetically feasible to explain brittle-to-ductile transition temperatures in the experimentally observed ranges.

INTRODUCTION

Abrupt transitions in fracture between energy absorbing ductile forms and brittle cleavage, with decreasing temperature and increasing strain rate have been, and still continue to be of concern in many structural materials. While the phenomenon has been known in engineering practice since at least the celebrated molasses tank fracture in Boston in 1919 (for a discussion of an historical perspective of non-ship fractures see Shank, [1]), it became of crisis proportions only during World War II through the rash of major fractures of Liberty ships. In the early post-war years the problem received attention through semi-quantitative studies of notch effects and strain rate [2], and through some studies of effects of microstructure and of alloying to suppress the ductile to brittle transition temperature (for a summary see Parker, [3]). In the 50s and early 60s a fundamental recognition was reached that brittle behavior is usually triggered by deformation induced cleavage microcracks introduced into the system by dislocation pile-ups [5,7] by intersection of deformation twins [8] or by cracking of elongated grain boundary carbides [9]. In the range of the transition temperature a substantial concentration of such microcracks are "injected" into the system. Eventual brittle behavior results when one such microcrack succeeds, without being rearrested, to break through grain boundary barriers and propagates long distances [9-11]. The triggering conditions for this final transition in polycrystalline metals were also studied theoretically [12-15].

A fundamental perspective on the class of materials which are capable of fracture transitions starts with Kelly et al [16], and more specifically with Rice and Thomson [17] who have conceived a fundamental behavior pattern for a theoretical criterion establishing in-

Mat. Res. Soc. Symp. Proc. Vol. 409 © 1996 Materials Research Society

trinsic brittleness vs intrinsic ductile behavior in materials. According to this criterion an atomically sharp crack has means of governing the behavior of a material in the absence of any other form of plastic response of the background, by either nucleating dislocations from its tip or by propagating in a cleavage mode by virtue of the presence of an energy barrier to the emission of such dislocations. In the first instance the material is designated as intrinsically ductile and incapable of exhibiting a fracture transition, while in the second instance it is designated as intrinsically brittle and capable of undergoing a transition from brittle cleavage to ductile forms at a characteristic transition temperature T_{BD}, affected by the rate of loading. Although many experimental studies have demonstrated that mere nucleation of some dislocations from a crack tip does not assure ductile behavior [18,19], the Rice Thomson mechanism comes close to a threshold process that triggers ductile behavior in a class of intrinsically brittle solids with relatively high dislocation mobility such as the BCC transition metals and most alkali halides. However, fully satisfactory experimental confirmation of this limiting response is rare, outside of an elegant experiment by Gilman et al [20] of crack arrest in LiF.

In distinction to the nucleation controlled response is the well established response of Si, and presumably, many other covalent materials and compounds with sluggish dislocation mobility, where the transition between brittle to tough behavior is governed by the mobility of groups of dislocations away from the crack tip [21-25]. In either the nucleation or the mobility controlled dislocation emission scenarios it is now well recognized that, emission of such dislocations from a crack tip occurs preferentially from specific crack tip sites and that assurance for full ductile behavior requires that all parts of the crack front be shielded to prevent continued brittle behavior by local break-out of the cleavage crack from unshielded portions of the crack front [24]. Since even the ductile to brittle transition is triggered by the continued propagation of an "injected" cleavage microcrack, it is now generally accepted that the fundamental fracture transition is governed by the behavior of a cleavage crack. Most modeling studies have been developed around this concept.

The fundamental supposition of the brittle-to-ductile transition models based on the Rice and Thomson scenario [17] is that while background plastic relaxations can serve to suppress the transition temperature, the ultimate arbiter of the transition is the ability, of the crack tip to emit dislocations that can shield the entire crack front and trigger widespread plastic deformation before the crack can propagate by cleavage. However, the approach of the Rice and Thomson model in which the activation configuration consisted of a fully developed dislocation line have proved to seriously over estimate the energy barriers to nucleation of dislocations [26], even after incorporating such refinements as crack tip non-linearity and tension softening [27] across the slip plane. This indicated that the activation configurations must involve imperfect dislocations which must incorporate at least a minimum of atomistic information [26].

The accumulating experimental evidence on Si [21-25] and the insight provided by the most recent modeling studies of Schöck and Püschl, [28], Rice and Beltz [29], Xu et al., [30] suggest that the activation configuration of a dislocation embryo is in the form of a double kink of dislocation core matter. The observation permits the identification of two distinct types of B-D transitions. In the BCC transition metals where barriers to kink mobility along the dislocation are low, the B-D transition is likely to be governed directly by the formation of dislocation embryos at the crack tip, resulting in a nucleation-controlled transition. By

contrast, in semi-conductors and compounds the evidence suggests [31-35], and modeling verifies [36], that kink mobility is hindered by substantial energy barriers, rendering the B-D transition controlled by dislocation mobility away from the crack tip.

Ultimately, a full understanding of the B-D transitions must come from atomistic models of the formation and outward propagation of the dislocation embryo at the crack tip. Before such modeling can be attempted, however, much progress can be made by recourse to hybrid continuum-atomistic approaches [28,29,30,37] based on the use of a Peierls interplanar potential [38-40]. In a recent development of this technique by Xu et al [30], an additional surface production resistance was introduced into the interplanar potential, and the appropriate saddle point configurations of the dislocation embryos were determined by recourse to a variational boundary integral method advanced by Xu and Ortiz earlier [41]. Xu et al [30] concluded that the energetics of dislocation embryo formation on inclined slip planes containing the crack tip, against an additional surface production resistance, is quite unfavorable and does not explain the known B-D transition temperatures. It was then conjectured that nucleation may be more favorable on oblique slip planes or, may occur heterogeneously at crack front ledges.

In the present communication we briefly take into account the earlier findings of Xu et al [30] and present new findings on saddle-point configurations and their energies on oblique planes in the interior and near free surfaces, and finally, on cleavage surface ledges at the crack front. In what follows we begin by describing the nucleation controlled alternative mechanisms to be appraised. Following a brief description of the fundamental methodology employed in calculations, results of three nucleation mechanisms are presented. Finally in a discussion, the B-D transition temperatures are estimated from the calculated activation energies, and findings are put in general perspective.

MODES OF DISLOCATION NUCLEATION

Several alternative modes of dislocation nucleation from crack tips have been contemplated in the past. The modes differ mainly in the relative geometry of the slip plane, the crack surface and the crack front. The configurations considered include: nucleation of dislocations on the extension of the crack surface, Fig. 1a; nucleation on an inclined plane containing the crack front, Fig. 1b; nucleation on an oblique plane, Fig. 1c; and nucleation on a cleavage ledge, Fig. 1d.

Of these modes that shown in Fig. 1a is the simplest since it involves no tension across the potential slip plane and no production of a free surface. It has been investigated by Rice, [45] and Rice et al [37] in a two dimensional setting and by Schöck and Püschl [28] in a three dimensional setting of a simple double kink shaped activation configuration. This was also done by a more elegant perturbation analysis by Rice and Beltz [29]. These analyses that have used a conservative tension-shear potential based on a Peierls-Nabarro model to represent the periodic interplanar shear resistance of a slip plane and a tension softening effect have demonstrated that the activation configuration did indeed consist only of dislocation core matter. In 2-D this produces an inelastic crack tip displacement equal to one half of a Burgers displacement and results in a critical energy release rate equal to the unstable stacking energy associated with a half step shear across the slip plane. Rice et al [37] have extended their approach to also deal with the mode of Fig. 1b involving dislocation

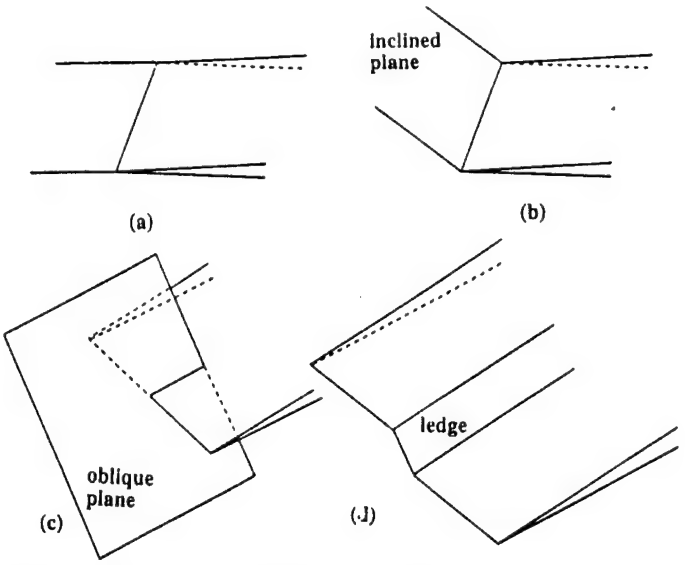

Fig. 1 Alternative modes of dislocation nucleation from a crack tip.

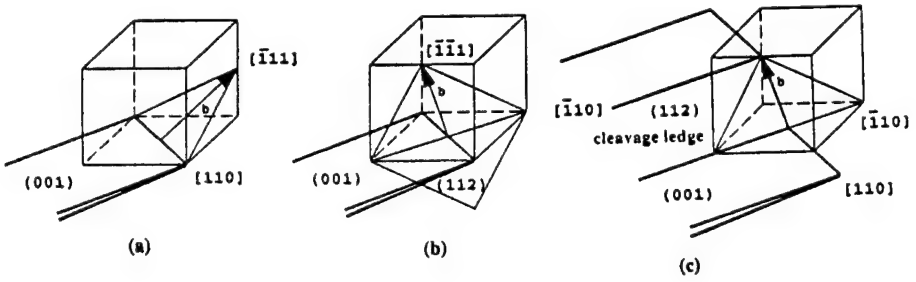

Fig. 2. Modes of dislocation nucleation from crack tips in α-Fe: a) inclined plane; b) oblique plane; c) cleavage ledge.

nucleation on an inclined plane-albeit without the affect of surface ledge production. To deal with such problems more definitively, a surface production resistance was incorporated into their model by Xu et al [30] who have concluded that this effect raises the energy barrier to such a degree that it all but rules out dislocation nucleation on inclined planes.

Experimental observations of Burns and Webb, [18] and considerations of peak stress levels [26] point to the possibility of nucleating dislocations on oblique planes as shown in Fig.1c. However, approximate analysis of this nucleation mode by the Rice and Thomson method have led to very large energy barriers. This conclusion is reinforced by our more accurate analysis presented below. Finally, experimental observations of George and Michot, [25] have indicated that actual dislocation nucleation occurs very frequently on cleavage ledges on the crack front and near free surfaces. We analyze this possibility in Section 4.4 and show that conditions are indeed quite favorable for this mode. Since nucleation controlled fracture transitions are likely to be limited only to BCC transition metals and to some alkali halides, we have performed our analyses for α-Fe. Figures 2a-2c show the specific

geometrical settings for Fe that have been considered where the cleavage plane in (001) and the crack front is parallel to the [110] directions which is the prevalent direction of the crack front in Fe giving a minimum of energy release rate [47].

METHOD OF ANALYSIS

The analysis employs a variant of the variational boundary integral method of Xu and Ortiz [41] to encompass problems of dislocation nucleation from atomically sharp cracks. In this model, a slip plane connected to the crack front is viewed as an extension of the crack surfaces with a nonlinear interlayer potential acting across it. Thus, the crack and the slip plane on which the dislocation nucleates are jointly regarded as a three-dimensional crack system embedded in the linear elastic solid. The interlayer potential acting across the slip plane is modeled by combining the universal binding energy relation of Rose et al [48] with a skewed shear resistance profile [40]. The interplanar displacements and the crack opening displacements are represented by a continuous distribution of curved dislocations. This approach introduces no artificial discontinuity between the elastic crack opening and inelastic interplanar slip and separation. The technique has been described in complete detail by Xu and Ortiz [41] and its application to the present study by Xu et al, [30,47]. In this section, we briefly outline those aspects of the method which are pertinent to the treatment of the special activation configurations described in the previous section.

We consider a semi-infinite cleavage crack and a slip plane intersecting the crack front as shown in Fig. 1b. The crack/slip plane system is loaded remotely by a K-field. The crystallographic slip plane is chosen to be the most advantageous for slip. As the driving force increases, an embryonic dislocation forms progressively until it reaches an unstable equilibrium configuration. The load corresponding to this unstable configuration is defined as the critical driving force for nucleation. The embryonic dislocation profile is characterized as a distribution of interplanar inelastic displacements, defined by Rice [45] as:

$$\delta = \Delta - \Delta^e \tag{1}$$

where Δ and Δ^e denote the total and the elastic interplanar displacements respectively. The opening displacements $\mathbf{u}$ of the crack surface, including the inelastic displacements along the slip plane, can be written as:

$$u = \overline{u} + \delta \tag{2}$$

where $\overline{u}$ is the displacement of a standard K-field for a reference semi-infinite crack. The term $\overline{u}$ matches the behavior of the opening displacements of the crack far away from the crack tip and serves as a boundary condition of the system. Consequently, the additional term δ, modifying the former, and which is the primary unknown in the analysis, is expected to decay rapidly to zero with distance away from the crack tip in either direction. In this manner, δ can be considered in a finite domain around the crack front on the crack surface and on the slip plane connected to the crack.

Following the procedure introduced by Xu et al, [30,47] the potential energy of the whole system can be written in the form.

$$\Pi[\overline{u}+\delta] = W[\overline{u}+\delta] + V[\delta] = W_1[\overline{u} + W_1[\delta] + W_2[\overline{u},\delta] + V[\delta], \tag{3}$$

where we identify $W_1[\overline{u}]$ as the elastic strain energy of the system, free of inelastic modifications, $W_1[\delta] + V[\delta]$ as the self energy of the system of inelastic modifications consisting of the distributed dislocations and the interplanar interaction energy on the slip plane, and $W_2[\overline{u},\delta]$ is the interaction energy of the initial unmodified system with the second system of modifications. Of these energies the ones of relevance in the variational approach are those that depend on the unknown inelastic modification δ. Their specific forms have been given elsewhere [30, 47].

The potential energy $V[\delta]$ of the interplanar inelastic deformation on the slip plane is a key ingredient of the method and is given as:

$$V[\delta] = \int_{\hat{S}_s} \Phi[\delta] dS, \tag{4}$$

where $\Phi[\delta]$ is the interplanar tension/shear potential, defined per unit area of the slip plane $\hat{S}_s$. It adopts the constrained displacement hypothesis of Rice [45] and Sun et al [49], in which the interplanar shear displacement Δ_r is constrained along the Burgers vector direction. The shear and tension separation resistances, τ and σ respectively, follow as functions of the inelastic shear displacements δ_r and tensile separation displacement δ_θ on the slip plane. The associated traction-displacement relation has been modeled by Rice et al [37] and was modified somewhat by Xu et al [30] to incorporate an element of skewness and a surface production resistance. The resulting forms have been presented in detail elsewhere [30].

The unknown displacements follow by rendering the potential energy $\Pi[\overline{u}+\delta]$ stationary. This is achieved by discretizing the integral equation with six noded elements distributed on the crack surface. The non-linear equations are solved by a Newton-Raphson iteration. The saddle point configurations are activated by introducing a small perturbation into the system at the bifurcation point, based on the solution of a first-order eigen-value problem if necessary. Solutions are obtained by recourse to interplanar displacement control achieved through the introduction of Lagrange multipliers [30,47].

The material constants for α-Fe used in the present calculations are given in Table I.

Table I. Material Properties for α-Fe [47]

slip system	T (°K)	μ (10^5MPa)	c	$\gamma_{us}^{(u)}$ (Jm^{-2})	$2\gamma_s$
$(1/2)[111](1\bar{1}0)$	4.2	0.756	3.125	0.517	3.33
$(1/2)[\bar{1}\bar{1}1](112)$	4.2	0.756	3.125	0.581	3.80

where

μ	shear modulus
c	uniaxial strain elastic modulus
$\gamma_{us}^{(u)}$	unrelaxed unstable stacking energy
γ_s	surface energy

RESULTS

Nucleation of Dislocations from a Shear Crack in Mode II

Because of its simplicity and the ease of systematically incorporating important effects, we consider first the nucleation analysis in Mode II as indicated in Fig. 1a. The crack surface coincides with the (001) plane, the crack front with the [110] direction and the slip plane with the $(1\bar{1}2)$ plane, Fig.2a. The crack/slip plane system is subjected to pure mode II loading. Two representative saddle point configurations of the dislocation embryo corresponding to normalized load levels G_{II}/G_{IIcd} =0.75 and 0.50 are shown in Figs 3 and 4, respectively. In the figures $x_1 = 0$ indicates the initial crack front and the level contours represent the shear displacements between the crack faces (for $x_1 < 0$), and the inelastic displacements across the slip plane (for $x_1 > 0$). The double-kink nature of the saddle point configuration is clearly visible. The dependence of the activation energy on the crack driving force is plotted in Fig. 5. The crack driving force G_{II} has been scaled with the athermal driving force G_{IIcd} for the 2-D release of a dislocation line from the entire crack front, where G_{IIcd} is the unrelaxed unstable stacking energy $\gamma_{us}^{(u)}$.

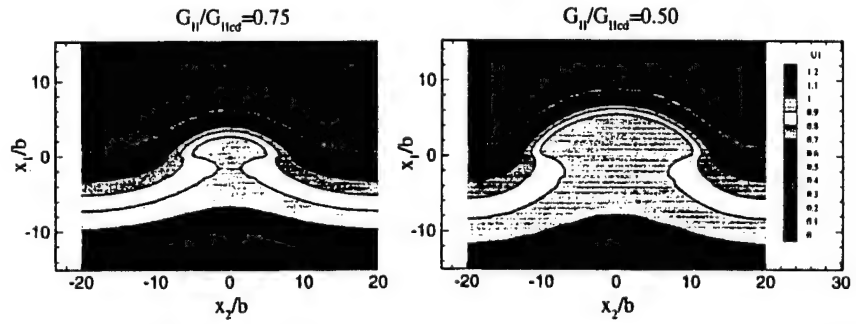

Figs. 3 & 4. Saddle-point configurations at a crack tip under Mode II loading for $G_{II}/G_{IIcd} = 0.75$, and 0.5.

Nucleation of Dislocations on Inclined Planes in Mode I.

To obtain from the results of the section above the condition for nucleating dislocations on inclined planes two modifications need to be considered.

First, on any inclined slip plane passing through a Mode I crack the nucleation of a dislocation will occur under a mixture of effective Modes II and Mode I where the local effective Modes I and II are related to the Mode I acting across the crack by [50],

$$K_I^{eff} = K_I cos^3(\theta/2) \;\; \therefore \; K_{II}^{eff} cos^2(\theta/2) sin(\theta/2) \qquad (5a,b)$$

Instead of solving the specific problem of Fig. 2b at hand, we examine the general modifying effect on K_{II} of a K_I^{eff} acting across the slip planes, that is required to achieve an athermal 2-D release of a straight dislocation on this plane. This result is given in Fig. 6 [30] and demonstrates that while the effect of a K_I^{eff} acting across the slip plane does indeed produce some reduction in the required K_{II}^{eff}, this reduction is relatively minor.

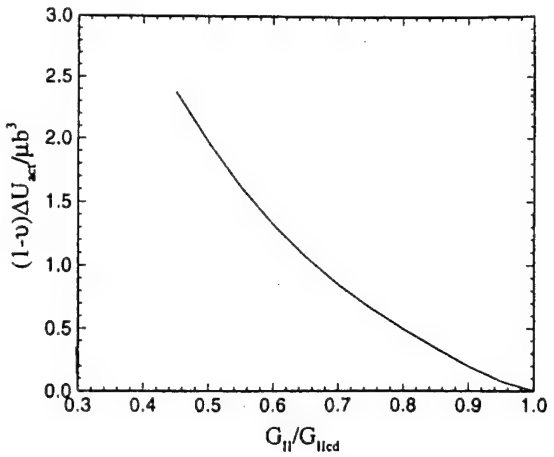

Fig. 5. The activation energy for dislocation emission under pure mode loading.

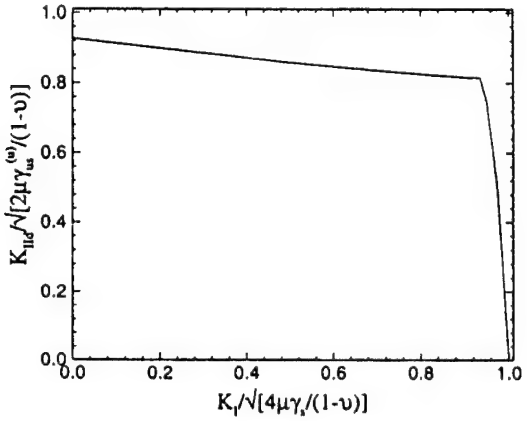

Fig. 6. Dependence of critical K_{II} for dislocation emission on K_I present on the $\frac{1}{2}[\bar{1}\bar{1}1](112)$ system of α-Fe.

Second, on any inclined slip plane the nucleation of a dislocation will produce a free surface ledge after the dislocation is emitted and has been sent into the background. During the actual nucleation process when the incipient surface is not yet relaxed the effect must be considered as an additional surface production resistance to be added to the shear resistance of the tension shear potential [30, 51] to at least the first row of atoms that will be bared as a free surface. The result of a specific analysis of this effect is shown in Fig. 7 again for the release of a straight dislocation from the crack tip onto an inclined plane making an angle of 45° with the crack plane. The dependence of the critical energy release rate G_{cd}, normalized with the crack driving force G_{IC} on the parameter $q = \gamma_{us}/2\gamma_s$ is shown for a case with no surface production resistance ($\lambda = 0$) and for a surface production resistance

affecting substantially only the first row of atoms ($\lambda = 1$). The slanted dash-dotted line shows a somewhat more approximate estimate of Rice for no surface production resistance [45], while the horizontal dashed line gives the condition where cleavage is obtained on the slip plane. $G_{cd}/G_{IC} < 1.0$ indicates nucleation of a dislocation prior to propagation of the crack. The solutions including the surface production resistance indicates that for all values of q crack propagation on the cleavage plane will precede athermal release of a dislocation on the 45° inclined plane. Values of q range from 0.081 for Al to 0.091 for Ni (both for Shockley partial dislocations) to 0.217 for α-Fe and 0.376 for Si (Shockley partial) [30]. Regardless of the values of q, since all cases lie above G_{cd}/G_{IC} of 1.0, it must be concluded that homogenous nucleation of dislocations on inclined planes is not possible prior to crack propagation for any material, regardless of whether it is intrinsically brittle or ductile [30].

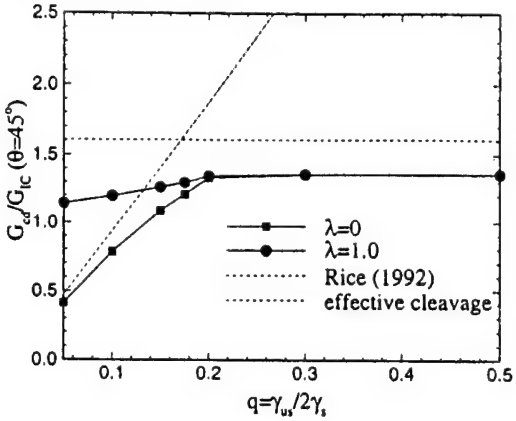

Fig. 7. Dependence of the critical energy release rate G_{cd}/G_{IC} on the factor $q = \gamma_{us}/2\gamma_s$ for dislocation nucleation at 45°.

Nucleation of Dislocations on the Oblique Plane.

As remarked above, dislocation nucleation on oblique planes has been put forth as a likely mode. However, the capability required for the analysis of this mechanism had been heretofore unavailable. Approximate analyses based on the Rice and Thomson method have led to estimates of the B-D transition temperatures several orders of magnitude higher than what is experimentally observed, prompting suggestions that nucleation should involve fractional dislocation [26].

Here we provide a direct analysis of the formation of dislocation embryos on oblique planes in α-Fe in the configuration of Fig. 2c as the most favorable for such nucleation. In the analysis, we have artificially constrained the cleavage plane from propagating to enable the computation of the critical driving force for dislocation nucleation. If the resulting athermal critical driving force is less than G_{IC} for cleavage, the crystal is intrincsically ductile. Contrariwise, if the critical driving force is greater than that for cleavage, the crystal is cleavable or intrinsically brittle. However, on a crack, on the verge of crack propagation by cleavage, a dislocation can still be nucleated through thermal activation. The calculation of the activation energy for such thermally assisted dislocation nucleation was performed for Fe in the configuration of Fig. 2c [47].

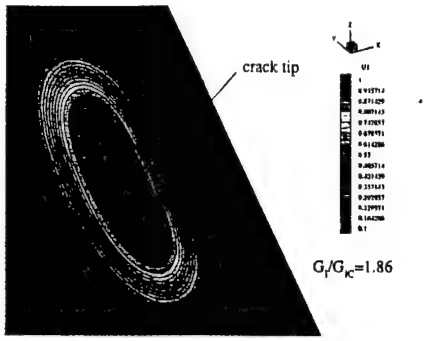

Fig. 8. Saddle-point configuration of a dislocation embryo emitted from a crack tip on an oblique plane.

A typical saddle point configuration of an embryonic dislocation loop emanating from the crack tip is shown in Fig. 8. The resulting calculated dependence of the activation energy on the crack driving force, near the athermal threshold is shown in Fig. 9. The critical driving force at the athermal threshold, and the attendant activation energies are so high that they render the nucleation mechanism most unlikely. The activation energy at $G_I/G_{IC} = 1.0$ can be estimated from the extrapolated curve, and forms an adequate basis for reaching a firm negative conclusion on the likelihood of nucleating a dislocation in the interior by this mechanism. A very different conclusion can be reached, however, for this mechanism where the crack front reaches a free surface. Here, no plane strain stress constraint exists and the resolved shear stresses on the oblique planes become much higher. An estimate of this is readily obtained by re-scaling the driving forces in Fig. 9 in proportion to the resolved shear stresses on the oblique slip planes near the surface vs those in the interior as (for the geometry of Fig. 2b):

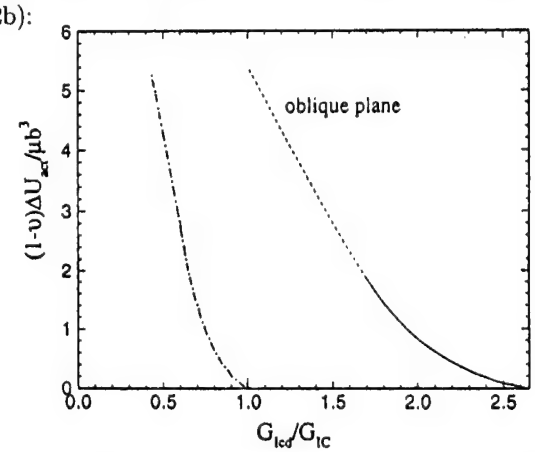

Fig. 9. Activation energies for dislocation nucleation on an oblique plane. Dash-dotted curve for such a plane near the surface.

$$\frac{G_{Is}}{G_{Ii}} = \left(\frac{3-4\nu}{3}\right)^2 \tag{6}$$

where G_{Is} and G_{Ii} are the respective energy release rates for initiation near the surface and in the interior. The result for Fe with $\nu = 0.291$ is shown as the dash-dotted curve in Fig. 9, which now suggests almost spontaneous nucleation near the surface. This, however, is not true since in this instance some surface ledge needs to be produced which will make the nucleation more difficult, but presumably still much easier than in the interior.

Nucleation of Dislocations on a Cleavage Ledge

Cleavage surfaces in metallic crystals invariably contain ledges parallel to the direction of crack propagation. These are likely to form when the direction of the principal tension driving the crack deviates slightly on a local scale, requiring the crack to make small adjustments along its front. This unavoidable micro-roughness of the cleavage surface depends on the crystallography of the cleavage planes and the crack propagation direction, as well as on temperature. The height of the observed ledges can range from several atomic spacings to microns. Numerous observations [24,25,42] have revealed that dislocation nucleation at a crack front is a relatively rare phenomenon associated with such crack front heterogeneities [52]. In what follows we analyse this mechanism as it is likely to operate in α-Fe.

Consider a cleavage crack propagating under Mode I loading, and containing ledges of a width of roughly a hundred atomic spacings distributed along its front. The presence of a considerable local Mode III stress intensity factor acting on the ledge, the fact that no free surface is produced, and that the nucleated embryo will be nearly screw in nature are all expected to promote nucleation.

The distribution of stress intensity factors on the crack front can be readily calculated by the boundary element method [41]. On the ledge, the dominant stress intensity factors are $K_I^{ledge} \sim 0.81 K_{IC}$ and $K_{III}^{ledge} \sim 0.35 K_{IC}$ at the verge of brittle propagation.

The athermal condition for nucleating a dislocation in Mode III loading, as it exists on the ledge, was determined by Rice [45], as:

$$K_{IIIcd} = \sqrt{(1-\nu)\gamma_{us}/2\gamma_s} K_{IC} = 0.357 K_{IC} > 0.350 K_{IC} \tag{7}$$

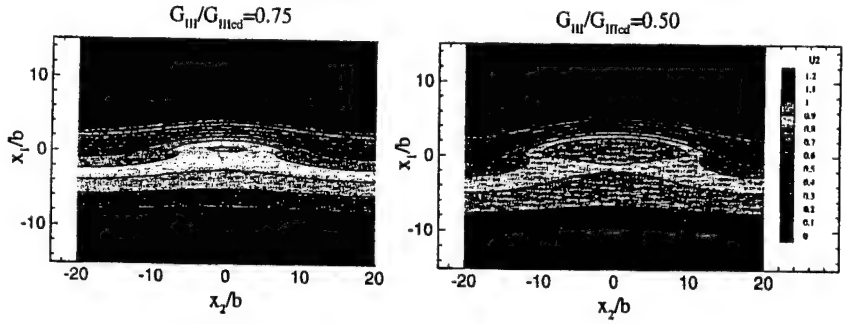

Figs. 10 & 11. Saddle-point configurations of a dislocation embryo on a cleavage ledge at $G_{III}/G_{IIIcd} = 0.75$, and 0.5.

Although, this suggests that dislocation formation on the ledges should be close to spontaneous according to this simple estimate, we merely conclude that it should be in the range to initiate thermally assisted embryo formation. To analyse such thermally assisted embryo formation we consider a saddle point analysis of a crack in pure Mode III, to apply to the problem at hand, of the cleavage ledge loaded in Mode III. Figures 10 and 11 show the saddle point configuration under normalized load levels of G_{III}/G_{IIIcd} of 0.75 and 0.5 respectively. The resulting dependence of the activation energies for such configurations on actual normalized crack driving forces G_I/G_{IC} are shown in Fig. 12, for a case with no K_I component acting across the ledge ($\bigtriangledown$) and the case with the appropriate K_I component of $0.81K_{IC}$ (o) acting across the ledge as it should be the case of the geometry of Fig. 2c. The differences are small.

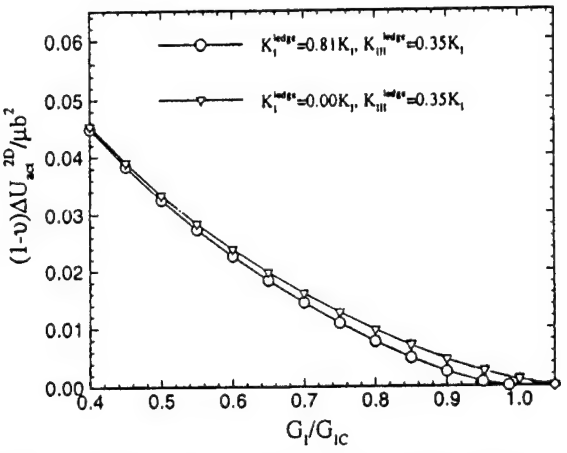

Fig. 12. Activation energies for dislocation nucleation on a cleavage ledge.

DISCUSSION

Estimates of the B-D Transition Temperature

As noted in the introduction, the B-D transition in BCC transition metals, and particularly in α-Fe, is most likely controlled solely by dislocation nucleation. Therefore, the preceding results can be used to estimate the B-D transition temperatures attendant to the three main nucleation modes considered. No precise experimental measurements of the transition temperature of single crystal α-Fe are available. The transition temperature for polycrystal low carbon steel is about $250°K$, as determined from Charpy impact experiments [53]. Based on this, we take the transition temperature for α-Fe to be in the range of $250 - 300°K$. A B-D transition scenario proposed by Argon [26] consists of the arrest, at T_{BD}, of a cleavage crack propagating with a velocity v against a temperature gradient. This gives the relation,

$$T_{BD} = \left[\frac{ln(c/v)}{\alpha} + \eta\frac{T_o}{T_m}\right]^{-1} T_o \tag{8}$$

where $T_o \equiv \mu b^3/k(1-\nu) \sim 1.2\text{x}10^5 K$; the melting temperature $T_m = 1809K$ for α-Fe; $\alpha = (1-\nu)\Delta U_{act}/\mu b^3$ is the normalized activation energy; c is speed of sound; $v \sim 1cm/s$ is a typical crack propagation velocity, giving $\ln(c/v) \sim 10$; $\eta \sim 0.5$ is a coefficient describing the temperature dependence of the shear modulus which, to a first approximation, is presumed of the form $\mu = \mu_o(1-\eta(T/T_m))$.

The activation energy at the critical driving force for cleavage , i.e., at $G_I/G_{IC} = 1$, determines the transition temperature through Eqn. 8. This relation is plotted in Fig. 13 together with reasonable ranges of activation energies for nucleation on inclined planes, oblique planes and on ledges. The results for the oblique plane near a free surface should be close to that for cleavage ledges. Also shown in the figure is the value of the transition temperature for polycrystalline Fe and its melting temperature. It is evident that only nucleation on cleavage ledges and on oblique planes near a free surface result in transition temperatures that approach the expected value for α-Fe. The dislocation loops which eventually shield the entire crack are apparently emitted from ledges distributed along the crack front as was noted by George and Michot [25].

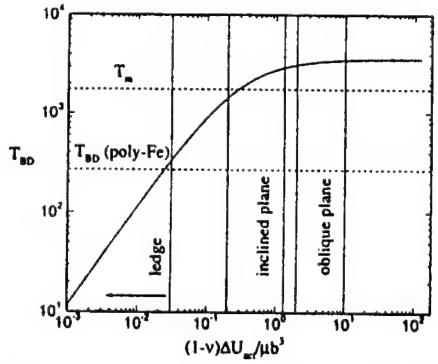

Fig. 13. Estimates of B-D transition temperatures in α-Fe vis-a-vis the three nucleation configurations considered.

Other Possibilities

The fracture transition modeled in the present study is meant for dislocation-nucleation-controlled- transitions, characteristic of BCC transition metals, and not for transitions controlled by the mobility of dislocations away from the crack tip [44] which is typical of semiconductors and compounds. The distinguishing characteristic between these two behaviors is the mobility of kinks on dislocations, which is high in BCC transition metals, and very low in Si and other compounds for which good information on dislocation mobility exists [31-35].

An additional effect which can influence fracture behavior is crack-tip shielding by general 'background' plasticity. A particularly elegant and compelling analysis of this mechanism was advanced by Freund and Hutchinson [54], who have demonstrated that brittle-like fracture should take place at high crack propagation velocities with progressively diminishing inelastic response. However, this transition is smooth and spread out, and far from being abrupt.

The importance of background plasticity effects has been demonstrated experimentally by Hirsch et al [24] who have shown that the sharp B-D transition in dislocation-free Si becomes diffuse and moves to somewhat lower temperatures-when the crystals are initially dislocated by a pre-deformation step. The effect of background plasticity can therefore be regarded to modulate the B-D transition, with the ultimate controlling mechanism still residing in crack-tip initiated processes.

In closing, we note that the ability of dislocation nucleation at the crack tip to account for the exceedingly sharp transitions observed in some materials has been questioned by Khanta et al [55, 56] who have advocated a critical phenomena approach, akin to defect- mediated melting. However, the preponderance of the observational evidence appears to support the crack-tip dislocation nucleation mechanism. Indeed, the detailed and meticulous direct X-ray imaging experiments of George and Michot [25] of the stages of evolution of the crack tip plastic response, starting from nucleation at crack tip heterogeneities and followed by the very rapid spread and multiplication of dislocation length from such sources, is a convincing direct demonstration of the vast numbers of degrees of freedom available to dislocations for populating the highly stresses crack tip zone. We know of no present experimental evidence for the large thermal equilibrium concentrations of stiffness-attenuating dislocation dipoles that are predicted by the model of Khanta et al.

ACKNOWLEDGMENTS

This research was supported by the Office of Naval Research (ONR) under contract N00014-92-J-4022 at MIT, and from the ONR contract No. N00014-90-J1758 at Brown University. The computations were carried out in the facilities of the Mechanics of Materials Group at MIT, and those of the Solid Mechanics Group at Brown University.

REFERENCES

1. M.E. Shank, *Mech. Eng.*, *76*, 23 (1954).
2. E. Orowan, in "Repts. Prog. Physics", vol 12, p.185 (1949).
3. E.R. Parker, ``Brittle Behavior of Engineering Structures", J. Wiley, New York (1957).
4. C. Zener, in ``Fracturing of Metals", ASM, Metals Park Ohio, p.3 (1949).
5. A.N. Stroh, *Proc. Roy. Soc.*, *A223*, 404, (1954).
6. A.N. Stroh, *Proc. Roy. Soc.*, *A232*, 548 (1955).
7. D. Hull, *Acta Metall*, *8*, 11 (1960).
8. C. McMahon, "Micromechanisms of Cleavage Fracture in Polycrystalline Iron", ScD Thesis, M.I.T., Cambridge, MA (1963).
9. G.T. Hahn, B.L. Averbach, W.S. Owen, and M. Cohen, in ``Fracture", edited by B.L. Averbach et al, MIT Press, Cambridge, MA, 91 (1959).
10. J.F. Knott and A.H. Cottrell, *J. Iron Steel Inst.*, *201*, 249 (1963).

11. M. Cohen and M.R. Vukcevich, in "Physics of Strength and Plasticity", edited by A.S. Argon, MIT Press, Cambridge, MA p.295 (1969).
12. A.N. Stroh, *Adv. Phys.*, *6*, 418 (1957).
13. R.O. Ritchie, J.F. Knott and J.R. Rice, *J. Mech. Phys. Solids*, *21*, 395 (1973).
14. T. Lin, A.G. Evans and R.O. Ritchie, *J. Mech. Phys. Solids*, *34*, 477 (1986).
15. T. Lin, A.G. Evans and R.O. Ritchie, *Met. Trans.*, *18A*, 641 (1987).
16. A. Kelly, W.R. Tyson and A.H. Cottrell, *Phil. Mag.*, *15*, 567 (1967).
17. J.R. Rice and R. Thomson, *Phil. Mag.*, *29*, 73 (1974).
18. S.J. Burns and W.W. Webb, *J. Appl. Phys.*, *41*, 2078 (1970).
19. S.J. Burns and W.W. Webb, *J. Appl. Phys.*, *41*, 2086 (1970).
20. J.J. Gilman, C. Knudsen and W.P. Walsh, *J. Appl. Phys.*, *29*, 600 (1958).
21. C. StJohn, *Phil. Mag.*, *32*, 1193 (1975).
22. M. Brede and P. Haasen, *Acta Metall*, *36*, 2003 (1988).
23. P.B. Hirsch, J. Samuels, and S.G. Rloberts, *Proc. Roy. Soc.*, *A421*, 25 (1989).
24. P.B. Hirsch, S.G. Roberts, J. Samuels and P.D. Warner, in "Advances in Fracture Research" edited by K. Salama et al, Pergamon, Oxford vol 1, p.139 (1989).
25. A. George and G. Michot, *Mater. Sci. Engng.*, *A164*, 118 (1993).
26. A.S. Argon, *Acta Metall.*, *35*, 185 (1987).
27. K.S. Cheung, A.S. Argon and S. Yip, *J. Appl. Phys.*, *69*, 2088 (1991).
28. G. Schöck and W. Püschl, *Phil. Mag.*, *A64*, 931 (1991).
29. J.R. Rice and G.E. Beltz, *J. Mech. Phys. Solids*, *42*, 333 (1994).
30. G. Xu, A.S. Argon and M. Ortiz, *Phil. Mag.*, *72*, 415 (1995).
31. K. Sumino, in ``Structure and Properties of Dislocations in Semiconductors", edited by S.G. Roberts et al, Inst. Phys., Bristol, England, p.245 (1989).
32. K. Maeda and Y. Yamashita, same as Ref. 31, p.269 (1989).
33. I. Yonenaga, U. Oriose and K. Sumino, *J. Mater. Res.*, *2*, 252 (1987).
34. I. Yonenaga, K. Sumino, G. Izawa, H. Watanabe and J. Matsui, *J. Mater. Res.*, *4*, 361 (1989).
35. I. Yonenaga, and K. Sumino, *J. Mater. Res.*, *4*, 355 (1989).
36. V.V. Bulatov, S. Yip, and A.S. Argon, *Phil. Mag.*, *72*, 452 (1995).

37. J.R. Rice, G.E. Beltz, and Y. Sun, in ``Topics in Fracture and Fatigue", edited by A.S. Argon, Springer, Berlin, p.1 (1992).
38. R.E. Peierls, *Proc. Phys. Soc., A52*, 34 (1940).
39. F.R.N. Nabarro, *Proc. Phys. Soc., A59*, 256 (1947).
40. A.J. Foreman, M.A. Jaswon, and J.K. Wood, *Proc. Phys. Soc., A64*, 156 (1951).
41. G. Xu and M. Ortiz, Intern. *J. Num. Methods Engng., 36*, 3675 (1993).
42. Chiao, Y-H, and D.R. Clarke, *Acta Metall., 47*, 203 (1989).
43. J. Samuels and S.G. Roberts, *Proc. Roy. Soc., A421*, 1 (1989).
44. M. Brede, *Acta Metall., et Mater., 41*, 211 (1993).
45. J.R. Rice, *J. Mech. Phys. Solids, 40*, 235 (1992).
46. A.S. Argon and D. Deng, unpublished research, available on request.
47. G. Xu, A.S. Argon and M. Ortiz, submitted to Phil. Mag.
48. J.H. Rose, J. Ferrante and J.R. Smith, *Phys. Rev. Letters., 47*, 675 (1981).
49. Y. Sun, G.E. Beltz and J.R. Rice, *Mater. Sci. Engng., A170*, 67 (1993).
50. B. Cotterell and J.R. Rice, *Intern. J. Fract., 16*, 155 (1980).
51. E. Kaxiras and Y. Juan, private communication, to be published.
52. S.J. Zhou and R. Thomson, *J. Mater. Res., 6*, 639 (1991).
53. F.A. McClintock and A.S. Argon ``Mechanical Behavior of Material", Addison Wesley, Reading MA (1966).
54. L.B. Freund and J.W. Hutchinson, *J. Mech.Phys.Solids, 33*, 169 (1985).
55. M. Khanta, D.P. Pope and V. Vitek, *Phys. Rev. Letters, 73*, 684 (1994).
56. M. Khanta, D.P. Pope and V. Vitek, *Scripta Metall et Mater., 31*, 1349 (1994).

REPORT DOCUMENTATION PAGE

Form Approved
OMB No. 0704-0188

1. AGENCY USE ONLY (Leave blank)	2. REPORT DATE	3. REPORT TYPE AND DATES COVERED
	May 22, 1997	Final: 9/1/1992-11/30/1995

4. TITLE AND SUBTITLE
Critical Configurations for Dislocation Nucleation from Crack Tips

5. FUNDING NUMBERS
C-N00014-92-J-4022

6. AUTHOR(S)
G.Xu, A.S. Argon and M. Ortiz

7. PERFORMING ORGANIZATION NAME(S) AND ADDRESS(ES)
Massachusetts Institute of Technology
Room 1-306
Cambridge, MA 02139 (A.S. Argon)

8. PERFORMING ORGANIZATION REPORT NUMBER
1-6

9. SPONSORING/MONITORING AGENCY NAME(S) AND ADDRESS(ES)
ONR Solid Mechanics Program (Attn: Dr. R. Barsoum)
ONR Code 1132
800 N. Quincy Street - Ballston Tower 1
Arlington, VA 22217-5000

10. SPONSORING/MONITORING AGENCY REPORT NUMBER

11. SUPPLEMENTARY NOTES
Paper published in "Philosophical Magazine", 75, 341-367, (1997)
(Reprint attached)

12a. DISTRIBUTION/AVAILABILITY STATEMENT
Unlimited

12b. DISTRIBUTION CODE

13. ABSTRACT *(Maximum 200 words)*

In the present paper, we analyze several activation configurations of embryonic dislocations nucleated from the tip of a cleavage crack. The activation configurations include nucleation on inclined planes, on oblique planes and on cleavage ledges and are treated within the classical framework of Peierls. A variational boundary integral method with an interplanar tension-shear potential developed earlier is used to solve for the saddle-point configurations of embryonic dislocation loops and their associated energies. Based on the assumption that the brittle-to-ductile transition in cleavage fracture is a nucleation-controlled process (as is expected to be the case in bcc transition metals such as α - Fe) the results of the calculations are used to estimate the brittle-to-ductile transition temperatures. It is concluded that only dislocation nucleation on cleavage ledges furnishes realistic values of the transition temperature. The homogeneous nucleation of dislocations on either inclined or oblique planes requires transition temperatures well above the melting point. This implies that nucleation of dislocations from a crack tip in intrinsically brittle crystals is only possible at local crack front heterogeneities such as cleavage ledges, and that the homogeneous nucleation of dislocations from a straight crack front is not possible. This conclusion is supported by the experimental observation that dislocation nucleation from a crack tip is a rare event which occurs preferentially at heterogeneities.

14. SUBJECT TERMS
A computational study of the critical activation configurations of dislocation embryos at crack tips

15. NUMBER OF PAGES
26

16. PRICE CODE

17. SECURITY CLASSIFICATION OF REPORT	18. SECURITY CLASSIFICATION OF THIS PAGE	19. SECURITY CLASSIFICATION OF ABSTRACT	20. LIMITATION OF ABSTRACT
Unclassified	Unclassified	Unclassified	None

PHILOSOPHICAL MAGAZINE A, 1997, VOL. 75, NO. 2, 341–367

Critical configurations for dislocation nucleation from crack tips

By G. XU†, A. S. ARGON‡

Massachusetts Institute of Technology, Cambridge, Massachusetts 02139, USA

and M. ORTIZ

California Institute of Technology, Pasadena, California 91125, USA

[*Received 25 January 1996 and accepted in revised form 16 June 1996*]

ABSTRACT

In the present paper, we analyse several activation configurations of embryonic dislocations nucleated from the tip of a cleavage crack. The activation configurations include nucleation on inclined planes, on oblique planes and on cleavage ledges and are treated within the classical framework of Peierls. A variational boundary integral method with an interplanar tension–shear potential developed earlier is used to solve for the saddle-point configurations of embryonic dislocation loops and their associated energies. Based on the assumption that the brittle-to-ductile transition in cleavage fracture is a nucleation-controlled process (as is expected to be the case in bcc transition metals such as α-Fe) the results of the calculations are used to estimate the brittle-to-ductile transition temperatures. It is concluded that only dislocation nucleation on cleavage ledges furnishes realistic values of the transition temperature. The homogeneous nucleation of dislocations on either inclined or oblique planes requires transition temperatures well above the melting point. This implies that nucleation of dislocations from a crack tip in intrinsically brittle crystals is only possible at local crack front heterogeneities such as cleavage ledges, and that the homogeneous nucleation of dislocations from a straight crack front is not possible. This conclusion is supported by the experimental observation that dislocation nucleation from a crack tip is a rare event which occurs preferentially at heterogeneities.

§ 1. INTRODUCTION

The abrupt transition in the fracture behaviour of some materials from ductile to brittle (or brittle to ductile) with small changes in temperatures remains a key concern in many structural applications. This phenomenon has been viewed from two different perspectives. In applications where the ductility of a material is relied upon, the transition is viewed as the sudden onset of brittleness. The complex phenomena associated with a ductile-to-brittle (D–B) transition in polycrystalline steels, involving as a key step the deformation-induced production of propagating cleavage microcracks, have been studied experimentally in detail (Hahn, Averbach, Owen and Cohen 1959) and have been modelled theoretically to some degree (Stroh 1954, 1955, 1957, Lin, Evans and Ritchie 1986, 1987).

†Present address: TerraTek, Inc., 420 Wakara Way, Salt Lake City, Utah 84108, USA.
‡Author for correspondence.

By contrast, in the brittle-to-ductile (B–D) transition a competition is believed to take place between cleavage fracture and plastic shielding, with eventual blunting of the propagating cleavage crack either by dislocation emission from the crack tip or by background plastic relaxation. The crack arrest and eventual blunting mechanism depends upon temperature, loading rate and the ability of the vicinity of the crack tip to undergo plastic deformation. This B–D transition has been explained either in the static framework of a stationary crack (St John 1975, Brede and Haasen 1988, Hirsch, Roberts, Samuels and Warner 1989a, Hirsch, Samuels and Roberts 1989b, George and Michot 1993), or in the dynamical framework of the arrest of a propagating cleavage crack with increasing temperature and decreasing loading rate (Gilman, Knudsen and Walsh 1958, Brede, Hsia and Argon 1991, Hsia and Argon 1994).

Models of the B–D transition just described (Kelly, Tyson and Cottrell 1967, Rice and Thomson 1974) have led to the notion of intrinsically ductile materials (most fcc metals, some hcp metals and bcc tantalum), which do not cleave and do not undergo a fracture transition. The remaining solids, including most bcc transition metals, are intrinsically brittle, that is cleavable, and are therefore susceptible to a B–D transition. The fundamental supposition is that, while background plastic relaxations can suppress the transition temperature, the ultimate arbiter of the transition is the ability, or the lack of it, of the crack tip to emit dislocations that can shield the crack and trigger widespread plastic deformation before the crack can propagate by cleavage.

The accumulating experimental evidence on Si (St John 1975, Brede and Haasen 1988, Hirsch *et al.* 1989a, b, George and Michot 1993) and the insight provided by the most recent modelling studies (Schöck and Püschl 1991, Rice and Beltz 1994, Xu, Argon and Ortiz 1995a) suggest that the activation configuration of a dislocation embryo is in the form of a double kink. This observation permits the identification of two distinct types of B–D transition. In the bcc transition metals where barriers to kink mobility are low, the B–D transition is likely to be governed directly by the formation of dislocation embryos at the crack tip, resulting in a nucleation-controlled transition. By contrast, in semiconductors and compounds the observational evidence suggests (Yonenaga, Onose and Sumino 1987, Maeda and Yamashita 1989, Sumino 1989, Yonenaga *et al.* 1989, Yonenaga and Sumino 1989), and modelling verifies (Bulatov, Yip and Argon 1995), that kink mobility is hindered by substantial energy barriers, rendering the B–D transition controlled by dislocation mobility away from the crack tip.

Ultimately, a full understanding of the nucleation-controlled or the mobility-controlled B–D transitions must come from atomistic models of the formation and outward propagation of the dislocation embryo at the crack tip. Before such modelling can be meaningfully attempted, much progress can be made by recourse to hybrid continuum-atomistic approaches (Schöck and Püschl 1991, Rice, Beltz and Sun 1992, Rice and Beltz 1994, Xu *et al.* 1995a) based on the use of a Peierls interplanar potential (Peierls 1940, Nabarro 1947, Foreman, Jaswon and Wood 1951). In a recent development of this technique by Xu *et al.* (1995a), an additional surface production resistance was introduced into the interplanar potential, and the appropriate saddle-point configurations of the dislocation embryo were determined by recourse to a variational boundary integral method advanced by Xu and Ortiz (1993). Xu *et al.* (1995a) concluded that the energetics of dislocation embryo formation on inclined slip planes containing the crack tip, against an additional surface

production resistance, is quite unfavourable and does not explain the known B–D transition temperatures. On this basis, it was conjectured that nucleation may be more favourable on oblique slip planes or, as numerous experimental observations have suggested, may occur heterogeneously at the crack front (Chiao and Clarke 1989, Samuels and Roberts 1989, George and Michot 1993). These dislocation nucleation mechanisms are investigated in this communication.

In § 2 we begin by describing the three alternative mechanisms to be appraised, namely nucleation on inclined planes, on oblique planes and on cleavage ledges on the crack front. Following a brief description in § 3 of the fundamental methodology employed in calculations, the three nucleation mechanisms are analysed in turn in § 4. In particular, the B–D transition temperature is estimated from the calculated activation energies. We find that only nucleation on cleavage ledges leads to realistic estimates of the transition temperature. In § 5 we endeavour to put our findings in general perspective.

§ 2. Dislocation nucleation modes

Several alternative modes of dislocation nucleation from crack tips have been contemplated in the past. The modes differ mainly in the relative geometry of the slip plane, the crack surface and the crack front. The configurations considered include nucleation of dislocations on the extension of the crack surface (fig. 1 (*a*)), nucleation on an inclined plane containing the crack front (fig. 1 (*b*)), nucleation on an oblique plane (fig. 1 (*c*)) and nucleation on a cleavage ledge (fig. 1 (*d*)).

Fig. 1

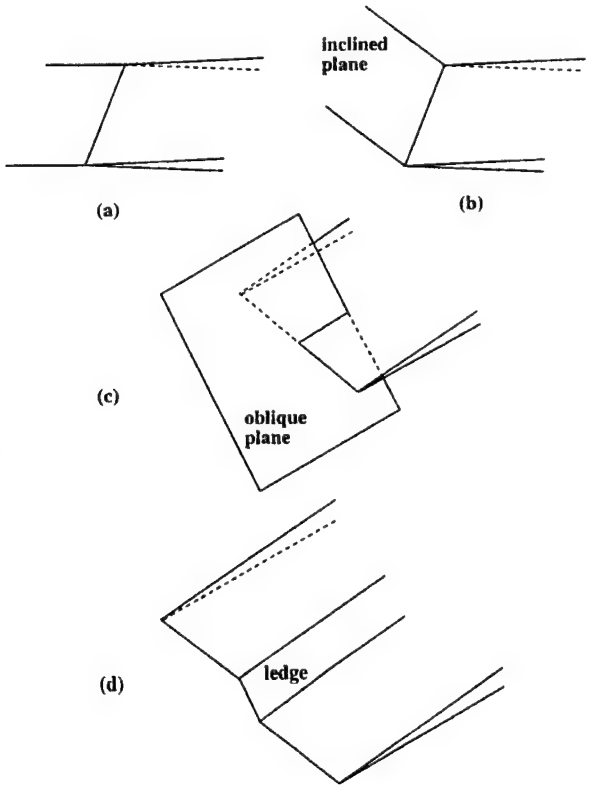

Alternative modes of dislocation nucleation from a crack tip.

Using the Peierls model of interplanar slip, Rice (1992) and Rice *et al.* (1992) analysed the athermal nucleation of straight dislocations on the extension of the crack surface under pure mode II and mixed mode loading (fig. 1 (*a*)). From this pioneering analysis, Rice *et al.* concluded that nucleation occurs when the crack tip energy release rate attains the unstable stacking energy of the slip plane, at which point half a dislocation core has been formed at the crack tip. Rice and Beltz (1994) have performed a three-dimensional perturbation analysis of dislocation nucleation on the extension of the crack surface which gives the saddle-point configurations and their dependence on the applied energy release rate. Rice and Beltz (1994) also compared their analysis with an earlier approximate calculation of Schöck and Püschl (1991). Xu *et al.* (1995a) have applied a variational boundary integral method to the same problem. In the Xu *et al.* (1995a) approach, the tension–shear potential is modified so as to account for surface production resistance. The results of these calculations indicate that, with the incorporation of surface production, homogeneous nucleation of dislocations on inclined planes is unlikely. This observation notwithstanding, in the interest of completeness we revisit this mode of nucleation in § 4.2 for a particular configuration pertaining to α-Fe.

Experimental observations (Burns and Webb 1970a, b), and the consideration of peak stress levels at the crack tip (Argon 1987), point to dislocation nucleation on oblique planes, such as shown in fig. 1 (*c*), as a likely dislocation nucleation mechanism. This mechanism has the additional advantage of involving nearly no free surface production. Moreover, as observed by Burns and Webb (1970a, b) and pointed out by Argon (1987), the nucleated dislocation can extent self-similarly as a loop attached to the crack tip, which results in steadily increasing shielding. These favourable features notwithstanding, approximate analyses carried out by Argon (1987) and A. S. Argon and D. Deng (1987, unpublished research available on request) suggest that this mode of nucleation also fails to furnish realistic values of the transition temperature. This conclusion is reinforced by the more accurate analysis of § 4.3.

The nucleation modes just described are examples of homogeneous nucleation, inasmuch as all points along the crack front are accorded an equal probability of being a nucleation site. However, numerous experiments (Chiao and Clarke 1989, Samuels and Roberts 1989, George and Michot 1993) have shown that actual dislocation nucleation events are rare and occur only at special sites along the crack front, namely at heterogeneities. Extensive documentation of these special sites by George and Michot (1993) has shown them to be mostly cleavage ledges. These ledges form frequently in response to local deviations of the crack driving force away from the crack plane. In cases in which the local stress intensity factor on the cleavage ledge has a substantial K_{III} component, a dislocation of screw type can be nucleated at the ledge without surface production. Moreover, a usually present substantial K_I component acting across the plane of the ledge should further promote this mode of nucleation. The analysis presented in § 4.4 reveals that, of all the modes considered, dislocation nucleation on ledges is the most energetically favourable and that which leads to the most realistic estimates of the B–D transition temperature. For definiteness, we restrict our attention to α-Fe and the geometries displayed in fig. 2.

The preferred growth direction of a {100} cleavage crack in α-Fe can be ascertained by computing the dependence of the energy release rate on the crack front direction within the framework of anisotropic linear elasticity. For pure mode I

Fig. 2

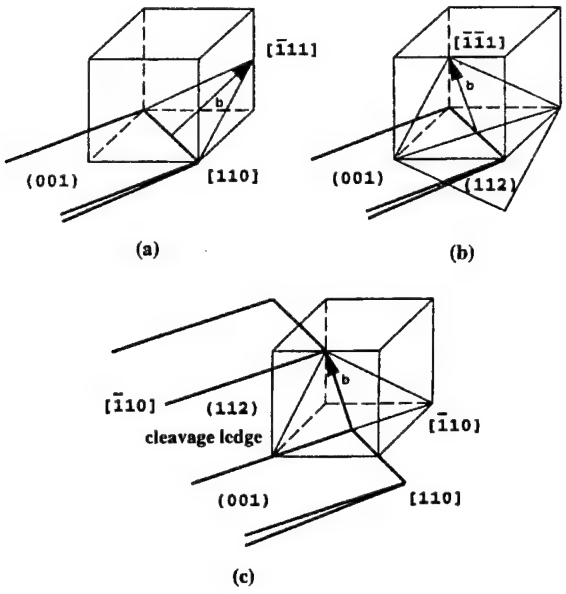

Alternative modes of dislocation nucleation from crack tips in α-Fe: (*a*) inclined plane; (*b*) oblique plane; (*c*) cleavage ledge.

loading, the analysis consigned to the Appendix reveals that the energy release rate is minimum for a crack front in the ⟨110⟩ direction, which is therefore taken to define the most likely crack front direction. Figure 2 displays the crystallography of the nucleation modes: a $\frac{1}{2}[\bar{1}11]$ dislocation nucleating in an inclined $(1\bar{1}2)$ plane in fig. 2(*a*), a $\frac{1}{2}[\bar{1}\bar{1}1]$ dislocation nucleating in an oblique (112) plane in fig. 2(*b*) and a $\frac{1}{2}[\bar{1}\bar{1}1]$ dislocation nucleating in a cleavage ledge on the (112) plane in fig. 2(*c*). In our estimation, these cases represent the most likely configurations for each nucleation mode.

§ 3. Method of analysis

The analysis builds on the recent developments of Xu *et al.* (1995a), who have extended the scope of the variational boundary integral method of Xu and Ortiz (1993) to encompass problems of dislocation nucleation from atomically sharp cracks. In this model, a slip plane connected to the crack is viewed as an extension of the crack surfaces with a nonlinear interlayer potential acting across it. Thus the crack and the slip plane on which the dislocation nucleates are jointly regarded as a three-dimensional crack system embedded in the linear elastic solid. The interlayer potential acting across the slip plane is modelled by combining the universal binding energy relation of Rose, Ferrante and Smith (1981) with a skewed shear resistance profile (Foreman *et al.* 1951). The interplanar displacements and the crack-opening displacements are represented by a continuous distribution of curved dislocations. This approach introduces no artificial discontinuity between the elastic crack opening and inelastic interplanar slip and separation. The technique has been described in complete detail by Xu and Ortiz (1993) and Xu *et al.* (1995a). In this section, we

briefly outline those aspects of the method which are pertinent to the treatment of the special activation configurations described in § 2.

We consider a semi-infinite cleavage crack and a slip plane intersecting the crack front. The crack–slip plane system is loaded remotely by a K field. The crystallographic slip plane is chosen to be the most advantageous for slip. As the driving force increases, an embryonic dislocation forms progressively until it reaches an unstable equilibrium configuration. The load corresponding to this unstable configuration is defined as the critical driving force for nucleation. The embryonic dislocation profile is characterized as a distribution of interplanar inelastic displacements, defined by Rice (1992) as

$$\boldsymbol{\delta} = \boldsymbol{\Delta} - \boldsymbol{\Delta}^{\mathrm{e}}, \tag{1}$$

where $\boldsymbol{\Delta}$ and $\boldsymbol{\Delta}^{\mathrm{e}}$ denote the total and elastic interplanar displacements respectively. The opening displacement $\mathbf{u}$ of the crack surface, including the inelastic displacements along the slip plane, can be written as

$$\mathbf{u} = \bar{\mathbf{u}} + \boldsymbol{\delta}, \tag{2}$$

where $\bar{\mathbf{u}}$ represents the standard K displacement field for a reference semi-infinite crack. The term $\bar{\mathbf{u}}$ matches the behaviour of the crack-opening displacements far away from the tip. Consequently, the additional term $\boldsymbol{\delta}$ modifying $\bar{\mathbf{u}}$, which is the primary unknown in the analysis, is expected to decay rapidly to zero with distance away from the crack tip. In this manner, $\boldsymbol{\delta}$ can be restricted to a finite domain $\hat{S}_{\mathrm{c}} \cup \hat{S}_{\mathrm{s}}$, where $\hat{S}_{\mathrm{c}}$ lies on the crack surface and $\hat{S}_{\mathrm{s}}$ on the slip plane, connected to the crack front.

Following the procedure introduced by Xu *et al.* (1995a) and Xu and Ortiz (1993), the potential energy of the whole system can be written in the form

$$\Pi[\bar{\mathbf{u}} + \boldsymbol{\delta}] = W[\bar{\mathbf{u}} + \boldsymbol{\delta}] + V[\boldsymbol{\delta}] = W_1[\bar{\mathbf{u}}] + W_1[\boldsymbol{\delta}] + W_2[\bar{\mathbf{u}}, \boldsymbol{\delta}] + V[\boldsymbol{\delta}], \tag{3}$$

where we identify $W_1[\bar{\mathbf{u}}]$ as the elastic strain energy of the system, free of inelastic modifications, $W_1[\boldsymbol{\delta}] + V[\boldsymbol{\delta}]$ as the self-energy of the system of inelastic modifications consisting of the distributed dislocations and the interplanar interaction energy on the slip plane, and $W_2[\bar{\mathbf{u}}, \boldsymbol{\delta}]$ is the interaction energy of the initial unmodified system with the second system of modifications. Of these energies those of relevance in the variational approach are those that depend on the unknown inelastic modification $\boldsymbol{\delta}$. They have the forms given below. The self-energy of the inelastic modification is given as

$$\begin{aligned} W_1[\boldsymbol{\delta}] = {} & \frac{\mu}{4\pi} \int_{\hat{S}_{\mathrm{c}}+\hat{S}_{\mathrm{s}}} \int_{\hat{S}_{\mathrm{c}}+\hat{S}_{\mathrm{s}}} \frac{[\mathbf{e}_i \cdot (\mathbf{n} \times \nabla \delta_j)_2][\mathbf{e}_j \cdot (\mathbf{n} \times \nabla \delta_i)_1]}{R} \, \mathrm{d}S_1 \, \mathrm{d}S_2 \\ & - \frac{\mu}{8\pi} \int_{\hat{S}_{\mathrm{c}}+\hat{S}_{\mathrm{s}}} \int_{\hat{S}_{\mathrm{c}}+\hat{S}_{\mathrm{s}}} \frac{[\mathbf{e}_i \cdot (\mathbf{n} \times \nabla \delta_i)_1][\mathbf{e}_j \cdot (\mathbf{n} \times \nabla \delta_j)_2]}{R} \, \mathrm{d}S_1 \, \mathrm{d}S_2 \\ & + \frac{\mu}{8\pi(1-\nu)} \int_{\hat{S}_{\mathrm{c}}+\hat{S}_{\mathrm{s}}} \int_{\hat{S}_{\mathrm{c}}+\hat{S}_{\mathrm{s}}} [\mathbf{e}_i \times (\mathbf{n} \times \nabla \delta_i)_1] \cdot \mathbf{T} \cdot [\mathbf{e}_j \times (\mathbf{n} \times \nabla \delta_j)_2] \, \mathrm{d}S_1 \, \mathrm{d}S_2, \end{aligned} \tag{4}$$

where $(.)_1$ and $(.)_2$ denote two different points on the domain $\hat{S}_{\mathrm{c}} \cup \hat{S}_{\mathrm{s}}$, R is the distance between these two points, $\mathbf{e}_i, i = 1, 2, 3$, are Cartesian basis vectors, $\mathbf{n}$ is the normal vector to the crack surface or the slip plane and $\mathbf{T}$ is a tensor with components

$$T_{ij} = \frac{\partial^2 R}{\partial x_i \partial x_j}. \tag{5}$$

The interaction energy between the elastic crack field and the inelastic modifications is

$$W_2[\bar{\mathbf{u}}, \boldsymbol{\delta}] = K_{\mathrm{I}} Q_{\mathrm{I}}[\boldsymbol{\delta}] + K_{\mathrm{II}} Q_{\mathrm{II}}[\boldsymbol{\delta}] + K_{\mathrm{III}} Q_{\mathrm{III}}[\boldsymbol{\delta}], \tag{6}$$

where

$$Q_{\mathrm{I}}[\boldsymbol{\delta}] = \int_{\hat{S}_c + \hat{S}_s} \mathbf{n} \cdot \boldsymbol{\sigma}_{\mathrm{I}} \cdot \boldsymbol{\delta} \, \mathrm{d}S, \tag{7a}$$

$$Q_{\mathrm{II}}[\boldsymbol{\delta}] = \int_{\hat{S}_c + \hat{S}_s} \mathbf{n} \cdot \boldsymbol{\sigma}_{\mathrm{II}} \cdot \boldsymbol{\delta} \, \mathrm{d}S, \tag{7b}$$

$$Q_{\mathrm{III}}[\boldsymbol{\delta}] = \int_{\hat{S}_c + \hat{S}_s} \mathbf{n} \cdot \boldsymbol{\sigma}_{\mathrm{III}} \cdot \boldsymbol{\delta} \, \mathrm{d}S, \tag{7c}$$

and $\boldsymbol{\sigma}_{\mathrm{I}}$, $\boldsymbol{\sigma}_{\mathrm{II}}$ and $\boldsymbol{\sigma}_{\mathrm{III}}$ are stresses of the standard K fields in modes I, II and III respectively, for unit stress intensity factor. The integration is partly extended over the real crack surface since the front of the reference semi-infinite crack is actually located some distance away from the physical crack front. This treatment permits the use of a non-singular Dugdale–Barenblatt crack as a reference crack to improve systematically the quality of the numerical solution (Xu and Ortiz 1993). Finally, the potential energy of the interplanar inelastic deformation on the slip plane is

$$V[\boldsymbol{\delta}] = \int_{\hat{S}_s} \Phi[\boldsymbol{\delta}] \, \mathrm{d}S, \tag{8}$$

where $\Phi[\boldsymbol{\delta}]$ is an interplanar potential defined per unit area of the slip plane. It is possible to model the general potential $\Phi[\boldsymbol{\delta}]$ with shear displacements allowed in all directions on the slip plane. However, atomistic simulations have shown that displacements and the attendant shear resistance take place predominantly in the direction of the dominant Burgers vector (Yamaguchi, Vitek and Pope 1981, Sun *et al.* 1991, Juan and Kaxiras 1996). Therefore we adopt the constrained displacement hypothesis of Rice (1992) and Sun *et al.* (1994), whereby the interplanar shear displacement Δ_r is constrained to be aligned with the Burgers vector direction. The shear separation resistance τ and tension separation resistance σ follow from the inelastic shear displacements δ_r and tensile separation displacement δ_θ through the relations (Beltz and Rice 1991, Xu *et al.* 1995a)

$$\delta_r = \Delta_r - \frac{h}{\mu} \tau(\Delta_r, \Delta_\theta), \tag{9a}$$

$$\delta_\theta = \Delta_\theta - \frac{h}{c} \sigma(\Delta_r, \Delta_\theta), \tag{9b}$$

and

$$\tau(\Delta_r, \Delta_\theta) = A(\Delta_\theta) \left[\sin\left(\frac{2\pi\Delta_r}{b}\right) + \frac{\beta - 1}{2} \sin\left(\frac{4\pi\Delta_r}{b}\right) \right], \tag{10a}$$

$$\sigma(\Delta_r, \Delta_\theta) = \left[B(\Delta_r)\left(\frac{\Delta_\theta}{L}\right) - C(\Delta_r) \right] \exp\left(-\frac{\Delta_\theta}{L}\right), \tag{10b}$$

with

$$A(\Delta_\theta) = \frac{\pi\gamma_{us}^{(u)}}{b}\left[1 + \frac{1}{q}\frac{q-p}{1-p}\frac{\Delta_\theta}{L}\right]\exp\left(-\frac{\Delta_\theta}{L}\right), \tag{11a}$$

$$B(\Delta_r) = \frac{2\gamma_s}{L}\left\{1 - \frac{q-p}{1-p}\left[\sin^2\left(\frac{\pi\Delta_r}{b}\right) + \frac{\beta-1}{4}\sin^2\left(\frac{2\pi\Delta_r}{b}\right)\right]\right\}, \tag{11b}$$

$$C(\Delta_r) = \frac{2\gamma_s}{L}\frac{p(1-q)}{1-p}\left[\sin^2\left(\frac{\pi\Delta_r}{b}\right) + \frac{\beta-1}{4}\sin^2\left(\frac{2\pi\Delta_r}{b}\right)\right], \tag{11c}$$

$$q = \frac{\gamma_{us}^{(u)}}{2\gamma_s}, \tag{12a}$$

$$p = \frac{\Delta_\theta^*}{L}, \tag{12b}$$

where:

μ is the shear modulus,
c is the uniaxial strain elastic modulus,
b is the magnitude of Burgers vector,
h is the interatomic layer spacing,
L is the interplanar tensile displacement at $\sigma = \sigma_{max}$,
$\gamma_{us}^{(u)}$ is the unrelaxed unstable stacking energy,
γ_s is the surface energy,
Δ_r is the total interplanar shear displacement,
Δ_θ is the total interplanar normal displacement, and
Δ_θ^* is the relaxed interplanar tensile displacement at $\sigma = 0$ in the saddle-point configuration and
β is the skewness parameter in the interplanar shear resistance.

A traction–displacement relation including the effect of surface production on an inclined slip plane at the crack tip has been proposed by Xu *et al.* (1995a). The material constants for α-Fe used in calculations are taken from table 1 of Xu *et al.* (1995a) and are reproduced here for convenience in table 1.

The unknown displacements $\boldsymbol{\delta}$ follow by rendering the potential energy $\Pi[\bar{\mathbf{u}} + \boldsymbol{\delta}]$ stationary. This is achieved by discretizing the integral equation with six noded elements distributed on the crack surface. The nonlinear equations are solved by a Newton–Raphson iteration. The saddle-point configurations are activated by introducing a small perturbation into the system at the bifurcation point, based on the solution of a first-order eigenvalue problem if necessary. Solutions are obtained by

Table 1. Material properties for α-Fe.

Slip system	T (K)	μ (10^5 MPa)	c	$\gamma_{us}^{(u)}$ (J m^{-2})	$2\gamma_s$ (J m^{-2})	β	p	q	L/b
$\frac{1}{2}[111](1\bar{1}0)$	4·2	0·756	3·125	0·517	3·33	2·25	0·217	0·155	0·187
$\frac{1}{2}[\bar{1}\bar{1}1](112)$	4·2	0·756	3·125	0·581	3·80	1·74	0·210	0·153	0·215

recourse to interplanar displacement control achieved through the introduction of Lagrange multipliers.

§ 4. Dislocation nucleation analysis

4.1. *Three modes of nucleation*

In this section we analyse the nucleation of dislocations from a cleavage crack in α-Fe as processes typical of bcc metals in which kink mobility is high. We consider the three competing mechanisms discussed in § 2, namely nucleation on an inclined plane, on an oblique plane, and on a cleavage ledge. The principal objective of the calculations is the determination of the saddle-point configurations and the dependence of the corresponding activation energies on the crack driving force. These results are subsequently used to estimate the B–D transition temperatures for each geometry. The geometry furnishing the most realistic value of the B–D transition temperature may be reasonably identified with the preferred nucleation configuration in α-Fe.

4.2. *Nucleation of dislocations on the inclined plane*

The previous analysis of Xu *et al.* (1995a) showed that nucleation of dislocations on the inclined planes is quite unlikely for most crystals. Nevertheless, for comparison with the other modes of nucleation, we shall re-examine the nucleation of dislocations on the inclined plane $(1\bar{1}2)$ in α-Fe as depicted in fig. 2(*a*).

We begin by solving the saddle-point configuration of a dislocation under a pure mode II type of loading. The crack surface on the (001) plane probes the $(1\bar{1}2)$ slip plane with the crack front being parallel to the [110] direction. Two representative saddle-point configurations of the dislocation embryo under normalized loading levels G_{II}/G_{IIcd} of 0·75 and 0·50 are illustrated in fig. 3 and fig. 4 respectively. The dependence of the activation energy on the crack front driving force from a series of such solutions is plotted in fig. 5.

Fig. 3

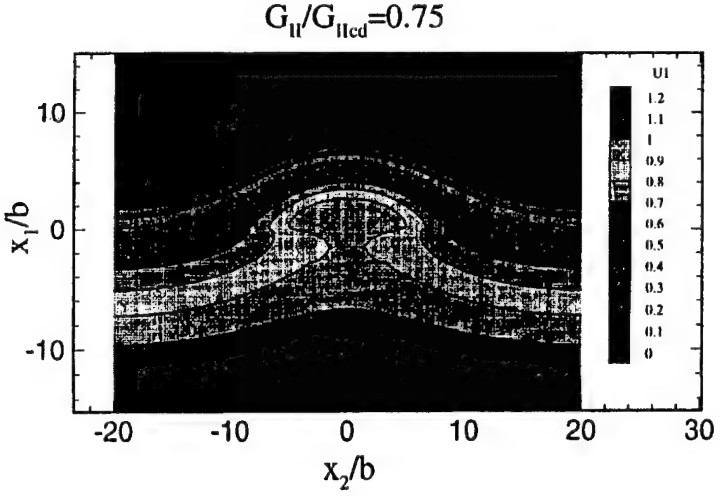

The saddle-point configuration at $G_{II}/G_{IIcd} = 0{\cdot}75$ under mode II loading.

Fig. 4

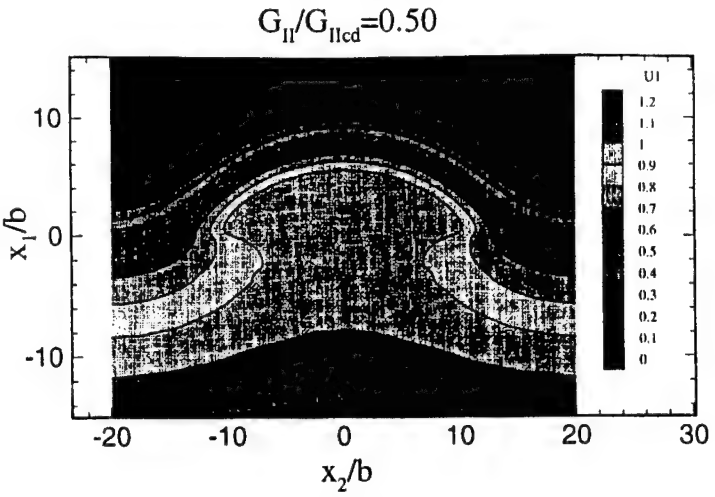

The saddle-point configuration at $G_{II}/G_{IIcd} = 0{\cdot}50$ under mode II loading.

Fig. 5

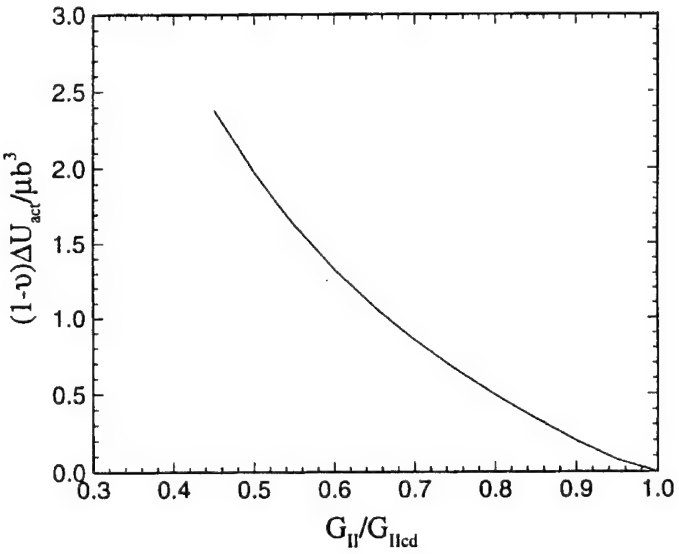

The activation energy for dislocation emission under pure mode II loading.

To obtain remote mode I loading, we assume that the nucleation process is essentially equivalent to the mode II crack case under a loading equal to the effective stress intensity factors on the inclined plane, which are,

$$K_I^{\text{eff}} = K_I \cos^3\left(\frac{\theta}{2}\right), \tag{13a}$$

$$K_{II}^{\text{eff}} = K_I \cos^2\left(\frac{\theta}{2}\right) \sin\left(\frac{\theta}{2}\right). \tag{13b}$$

More precisely, these stress intensity factors are those at the tip of a small crack emanating from the crack tip in the direction of the slip plane (Cotterell and Rice 1980). The critical mode I loading for nucleation of a straight dislocation in two dimensions on the inclined plane can then be estimated from the analysis of Rice using eqn. (13*b*) and is given by

$$\frac{G_{\mathrm{Icd}}}{G_{\mathrm{Ic}}} = \frac{8}{(1+\cos\theta)\sin^2\theta}\,\frac{\gamma_{\mathrm{us}}}{2\gamma_{\mathrm{s}}}. \tag{14}$$

However, this estimate which considers neither tension softening nor surface production resistance underestimates the energetics of the configuration for most transition metals and intermetallics (Xu *et al.* 1995a) because, while the tension softening does make nucleation somewhat easier, the surface production resistance makes it comparatively much more difficult. The dependence of the activation energy of the actual three-dimensional saddle-point configuration analysis on the remote mode I loading is shown in fig. 6, as rescaled from fig. 5 through eqn. (13*b*).

4.3. *Nucleation of dislocations on the oblique plane*

As remarked in § 2, dislocation nucleation on oblique planes has been put forth as a likely mode of nucleation. However, the capability required for the analysis of this mechanism had been heretofore unavailable. Approximate analyses based on the consideration of perfect dislocations and the introduction of a core cut-off radius have led to estimates of the B–D transition temperatures several orders of magnitude higher than what is experimentally observed, prompting suggestions that nucleation should involve fractional dislocations (Argon 1987).

In this section, we provide a direct analysis of the formation of dislocation embryos on oblique planes in α-Fe. A comparison of resolved shear stresses on all

Fig. 6

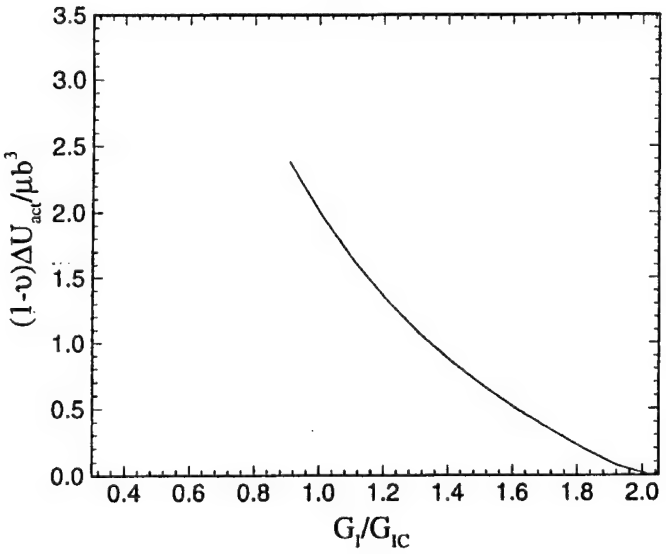

Dependence of the activation energy for dislocation nucleation on the inclined {112} planes on the remote mode I loading.

potentially active slip systems points to the configuration in fig. 2(*b*) as the most favourable for nucleation. In calculations, we artificially constrain the cleavage plane from propagating to enable the computation of the critical driving force for dislocation nucleation. If the resulting athermal critical driving force is less than G_{Ic} for cleavage, the crystal is intrinsically ductile. Contrariwise, if the critical driving force is greater than that for cleavage, the crystal is cleavable or intrinsically brittle. However, on the verge of crack propagation by cleavage, a dislocation can still be nucleated through thermal activation. The calculation of the activation energy for such thermally assisted dislocation nucleation is therefore of primary interest.

Figure 7 shows the geometry of the problem and the mesh used in the analysis. A close-up view of a typical saddle-point configuration of an embryonic dislocation loop emanating from the crack tip is shown in fig. 8 for the geometry of fig. 2(*b*). The calculated dependence of the activation energy on the crack driving force near the athermal threshold is shown in fig. 9. The critical driving force at the athermal threshold and the attendant activation energies are so high that they render the nucleation mechanism highly improbable. The calculation was discontinued at $G_I/G_{Ic} = 1{\cdot}6$ when the improbability of the mechanism had become amply clear. The activation energy at $G_I/G_{Ic} = 1{\cdot}0$ can be estimated by extrapolation, which provides an adequate basis for reaching a firm negative conclusion *vis-à-vis* the likelihood of the mechanism. One factor which contributes to rendering the mechanism ineffective is the fact that the resolved shear stress decays away from the crack tip in all directions, making the area-averaged shear stress smaller than that on the inclined plane.

It should be noted that in the above analysis the inelastic displacements across the slip plane were treated as total displacements for computational convenience. This tends to underestimate slightly the activation energy as will be demonstrated subsequently. Moreover, we have only considered two-sided activation configura-

Fig. 7

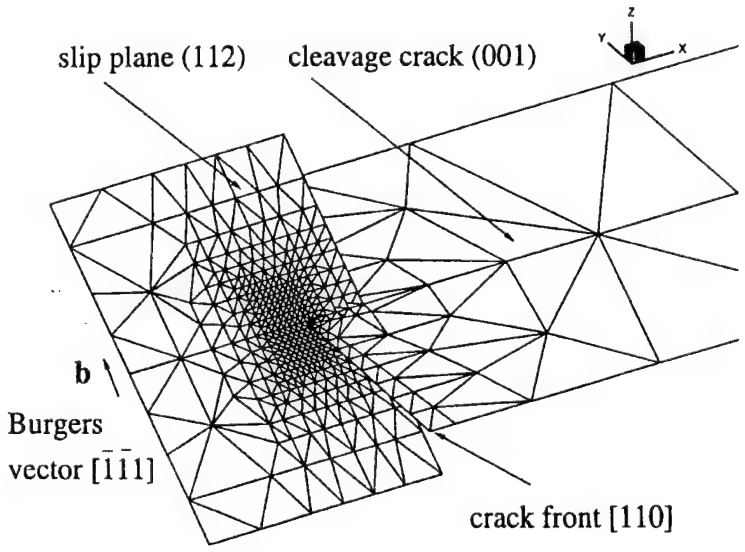

Mesh used in the analysis of dislocation nucleation on an oblique plane in α-Fe for the geometry shown in fig. 2(*b*).

Fig. 8

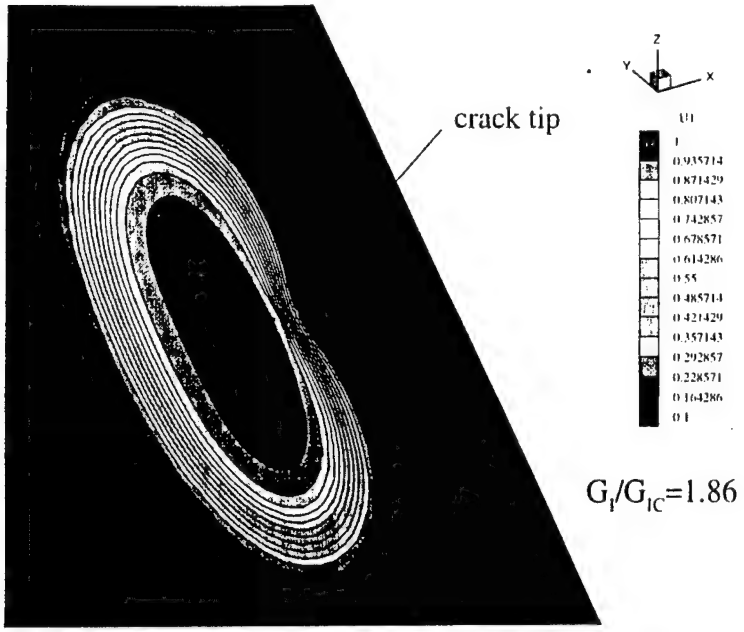

The saddle-point configuration of a dislocation embryo emitted from the crack tip on an oblique plane in the interior.

Fig. 9

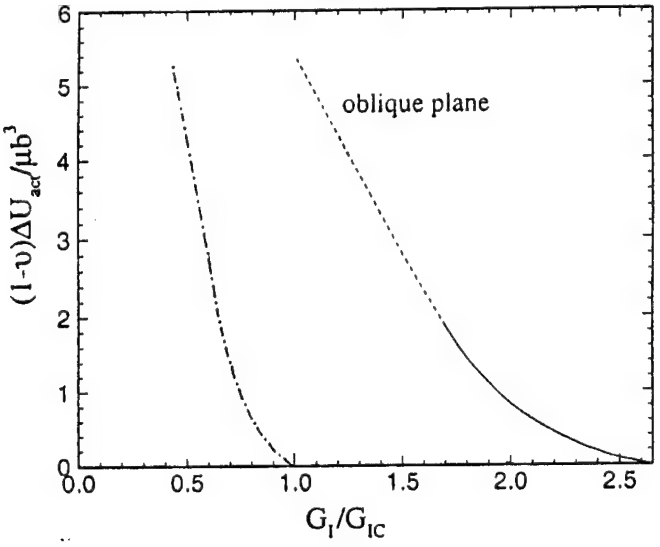

Activation energy for dislocation nucleation on an oblique plane in the interior (- - - -, ——) and near a free surface (— · —).

tions in our analysis. One-sided configurations, in which dislocation embryos expand primarily on one side of the oblique plane, might conceivably require lower activation energies. However, in view of the results just described, it seems unlikely that this reduction in the activation energy should be sufficient to justify a detailed analysis of one-sided configurations.

The above analysis establishes convincingly that nucleation of dislocations on oblique planes in the interior of the cracked solid is most unlikely. A very different conclusion can be reached, however, for this mechanism where the crack front reaches a free surface where no plane strain stress is present, and the resolved shear stresses on the oblique planes become much higher. An estimate of this enhanced nucleation probability on the oblique plane near the surface is easily obtained by rescaling the driving forces in fig. 9, in proportion to the resolved shear stresses on the oblique slip planes near the free surface against those in the interior as (for the geometry of fig. 2(*b*))

$$\frac{G_{\mathrm{Is}}}{G_{\mathrm{Ii}}} = \left(\frac{3-4\nu}{3}\right)^2, \tag{15}$$

where G_{Is} and G_{Ii} are respective energy release rates required for initiation of a dislocation near the free surface and in the interior. The result for α-Fe with $\nu = 0{\cdot}291$ is shown as the chain curve in fig. 9, which now suggests almost spontaneous embryo formation near the free surface. This, however, is not true, since in this case at least a partial surface ledge must be produced, which will make the nucleation more difficult, but presumably still much easier than in the interior. An abundance of such nucleation events has been observed by George and Michot (1993).

4.4. *Nucleation of dislocations on a cleavage ledge*

Cleavage surfaces in metallic crystals invariably contain ledges parallel to the direction of crack propagation. These are likely to form when the principal tension driving the crack deviates slightly on a local scale, requiring the crack to make small adjustments along its front. This microroughness of the cleavage surface depends also on the crystallography of the cleavage planes and crack propagation direction as well as on temperature. The height of the observed ledges can range from several atomic spacings to microns. Numerous observations (Chiao and Clarke 1989, Hirsch *et al.* 1989a, b, George and Michot 1993) have revealed that dislocation nucleation at a crack front is a relatively rare phenomenon associated with crack front heterogeneities. This strongly suggests that ledges are likely sites for heterogeneous nucleation of dislocations (Zhou and Thomson 1991). In what follows we analyse this mechanism as it is likely to operate in α-Fe.

Consider a cleavage crack propagating under mode I loading. The crack contains ledges of a width of roughly a hundred atomic spacings distributed along its front, as depicted later in fig. 11. The presence of a considerable local mode III stress intensity factor acting on the ledge is expected to promote nucleation. Moreover, the direction of the Burgers vector of the dislocation embryo, which is parallel to the local crack front on the ledge, requires no fresh surface production. In view of the mesh size requirements to resolve adequately the dislocation embryo, a direct simulation of the complete system does not appear possible at present. This difficulty can be sidestepped by the approximate two-scale approach sketched in fig. 10. The distribution of stress intensity factors along the front of the crack, including the ledge, is first calculated by recourse to a linear elastic analysis. The small stretch of ledge on which the dislocation embryo nucleates is then idealized as a semi-infinite crack subjected to the local stress intensity factors determined in the first analysis. Because of the vastly disparate scales of the ledge and the activation configuration, the results

Fig. 10

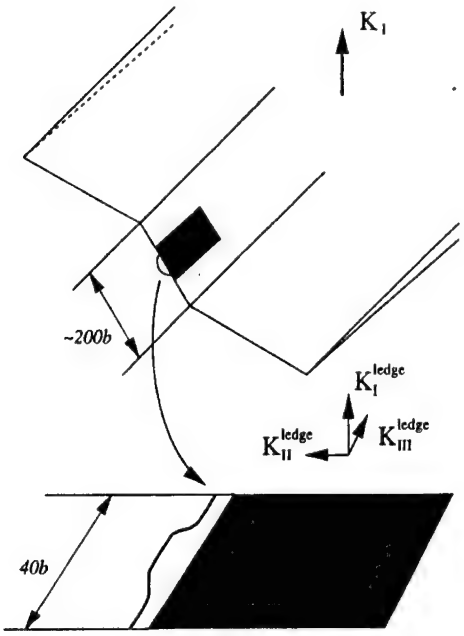

Dislocation nucleation on a cleavage ledge.

obtained in the manner just outlined should be ostensibly identical with those obtained from a direct simulation.

The distribution of stress intensity factors on the crack front can be readily calculated by the boundary element method of Xu and Ortiz (1993). The mesh used in the analysis is shown in fig. 11. As is evident from the figure, two symmetric ledges are included in the mesh. This permits the enforcement of periodic boundary

Fig. 11

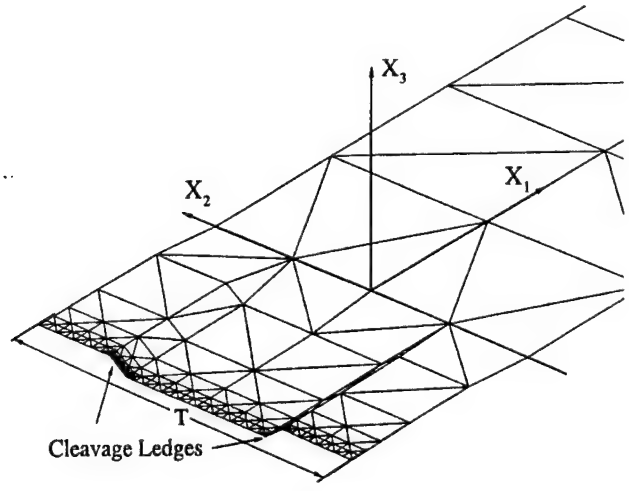

Mesh used in the computation of the stress intensity factors along a crack front containing cleavage ledges.

conditions, which greatly facilitates the calculations (Xu and Ortiz 1993). For small width-to-separation ratios, the interaction between the ledges may be expected to be negligible. The calculated stress intensity factors are shown in fig. 12. On the ledge, the dominant stress intensity factors are $K_{\mathrm{I}}^{\mathrm{ledge}} \approx 0{\cdot}81K_{\mathrm{I}}$ and $K_{\mathrm{III}}^{\mathrm{ledge}} \approx 0{\cdot}35K_{\mathrm{I}}$. On the verge of brittle fracture, it therefore follows that $K_{\mathrm{III}}^{\mathrm{ledge}} \approx 0{\cdot}35K_{\mathrm{Ic}}$. For mode III loading, Rice (1992) has determined the athermal critical condition for nucleation of a screw dislocation to be

$$G_{\mathrm{IIIcd}} = \gamma_{\mathrm{us}} = \frac{1}{2\mu} K_{\mathrm{IIIcd}}^2. \tag{16}$$

Using the relation

$$G_{\mathrm{Ic}} = 2\gamma_{\mathrm{s}} = \frac{1-\nu}{2\mu} K_{\mathrm{Ic}}^2, \tag{17}$$

we obtain

$$K_{\mathrm{IIIcd}} = \left(\frac{(1-\nu)\gamma_{\mathrm{us}}}{2\gamma_{\mathrm{s}}}\right)^{1/2} K_{\mathrm{Ic}} = 0{\cdot}357K_{\mathrm{Ic}} > 0{\cdot}350K_{\mathrm{Ic}}. \tag{18}$$

This calculation suggests that screw dislocations cannot be nucleated spontaneously below the critical condition for cleavage, which is consistent with the expectation that α-Fe single crystals be intrinsically brittle. However, the small difference between the numerical factors is most likely to be below the accuracy of the calculation, which viciates the argument to a considerable extent. Indeed, consideration of tension softening, the effect of anisotropy and uncertainties in the material parameters can all change eqn. (18) to some degree. The calculation does nevertheless provide a first indication that screw dislocation nucleation from a ledge may indeed be much easier than nucleation on inclined and oblique planes.

Next we consider a semi-infinite crack under simple mode III loading. Tension softening has been shown to be of little consequence up to values of K_{I} of the order of $0{\cdot}9K_{\mathrm{Ic}}$ (Xu *et al.* 1995a) and can therefore be safely neglected. Figures 13 and 14 show two saddle-point configurations of the embryonic screw dislocations for nor-

Fig. 12

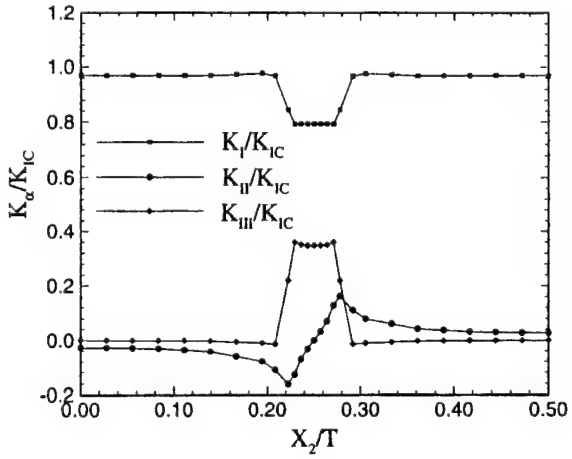

Distribution of stress intensity factors on a cleavage ledge.

Fig. 13

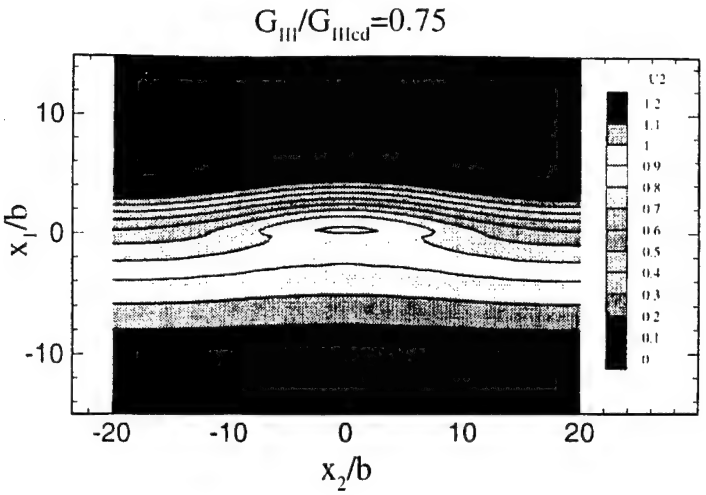

The saddle-point configuration for nucleation of a screw dislocation from a cleavage ledge, $G_{III}/G_{IIIcd} = 0{\cdot}75$.

Fig. 14

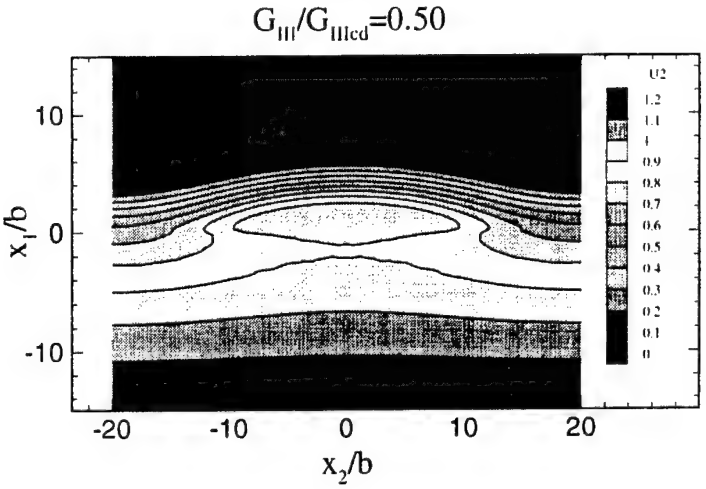

The saddle-point configuration for nucleation of a screw dislocation from a cleavage ledge, $G_{III}/G_{IIIcd} = 0{\cdot}50$.

malized load levels $G_{III}/G_{IIIcd} = 0{\cdot}75$ and $0{\cdot}50$. Interestingly, these saddle-point configurations are flatter than those of edge dislocations, shown in figs. 3 and 4, as befits the lower line energies of screw dislocations. As the screw dislocation bows out, it tends to form double kinks with short edge components. By way of contrast, the screw double kinks of the edge dislocation embryo tend to be longer and the edge segment shorter (figs. 3 and 4). Computationally, this requires a larger periodic domain in the case of the screw embryo, which inevitably increases the size of the problem. The dependence of the activation energy on the crack driving force is

shown in fig. 15. The low values of the activation energy relative to those computed for nucleation on inclined and oblique planes is particularly noteworthy.

Finally, we endeavour to ascertain the magnitude of the errors incurred as a result of the various simplifications adopted in the calculations. In order to estimate the effect of tension softening, we consider the simple two-dimensional problem of a semi-infinite crack subjected to mixed mode I and III. We take the ratio K_{III}/K_I to be $0{\cdot}35/0{\cdot}81 = 0{\cdot}43$, which is the case of interest in the ledge problem. We also wish to estimate the effect of identifying the interlayer inelastic displacements with the total displacements, that is of setting $\Delta = \delta$, a simplification which has been adopted for computational convenience. Physically, this corresponds to taking the interplanar distance h across the slip plane to be zero. In the ledge problem, we have additionally set the parameter $p = 0$ for want of a better estimate. Figure 16 shows the effect on the activation energy of variations in these parameters. As is evident from the figure, the $h = 0$ approximation accounts for modest errors of the order of 15% at most, over much of the range of G_I/G_{Ic}. The effect of tension softening in the range $0 \leqslant K_I \leqslant 0{\cdot}43K_{III}$ is indeed seen to be negligible. The lowest curve for the activation energy has been calculated for $p = 0{\cdot}217$ as a reasonable estimate. It shows that non-zero values of p can reduce the activation energy significantly, which indicates the need for more reliable estimates of this parameter. The effect of the periodicity of the computational model on the activation energy was found by Xu *et al.* (1995a) to decay rapidly with increasing size of the period.

4.5. *Estimates of the brittle-to-ductile transition temperature*

As noted in the foregoing, the B–D transition in bcc transition metals, and particularly in α-Fe, is most likely probably controlled solely by dislocation nucleation. Therefore, the preceding results can be used to estimate the B–D transition temperatures attendant to the three nucleation modes considered, namely nucleation on inclined planes, on oblique planes, or on cleavage ledges. No precise experimental

Fig. 15

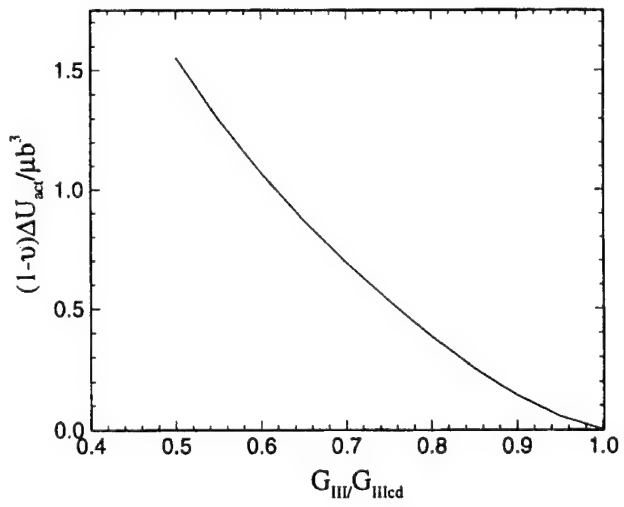

The activation energy for dislocation emission in simple mode III loading, at the cleavage ledge.

Fig. 16

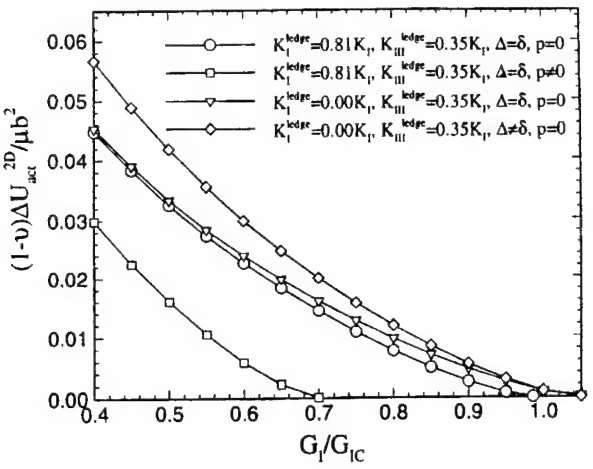

Parametric sensitivity of the activation energy for dislocation emission on cleavage ledges.

measurements of the transition temperature of single-crystal α-Fe are available. The transition temperature for polycrystalline low-C steel is about 250 K, as determined from Charpy impact experiments (McClintock and Argon 1966). In the absence of more direct measurements, we shall suppose the transition temperature for pure α-Fe to be in the range 250–300 K. A B–D transition scenario achievable experimentally was proposed by Argon (1987) and consists of the arrest of a cleavage crack propagating against a temperature gradient.

The evaluation of the B–D transition temperature from the activation energy can be effected as suggested by Xu *et al.* (1995a), who give the relation

$$T_{BD} = \left(\frac{\ln(c/v)}{\alpha} + \eta\frac{T_0}{T_m}\right)^{-1} T_0. \tag{19}$$

Here $T_0 \equiv \mu b^3/k(1-\nu) \approx 1{\cdot}2 \times 10^5$ K; the melting temperature $T_m = 1809$ K for α-Fe; $\alpha = (1-\nu)\,\Delta U_{act}/\mu b^3$ is the normalized activation energy; c is the speed of sound; $v \approx 1\,\mathrm{cm\,s^{-1}}$ is a typical crack propagation velocity, giving $\ln(c/v) \approx 10$; $\eta \approx 0{\cdot}5$ is a coefficient describing the temperature dependence of the shear modulus which, to a first approximation, is presumed of the form

$$\mu = \mu_0\left(1 - \eta\frac{T}{T_m}\right). \tag{20}$$

The dependence of the activation energy for nucleation of dislocation embryos on the energy release rate G_I is shown in fig. 17 for each of the three modes of nucleation considered in the foregoing. The activation energy at the critical driving force for cleavage, that is, at $G_I/G_{Ic} = 1$, determines the transition temperature through eqn. (19). This relation is plotted in fig. 18, together with the activation energies for nucleation on inclined planes, oblique planes and ledges. Also shown in the figure is the value of the transition temperature for polycrystalline Fe. It is evident from this comparison that only nucleation on cleavage ledges results in transition temperatures which approach the expected value for α-Fe. The remaining two mechan-

Fig. 17

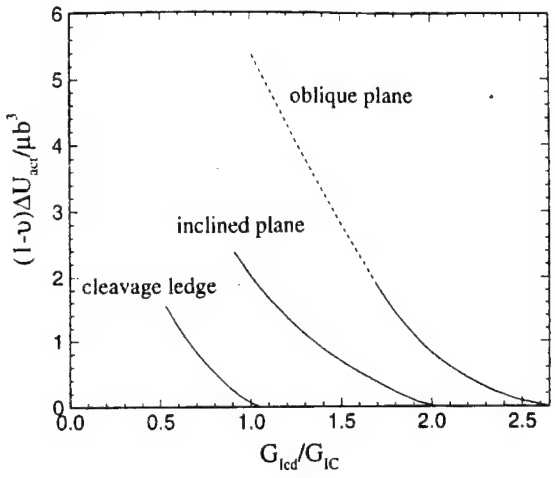

The activation energies for dislocation nucleation at a crack tip in α-Fe, for three different modes of nucleation.

Fig. 18

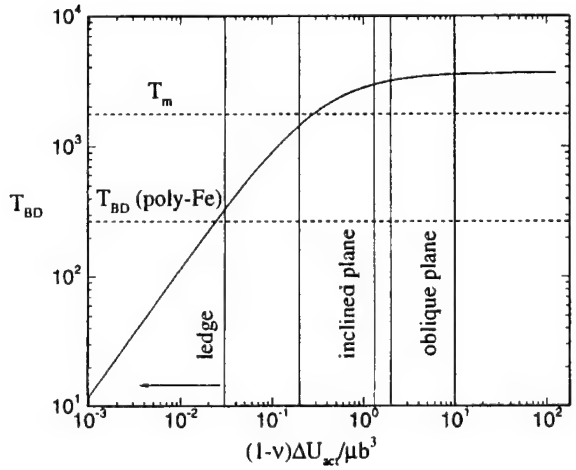

The estimated B–D transition temperatures in α-Fe.

isms grossly overestimate the transition temperature. These results strongly suggest that dislocation nucleation from a crack tip in α-Fe is an inhomogeneous process. The dislocation loops which eventually shield the crack are emitted from ledges distributed along the crack front.

§ 5. Discussion

We have viewed the transition in fracture behaviour from ductile to brittle or, more fundamentally, from brittle to ductile as a manifestation of crack-tip-initiated plasticity counteracting the tendency for brittle behaviour by cleavage cracking. In this regard, we have distinguished two different behaviours: that in which the transi-

tion is controlled by nucleation of dislocation embryos from the crack tip, which is characteristic of bcc transition metals, and that in which the transition is controlled by the mobility of dislocations away from the crack tip, which is typical of semiconductors and compounds. The distinguishing characteristic between these two behaviours is the mobility of kinks on dislocations. Experiments indicate that in bcc transition metals (at anything but the lowest temperatures) there is little resistance to the motion of kinks along dislocation lines. By contrast, in semiconductors such as Si and other compounds for which good information on dislocation mobility exists (Yonenaga *et al.* 1987, 1989, Yonenaga and Sumino 1989) it is known that the stress dependence of the dislocation velocity is nearly linear, implying that a process of kink drift controls dislocation motion. Computer simulations (Bulatov *et al.* 1995) confirm that kink motion along dislocations is indeed hindered by very substantial energy barriers in Si. These observations suggest that the B–D transition is nucleation controlled in bcc transition metals and mobility controlled in semiconductors and semiconducting compounds.

An additional mechanism which can influence fracture behaviour is crack-tip shielding by general 'background' plasticity. A particularly elegant and compelling analysis of this mechanism was advanced by Freund and Hutchinson (1985). Based on the known rate dependence characteristics of steels, which exhibit a marked stress upturn at high strain rates, Freund and Hutchinson (1985) demonstrated that brittle fracture can take place at high crack propagation velocities. This results in progressively diminishing inelastic response but that the transition is smooth and spread out, and far from being abrupt. The importance of background plasticity effects has been demonstrated experimentally by Hirsch *et al.* (1989a), who have shown that the sharp B–D transition in dislocation-free Si becomes diffuse, and moves to somewhat lower temperatures, when the crystals are initially dislocated by a pre-deformation step. The effect of background plasticity can therefore be regarded as one of modulating the B–D transition, with the ultimate controlling mechanism residing in crack-tip-initiated processes.

It is observed that intrinsically brittle materials such as crack-free Fe (Allen 1959) and W (Argon and Maloof 1966a) single crystals can often be plastically deformed at cryogenic temperatures with low plastic resistance when they are in pure form but fracture in a brittle manner when they are less pure and exhibit a high plastic resistance. This observation has been used as an argument in support of the background plasticity model of the fracture transition. This is partly correct. An intrinsically brittle solid only demonstrates its brittle characteristics when a crack is present. In well prepared Fe and W crystals, cracks do not exist initially and need to be produced by plastic deformation, most prominently by the intersection of deformation twins (Argon and Maloof 1966b). This requires a relatively high stress to nucleate the twins. In pure metallic crystals, the plastic yield stress is usually below the critical stress required for twinning, and brittle microcracks are not produced until the flow stress is raised by strain hardening to a sufficient level for twinning.

In the present paper we have reported on the key process of dislocation nucleation from crack tips in bcc transition metals, and particularly in α-Fe, where nucleation is expected be the controlling process. We have noted that, as is now well established (Schöck and Püschl 1991, Rice *et al.* 1992, Rice and Beltz 1994, Xu *et al.* 1995a), at the saddle point the critical activation configuration of the nucleated dislocation consists only of partially completed core matter. Consequently, we have termed these configurations dislocation embryos.

We note that a cursory examination of the shapes of the dislocation embryos shown in figs. 3 and 4, for the case of the inclined plane, and to a lesser extent, those in figs. 13 and 14, for the substantially screw-type embryos on cleavage ledges might give the counter-intuitive appearance of closed loops that are in the process of formation. This is an illusion since the level contours shown in these figures pertain to the total displacements at the crack tip where only the bulged portions of these, in the region of $x_1/b > 0$, could be associated with the inelastic displacements of the embryo. A reference line passed through $x_1/b = 0$ (the initial geometrical crack front) shows clearly that the embryo approximates to somewhat less than a half-ellipse but results in the partial penetration of the crack tip displacements into the embryo, giving an overall mushroom-type appearance.

The present study, as was our original work, as well as that of Rice *et al.* (1992), is based on the Peierls concept of describing the fundamental inelastic response by an interplanar tension–shear potential. The analysis of the shapes of the embryos and the dependence of the activation energies for their formation on the applied energy release rates were performed self-consistently, utilizing quantities such as μ, γ_{us} and γ_s that had been determined by the best available atomistic approaches (Sun, Beltz and Rice 1993) and were presented also by us earlier (Xu *et al.* 1995a). Thus, while published information of these quantities based on experimental measurements may have a considerable latitude in certainty, our results should have greater accuracy in the relative placement of the modes of response that we have simulated. Clearly, however, on an absolute basis, such as in the determination of the transition temperatures of fig. 18, the results should be viewed with more caution. Nevertheless, the energetics of the embryos that we have analysed indicate that the very large uncertainties in the transition temperatures of previous considerations (discussed by Xu *et al.* (1995a)) have now been eliminated.

In our present study we have examined three plausible modes of nucleation: on inclined planes containing the crack front, on oblique planes intersecting the crack front, in the interior and near a free surface and, finally, on cleavage ledges along the crack front. Our analysis has confirmed our earlier finding (Xu *et al.* 1995a) that nucleation on inclined planes in α-Fe entails energy barriers that are too high to be overcome, at impending crack advance, at temperatures below the melting point. Contrary to expectations, our analysis has also established that dislocation nucleation on oblique planes in α-Fe requires even higher energies in the interior of the solid, which translates into transition temperatures well above the melting point. Since in this mode of nucleation no significant free surface is produced, the finding is surprising but can be explained by noting that, while the peak shear stress near the crack tip is higher on the oblique planes than on inclined planes, the area-averaged shear stress is significantly lower in the former case, owing to the rapid decay of stresses in all directions away from the tip. A rather different conclusion was reached, however, for oblique planes near a free surface where no plane-strain stress exists and shear stresses on oblique planes are much higher. Here, were it not for a need of some surface ledge production, emission of dislocations should be nearly spontaneous. Such preponderance of dislocation emission where the crack reaches free surfaces has been observed by George and Michot (1993).

Both the inclined plane modes and the oblique plane modes are instances of homogeneous nucleation, inasmuch as every segment of the crack front constitutes an equally likely nucleation site. However, numerous experiments (Chiao and Clarke 1989, Samuels and Roberts 1989, George and Michot 1993) have demonstrated that

nucleation is a rare event and occurs only at particular sites along the crack front. These sites are nearly always associated with cleavage ledges. A preliminary analysis of heterogeneous nucleation at ledges had been carried out by Zhou and Thomson (1991), who found the mechanism to be quite favourable.

We have analysed dislocation nucleation on cleavage ledges in α-Fe, where we have taken the crack front to coincide with the ⟨110⟩ direction and the ledges to be on {112} planes. This mode is favoured in two important ways. Firstly, the embryo is of a predominantly screw type and, hence, has a low line energy; it involves no surface production. Indeed, our results show that the energetics of this mode in α-Fe are so favourable that it borders on being a spontaneous process. The B–D transition temperatures that are estimated for this mode are well within the expected range for low-C steel, that is around 250–300 K. This mode of initiation of dislocation activity also furnishes a ready explanation for the observation of Michot (1988) and George and Michot (1993) that such activity often occurs on planes with low resolved shear stress.

Analyses based on Peierls potentials represent the best minimum-commitment approach to an atomistic analysis. Consequently, we view our results as less than a final answer. These limitations notwithstanding, it can be safely argued that the previously existing gap between experiment and theory pointed out by Argon (1987) has been substantially closed at present. Our finding that the key event is a process of heterogeneous nucleation is well in keeping with most other nucleation-controlled phenomena in nature (see Martin and Doherty (1976) for a discussion). Further refinements of the model can be derived from the direct atomistic simulation of the crack-tip processes. These, which have proven unwieldly in the past, can now be more readily attempted using our activation configurations as a first guess of the initial position of the crack-tip atoms. One outstanding problem that remains to be addressed concerns the mobility-controlled fracture transition. A perceptive model of Brede (1993) should be amenable to a more rigorous analysis by our variational boundary integral method. In particular, it should be possible to account for rate effects within the present theory by introducing a rate and temperature-dependent resistance law for dislocation motion.

In closing, we note that the ability of dislocation nucleation at the crack tip to account for the exceedingly sharp transitions observed in some materials has been questioned by Khanta, Pope and Vitek (1994a,b), who have advocated a critical phenomena approach akin to statistical mechanical theories of defect-mediated melting. However, the preponderance of the observational evidence appears to support the crack-tip dislocation nucleation mechanism. Indeed, the detailed and meticulous direct X-ray imaging experiments of George and Michot (1993) of the stages of evolution of the crack tip plastic response, starting from nucleation at crack tip heterogeneities and followed by the very rapid spread and multiplication of dislocation length from such sources, is a convincing direct demonstration of the vast number of degrees of freedom available to dislocations for populating the highly stressed crack tip zone. We know of no present experimental evidence for the large thermal equilibrium concentrations of stiffness-attenuating dislocation dipoles that are predicted by the model of Khanta *et al.* (1994a,b).

Acknowledgements

This research was supported by the Office of Naval Research (ONR) under Contract No. N00014-92-J-4022, with an additional supplement for the present

simulation for which we are grateful to Dr R. Barsoum of that agency. M.O. gratefully acknowledges support from the ONR under Contract No. N00014-90-J1758. We acknowledge fruitful discussions with Professor J. R. Rice and Professor E. Kaxiras of Harvard University and Dr R. Thomson of the National Institute of Standards and Technology. Moreover, we acknowledge support from the Army Research Office under a Supplementary Equipment Grant No. P-33768-MA-RIP for purchases of computer equipment used in this work. The computations were carried out in the facilities of the Mechanics of Materials group at Massachusetts Institute of Technology, and those of the Solid Mechanics group at Brown University.

APPENDIX

Asymptotic solutions of the crack tip in the anisotropic solid

Cracks and dislocations in anisotropic solids were investigated by Stroh (1958) in the manner most useful to our present study. A comprehensive review of the theory of dislocations in anisotropic solids has recently been given by Lothe (1992). The asymptotic solutions of the semi-infinite crack in anisotropic solids used here are obtained by taking the limit of the solution of a slit crack given by Barnett and Asaro (1972), who modelled the slit crack as the superposition of three sets of straight dislocations. The variational boundary integral method developed by Xu and Ortiz (1993) and Xu *et al.* (1995b) is an extension of this approach to three dimensions.

With reference to fig. A 1, the three stress intensity factors $K_i (i = 1, 2, 3)$ are defined as

$$\sigma_{i2}|_{x_1 \to 0, x_2 = 0} = \frac{K_i}{(2\pi x)^{1/2}} + \text{non-singular terms.} \tag{A 1}$$

The opening displacements u_i are given by

Fig. A 1

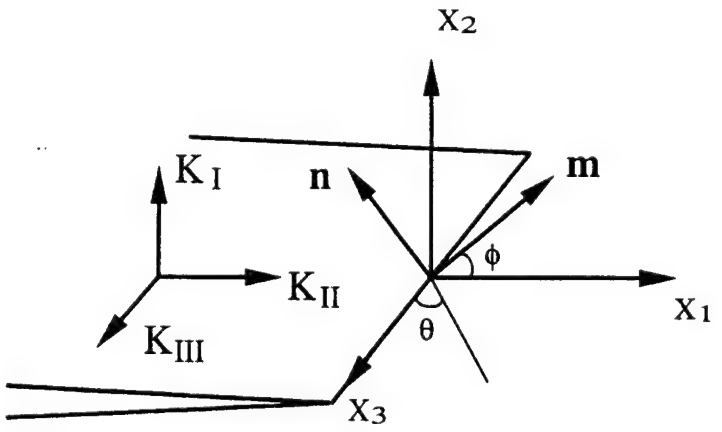

A semi-infinite crack in an anisotropic solid.

$$u_i = 4B_{ij}^{-1}K_j\left(\frac{-x_1}{2\pi}\right)^{1/2}, \tag{A 2}$$

and the energy release rate G for crack extension is

$$G = \tfrac{1}{2}K_iB_{ij}^{-1}K_j. \tag{A 3}$$

Here **B** is a positive-definite symmetric second-rank tensor that depends only on the direction of the crack front. For isotropic solids, **B** takes the diagonal form

$$B_{11} = B_{22} = \frac{\mu}{1-\nu}, \qquad B_{33} = \mu. \tag{A 4}$$

For anisotropic solids, **B** is given by the integral

$$\mathbf{B} = -\frac{1}{2\pi}\int_0^{2\pi}[(mn)(nn)^{-1}(nm) - (mm)]\,\mathrm{d}\phi, \tag{A 5}$$

where **m** and **n** are mutually orthogonal unit vectors normal to the crack front; the matrix (mn) is, in components, $(mn)_{jk} = m_ic_{ijkl}n_l$, and c_{ijkl} are elastic constants of the solid.

For α-Fe, $c_{11} = 2{\cdot}431 \times 10^5$ MPa, $c_{12} = 1{\cdot}381 \times 10^5$ MPa and $c_{44} = 1{\cdot}219 \times 10^5$ MPa. The resulting dependence of the energy release rate on crack front orientation is plotted in fig. A 2, where G_{iso} is the energy release rate computed from average elastic constants. Similar results are shown for Si on (111) and (110) planes, in which case $c_{11} = 1{\cdot}677 \times 10^5$ MPa, $c_{12} = 0{\cdot}650 \times 10^5$ MPa and $c_{44} = 0{\cdot}804 \times 10^5$ MPa. It follows from this calculation that the preferred crack front orientation for cleavage fracture on the (001) plane in α-Fe is parallel to the [110] direction. Likewise, the directions [110] and [111] are preferred for cleavage on (110) and (111) planes respectively in Si.

Fig. A 2

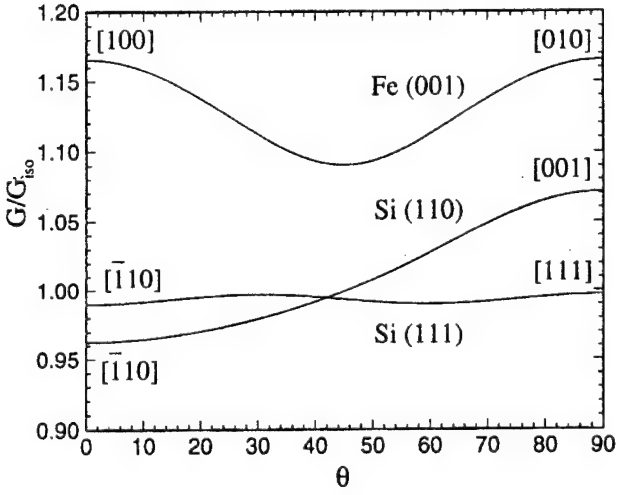

The variation in energy release rate with crack front orientation in Fe and Si.

References

Allen, N. P., 1959, *Fracture*, edited by B. L. Averbach, D. K. Felbeck, G. T. Hahn and D. A. Thomas (Cambridge, Massachusetts: MIT Press), p. 123.

Argon, A. S., 1987, *Acta metall.*, **35**, 185.

Argon, A. S., and Maloof, S. R., 1966a, *Acta metall.*, **14**, 1449; 1966b, *Ibid.*, **14**, 1463.

Barnett, D. M., and Asaro, R. J., 1972, *J. Mech. Phys. Solids*, **20**, 253.

Beltz, G. E., and Rice, J. R., 1991, *Modeling the Deformation of Crystalline Solids: Physical Theory, Application and Experimental Comparisons*, edited by T. C. Lowe, A. D. Rollett, P. S. Follansbee and G. S. Daehn (Warrendale, Pennsylvania: Metallurgical Society of AIME), p. 457.

Brede, M., 1993, *Acta metall. mater.*, **41**, 211.

Brede, M., and Haasen, P., 1988, *Acta metall.*, **36**, 2003.

Brede, M., Hsia, K. J., and Argon, A. S., 1991, *J. appl. Phys.*, **70**, 758.

Bulatov, V. V., Yip, S., and Argon, A. S., 1995, *Phil. Mag.* B, **72**, 452.

Burns, S. J., and Webb, W. W., 1970a, *J. appl. Phys.*, **41**, 2078; 1970b, *J. appl. Phys.*, **41**, 2086.

Chiao, Y.-H., and Clarke, D. R., 1989 *Acta metall.*, **47**, 203.

Cotterell, B., and Rice, J. R., 1980, *Int. J. Fract.*, **16**, 155.

Foreman, A. J., Jaswon, M. A., and Wood, J. K., 1951, *Proc. phys. Soc.* A, **64**, 156.

Freund, L. B., and Hutchinson, J. W., 1985, *J. Mech. Phys. Solids*, **33**, 169.

George, A., and Michot, G., 1993, *Mater. Sci. Engng*, **A164**, 118.

Gilman, J. J., Knudsen, C., and Walsh, W. P., 1958, *J. appl. Phys.*, **29**, 600.

Hahn, G. T., Averbach, B. L., Owen, W. S., and Cohen, M., 1959, *Fracture*, edited by B. L. Averbach, D. K. Felbeck, G. T. Hahn and D. A. Thomas (Cambridge, Massachusetts: MIT Press), p. 91.

Hirsch, P. B., Roberts, S. G., Samuels, J. and Warner, P. D., 1989a, *Advances in Fracture Research*, Vol. 1, edited by K. Salama, K. Ravi-Chandar, D. M. R. Taplin and P. Rama Rao (Oxford: Pergamon), p. 139.

Hirsch, P. B., Samuels, J., and Roberts, S. G., 1989b, *Proc. R. Soc.* A, **421**, 25.

Hsia, K. J., and Argon, A. S., 1994, *Mater. Sci. Engng.* A, **176**, 111.

Juan, Y., and Kaxiras, E., 1996 *Phil. Mag.* A, **74**, 1367.

Kelly, A., Tyson, W. R., and Cottrell, A. H., 1967, *Phil. Mag.*, **15**, 567.

Khanta, M. Pope, D. P., and Vitek, V., 1994a, *Phys. Rev. Lett.*, **73**, 684; 1994b, *Scripta metall. mater.*, **31**, 1349.

Lin, T., Evans, A. G., and Ritchie, R. O., 1986, *J. Mech. Phys. Solids*, **34**, 477; 1987, *Metall. Trans.* A, **18**, 641.

Lothe, J., 1992, *Elastic Strain Fields and Dislocation Mobility*, edited by V. L. Indenbom and J. Lothe (Amsterdam: Elsevier), p. 269.

McClintock, F. A., and Argon, A. S., 1966, *Mechanical Behavior of Materials* (Reading, Massachusetts: Addison-Wesley), chapter 17.

Maeda, K., and Yamashita, Y., 1989, *Structure and Properties of Dislocations in Semiconductors*, edited by S. G. Roberts, D. B. Holt and P. R. Wilshaw (Bristol: Institute of Physics), p. 269.

Martin, J. W., and Doherty, R. D., 1976, *Stability of Microstructure in Metallic Systems* (Cambridge University Press).

Michot, G., 1988, *Crystal Properties and Preparation*, Vols. 17 and 18 (Aedermannsdorf, Switzerland: Trans Tech Publ.), p. 55.

Nabarro, F. R. N., 1947, *Proc. phys. Soc.* A, **59**, 256.

Peierls, R. E., 1940, *Proc. phys. Soc.* A, **52**, 34.

Rice, J. R., 1992, *J. Mech. Phys. Solids*, **40**, 235.

Rice, J. R., and Beltz, G. E., 1994, *J. Mech. Phys. Solids*, **42**, 333.

Rice, J. R., Beltz, G. E., and Sun, T., 1992, *Topics in Fracture and Fatigue*, edited by A. S. Argon (Berlin: Springer), p. 1.

Rice, J. R., and Thomson, R., 1974, *Phil. Mag.*, **29**, 73.

Rose, J. H., Ferrante, J., and Smith, J. R., 1981, *Phys. Rev. Lett.*, **47**, 675.

Samuels, J., and Roberts, S. G., 1989, *Proc. R. Soc.* A, **421**, 1.

Schöck, G., and Püschl, W., 1991, *Phil. Mag.* A, **64**, 931.

St John, C., 1975, *Phil. Mag.*, **32**, 1193.

Stroh, A. N., 1954, *Proc. R. Soc.* A, **223**, 404; 1955, *Ibid.*, **232**, 548; 1957, *Adv. Phys.*, **6**, 418; 1958, *Phil. Mag.*, **3**, 625.

Sumino, K., 1989, *Structure and Properties of Dislocations in Semiconductors*, edited by S. G. Roberts, D. B. Holt and P. R. Wilshaw (Bristol: Institute of Physics), p. 245.

Sun, Y., Beltz, G. E., and Rice, J. R., 1993, *Mater. Sci. Engng*, **A170**, 67.

Sun, Y., Rice, J. R., and Truskinovsky, L., 1991, *High Temperature Ordered Intermetallic Alloys IV*, Materials Research Society Symposium Proceedings, Vol. 213, edited by L. A. Johnson, D. T. Pope, and J. O. Stiegler (Pittsburgh, PA: Materials Research Society), p. 243.

Xu, G., and Ortiz, M., 1993, *Int. J. Numer. Methods Engng*, **36**, 3675.

Xu, G. Argon, A. S., and Ortiz, M., 1995a, *Phil. Mag.* B, **72**, 415.

Xu, G., Argon, A. S., Ortiz, M., and Bower, A. F., 1995b, *Computational Mechanics '95, Theory and Applications*, Vol. 2, edited by S. N. Atluri, G. Yagawa, and T. A. Cruse (Berlin: Springer), p. 2874.

Yamaguchi, M., Vitek, V., and Pope, D., 1981, *Phil. Mag.* A, **43**, 1027.

Yonenaga, I., Onose, U., and Sumino, K., 1987, *J. Mater. Res.*, **2**, 252.

Yonenaga, I., and Sumino, K., 1989, *J. Mater. Res.*, **4**, 355.

Yonenaga, I., Sumino, K., Izawa, G., Watanabe, H., and Matsui, J., 1989, *J. Mater. Res.*, **4**, 361.

Zhou, S. J., and Thomson, R., 1991, *J. Mater. Res.*, **6**, 639.

REPORT DOCUMENTATION PAGE

Form Approved
OMB No. 0704-0188

1. AGENCY USE ONLY (Leave blank)	2. REPORT DATE	3. REPORT TYPE AND DATES COVERED
	May 22, 1997	Final: 9/1/1992-11/30/1995

4. TITLE AND SUBTITLE
Kinetics of the Crack-Tip-Governed Brittle to Ductile Transitions in Intrinsically Brittle Solids

5. FUNDING NUMBERS
C-N00014-92-J-4022

6. AUTHOR(S)
A.S. Argon, G. Xu and M. Ortiz

7. PERFORMING ORGANIZATION NAME(S) AND ADDRESS(ES)
Massachusetts Institute of Technology
Room 1-306
Cambridge, MA 02139 (A.S. Argon)

8. PERFORMING ORGANIZATION REPORT NUMBER
1-7

9. SPONSORING/MONITORING AGENCY NAME(S) AND ADDRESS(ES)
ONR Solid Mechanis Program (Attn: Dr. R. Barsoum)
ONR Code 1132
800 N. Quincy Street - Ballston Tower 1
Arlington, VA 22217-5000

10. SPONSORING/MONITORING AGENCY REPORT NUMBER

11. SUPPLEMENTARY NOTES
Paper to be published in "Cleavage Fracture: Theory, Experimentation and Modeling", TMS: Warrendale, PA (1997).

12a. DISTRIBUTION/AVAILABILITY STATEMENT
Unlimited

12b. DISTRIBUTION CODE

13. ABSTRACT *(Maximum 200 words)*

Brittle-to-ductile transitions in the fracture of intrinsically brittle solids manifest themselves in two fundamentally different forms. In the first type of solids exemplified by the BCC transition metals and some alkali halides in which dislocation mobility against the lattice resistance is governed by double kink nucleation, the corresponding fracture transition appears to be controlled by formation of dislocation embryos at crack tips. In the second type of solids exemplified by Si, and possibly all other compounds, dislocation mobility is governed not only by double kink nucleation but by kink mobility as well. In these solids the B-D transitions are known to be controlled by dislocation mobility. Here we report first on recent simulations of dislocation embryo formation from Mode I cracks in α - Fe as generic cases of BCC transition metals, and then on a new model of the mobility controlled transitions, typically in *Si*. Both models find good experimental confirmation.

14. SUBJECT TERMS
A summary of computational and analytic simulations of crack tip dislocation emissions in Fe and Si

15. NUMBER OF PAGES
11

16. PRICE CODE

17. SECURITY CLASSIFICATION OF REPORT	18. SECURITY CLASSIFICATION OF THIS PAGE	19. SECURITY CLASSIFICATION OF ABSTRACT	20. LIMITATION OF ABSTRACT
Unclassified	Unclassified	Unclassified	None

To be presented at the TMS Symposium on Cleavage Fracture: Theory, Experimentation, and Modeling in Indianapolis, Sept. 14-18. 1997

KINETICS OF THE CRACK-TIP-GOVERNED BRITTLE TO DUCTILE TRANSITIONS IN INTRINSICALLY BRITTLE SOLIDS

A.S. Argon *, G. Xu *†, M. Ortiz ‡
* Massachusetts Institute of Technology, Cambridge, MA 02139
† present address: Terra Tek, Inc, Salt Lake City, Utah 84108
‡ California Institute of Technology, Pasadena, CA 91125

Abstract

Brittle-to-ductile transitions in the fracture of intrinsically brittle solids manifest themselves in two fundamentally different forms. In the first type of solids examplified by the BCC transition metals and some alkali halides in which dislocation mobility against the lattice resistance is governed by double kink nucleation, the corresponding fracture transition appears to be controlled by formation of dislocation embryos at crack tips. In the second type of solids exemplified by Si, and possibly all other compounds, dislocation mobility is governed not only by double kink nucleation but by kink mobility as well. In these solids the B-D transitions are known to be controlled by dislocation mobility. Here we report first on recent simulations of dislocation embryo formation from Mode I cracks in $\alpha - Fe$ as generic cases of BCC transition metals, and then on a new model of the mobility controlled transitions, typically in *Si*. Both models find good experimental confirmation.

Introduction

Abrupt transitions in fracture between energy absorbing ductile forms and brittle cleavage, with decreasing temperature and increasing strain rate have been, and still continue to be of concern in many structural materials. While the phenomenon has been known in engineering practice since at least the celebrated molasses tank fracture in Boston in 1919 (for a discussion of an historical perspective of non-ship fractures see Shank, [1]), it became of crisis proportions only during World War II through the rash of major fractures of Liberty ships. In the early post-war years the problem received attention through semi-quantitative studies of notch effects and strain rate [2], and through some studies of effects of microstructure and of alloying to suppress the ductile to brittle transition temperature (for a summary see Parker, [3]). In the 50s and early 60s a fundamental recognition was reached that brittle behavior is usually triggered by deformation induced cleavage microcracks introduced into the system by dislocation pile-ups [4-6] by intersection of deformation twins [7] or by cracking of elongated grain boundary carbides [8]. In the range of the transition temperature a substantial concentration of such microcracks are "injected" into the system. Eventual brittle behavior results when one such microcrack succeeds, without being rearrested, to break through grain boundary barriers and propagates long distances [9-11]. The triggering conditions for this final transition in polycrystalline metals were also studied theoretically [12-15].

A fundamental perspective on the class of materials which are capable of fracture transitions starts with Kelly et al [16], and more specifically with Rice and Thomson [17] who have conceived a fundamental behavior pattern for a theoretical criterion establishing intrinsic brittleness vs intrinsic ductile behavior in materials. According to this criterion an atomically sharp crack has means of governing the behavior of a material in the absence of any other form of plastic response of the background, by either nucleating dislocations from its tip or by propagating in a cleavage mode by virtue of the presence of an energy barrier to the emission of such dislocations. In the first instance the material is designated as intrinsically ductile and incapable of exhibiting a fracture transition, while in the second instance it is designated as intrinsically brittle and capable of undergoing a transition from brittle cleavage to ductile forms at a characteristic transition temperature T_{BD}, affected by the rate of loading. Although many experimental studies have demonstrated that mere nucleation of some dislocations from a crack tip does not assure ductile behavior [18,19], the Rice Thomson mechanism comes close to a threshold process that triggers ductile behavior in a class of intrinsically brittle solids with relatively high dislocation mobility, such as the BCC transition metals and most alkali halides. However, fully satisfactory experimental confirmation of this limiting response is rare, outside of an elegant experiment by Gilman et al. [20] of crack arrest in *LiF*.

In distinction to the nucleation controlled response is the well established response of Si, and presumably, many other covalent materials and compounds with sluggish dislocation mobility, where the transition between brittle to tough behavior is governed by the mobility of groups of dislocations away from the crack tip [21-25]. In either the nucleation or the mobility controlled dislocation emission scenarios it is now well recognized that, emission of such dislocations from a crack tip occurs preferentially from specific crack tip sites and that assurance for full ductile behavior requires that

all parts of the crack front be shielded to prevent continued brittle behavior by local break-out of the cleavage crack from unshielded portions of the crack front [24]. Since even the ductile to brittle transition is triggered by the continued propagation of an "injected" cleavage microcrack, it is now widely accepted that the fundamental fracture transition is governed by the behavior of a cleavage crack. Most modeling studies have been developed around this concept.

The fundamental supposition of the brittle-to-ductile transition models based on the Rice and Thomson scenario [17] is that while background plastic relaxations can serve to suppress the transition temperature, the ultimate arbiter of the transition is the ability, of the crack tip to emit dislocations that can shield the entire crack front and trigger widespread plastic deformation before the crack can propagate by cleavage. However, the approach of the Rice and Thomson model in which the activation configuration consisted of a fully developed dislocation line have proved to seriously over estimate the energy barriers to nucleation of dislocations [26], even after incorporating such refinements as crack tip non-linearity and tension softening [27] across the slip plane. This indicated that the activation configurations must involve imperfect dislocations which must incorporate at least a minimum of atomistic information [26].

The accumulating experimental evidence on Si [21-25] and the insight provided by the most recent modeling studies of Schöck and Püschl, [28], Rice and Beltz [29], Xu et al., [30] suggest that the activation configuration of a dislocation embryo is in the form of a double kink of dislocation core matter. The observation permits the identification of two distinct types of B-D transitions. In the BCC transition metals where barriers to kink mobility along the dislocation are low, the B-D transition is likely to be governed directly by the formation of dislocation embryos at the crack tip, resulting in a nucleation-controlled transition. By contrast, in semi-conductors and compounds the evidence suggests [31-35], and modeling verifies [36], that kink mobility is hindered by substantial energy barriers, rendering the B-D transition controlled by dislocation mobility away from the crack tip.

Ultimately, a full understanding of the B-D transitions must come from atomistic models of the formation and outward propagation of the dislocation embryo at the crack tip. Before such modeling can be attempted, however, much progress can be made by recourse to hybrid continuum-atomistic approaches [28-30,37] based on the use of a Peierls interplanar potential [38-40]. In a recent development of this technique by Xu et al. [30], an additional surface production resistance was introduced into the interplanar potential, and the appropriate saddle point configurations of the dislocation embryos were determined by recourse to a variational boundary integral method advanced by Xu and Ortiz earlier [41]. Xu et al. [30] concluded that the energetics of dislocation embryo formation on inclined slip planes containing the crack tip, against an additional surface production resistance, is quite unfavorable and does not explain the known B-D transition temperatures. It was then conjectured that nucleation may be more favorable on oblique slip planes or, may occur heterogeneously at crack front ledges.

In the present communication we first review briefly the recent findings of Xu et al. [30,42] on the dislocation emission processes that most likely govern the brittle to ductile transition in BCC transition metals. These findings demonstrate the power of the special hybrid continuum - atomistic approach, based on the recently developed technique of Rice and coworkers [37], in fairly accurately predicting the transition temperature and the specific modes of dislocation embryo formation that govern it. We then present a new development for the B-D transition in fracture in Si where this transition is governed by dislocation mobility away from the crack tip. It is worth noting that even in this latter case the specific process of dislocation embryo formation at the crack tip will occur and often govern the mode of the crystal plasticity of the crack tip but do not govern the kinetics of the transition.

Modes of Dislocation Nucleation at a Crack Tip

Several alternative modes of dislocation nucleation from crack tips have been contemplated in the past. The modes differ mainly in the relative geometry of the slip plane, the crack surface and the crack front. The configurations considered include: nucleation of dislocations on the extension of the crack surface, Fig. 1a; nucleation on an inclined plane containing the crack front, Fig. 1b; nucleation on an oblique plane, Fig. 1c; and nucleation on a cleavage ledge, Fig. 1d.

Of these modes, that shown in Fig. 1a is the simplest, since it involves no tension across the potential slip plane and no production of a free surface. It has been investigated by Rice, [43] and Rice et al. [37] in a two dimensional setting and by Schöck and Püschl [28] in a three dimensional setting of a simple double kink shaped activation configuration. This was also done by a more elegant perturbation analysis by Rice and Beltz [29]. These analyses that have used a conservative tension-shear potential based on a Peierls-Nabarro model to represent the periodic interplanar shear resistance of a slip plane and a tension softening effect have demonstrated that the activation configuration did indeed consist only of dislocation core matter. In 2-D this produces an inelastic crack tip displacement equal to one half of a Burgers displacement and results in a critical energy release rate equal to the unstable stacking energy associated with a half step shear across the slip plane. Rice et al. [37] have extended their approach to also deal with the mode of Fig. 1b involving dislocation nucleation on an inclined plane-albeit without the affect of surface ledge production. A surface production resistance was incorporated into the Rice model by Xu et al. [30] who have concluded that this effect raises the energy barrier to such a degree that it all but rules out dislocation nucleation on inclined planes.

Experimental observations of Burns and Webb, [18] and considerations of local peak stress levels [26] point to the possibility of nucleating dislocations on oblique planes as shown in Fig.1c. However, approximate analysis of this nucleation mode by the Rice and Thomson method have led to very large energy barriers. This conclusion is reinforced

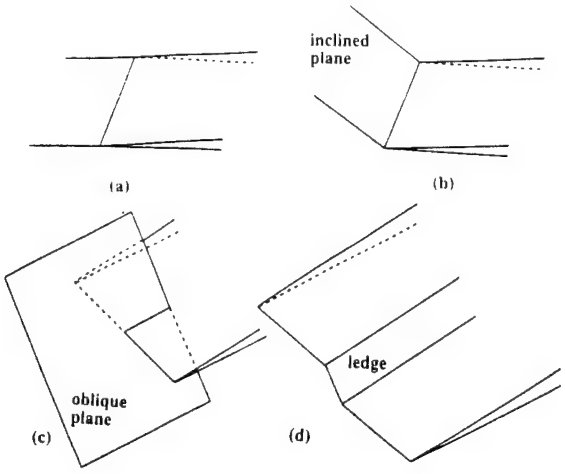

Fig. 1 Alternative modes of dislocation nucleation from a crack tip, ([42], courtesy of Taylor & Francis).

by a more accurate analysis of Xu et al. [42] that we present below. Finally, experimental observations of George and Michot, [25] have indicated that actual dislocation nucleation occurs very frequently on cleavage ledges on the crack front and near free surfaces. This possibility is analysed further below and shows that conditions are indeed quite favorable for it. Since nucleation controlled fracture transitions are likely to be limited only to BCC transition metals and to some alkali halides, the analysis of Xu et al. was performed for $\alpha - Fe$. Figures 2a-2c show the specific geometrical settings for Fe that were considered, where the cleavage plane is (001) and the crack front is parallel to the [110] directions which are the prevalent directions of the crack front in Fe giving a minimum of energy release rate [42].

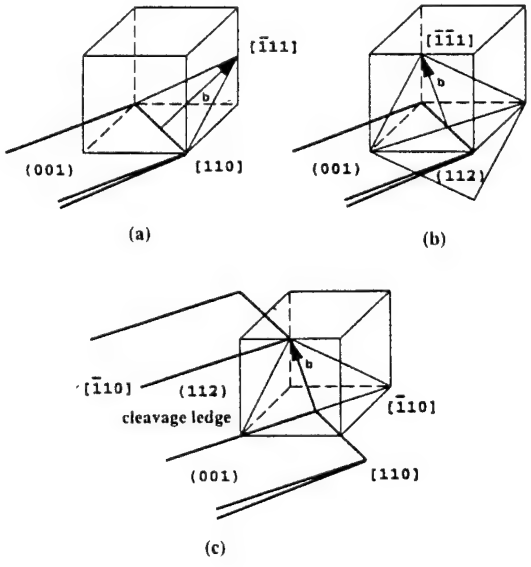

Fig. 2. Modes of dislocation nucleation from crack tips in $\alpha - Fe$: a) inclined plane; b) oblique plane; c) cleavage ledge, ([42], courtesy of Taylor & Francis)

Method of Analysis for Dislocation Embryos

The analysis for dislocation embryos employs a variant of the variational boundary integral method of Xu and Ortiz [41] to encompass problems of dislocation nucleation from atomically sharp cracks. In this model, a slip plane connected to the crack front is viewed as an extension of the crack surfaces with a nonlinear interlayer potential acting across it. Thus, the crack and the slip plane on which the dislocation nucleates are jointly regarded as a three-dimensional crack system embedded in the linear elastic solid. The interlayer potential acting across the slip plane is modeled by combining the universal binding energy relation of Rose et al. [44] with a skewed shear resistance profile [40]. The interplanar displacements and the crack opening displacements are represented by a continuous distribution of curved dislocations. This approach introduces no artificial discontinuity between the elastic crack opening and inelastic interplanar slip and separation. The technique has been described in complete detail by Xu and Ortiz [41] and its application to the present study by Xu et al. [30,42]. In this section, we briefly outline those aspects of the method which are pertinent to the treatment of the special activation configurations described in the previous section.

Consider a semi-infinite cleavage crack and a slip plane intersecting the crack front as shown in Fig. 1b. The crack/slip plane system is loaded remotely by a K-field. The crystallographic slip plane is chosen to be the most advantageous for slip. As the driving force increases, an embryonic dislocation forms progressively until it reaches an unstable equilibrium (saddle-point) configuration. The load corresponding to this unstable configuration is defined as the critical driving force for nucleation. The embryonic dislocation profile is characterized as a distribution of interplanar inelastic displacements, defined by Rice [43] as:

$$\delta = \Delta - \Delta^e \tag{1}$$

where Δ and Δ^e denote the total and the elastic interplanar displacements respectively. The opening displacements u of the crack surface, including the inelastic displacements along the slip plane, can be written as:

$$u = \overline{u} + \delta \tag{2}$$

where $\overline{u}$ is the displacement of a standard K-field for a reference semi-infinite crack. The term $\overline{u}$ matches the behavior of the opening displacements of the crack far away from the crack tip and serves as a boundary condition of the system. Consequently, the additional term δ, modifying the former, and being the primary unknown in the analysis, is expected to decay rapidly to zero with distance away from the crack tip in either direction. In this manner, δ can be considered in a finite domain around the crack front on the crack surface and on the slip plane connected to the crack.

Following the procedure introduced by Xu et al. [30,42], the potential energy of the whole system can be written in the form.

$$\Pi[\overline{u}+\delta] = W[\overline{u}+\delta] + V[\delta]$$
$$= W_1[\overline{u}] + W_1[\delta] + W_2[\overline{u},\delta] + V[\delta], \quad (3)$$

where we identify $W_1[\overline{u}]$ as the elastic strain energy of the system, free of inelastic modifications, $W_1[\delta]+V[\delta]$ as the self energy of the system of inelastic modifications consisting of the distributed dislocations and the interplanar interaction energy on the slip plane, and $W_2[\overline{u},\delta]$ is the interaction energy of the initial unmodified system with the second system of modifications. Of these energies the ones of relevance in the variational approach are those that depend on the unknown inelastic modification δ. Their specific forms have been given elsewhere [30, 42].

The potential energy $V[\delta]$ of the interplanar inelastic deformation on the slip plane is a key ingredient of the method and is given as:

$$V[\delta] = \int_{\hat{S}_s} \Phi[\delta] dS, \quad (4)$$

where $\Phi[\delta]$ is the interplanar tension/shear potential, defined per unit area of the slip plane, $\hat{S}_s$. It adopts the constrained displacement hypothesis of Rice [43] and Sun et al. [45], in which the interplanar shear displacement Δ_r is constrained along the Burgers vector direction. The shear and tension separation resistances, τ and σ respectively, follow as functions of the inelastic shear displacements δ_r and tensile separation displacement δ_θ on the slip plane. The associated traction-displacement relation has been modeled by Rice et al. [37] and was modified by Xu et al. [30] to incorporate an element of skewness and a surface production resistance. The resulting forms have been presented in detail elsewhere [30].

The unknown displacements follow by rendering the potential energy$\Pi[\overline{u}+\delta]$ stationary. This is achieved by discretizing the integral equation with six noded elements distributed on the crack surface. The non-linear equations are solved by a Newton-Raphson iteration. The saddle-point configurations are activated by introducing a small perturbation into the system at the bifurcation point, based on the solution of a first-order eigen-value problem if necessary. Solutions are obtained by recourse to interplanar displacement control, achieved through the introduction of Lagrange multipliers [30,42].

The material constants for α-Fe used in the present calculations are given in Table I.

Table I. Material Properties for α-Fe [42]

slip system	T (°K)	μ (10^5MPa)	c	$\gamma_{us}^{(u)}$ (Jm^{-2})	$2\gamma_s$
$(1/2)[111](1\bar{1}0)$	4.2	0.756	3.125	0.517	3.33
$(1/2)[\bar{1}\bar{1}1](112)$	4.2	0.756	3.125	0.581	3.80

where

μ	shear modulus
c	uniaxial strain elastic modulus
$\gamma_{us}^{(u)}$	unrelaxed unstable stacking energy
γ_s	surface energy

Embryo Configurations and Energies

Nucleation of Dislocations from a Shear Crack in Mode II

This configuration which is easiest to analyse was the one considered first by Rice[43] to establish that in the athermal limit of emission of a straight dislocation, the critical configuration consists entirely of dislocation core material with a total inelastic crack-tip shear displacement of one half Burgers displacement and an energy G_{IIcd} equal to the unrelaxed unstable stacking energy $\gamma_{us}^{(u)}$. It is of little realistic interest, even in its 3-D saddle point forms at driving forces $G_{II} < G_{IIcd}$ that were analysed by Xu et al. [30,42].

Nucleation of Dislocations on Inclined Planes in Mode I.

The nucleation of a dislocation on any inclined slip plane passing through a Mode I crack will occur under a mixture of effective Modes II and Mode I where the local effective Modes I and II are related to the overall Mode I acting across the crack by [46],

$$K_I^{eff} = K_I cos^3(\theta/2) \;\; \therefore K_{II}^{eff} cos^2(\theta/2) sin(\theta/2) \quad (5a,b)$$

To better appreciate this mixture of modes we have examined the general modifying effect on K_{II} of a K_I^{eff} acting across a slip plane, that is required to achieve an athermal 2-D release of a straight dislocation on this plane. This result is given in Fig. 3 [30] and demonstrates that while the effect of a K_I^{eff} acting across the slip plane does indeed produce some reduction in the required K_{II}^{eff}, this reduction is relatively minor. Xu et al. [30] have shown that this comes about from the lack of spatial coincidence of the non-linear opening displacements and shear displacements at the crack tip.

On any inclined slip plane the nucleation of a dislocation must produce a free surface ledge after the dislocation is emitted and has been sent into the background. During the actual nucleation process when the incipient surface is not

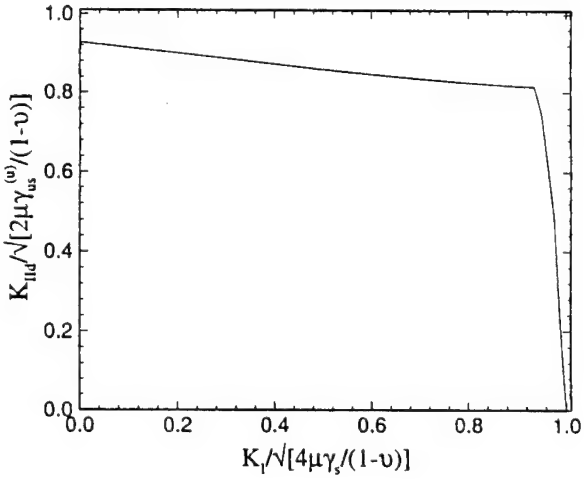

Fig. 3. Dependence of critical K_{II} for dislocation emission on K_I present on the $\frac{1}{2}[\bar{1}\bar{1}1](112)$ system of α-Fe ([30], courtesy of Taylor & Francis).

yet relaxed the effect must be considered as an additional surface production resistance to be added to the shear resistance of the tension shear potential [30, 47] to at least the first row of atoms that will be bared as a free surface. The result of a specific analysis of this effect is shown in Fig. 4 again for the release of a straight dislocation from the crack

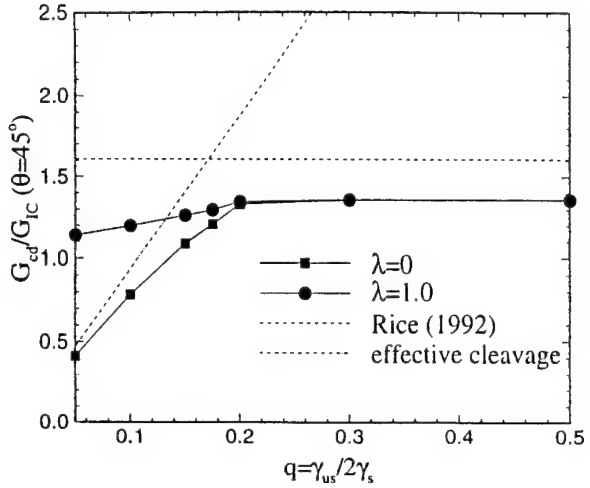

Fig. 4. Dependence of the critical energy release rate G_{cd}/G_{IC} on the factor $q = \gamma_{us}/2\gamma_s$ for dislocation nucleation at 45°, ([30], courtesy of Taylor & Francis).

tip onto an inclined plane making an angle of 45° with the crack plane. The dependence of the critical energy release rate G_{cd}, normalized with the crack driving force G_{IC} on the parameter $q = \gamma_{us}/2\gamma_s$ is shown for a case with no surface production resistance ($\lambda = 0$) and for a surface production resistance affecting substantially only the first row of atoms ($\lambda = 1$). The slanted dash-dotted line shows a somewhat more approximate estimate of Rice for no surface production resistance [43], while the horizontal dashed line gives the condition where cleavage is obtained on the slip plane. $G_{cd}/G_{IC} < 1.0$ indicates nucleation of a dislocation prior to propagation of the crack. The solutions including the surface production resistance indicates that for all values of q crack propagation on the cleavage plane will precede athermal release of a dislocation on the 45° inclined plane. Values of q range from 0.081 for Al to 0.091 for Ni (both for Shockley partial dislocations) to 0.217 for $\alpha - Fe$ and 0.376 for Si (Shockley partial) [30]. Since all cases lie above G_{cd}/G_{IC} of 1.0, it must be concluded that homogenous nucleation of dislocations on inclined planes is not possible prior to crack propagation for any material, regardless of whether it is intrinsically brittle or ductile [30].

Nucleation of Dislocations on an Oblique Plane.

Dislocation nucleation on oblique planes has frequently ben suggested as a likely mode. Approximate analyses based on the Rice and Thomson method have led to estimates of the B-D transition temperatures several orders of magnitude higher than what is experimentally observed, prompting suggestions that nucleation should involve a fractional dislocation [26].

The problem of the formation of a dislocation embryo on an oblique plane in $\alpha - Fe$ in the configuration of Fig. 2c was considered.

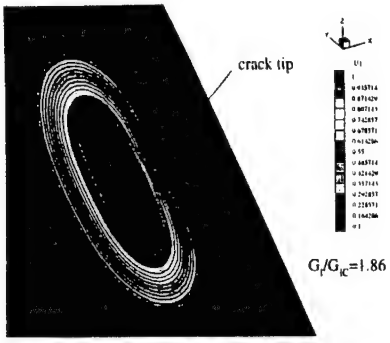

Fig. 5. Saddle-point configuration of a dislocation embryo emitted from a crack tip on an oblique plane, ([42], courtesy of Taylor & Francis).

A typical saddle-point configuration of such an embryonic dislocation loop emanating from the crack tip is shown in Fig. 5. The resulting calculated dependence of the activation energy on the crack driving force, near the athermal threshold is shown in Fig. 6. The critical driving force at the athermal threshold, and the attendant activation energies are so high that they render the nucleation mechanism most unlikely. The activation energy at $G_I/G_{IC} = 1.0$ can be estimated from the extrapolated curve, and forms an adequate basis for reaching a firm negative conclusion on the likelihood of nucleating a dislocation in the interior by this mechanism. A very different conclusion can be reached, however, for this mechanism where the crack front reaches a free surface. Here, no plane strain stress constraint exists and the resolved shear stresses on the oblique planes become much higher. An estimate of this is readily obtained by re-scaling the driving forces in Fig. 6 in proportion to

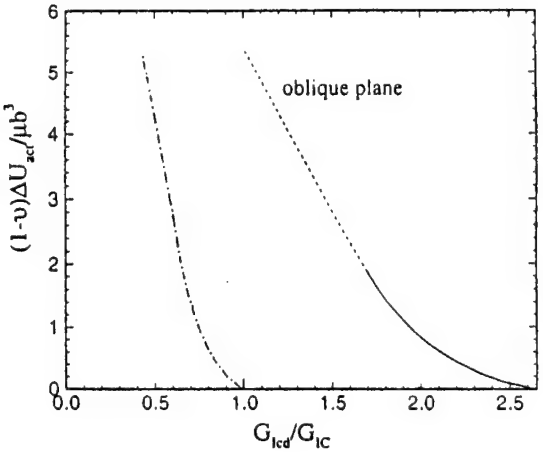

Fig. 6. Activation energies for dislocation nucleation on an oblique plane. Dash-dotted curve for such a plane near the surface, ([42], courtesy of Taylor & Francis).

the resolved shear stresses on the oblique slip planes near the surface vs those in the interior as (for the geometry of Fig. 2b):

$$\frac{G_{Is}}{G_{Ii}} = \left(\frac{3-4\nu}{3}\right)^2 \tag{6}$$

where G_{Is} and G_{Ii} are the respective energy release rates for initiation near the surface and in the interior. The result for *Fe* with $\nu = 0.291$ is shown as the dash-dotted curve in Fig. 6, which now suggests almost spontaneous nucleation near the surface. This, however, is not quite the case since in this instance some surface ledge needs to be produced on the side surfaces which will make the nucleation more difficult, but presumably still much easier than in the interior.

Nucleation of Dislocations on a Cleavage Ledge

Cleavage surfaces in metallic crystals invariably contain ledges parallel to the direction of crack propagation. These are likely to form when the direction of the principal tension driving the crack deviates slightly on a local scale, requiring the crack to make small adjustments along its front. This unavoidable micro-roughness of the cleavage surface depends on the crystallography of the cleavage planes and the crack propagation direction, as well as on temperature. The height of the observed ledges can range from several atomic spacings to microns. Numerous observations [24,25,48] have revealed that dislocation nucleation at a crack front is a relatively rare phenomenon associated with such crack front heterogeneities [49].

Consider a cleavage crack propagating under Mode I loading, and containing ledges of a width of roughly a hundred atomic spacings distributed along its front. The presence of a considerable local Mode III stress intensity factor acting on the ledge, the fact that no free surface is produced, and that the nucleated embryo will be nearly screw in nature are all expected to promote such nucleation.

The distribution of stress intensity factors on the crack front can be readily calculated by the boundary element method [41]. On the ledge, the dominant stress intensity factors are $K_I^{ledge} \sim 0.81 K_{IC}$ and $K_{III}^{ledge} \sim 0.35 K_{IC}$ at the verge of brittle propagation of the crack.

The athermal condition for nucleating a dislocation in Mode III loading, as it exists on the ledge, was determined by Rice [43], as:

$$\begin{aligned} K_{IIIcd} &= \sqrt{(1-\nu)\gamma_{us}/2\gamma_s}\, K_{IC} \\ &= 0.357 K_{IC} > 0.350 K_{IC} \end{aligned} \tag{7}$$

This result suggests that dislocation formation on crack front cleavage ledges should be close to spontaneous according to this simple estimate. However, we merely conclude that it should be in the range to initiate thermally assisted embryo formation. To analyse such thermally assisted embryo formation a saddle point analysis of a crack in pure Mode III, to apply to the problem at hand, of the cleavage ledge loaded in Mode III. Figures 7a and 7b show the saddle point configuration under normalized load levels of

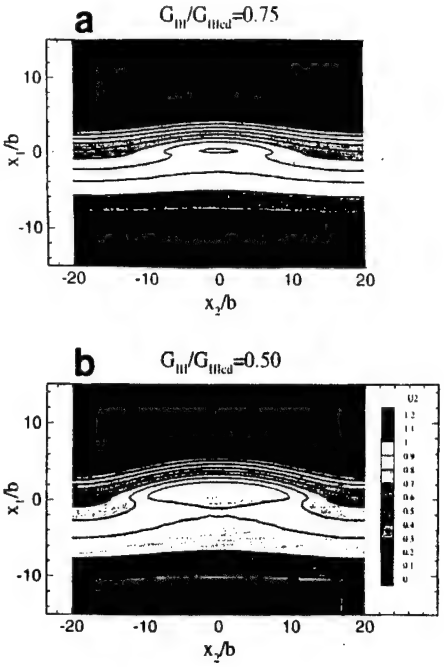

Figs. 7a & b. Saddle-point configurations of a dislocation embryo on a cleavage ledge at $G_{III}/G_{IIIcd} = 0.75$, and 0.5, ([42], courtesy of Taylor & Francis).

G_{III}/G_{IIIcd} of 0.75 and 0.5 respectively. The resulting dependence of the activation energies for such configurations on actual normalized crack driving forces G_I/G_{IC} are shown in Fig. 8, for a case with no K_I component acting across the ledge (∇) and the case with the appropriate K_I component of $0.81 K_{IC}$ (o) acting across the ledge, as it should be the case of the geometry of Fig. 2c. The differences are small.

The B-D Transition Temperature in α-Fe

The preceding results can be used to estimate the B-D transition temperatures attendant to the three main nucleation modes considered. No precise experimental measurements of the transition temperature of single crystal $\alpha - Fe$ are available. The transition temperature for polycrystal low carbon steel is about $250^o K$, as determined from Charpy impact experiments [50]. Based on this, we take the transition temperature for $\alpha - Fe$ to be in the range of $250 - 300^o K$. A B-D transition scenario proposed by Argon [26] consists of the arrest, at T_{BD}, of a cleavage crack propagating with a velocity v against a temperature gradient. This gives the relation,

$$T_{BD} = \left[\frac{ln(c/v)}{\alpha} + \eta\frac{T_o}{T_m}\right]^{-1} T_o \tag{8}$$

where $T_o \equiv \mu b^3/k(1-\nu) \sim 1.2 \text{x} 10^5 K$; the melting temperature $T_m = 1809K$ for $\alpha - Fe$; $\alpha = (1-\nu)\Delta U_{act}/\mu b^3$ is the normalized activation energy; c is speed of sound; $v \sim 1\ cm/s$ is a typical crack propagation velocity, giving $\ln(c/v) \sim 10$; $\eta \sim 0.5$ is a coefficient describing the temperature dependence of the shear modulus which, to a first approximation, is taken to be of the form $\mu = \mu_o(1 - \eta(T/T_m))$.

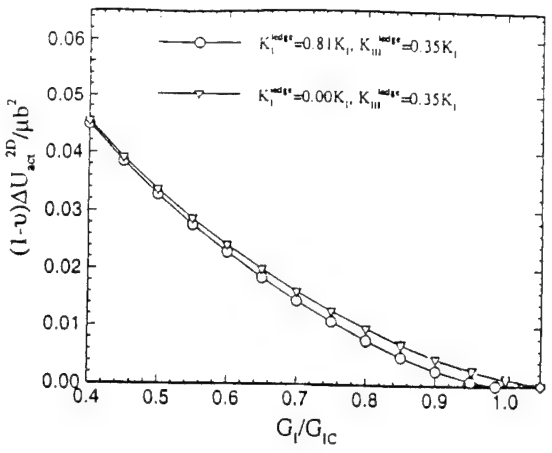

Fig. 8. Activation energies for dislocation nucleation on a cleavage ledge, ([42], courtesy of Taylor & Francis).

The activation energy at the critical driving force for cleavage , i.e., at $G_I/G_{IC} = 1$, determines the transition temperature through Eqn. 8. This relation is plotted in Fig. 9 together with reasonable ranges of activation energies for nucleation on inclined planes, oblique planes and on crack tip ledges. The results for the oblique plane near a free surface should be close to that for crack tip cleavage ledges. Also shown in the figure is the value of the transition temperature for polycrystalline *Fe* and its melting temperature. It is evident that only nucleation on cleavage ledges and on oblique planes near a free surface result in transition temperatures that approach the expected value for $\alpha - Fe$. The dislocation loops which eventually shield the entire crack are apparently emitted from ledges distributed along the crack front as was noted by George and Michot [25].

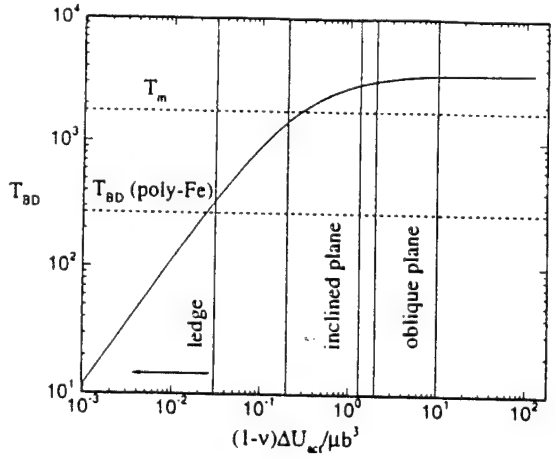

Fig. 9 Estimates of T_{BD} in $\alpha - Fe$, vis-a-vis the three primary nucleation configurations considered, ([42], courtesy of Taylor & Francis).

Dislocation Mobility Controlled B-D Transitions in Si

Stress Relaxation and Crack-Tip Shielding

That the B-D transition in *Si* single crystals is controlled by dislocation mobility is well established. The meticulously performed stress relaxation experiments of George and Michot [25] carried out at $K_I < K_{IC}$ levels have demonstrated that the development of crack tip shielding by the emitted dislocations leading to an eventual fracture transition is associated with a complex set of dislocations moving away from the crack tip on several crystallographic planes. The best available analyses of the spread of dislocations from the crack tip [51-53] have been too idealized and stylized to represent the real situation. Here we present a more homogenized approach that is based on the developments of Riedel and Rice [14] for sharp Mode I cracks undergoing stress relaxation by power-law creep from an initially elastic response. In their extensive characterization of the inelastic response of *Si* at elevated temperature Alexander and Haasen [55] have demonstrated that, once an initial stage of dislocation multiplication is completed, the steady state creep response of *Si* can be given by a nearly perfect power-law form of Eqn. 9 with a stress exponent of $n = 3$.

$$\dot{\epsilon} = \alpha exp\left(-\frac{U}{kT}\right)(\sigma/\sigma_o)^3 \tag{9}$$

where $\alpha/\sigma_o^3 = 1.34\text{x}10^3 MPa^{-3}s^{-1}$ and the activation energy $U = 2.4$ eV/atom.

The Riedel and Rice solution gives for creep stress relaxation around a Mode I crack at time t, for the tensile stress $\sigma_{\theta\theta}$ at the crack tip at $\theta = 0$ and $r = r_c = b$ the following form [56].

$$\sigma_{\theta\theta} = \sigma_o \left(\frac{K_I^2(1-\nu^2)/E}{\sigma_o \alpha exp(-U/kT) I_n (n+1) r_c t}\right)^{\frac{1}{n+1}} \tilde{\sigma}_{\theta\theta}^c(\theta, n) \tag{10}$$

where I_n is a well defined integration constant and $\tilde{\sigma_{\theta\theta}^c}(\theta, n)$ is another constant defining the angular dependence of the stress field around the crack. For the present purpose for *Si* with n=3 we represent the relaxing stress $\sigma_{\theta\theta}$ in a different form of

$$\sigma_{\theta\theta}(r_c) = \sigma_{ic}\tilde{\sigma}_{\theta\theta}^c(0,3)\left[\left(\frac{K_I}{K_{IC}}\right)^2 \frac{(1-\nu)^2}{\sigma_{ic}^2 E I_3}\left(\frac{\pi}{2}\right)\left(\frac{\sigma_o^3}{\alpha}\right)\frac{1}{texp(-\frac{U}{kT})}\right]^{0.25} \tag{11}$$

where we have introduced the ideal cohesive strength σ_{ic}, determined from the universal binding energy relation of Rose et al [57].

$$\sigma_{ic} = \frac{1}{e}\sqrt{\frac{2\chi_s E}{(1-\nu^2)b}} = \frac{K_{IC}}{\sqrt{2\pi r_c}} \tag{12}$$

This permits a simple statement of the time dependent development of creep-strain-induced-crack-tip-shielding ΔK_{ISh} as

$$\left|\frac{\Delta K_{ISh}}{K_{IC}}\right| = \frac{K_I}{K_{IC}} - \tilde{\sigma}_{00}^c(0,3)\left[\left(\frac{K_I}{K_{IC}}\right)^2 \frac{(1-\nu)^2}{\sigma_{ic}^2 E I_3}\left(\frac{\pi}{2}\right)\frac{\sigma_o^3}{\alpha texp(-\frac{U}{kT})}\right]^{0.25} \tag{13}$$

The utility of this expression can be tested first to explain the recent stress relaxation experiments of Xin and Hsia [58]

on Si single crystals containing cracks subjected to stress intensities $K_I < K_{IC}$ for 20 hrs at 500C followed by subsequent measurement of increases of K_{IC} to fracture the samples at room temperature. As reproduced in Fig. 10, Xin and Hsia have noted that above a threshold of $K_I = 0.4K_{IC}$ increasing crack tip shielding develops in 20 hrs of stress relaxation with increasing K_I. Xin and Hsia attribute the stress intensity threshold to result from initiation of crack tip dislocation nucleation at this stress intensity at 500C over this period of holding. While this interpretation is, no doubt correct, we use the observation in our framework as a level of K_I/K_{IC} at which, over the period of holding, no significant crack tip shielding develops, and proceed to obtain a fit from Eqn(13) by solving for α/σ_o^3 for the well defined physical and simulation parameters of $n = 3, I_3 = 5.386, \sigma_{ic} = 17.7GPa, E = 147GPa, \nu = 0.215, \tilde{\sigma}^c_{\theta\theta}(0,3) = 1.9$. The choice is for $\alpha/\sigma_o^3 = 2.94x10^{-2}$ MPa^{-3} sec^{-1} and a factor of $2.19x10^{-5}$ smaller than the steady state value reported by Alexander and Haasen [55] and given above. While this discrepancy, at first sight, appears depressing, it is quite within expectations if it is recognized that in the Alexander and Haasen creep experiments the mobile dislocation density was $4.9x10^{11}m/m^3$. In the experiments of Xin and Hsia as well as on other B-D transition experiments performed on initially perfect crystals of Si the dislocation density starts out from zero and builds up in a slow transient. Thus, the value of α/σ_o^3 obtained from the fit amounts to a local mobile dislocation density at the time of transition to about $10^7m/m^3$ which is quite acceptable. Using this value, the subsequent levels of K'_{IC} at fracture reported by Xin and Hsia following the stress relaxation treatments can be determined simply from,

$$\frac{K'_{IC}}{K_{IC}} = 1 + \left(\frac{\Delta K_{ISh}}{K_{IC}}\right) \tag{14}$$

This result is plotted in Fig. 10 as the slanted dashed line and shows a similar nearly linear rise of K'_{IC}/K_{IC} with increasing K_I/K_{IC}, used in the stress relaxation experiment, but at a level of about 0.42 of what was reported by Xin and Hsia. Since there is no real or operational means of accommodating this finding by another adjustment in the developments of Eqns. (11-14), we attribute the difference

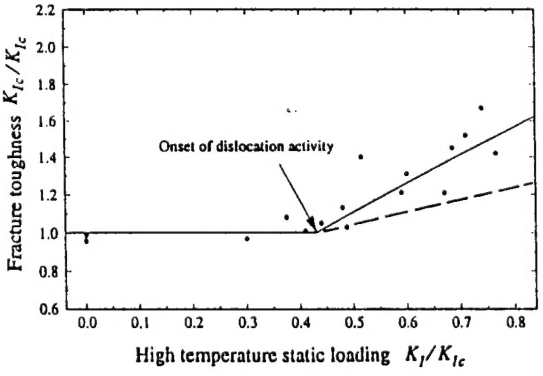

Fig. 10 Effect of crack tip stress relaxation at 500C for 20 hrs. for a cleavage crack on the (110) cleavage plane parallel to a [100] direction, on the subsequent fracture toughness. Dashed line represents Eqn. (14) (after Xin and Hsia [58], courtesy of Pergamon Press).

to a geometrical effect of fracture surface roughening, while the calculated effect presumably is what can be attributed to stress relaxation alone. Micrographs of fracture surfaces presented by Xin and Hsia show roughness levels that can readily account for the difference.

Brittle-to-Ductile Transitions in Constant Loading Rate Experiments

The B-D transition model presented by Brede [52], while quantitatively somewhat deficient, provides important insight into the dislocation-mobility-controlled-fracture-transition in Si. It demonstrates that a monotonic increase of the applied stress intensity factor K_I together with a concurrent crack tip stress relaxation results in a systematic reduction in the crack tip tensile stress from an otherwise linear increase with K_I in the absence of crack tip creep. At the range of the B-D transition, $\sigma_{\theta\theta}$ just manages to reach the ideal cohesive strength σ_{ic}, but the rate of increase in $\sigma_{\theta\theta}$ with time (orK_I) becomes zero. Thus, the B-D transition is a competition between elastic stress increase with a creep-induced-stress-relaxation process at a crack tip point $r = r_c$. Thus, the increase in the crack tip tensile stress $\sigma_{\theta\theta}(r = r_c)$ is,

$$d\sigma_{\theta\theta} = \left(\frac{\partial\sigma_{\theta\theta}}{\partial K_I}\right)_t dK_1 + \left(\frac{\partial\sigma_{\theta\theta}}{\partial t}\right)_{K_I} dt \tag{15}$$

where

$$\left(\frac{\partial\sigma_{\theta\theta}}{\partial K_I}\right)_t = \frac{1}{\sqrt{2\pi r_c}} = \frac{\sigma_{ic}}{K_{IC}} \tag{16a}$$

and

$$\left(\frac{\partial\sigma_{\theta\theta}}{\partial t}\right)_{K_I} = -\frac{\sigma_{ic}A}{4}\left(\frac{K_I}{K_{IC}}\right)^{\frac{1}{2}}\left(\frac{1}{t^5 exp(-\frac{U}{kT})}\right)^{\frac{1}{4}} \tag{16b}$$

obtainable directly from Eqn. (11) with,

$$A = \tilde{\sigma}^c_{\theta\theta}(0,3)\left|\frac{(1-\nu^2)}{\sigma_{ic}^2 E I_3}\left(\frac{\pi}{2}\right)\frac{\sigma_o^3}{\alpha}\right|^{\frac{1}{4}} = 1.28x10^{-3}(sec)^{0.25} \tag{16c}$$

for the quantities of Si given above.

At the B-D transition,

$$\sigma_{\theta\theta}(r = r_c) = \sigma_{ic} \quad \therefore \frac{d\sigma_{\theta\theta}(r = r_c)}{dt} = 0 \tag{17}$$

These two conditions with $t = K_I/\dot{K}_I$ and the use of Eqns. (15-16c) give a simple dependence of the brittle to ductile transition temperature T_{BD} on loading rate K_I as,

$$T_{BD} = T_o/ln(\dot{K}_o/\dot{K}_1) \tag{18}$$

where

$$T_o = \frac{U}{k} = 2.78x10^4 K \text{ and}$$

$$\dot{K}_o = \frac{4K_{IC}}{A^4} = 1.42x10^{12}\frac{MPa\sqrt{m}}{sec}$$

Moreover, the actual level of fracture toughness K'_{IC} at the verge of the fracture transition in units of the intrinsic frac-

ture toughness K_{IC} can be given as,

$$\frac{K'_{IC}}{K_{IC}} = \frac{1}{4}\frac{\dot{K}_o}{\dot{K}} exp(-U/kT) \qquad (19)$$

The experimental support of Eqn (18) is very good. Eqn. (18) gives,

$$\frac{d ln \dot{K}_I}{d(1/T_{BD})} = -T_o = -2.78 \text{x} 10^4 K \qquad (20)$$

while the values of this dependence reported by Brede and Haasen[22] range from 2.08 x 10^4K(G)[21] to 2.32 x 10^4K(E) and 2.67 x 10^4K(F)[62], and 2.10 x 10^4K(A)[22] all for intrinsic *Si*.

While this agreement of the predicted dependence of T_{BD} on $\dot{K}_I$ is pleasing, a check of the accuracy of the absolute value of T_{BD} through Eqn. (18) reveals a further discrepancy. The use of Eqn. (18) with the values for *Si* listed above adjusted to the experiment of Xin and Hsia, would give the characteristic line (1) plotted on Fig. 11 showing the various experimental results reported by Brede and Haasen [22]. A better fit given by line (2) would require a different adjustment for α/σ_o^3 to 1.63 x 10^{-4} MPa^{-3} sec^{-1} and a corresponding change of $\dot{K}_o$ to 7.89 x 10^9 MPA$\sqrt{m}$/sec. This would imply an even smaller dislocation density in the experiments of the fracture transition investigations [21,22,25] whose data is given in Fig. 11, below those required in the stress relaxation experiment of Xin and Hsia. This is not unlikely if it is noted that all the data reported in Fig. 11 involves a fracture transition on the {111} cleavage plane with the crack front being parallel to the <112> direction, while in the Xin and Hsia experiment the cleavage crack is on the {110} plane with the crack front being parallel to the <100> direction. The slip distribution for these two geometries is radically different [25].

Experimental verification of Eqn. (19) is more difficult since when a successful transition is initiated it follows continuously to much tougher behavior.

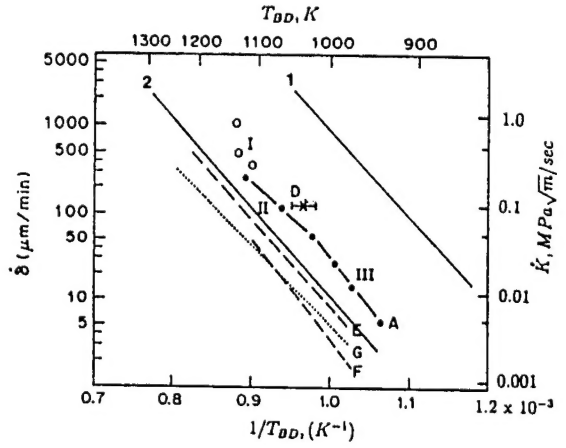

Fig. 11 Dependence of T_{BD} on loading rate $\dot{K}_I$ for a cleavage crack on (111) plane parallel to a [112] direction. Data from [22]. Line (1) results of Eqn. (18) based on Xin and Hsia data. Line (2) with adjustment for α/σ_o^3 more appropriate to the fracture transition experiments (after Brede and Haasen [22], courtesy of Pergamon Press).

Discussion

The models presented here relate to the fracture transition in both dislocation nucleation controlled solids, such as BCC transition metals and some alkali halides including *LiF, NaCl*, as well as in dislocation-mobility-controlled solids where *Si* is a principal example. In either case the processes are of key nature - more so in the initation-controlled solids then in the mobility-controlled solids where the actual toughening results from subsequent large scale plastic response, governed by extensive dislocation multiplication and spreading, rather than by the key process itself. The insight offered by the newly proposed approach using the Riedel-Rice solutions of continuum creep stress relaxation is particularly useful. It provides a good phenomenological framework in separating the two proccesses. Recently Roberts and coworkers[53,59] have advocated that all fracture transitions, including those in BCC transition metals, are governed by dislocation mobility on the basis of a good correspondence of the kinetics of the transition to the kinetics of dislocation mobility. We find this not convincing, first because the kinetics of dislocation glide in BCC metals exhibits a very different form from that in *Si*. In such materials the activation energy of glide against the lattice resistance is strongly stress dependent, manifesting itself in a very large phenomenolgical stress exponent in the range of 30-50 rather than 3, and a stress independent activation energy as is the case in *Si*. The resulting formalism following Eqns (11-19) while still useful, will indicate a near threshold type behavior in the fracture transitions. Nevertheless, the subject is still in need for further exploration in which our new developments could prove useful.

The two different adjustments that were necessary to the factor α/σ_o^3 representing the effective mobile dislocation density points out a number of important problems. First, in the range of transition to fully plastic behavior the evolution of a dislocation density is a complex process and as important as the kinetics of glide. Second, the actual B-D transition temperature (although not its dependence on loading rate) can depend sensitively on the particular kinematical distribution of the slip systems at the crack tip which is associated with the geometry of crystal plasticity and governs the effective density of dislocations that accomplish the transition. Finally, the adjustment exercise also points out the important role of mobilizable background dislocations, which through their polarization, will play a role in the crack tip shielding process. This is evident from the two cases considered. A formal increase in α/σ_o^3 shifts the T_{BD} toward lower levels.

There are many microstructural aspects of a B-D transition in polycrystalline solids in which microcrack, nucleation and processes of crack arrest at grain boundaries become very important, and will modulate the actual B-D transition temperature. Definitive understanding of these processes are still lacking. They too can benefit from more fundamental approaches of the type presented here.

Finally, we note that the ability of dislocation nucleation at the crack tip to account for the exceedingly sharp transitions observed in materials such as *Si* has been questioned by Khanta et al. [60, 61] who have advocated a critical phenomena approach, akin to defect- mediated melting where dislocation loops form and collapse in thermal equilibrium. The preponderance of the experimental evidence is against this proposition and supports the crack-tip dislocation mechanisms. Indeed, the detailed and meticulous direct X-ray imaging experiments of George and Michot [25] of the stages of evolution of the crack-tip plastic response, starting from nucleation at crack tip heterogeneities and followed by the very rapid spread and multiplication of dislocation length from such sources, is a convincing direct demonstration of the vast numbers of degrees of freedom available to dislocations for populating the highly stressed crack-tip zone. We know of no present experimental evidence nor any fundamental justification for the large thermal equilibrium concentrations of stiffness-attenuating dislocation dipoles that are predicted by the model of Khanta et al.

Acknowledgments

This research was supported by the Office of Naval Research (ONR) under contracts N00014-92-J-4022 and N00014-96-1-0629 with additional support from the ARO under Grant No. P-33768-MA-RIP for computer equipment acquisitions.

REFERENCES

1. M.E. Shank, *Mech. Eng., 76*, 23 (1954).
2. E. Orowan, in *Repts. Prog. Physics, vol 12*, p.185 (1949).
3. E.R. Parker, "*Brittle Behavior of Engineering Structures*", J. Wiley, New York (1957).
4. C. Zener, in "*Fracturing of Metals*", ASM, Metals Park Ohio, p.3 (1949).
5. A.N. Stroh, *Proc. Roy. Soc., A223*, 404, (1954).
6. A.N. Stroh, *Proc. Roy. Soc., A232*, 548 (1955).
7. D. Hull, *Acta Metall, 8*, 11 (1960).
8. C. McMahon, "*Micromechanisms of Cleavage Fracture in Polycrystalline Iron*", *ScD Thesis, M.I.T.*, Cambridge, MA (1963).
9. G.T. Hahn, B.L. Averbach, W.S. Owen, and M. Cohen, in "*Fracture*", edited by B.L. Averbach et al. MIT Press, Cambridge, MA, p. 91 (1959).
10. J.F. Knott and A.H. Cottrell, *J. Iron Steel Inst., 201*, 249 (1963).
11. M. Cohen and M.R. Vukcevich, in "*Physics of Strength and Plasticity*", edited by A.S. Argon, MIT Press, Cambridge, MA p.295 (1969).
12. A.N. Stroh, *Adv. Phys., 6*, 418 (1957).
13. R.O. Ritchie, J.F. Knott and J.R. Rice, *J. Mech. Phys. Solids, 21*, 395 (1973).
14. T. Lin, A.G. Evans and R.O. Ritchie, *J. Mech. Phys. Solids, 34*, 477 (1986).
15. T. Lin, A.G. Evans and R.O. Ritchie, *Met. Trans., 18A*, 641 (1987).
16. A. Kelly, W.R. Tyson and A.H. Cottrell, *Phil. Mag., 15*, 567 (1967).
17. J.R. Rice and R. Thomson, *Phil. Mag., 29*, 73 (1974).
18. S.J. Burns and W.W. Webb, *J. Appl. Phys., 41*, 2078 (1970).
19. S.J. Burns and W.W. Webb, *J. Appl. Phys., 41*, 2086 (1970).
20. J.J. Gilman, C. Knudsen and W.P. Walsh, *J. Appl. Phys., 29*, 600 (1958).
21. C. StJohn, *Phil. Mag., 32*, 1193 (1975).
22. M. Brede and P. Haasen, *Acta Metall, 36*, 2003 (1988).
23. P.B. Hirsch, J. Samuels, and S.G. Rloberts, *Proc. Roy. Soc., A421*, 25 (1989).
24. P.B. Hirsch, S.G. Roberts, J. Samuels and P.D. Warner, in *"Advances in Fracture Research"* edited by K. Salama et al. Pergamon, Oxford vol 1, p.139 (1989).
25. A. George and G. Michot, *Mater. Sci. Engng., A164*, 118 (1993).
26. A.S. Argon, *Acta Metall., 35*, 185 (1987).
27. K.S. Cheung, A.S. Argon and S. Yip, *J. Appl. Phys., 69*, 2088 (1991).
28. G. Schöck and W. Püschl, *Phil. Mag., A64*, 931 (1991).
29. J.R. Rice and G.E. Beltz, *J. Mech. Phys. Solids, 42*, 333 (1994).
30. G. Xu, A.S. Argon and M. Ortiz, *Phil. Mag., 72*, 415 (1995).
31. K. Sumino, in "*Structure and Properties of Dislocations in Semiconductors*", edited by S.G. Roberts et al, Inst. Phys., Bristol, England, p.245 (1989).
32. K. Maeda and Y. Yamashita, same as Ref. 31, p.269 (1989).
33. I. Yonenaga, U. Oriose and K. Sumino, *J. Mater. Res., 2*, 252 (1987).
34. I. Yonenaga, K. Sumino, G. Izawa, H. Watanabe and J. Matsui, *J. Mater. Res., 4*, 361 (1989).
35. I. Yonenaga, and K. Sumino, *J. Mater. Res., 4*, 355 (1989).
36. V.V. Bulatov, S. Yip, and A.S. Argon, *Phil. Mag., 72*, 452 (1995).

37. J.R. Rice, G.E. Beltz, and Y. Sun, in "*Topics in Fracture and Fatigue*", edited by A.S. Argon, Springer, Berlin, p.1 (1992).

38. R.E. Peierls, *Proc. Phys. Soc., A52*, 34 (1940).

39. F.R.N. Nabarro, *Proc. Phys. Soc., A59*, 256 (1947).

40. A.J. Foreman, M.A. Jaswon, and J.K. Wood, *Proc. Phys. Soc., A64*, 156 (1951).

41. G. Xu and M. Ortiz, *Intern. J. Num. Methods Engng., 36*, 3675 (1993).

42. G. Xu, A.S. Argon and M. Ortiz, *Phil. Mag., 75*, 341 (1997)

43. J.R. Rice, *J. Mech. Phys. Solids, 40*, 235 (1992).

44. J.H. Rose, J. Ferrante and J.R. Smith, *Phys. Rev. Letters., 47*, 675 (1981).

45. Y. Sun, G.E. Beltz and J.R. Rice, *Mater. Sci. Engng., A170*, 67 (1993).

46. B. Cotterell and J.R. Rice, *Intern. J. Fract., 16*, 155 (1980).

47. Y. Juan, Y. Sun and E. Kaxiras, *Phil. Mag. Lett., 73*, 233 (1996).

48. Y-H, Chiao, and D.R. Clarke, *Acta Metall., 47*, 203 (1989).

49. S.J. Zhou and R. Thomson, *J. Mater. Res., 6*, 639 (1991).

50. F.A. McClintock and A.S. Argon "*Mechanical Behavior of Material*", Addison Wesley, Reading MA (1966).

51. J. Samuels and S.G. Roberts, *Proc. Roy. Soc., A421*, 1 (1989).

52. M. Brede, *Acta Metall., et Mater., 41*, 211 (1993).

53. B. Devincre and S.G. Roberts, *Acta Material, 44*, 2891 (1996)

54. H. Riedel and J.R. Rice, in "*Fracture Mechanics: Twelfth Conference*" ASTM STP 700, edited by P.C. Paris, ASTM: Philadelphia PA p. 112, (1980).

55. H. Alexander and P. Hassen, in "*Solid State Physics*", edited by F. Seitz and D. Turnbull, Academic Press: New York, Vol. 22 p. 28 (1968)

56. H. Riedel, "*Fracture at High Temperatures*", Springer: Berlin (1987).

57. J.H. Rose, J. Ferrante, and J.R. Smith, *Phys. Rev. Letters, 47*, 675 (1981).

58. Y.-B. Xin and K.J. Hsia, *Acta Material, 44*, 845 (1996).

59. S.G. Roberts, M. Ellis and P.B. Hirsch, *Mater. Sci. Engng., A164*, 135 (1993).

60. M. Khanta, D.P. Pope and V. Vitek, *Phys. Rev. Letters, 73*, 684 (1994).

61. M. Khanta, D.P. Pope and V. Vitek, *Scripta Metall et Mater., 31*, 1349 (1994).

62. G. Michot and A. George, in *"Strength of Metals and Alloys"*, edited by H.J. McQueen et al. Pergamon: Oxford, Vol. 2, p. 1187 (1985).